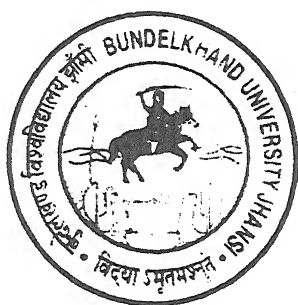


PETROGENESIS OF TIN BEARING GRANITOIDS OF KATEKALYAN AREA OF BASTAR, CENTRAL INDIA

By

Abhimanyu Singh



forwarded
21.4.2
26.5.2003

Head,

THESIS SUBMITTED FOR THE DEGREE OF Department of Geology
Bundelkhand University, JHANSI

Doctor of Philosophy

IN

Geology

OF THE

BUNDELKHAND UNIVERSITY
JHANSI – 284128
INDIA

Enrolment No. – 4005

May – 2003



*Dedicated
to my
Parents*

तार : विश्वविद्यालय
Gram : UNIVERSITY




टेलिफोन : कार्यालय : 320496
कुलसचिव : निवास : 321214
फैक्स : 0517 — : 320761

DEPARTMENT OF GEOLOGY
बुन्देलखण्ड विश्वविद्यालय, झाँसी
BUNDELKHAND UNIVERSITY, JHANSI

झाँसी (उ०प्र०)—284128

This is to certify that **Shri Abhimanyu Singh** has worked under my supervision on the problem "**Petrogenesis of Tin bearing Granitoids of Katekalyan Area of Bastar, Central India**" in the Department of Geology, Bundelkhand University, Jhansi. He completed the research work for the full period as prescribed under clause of the Ph. D ordinances and the thesis embodies the result of his investigation conducted during the period he worked as a Ph. D research scholar.


(S. P. Singh)
Supervisor

ACKNOWLEDGEMENTS

Whatever the matter, I am going to represent, was helped by my teachers and friends, who have made valuable suggestions, which I have incorporated in this research work.

As the mighty Himalayas are beyond measure and description so are the contributions of my revered supervisor **Prof. S. P. Singh**, Head, Department of Geology and Dean of the Faculty of Science. All I can say is that, to me, he is a "Guru". Immense gratitude and praises are the least I can offer to in return as he poured all the showers of knowledge to my shallow well. His sincerity, enthusiasm, tireless encouragements and the clear concept of the subject are only some of the qualities that had left a permanent work on me. He proved for me like a rudder to the boat or wings to the bird.

Words are there to express one's feelings, but some feelings are such that they cannot be expressed in words but still they have to be the kind help and humble suggestions of my respected **Prof. Santosh Kumar**, Department of Geology, Kumaon University, Nainital, will always be running through my nerves.

Thanks are also extended to **Dr. Satyendra Singh**, Department of Geology, B.H.U., who gave his time during research work.

I record to my admiration for the help extended by **Dr. P. P. Khanna** and **Dr. H. K. Sachan**, Wadia Institute of Himalayan Geology, Dehradun, for carrying out geochemical and fluid inclusion analyses of the samples.

I wish to express my heartfelt thanks to my colleagues **Dr. Ram Chandra**, **Dr. S. K. Singh**, **Dr. R.A. Singh**, **Dr. R. N. Yadav**, **Dr. B.C. Joshi**, **Dr. S. C. Bhatt**, **Dr. V.K. Singh**, **Sri. M.M. Singh**, **Dr. Anil Kumar Gupta** (Environmental Science), **Dr. P.K. Pandey**, **Mr. Brajesh Singh**, **Mr. Sahab Singh Yadav**, **Mr. Vidya Shankar Singh**, **Mr. Akhilesh Kumar Srivastava**, **Mr. Anupam Shukla**, **Mr. Shaktidhar Sahani**, **Ravi Kr. Sharma** and many others, for their constant help in various ways to accomplish this work successfully, as is said that "A friend in need is a friend indeed".

I would be failing to my duty if I do not acknowledge my wife **Smt. Gayatri Singh** and respected madams **Dr.(Smt.) Subra** and **Smt. Pushpa Singh**, for the continuous inspiration during the research work.

Finally I thank to all the members of the *Department Of Geology* for their support and encouragement.

Date:

ABZ 26/5/2023
(Abhimanyu Singh)

CONTENTS

	Page No.
Chapter I : INTRODUCTION	... 1-13
1.1: Introduction about granitoids	... 1-2
1.2: Tin occurrences and its locality in India	... 2-3
1.3: Tin bearing granitoids: a literature review	... 4-6
1.4: Location and approach of the Katekalyan	... 6-7
1.5: Climate, vegetation and other information	... 7
1.6: A brief resume of the previous work in and around Katekalyan	... 7-11
1.7: Nature and scope of the present investigation	... 11-13
 Chapter II : GEOLOGICAL SETTING	 ... 14-43
2.1 Introduction	... 14-15
2.2 Regional geology	... 16-21
2.2.1 Regional structure	... 21-24
2.2.2 Geochronology	... 24-29
2.3 Geology of the study area	... 30-32
2.3.1 Topography and drainage	... 32
2.3.2 Succession of the rocks of the area	... 33-34
2.3.3 Lithology, field relationships and structure	... 34-38
2.3.3.1 Metasediments	... 34-35
2.3.3.1.1 Andalusite, sericite schist	... 34
2.3.3.1.2 Quartz, sericite schist	... 34
2.3.3.1.3 Ferruginous quartzite	... 35
2.3.3.2 Metabasic extrusives	... 35
2.3.3.3 Metabasic intrusives	... 35-36
2.3.3.4 Granitoids (granite and granite gneiss)	... 36-38
2.3.3.5 Pegmatites (mineralised and non- mineralised)	... 38-41
2.3.3.6 Quartz reef	... 41
2.3.3.7 Younger metadolerite dyke	... 41
2.3.3.8 Alluvium	... 41-42
2.3.4 Mineralisation potential of the area	... 42-43

Contd...

Chapter III : PETROGRAPHY	... 44-63
3.1. Introduction	... 44
3.2. Metasediments	... 44-48
3.2.1. Andalusite sericite schist (A.S.S.)	... 44-45
3.2.2. Quartz sericite schist (Q.S.S.)	... 46
3.2.3. Banded ferruginous quartzite (BMQ/G.M.Q)	... 46-48
3.3. Metabasic extrusives (metabasalt)	... 48-49
3.4. Metabasic intrusives (metagabbro and amphibolite)	... 49-52
3.5. Granitoids [granite (KG) and granite gneiss (KGG)]	... 52-58
3.6. Pegmatites (mineralised and non-mineralised)	... 58-62
3.7. Quartz reef	... 62
3.8. Younger metadolerite dykes	... 62-63
 Chapter IV : GEOCHEMISTRY	 ... 64-80
4.1. Introduction	... 64
4.2. Major element geochemistry	... 64-72
4.2.1. Classification and nomenclature	... 65
4.2.2. Tectonic discrimination	... 68-69
4.2.3. Petrogenesis	... 69
4.2.4. Major oxide variation	... 70-72
4.3. Trace element geochemistry	... 72-73
4.3.1. Trace element variation	... 73-74
4.4. Rare earth element (REEs)	... 75
4.4.1. Introduction	... 75
4.4.2. Methodology	... 76-77
4.4.3. REE data presentation	... 78
4.4.4. Interpretation	... 79-80
 Chapter V : ORE PETROGRAPHY, ALTERATION AND GEOCHEMISTRY	 ... 81-90
5.1. Ore petrography	... 81-86
5.1.1. Introduction	... 81
5.1.2. Microscopic observations	... 81-86
5.2. Alteration environment	... 86-88
5.3. Geochemistry of cassiterite	... 88-90
5.3.1. Sample preparation method	... 88
5.3.2. Procedure of XRF analysis	... 88-89
5.3.3. Chemistry of cassiterite	... 89-90

Conta...

Chapter VI : FLUID INCLUSION STUDIES	... 91-101
6.1. Introduction	... 91-92
6.2. Method of sample preparation	... 92
6.3. Fluid inclusion petrography	... 92-95
6.4. Microthermometric analysis	... 95-96
6.5. Results of the microthermometric study	... 96-98
6.6. Conclusions	... 98-101
 Chapter VII : DISCUSSION	 ... 102-129
7.1. Introduction	... 102
7.2. Field evidences of tin mineralisation	... 102-103
7.3. Petrographical mineral assemblage of granite-gneiss (KGG) granite (KG) and its relationship with pegmatites (KP)	... 103-108
7.3.1. Granite-gneiss	... 103-104
7.3.2. Granite and its varieties	... 104-106
7.3.3. Pegmatite phase and its parents	... 106-108
7.4. Fluid rock interactions	... 108-109
7.5. Mineralogical evidences of boron and fluorine activity	... 109
7.6. Vapour phase separation from granitic magma and its role in Sn-mineralisation	... 109-111
7.7. Evidences from fluid-inclusion study	... 111-113
7.8. Evidences from wall-rock alteration	... 113-114
7.9. Geochemical evidences of the tin bearing granitoids	... 115
7.9.1. Major elements geochemistry	... 117-123
7.9.2. Trace elements geochemistry	... 123-126
7.9.3. Rare earth elements (REEs) geochemistry	... 126-127
7.10. Geochemical partial melting modeling	... 127-128
7.11. Geotectonic environments and its relevance to tin-bearing granitoids...	128-129
 Chapter VIII : CONCLUSION	 ... 130-141
 REFERENCES	 ... 142-158

LIST OF FIGURES

Figure No.	After page No.
Fig. 1.1. Map showing important occurrences of tin bearing granitoids deposits in India	2
Fig 1.2: Location map of the study area	6
Fig 2.1: Generalised regional geological map of the Southern Crustal Province (SCP) in the Central Indian Peninsular Shield (CIPS). The inset shows the major structural features of Peninsular India (KL= Kondagaon Lineament, BL= Bhomargarh Lineament).	16
Fig. 2.2: Regional geological map with radiometric dates (billion of years) of the primary tin mineralised belt in the southeastern part of Bastar Craton.	19
Fig. 2.3: Tectono-thermal events in Bastar Craton.	24
Fig. 2.4: Geological map of the Katekalyan area, district Dantewada, Chhattisgarh (Modified after T.M. Babu 1985).	30
Fig. 4.1: Na ₂ O vs K ₂ O (wt.%) plots for the Katekalyan granitoids, district Dantewada, Chhattisgarh (Harpum, 1963).	66
Fig. 4.2: Normative An-Ab-Or plots for Katekalyan granitoids, district Dantewada, Chhattisgarh (After O'Connor, 1965)	66
Fig. 4.3: The normative Q-A-P variation diagram after LeMaitre (1989) showing field of variation of the Katekalyan granitoids, district Dantewada (Chhattisgarh).	66
Fig. 4.4: The classification scheme is based on major element criteria of the Katekalyan granitoids using the parameters R ₁ and R ₂ (After De La Roche <i>et al.</i> , 1980), calculated from millication proportions.	66
Fig. 4.5: P vs Q diagram for the Katekalyan granitoids based on Debon and LeFort (1982). The parameters are expressed as gram atoms x 10 ³ of each element in 100 gm of material. Each pigeon hole of the classification grid corresponds to a petrographical group (1 to 12).	66
Fig. 4.6: Ternary diagram SiO ₂ -(FeO* + MgO + CaO) - (Al ₂ O ₃ + Na ₂ O + K ₂ O) of the tin bearing granitoids (a) and pegmatites (b) of the Katekalyan area, district Dantewada, Chhattisgarh (Greig-Stemprok, 1969).	66
Fig. 4.7: Ternary diagram of Silica-Total Mafics - Alkalies for the Katekalyan granitoids, district Dantewada (Chhattisgarh) along with tin-bearing granites of the world (After T.M. Babu, 1993).	66
Fig. 4.8 a: A vs B diagram of Katekalyan granitoids (After Debon and Le-Fort; 1982 and Debon <i>et al.</i> , 1986). The diagram is divided into six sectors numbered from I to VI. I. Mu > Bi, II. Bi > Mu, III. Bi ±, IV. Bi ± Hbl ± cpx ± opx ± ol ±, V. cpx ± hbl ±, VI. Di ±.	67

Contd...

Figure No.	After page No.
Fig. 4.8 b: Mole, $\text{Al}_2\text{O}_3/(\text{CaO} + \text{K}_2\text{O} + \text{Na}_2\text{O})$ vs SiO_2 plots for the Katekalyan granitoids and pegmatites (Chappel and White, 1974).	67
Fig. 4.9: A-F-M diagram plots for the Katekalyan granitoids (after Irvine and Baragar, 1971).	68
Fig. 4.10 a-d: Discrimination diagram for Katekalyan granitoids (Fields after Maniar and Piccoli, 1989).	68
Fig. 4.11: R_1 vs R_2 multicationic plots (a and b) of the Katekalyan granitoids (After De La Roche, 1964) modified by Batchelor and Bowden, 1985).	69
Fig. 4.12 a: $\text{K}_2\text{O}/\text{Al}_2\text{O}_3$ vs $\text{Na}_2\text{O}/\text{Al}_2\text{O}_3$ diagram for the Katekalyan granitoids (After Garrels and Mackenzie, 1971).	70
Fig. 4.12 b: Binary variation diagram between FELSIC and MAFIC constituents of the Katekalyan granitoids.	70
Fig. 4.13 a-h: Harkers variation diagrams of SiO_2 vs CaO , MgO , Na_2O , Al_2O_3 , Na_2O , K_2O , Al_2O_3 , Fe_2O_3^* , P_2O_5 , and TiO_2 for the granite (KG), granite gneiss (KGG) and pegmatites(KP).	70
Fig. 4.14: Rb-Sr log-log plot (Fields after Condie, 1973).	72
Fig. 4.15: Rb-Ba-Sr ternary diagram after El-Bouseilly and El-Sokkary (1975) with the distribution of Katekalyan granitoids (KG and KGG).	72
Fig. 4.16: Binary variation $\text{Zr} + \text{Nb} + \text{Ce} + \text{Y}$ vs FeO^*/MgO (wt.%) and $\text{Zr} + \text{Nb} + \text{Ce} + \text{Y}$ (ppm) vs $(\text{K}_2\text{O} + \text{Na}_2\text{O})/\text{CaO}$ (wt.%) diagrams (A and B) of the Katekalyan granitoids (After Whalen <i>et al.</i> , 1987).	72
Fig. 4.17: Discrimination diagrams for the Katekalyan granitoids (After Pearce <i>et al.</i> , 1984).	72
Fig. 4.18: Harkers variation diagrams of SiO_2 vs Cu, Zn, Rb, Ba, Sr, Zr, Nb and Ga	73
Fig. 4.19: Harkers variation diagrams of Sn vs TiO_2 , K_2O , MgO and Rb/Sr.	73
Fig. 4.20: Chondrite-normalized REE patterns for selected samples of the granitoids of the Katekalyan area. Open circles: biotite granite (KBG), closed circle: tourmaline granite (KTG) and closed squares: granite gneiss (KGG). The data are normalized to chondritic values given by Taylor and Mc Lennan; 1985 (1.5 x values of Evensen <i>et al.</i> ; 1978).	79
Fig. 6.1: Intersecting isochors for CO_2 and H_2O rich inclusion showing estimated P-T conditions for cassiterite associated with Katekalyan granitoids.	97
Fig. 7.1a: Rb/Sr vs SiO_2 plots for KG (KBG, KHG and KTG) and KGG. Note that the KG is evolved to a most SiO_2 differentiated and has affinity with Sn-granitic of Australia (Blevin and Chappel, 1995). See text for detail discussion.	124
Fig. 7.1b: $\text{FeO}^{\text{tot}}/(\text{FeO}^{\text{tot}} + \text{MgO})$ vs weight percent SiO_2 diagram plotted for KG and KGG and compared with ferroan plutons and magnesian plutons shown by continuous line (Frost <i>et al.</i> ; 2001). Bold dashed line is the boundary between calc-alkalic and tholeiitic magmas defined by Miyashiro (1970).	124

Contd...

Figure No.

After page No.

- Fig. 7.1c: $\text{Na}_2\text{O} + \text{K}_2\text{O} - \text{CaO}$ vs K_2O diagram plotted for KG and KGG ... 124
 compared with the compositional trends of Archaean tonalitic gneisses and Mesozoic granites of the Cordilleran batholiths a-c, alkali - calcic; c-a, calc-alkalic; c, calcic. The number refers to the position of the respective boundaries at that percentage of SiO_2 , $n=83$ for the cordilleran batholiths; $n=17$ for the Archaean Gneisses - as used by Frost *et al* (2001).
- Fig 7.2a: $\text{Na}_2\text{O} + \text{K}_2\text{O} - \text{CaO}$ vs SiO_2 diagram plotted for KG and KGG ... 125
 compared with the compositional trends of various plutons (Frost *et al*, 2001). The thick boundary lines separating the various series are taken after Frost *et al* (2001). See text for detail explanation.
- Fig 7.2b,c: Rb/Sr vs Sn (b) and TiO_2 vs Sn (c) variation diagrams (after ... 125
 Lehmann, 1982; Winchester and Max, 1983) contrasting Sn-rich and Sn-poor trends. Note that KG (KBG and KHG) and KGG mostly coincides with Sn-rich trends. The broken line separates the Sn-poor and Sn-rich fields.
- Fig. 7.3 a, b, c: Spider diagrams of the trace elements for the Katekalyan KGG ... 126
 (a), KG (b) and pegmatite (c). (After Taylor and Mc Lennan, 1985).
- Fig. 7.4 a, b: (a) Distribution of the KBG, KTG and KGG granitoid samples in ... 127
 the $\text{LREE} = (\text{La} + \text{Ce} + \text{Nd})$ in ppm vs $B = (\text{Fe} + \text{Mg} + \text{Ti})$ diagram. ($\text{La} + \text{Ce} + \text{Nd}$) is proportional to the amount of monazite. ($\text{Fe} + \text{Mg} + \text{Ti}$) reflects the amount of biotite content in granitoids. B values are calculated after Debon and Le Fort (1983) and Debon *et al* (1986).
- Fig. 7.4 (b) Distribution of KBG, KTG and KGG samples in the total REE (in ... 127
 ppm) vs $B = (\text{Fe} + \text{Mg} + \text{Ti})$ diagram.
- Fig. 7.5: Partial melting models (1 and 2) of bulk crust composition ($\text{Sr} = 260$... 127
 ppm, $\text{Rb} = 32$ ppm) of Taylor and Mc Lennan (1985) calculated at $D_{\text{Sr}} = 20$ and $D_{\text{Sr}} = 10$ respectively as shown by Gasparon *et al*. (1983) and compared with the variation of KG and KGG, approximately by 5-50% melting of average crust silicate. $D_{\text{Sr}} < 10$. See text for discussion.
- Fig. 7.6: Plots averages for Katekalyan granite (KG) and granite gneiss (KGG) ... 127
 in the $\text{Qz-Ab-Or-H}_2\text{O-F}$ system (Tuttle and Bowen, 1958; Manning *et al*, 1980).

LIST OF TABLES

<i>Table No.</i>	<i>After Page No.</i>
2.1 : Generalised Tectonostratigraphy of the Southern Crustal Province (SCP) in the Precambrian of Cenral India	... 14
2.2 : Litho – succession in the Bastar	... 16
2.3 : Lithostratigraphy in the Southern part of Bastar Craton	... 17
2.4 : Regional stratigraphy of Southern Bastar	... 18
2.5 : Geochronological data on Precambrian rocks of Bastar Craton	... 43
2.6 : Geochronostratigraphy of Southern Bastar	... 43
2.7 : Succession of the rocks of the Katekalyan area	... 43
4.1a : Major element analysis (in wt%) and CIPW weight norms of granite (KG) of Katekalyan area	... 80
4.1b : Major element analysis (in wt%) and CIPW weight norms of granite gneiss (KGG) of Katekalyan area	... 80
4.1c : Major elements analysis (in wt%) and CIPW weight norms of pegmatite (KP) of Katekalyan area	... 80
4.1d : Comparision of average major oxide values (in wt%) for granite (KG) and granite gneiss (KGG) compared with metallogenically specialized granite (Tischendorf, 1977) and average Low – Ca Granites (Turekian and Wedepohl, 1961)	... 80
4.2 : Criteria for distinguishing I- and S- type granites (Chappel and White, 1974; Takahasi <i>et al</i> ; 1980) applied for granite (KG) and granite gneiss (KGG)	... 80
4.3a: Major oxide criteria for tectonic environment (after Maniar and Piccoli; 1989)	... 80
4.3b: Inferred Tectonic Environment for granite (KG) and granite gneiss (KGG) based on discriminant function given in table 4.3a	... 80
4.4a: Trace element analysis (in ppm) of granite (KG) from Katekalyan..	80
4.4b: Trace element analysis (in ppm) of granite gneiss (KGG) from Katekalyan area	... 80

Contd...

Table No.**After Page No.**

4.4c: Average of Rb, Ba and Sr of the various granite group (El Bouseilly and El Sokkary, 1975) compared with granite (KG) and granite gneiss (KGG). The values for the High and Low-Ca granites take from Turekian and Wedepohl (1961)	... 80
4.4d: Trace element analysis (in ppm) of pegmatite (KP) of the Katekalyan area	... 80
4.5: Selected REE analysis and normalized chondrite values (in ppm) of Katekalyan granitoids (KG and KGG)	... 80
5.1: Element analysis of Cassiterite from Katekalyan area	... 88
6.1 : Type I CO ₂ inclusions in Cassiterite	... 101
6.2 : Type II CO ₂ – H ₂ O inclusions in Cassiterite	... 101
6.3 : Type IV H ₂ O- Nacl inclusions in Cassiterite	... 101
6.4 : Summary of microthermometric data of cassiterite	... 101
7.1: Different type of pegmatite and their mineralized characteristics	.. 114
7.2 : Ionic radii and Valencies of certain elements relevant to the geochemistry of Tin (after Hosking, 1965a)	... 115
7.3: Measured magnetic susceptibility (MS) related to samples of Katekalyan granite (KG) and granite gneiss(KGG)	... 119

LIST OF PLATES

<i>Plate No.</i>		<i>After page No.</i>
I, II, III	: Field photograph	63
IV, V, VI, VII, VIII	: Hand Specimen photograph	63
IX, X	: Metasediments (ASS, QSS, BFQ)	63
XI	: Metabasalt (MBE)	63
XII	: Metagabbro / amphibolite (MBI)	63
XIII	: Granite gneiss (KGG) and Biotite granite (KBG)	63
XIV	: Mylonitised granite (KG) and Biotite granite (KBG)	63
XV, XVI	: Biotite granite (KBG)	63
XVII	: Granite gneiss (KGG) and Biotite granite (KBG)	63
XVIII	: Hornblende granite (KHG)	63
XIX	: Tourmaline granite (KTG) and Pegmatite (KP)	63
XX, XXI	: Pegmatite (KP)	63
XXII	: Metadolerite	63
XXIII, XXIV, XXV	: Cassiterite and allied ore minerals	90
XXVI	: Fluid inclusions in cassiterite	101

ABBREVIATIONS USED FOR MINERALS

And	:	Andalusite
Ser	:	Sericite
Qz	:	Quartz
Grun	:	Grunerite
Mt	:	Magnetite
Plag	:	Plagioclase
Cpx	:	Clinopyroxene
Kf	:	K-feldspar
Zoi	:	Zoisite
Gt	:	Garnet
Hbl	:	Hornblende
Epi	:	Epidote
Chl	:	Chlorite
Fluo	:	Fluorite
Fels	:	Feldspar
Tour	:	Tourmaline
Zir	:	Zircon
Or	:	Orthoclase
Micro	:	Microcline
Alb	:	Albite
Bio	:	Biotite
Mus	:	Muscovite
Cass	:	Cassiterite
Ap	:	Apatite
Clv	:	Cleavelandite
Microl	:	Microlite
Tapi	:	Tapiolite
Colbt – Tanlt	:	Columbite - Tantalite
Wolf	:	Wolframite

INTRODUCTION

1.1. Introduction about granitoids

The tin fertile or specialized granites, ~~are~~^d mostly polyphase^d highly evolved, post – kinematics^d in nature, occur as intrusive fissure type, which are usually at the roofs of the batholiths. The tin-bearing granitoids are in general richer^d in ilmenite but poor in magnetite content. Topaz, tourmaline, fluorite, columbite-tantalite, beryl and cassiterite are characteristic accessories of these specialized granites.

The tin-bearing granitoids show wide occurrence through geological column. However, 63.1% of the tin deposits of the world are associated with Mesozoic granites, 18.1% with Upper Palaeozoic, 6.6% with Middle Palaeozoic granites and 3.3% with Precambrian granites (Evans, 1980) and very little occurrence ⁱⁿ with Tertiary granites. ^{is}

The tin content has been noticed from nearly every granitoid type. But tin deposit is restricted in little type of granitoids. Aranyakanon (1970) [?] opines that (a) The primitive granitoid i.e., hornblende granitoid yield^s lowest tin; (b) The coarse-grained secondary biotite granitoids yield moderate amount of the tin-ore, while (c) Altered metasomatic and pneumatolytised granitoid (Haad Som Pan granite type of Thailand) bear^s remarkably high values of tin. ^s

The temperature of formation of tin-bearing granites is generally lower than that of the tin-barren granite. But in case of assimilation with coarse-perthitic K-feldspar, the tin bearing granitoids ^{might} ^d may evolve^d at high temperature.

The tin-fertile granites in the world could be summed up as evolved ^{that} intrusive specialized granites are mostly polyphase, palingenetic, post to late kinematics^d in origin, formed in the last stages of orogeny. The granites with enriched tin content appear to have formed in hypabyssal intrusion level in the

mobile regions. These granites are concentrated mostly in the shallow dipping Benioff zones, continental–continental collision or intra-continental rift zones. The tin content rises up to 3 to 10 times more in stanniferous granites than the normal granites (about 6 ppm Sn).

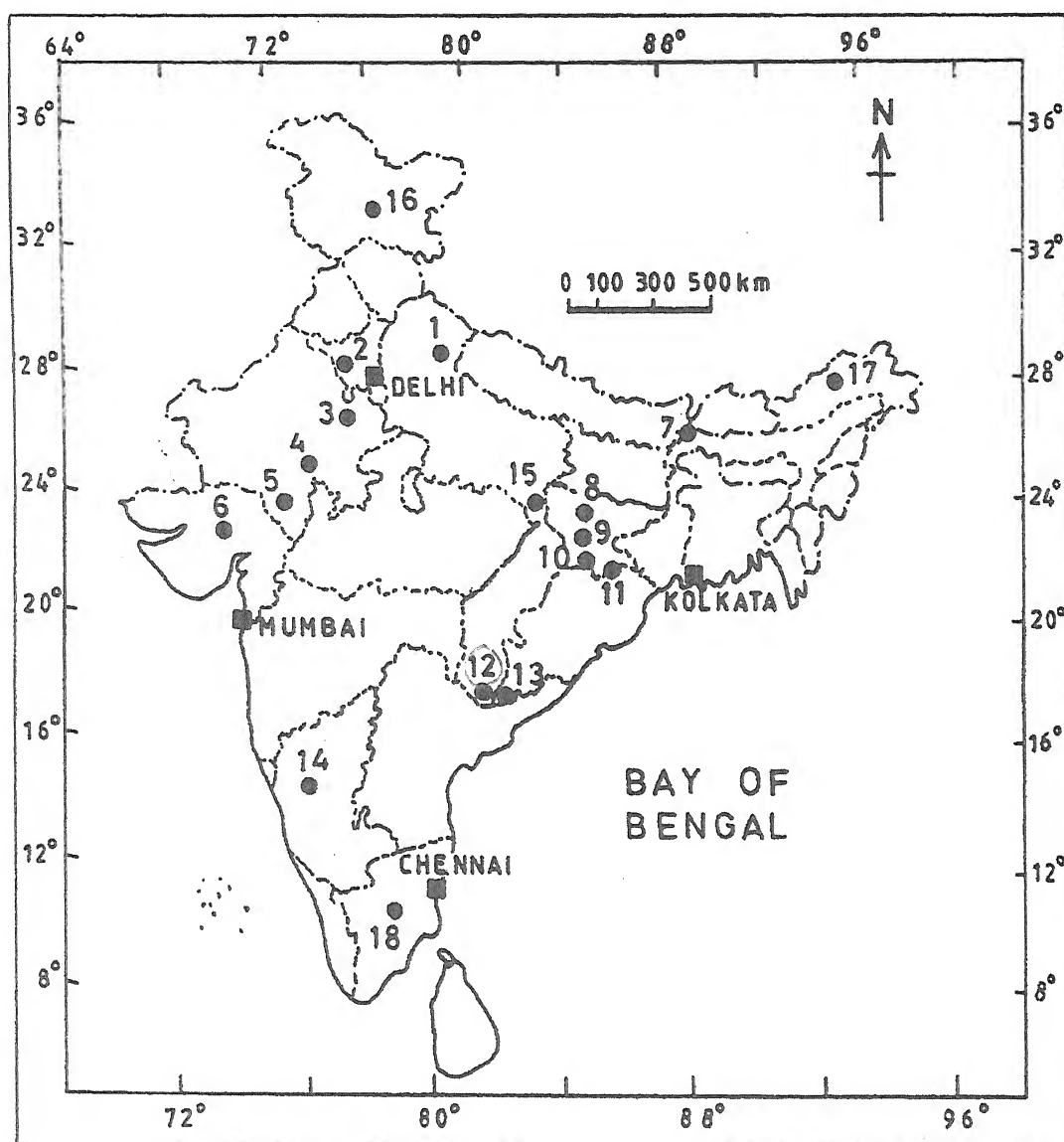
Stemprok (1970) stated that tin bearing granites do not differ substantially from non-stanniferous granite. There are no major differences in their textures or structures. However, distinct differences in the geochemical assemblage of elements can be suggested.

Differences between tin-bearing and tin-barren granites according to Pitakpaivan (1969) are; (a) In general, the tin bearing granite has more leucocratic felsic minerals (white/light gray white) than the tin-barren granite (dark gray, pink and mottled); (b) Tin bearing granites are more acidic with 29.9% free quartz while tin-barren granites contain 27% quartz; (c) Tin-bearing granites are often fine, medium to coarse-grained and vary in composition from alkaline to calc-alkaline but tin barren ones are often coarse to very coarse, porphyritic with feldspar phenocrysts. Hornblende granite and granodiorite are usually devoid of tin mineralisation; (d) Muscovite, tourmaline, albite, microcline, apatite and ilmenite increase, while orthoclase, hornblende, biotite and epidote decrease in tin-bearing granites.

According to Tischendorf (1977), trace elements like F, Rb, Li, Sn, Be, W and Mo can be used to distinguish between normal and tin-bearing granites. Compared to the average granite composition, the specialized granites are enriched in granitophile elements (B, Nb, Ta, Cs, U, Th, REE) whereas granitophobe elements (Ni, Cr, Co, V, Sr, Ba,) are impoverished.

1.2. Tin occurrences and its locality in India

The mankind knows about tin since the early historical times. It was mainly used in the alloy “bronze” after which the *Bronze Era* was named. In the beginning of modern time, tin started receiving more scientific and industrial applications. In fact, a number of unique properties of tin like non-toxic nature, high malleability, and chemical inertness, ease of forming amalgam with other metals have given it a special status among non-ferrous



INDEX

1. Almora (Distt. Almora)
2. Tosham (Distt. Bhiwani)
3. Bandraul (Distt. Alwar)
4. Paroli (Distt. Bhilwara)
5. Soniana (Distt. Udaipur)
6. Hosainpura (Distt. Banaskantha)
7. Munsang Singhik-Chungthank (Distt. North Sikkim)
8. Chhakkarbandah (Distt. Gaya)
9. Nurungo, Simratari, Pihara, Chhappatand (Distt. Hazaribagh)
10. Paharsingh (Distt. Ranchi)
11. Kalikapur (Distt. Singhbhum)
12. Katekalyan, Govindpal, Tongpal (Distt. Dantewada)
13. Munda-guda-Mathili Block (Distt. Koraput)
14. Dambal (Distt. Dharwar)
15. Dudhi Tehsil (Distt. Sonbhadra)
16. Kaplas-Jgmotha (Distt. Udhampur,) *Doda*
17. Rangavally (Distt. Lr. Suubansiri)
18. Kadavur (Distt. Tiruchi)

Fig. 1.1. Map showing important occurrences of tin bearing granitoids deposits in India

metals. Thus, tin ^{is} ^{only} has not become a strategic metal but also act^s as ^{an} essential metal of daily use.

Tin is one of the rare base metals in India. It occurs in acid magmatic rocks of different regions generally in the form of oxide and sulphide.

A detailed study of the Mineralisation Associated with Acid Magmatism (MAWAM) was under taken in India quite for some time in the past. Which was mostly initiated by the Geological Survey of India. Most of the Indian occurrences shown in Figure 1.1 of tin are only of academic interest except one in Bastar (Chhattisgarh), where preliminary work of exploration has reflected better and promising mineralisation. In addition, some other tin occurrences of academic interest are also known from Himalayan region. (Shukla and Singh, 1988; Singh *et al*, 1996).

However, tin resources have been estimated from three localities in India viz. Tosham, Dantewada (Bastar) and Koraput districts. The tin deposit of Tosham in Haryana includes the primary mineralized ore within rhyolites, granites and metasediments. The tin deposits of Dantewada district (Chhattisgarh) and Koraput district (Orissa) consist mainly pegmatite-derived secondary eluvial, colluvial and alluvial placers.

Out of the total (9.9 million tones) of Indian resources, about 8 million tones are in Bhiwani district (Haryana), 1.85 million tones are in Dantewada district (Bastar) in Chhattisgarh and the rest in Koraput district (Orissa). The requirement of tin metal in the country continues to be fulfilled mainly through imports.

The geological study about the different deposit of tin bearing rocks in India and world suggest that the tin as primary source is restricted to the acidic magmatism of late stage. Therefore an emphasis on detailed study of acidic magmatism should be given to find out the formation of tin bearing granitoids. The present study is therefore intended to examine in detail the different aspects of tin mineralisation and associated granitoids of Katekalyan area, Dantewada district in Chhattisgarh.

1.3. Tin bearing granitoids: a literature review

In India, the tin and its rare metal mineralisation associated with the Precambrian rocks are related to acid magmatic activity. These mineralisations are found in younger pegmatites, quartz veins and in a few cases with the intrusives of syn- to post-tectonic Proterozoic metamorphic complexes.

A brief description of ~~the~~ some important tin mineralisation and associated lithotypes in India is given here:

[a] Jharkhand and Bihar

- (i) In Nurango (district Hazaribagh), McClelland (1849) first reported the presence of tin in India particularly in Nurango area. Clegg (1944) described that in Nurango area, the ore zone occurs as cassiterite-granulite layer with 30% to 50% of cassiterite granules parallel to the foliation of gneiss. He recorded yield of 1.87% Sn and the grade of this deposit worked out to 268 lbs of metal per ton of ore. The country rocks in this area comprised of granite gneisses of Chotanagpur with relicts of Archaean metamorphics, amphibolites and schistose rocks. The younger granites, pegmatites and quartz veins represent the acid magmatic activity spatially and genetically related to the tin mineralisation.
- (ii) South-West (SW) of Pihara near Simratari, ~~where~~ a few crystals of cassiterite have been recovered from lenticular pockets of granite emplaced within mica schist. The granite is non-foliated leucocratic with lepidolite (Li mica) bearing pegmatite veins.
- (iii) Tin mineralisation was reported mainly from Chhakkarbandah, Dhaknawha, Dhanaras and Kanchanpur localities in Gaya district extending north into a part of Aurangabad district. Nag (1929) firstly reported the occurrence of tin in garnet crystals of micaschist in Dhanaras hill near Chhakkarbandah. According to Mukerjee and Rai (1978), the tin content of the mineralized rocks is between 0.4 to 0.5% and at places ~~might~~ go up to 1.5%. (iv) Occurrence of cassiterite is

it goes

known in Kalikapur locality of the Singhbhum district. It is associated with copper belt of the Singhbhum Shear Zone. Recently, Mukerjee and Bhattacharya (1990), has recorded Sn, Nb, REE etc. from this part of the Singhbhum mobile belt.

[b] Chhattisgarh

Occurrence of tin in Bastar district (now Dantewada); was first rereported by Fermor and Kellerschon (1909). In Bastar district, the tin and rare metal mineralisation are associated with granites and pegmatites of the Precambrian age. The stanniferous Paliam granite appears to be the source of pegmatites intrusive into fractures of metabasic sills emplaced within the Bengpal metasediments. This granite is therefore of post Bengpal age and the biotite hosted in it has indicated an age of 1345 ± 22 m.y. (Balasubrahmanian, 1977). The Darba granite (gneiss) appears to be of a little younger phase as compared to the Paliam granite. Both granites are related to the pegmatitic activity in the Bengpal metasediments and the metabasic rocks. Presumably, the pegmatites carrying tin are considered genetically related to the granites.

[c] Orissa

The tin deposits of Orissa are considered very potential in nature. Both the primary as well as secondary sources ~~are likely to~~ make the region rich in stanniferous (Acharya *et al.*, 1982). Tin mineralisation has been recently reported from the Mundaguda-Mathili block of the Koraput district. It appears to be a continuation of tin mineralisation of the Dantewada district (Bastar) according to (Sarangi and Das (1977).

[d] Haryana

Geological Survey of India (1983) discovered the tin deposit in Tosham area of Bhiwani district. It is situated about 90 km west of Delhi. At

present, this is a biggest tin prospect of the country and the extent of mineralisation occurs over several kilometers.

[e] Other states

Tin mineralisation has been reported from few other areas also besides those mentioned above. However, these deposits are of academic interest only. For example, cassiterite was found as a rare accessory such as in Soniana mica mine in Bhilwara (Rajasthan), minor grains of cassiterite associated with wolframite in Kadavur pegmatite in Tiruchi district (Tamilnadu), and also crystals of cassiterite in tourmaline bearing pegmatite near Hosainpura in Banaskantha district (Gujarat).

Mukerjee (1975) pointed out the possibility of finding tin-tungsten deposits in the Himalaya. Shukla and Singh (1988) have reported the occurrence of tin found as cassiterite in the Jalali area of Precambrian Ranikhet formation of Almora Group, Kumaun lesser Himalaya. Singh *et al*, (1996) have further studied the trace and rare earth elements geochemistry of host rocks of tin and tungsten minerals. It may not be out of place to mention that along the Himalayan belt there is younger granitic activity at many places. Such granitic rocks of Miocene-Pliocene age accompanied by pegmatitic-pneumatolytic phase may be potential for tin mineralisation. Tin mineralisation is also reported from Dhauladhar range of Lesser Himalayas in Jammu and Kashmir. The Kaplas and Jamotha granites of ca 456 Ma age found emplaced in Precambrian Bhadarwah slate Formation have ^{contain} contributed the tin mineralisation. / —

1.4. Location and approach of the Katekalyan

The study area for tin mineralisation is situated in the southeastern part of the Dantewada (Bastar) district of newly created Chhattisgarh state. This area lies North and South of the Dummam nadi between the longitudes $81^{\circ}35'$ E to $81^{\circ}40'$ E and latitudes $18^{\circ}45'$ N to $18^{\circ}50'$ N in the survey of India toposheet No. 65 F/9 (1933, Scale: 1" to 1 mile).

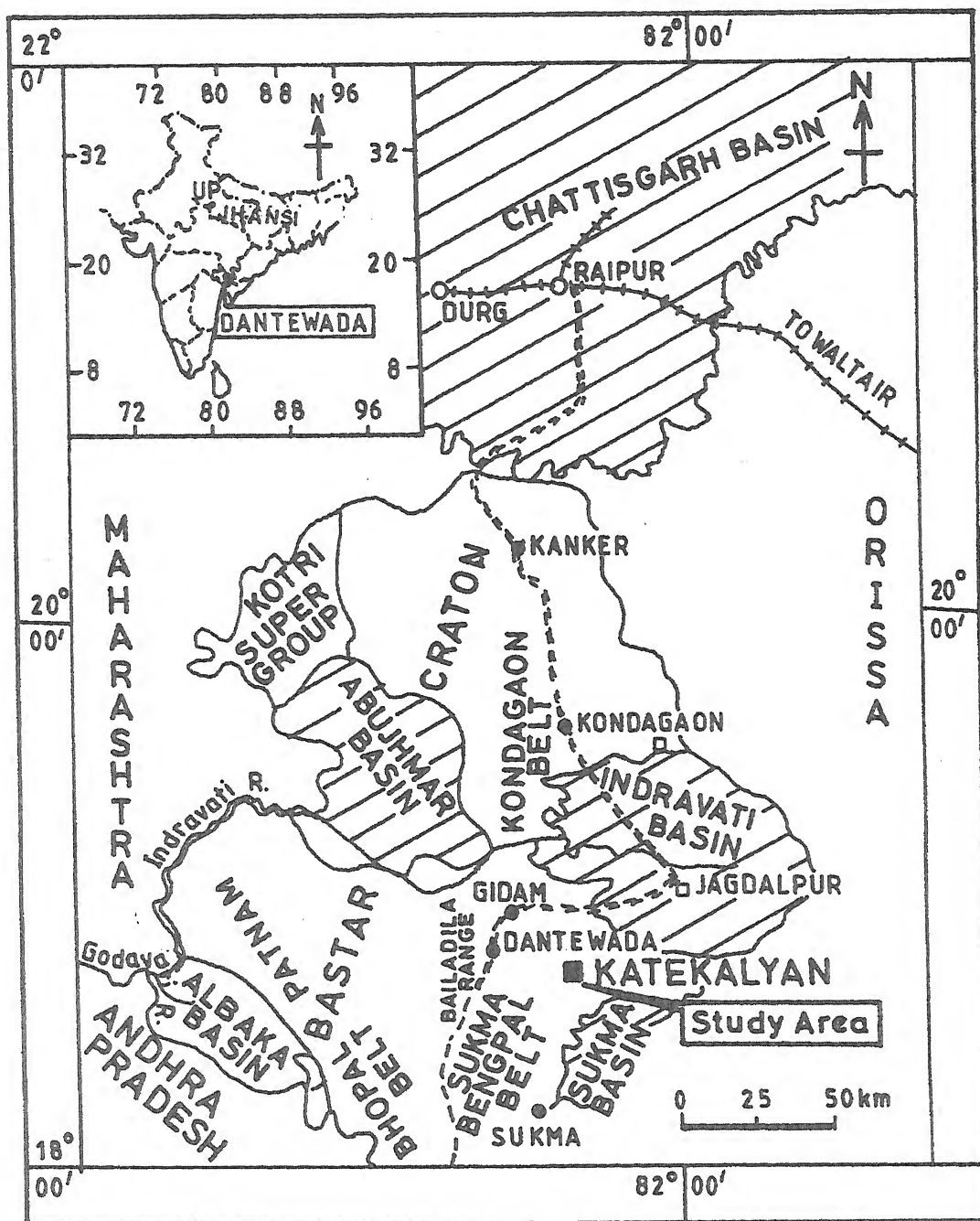


Fig 1.2. Location map of the study area

The Katekalyan area (Fig. 1.2) can be easily approached through Raipur city capital of Chhattisgarh state, situated on the main railway line between Howrah and Mumbai via Nagpur. From Raipur, a metalled road (N.H No. 43) passes through Jagdalpur which is 297 km south. Further 74 km in the west leads to Gidam from where one can go up to Dantewada. The study area i.e. Katekalyan is around 40 km towards east of Dantewada and is connected by non-metalled road.

1.5. Climate, vegetation and other information

The general climatic conditions of the area resemble to tropical. In summer, it is very hot and dry, and during winter it is quite pleasant but occasionally becomes very cold. Temperature reached maximum up to 39°C in summer reason while minimum temperature generally does not fall below 12°C. The highest rainfall of the area is about 35 cm and occurs mostly in the month of July.

Natural climatic conditions have been responsible for the growth of dense mixed forest all over the region. The plateau and steep scarps are forested mostly by tropical deciduous species. The most dominant vegetation in the area is Sal. However, other species like Teak, Sirsa, Palas, Tendu and Mahua etc. are also found appreciably. ??

The original inhabitants of Dantewada (Bastar) district are tribals. The major tribes living in the Dantewada are Muria, Maria, Gonds, Abhujmaria, Bison-horn Maria and Nahar etc.

The best season of the year for carrying out geological fieldwork is winter, preferably in the month of February. They're being no proper shelter in the area; the fieldwork was usually conducted from the base camp at Katekalyan town. ??

1.6. A brief resume of the previous works in and around Katekalyan

Bastar Craton exposes the well-developed sequence of rocks ranging from Archaean to Late Proterozoic. It forms the central part of the

Indian Peninsular Shield, occupying an area of 40,000 sq. km. It is flanked by the Chhattisgarh basin in the north, charnockite-khondalite granulites of Eastern Ghat Belt to the east, gneissic complex in the south and west and Pranhita-Godavari basin in the south-west.

The pioneer geological works in Bastar area are mostly carried out by Ball (1877), King (1881), Bose (1899-1900), Walker (1900), Fermor and Kellerschon (1909). Earlier Ball (1877) pointed out that the quartzites, shales and limestones along Jepore – Bastar border were same as those in Chhattisgarh i.e. Lower Vindhyan/Cuddapah. King (1881) also visited Bastar and said that the rocks observed by Ball (1877) were definitely the same as Cuddapah of Wardoha-Praolite valley.

Bose (1899, 1900) was the first to map the parts of Bastar district. He delineated the transition series of Bailadilla, Chhota Dongar and Rowghat as well as few other areas having resemblance with Dharwars of south India. He also referred to the extensive iron ores as hematite quartzites (Banded Iron Ores) in Bailadilla and other areas.

Walker (1900) worked mainly in Jepore region outside the Bastar region. Tin mineralisation in Bastar district (Dantewada) was first recorded by Fermor and Kellerschon (1909). Later during thirties, Fermor (1935) and Heron (1937 and 1938) described the geology of parts of Bastar district (Dantewada). All of them initiated preliminary geological investigation and other studies related to mineral deposits etc. of the state.

Middlemiss (1938a,) has dealt with charnockites of Bastar region, which are separated from the gneiss along its eastern margin by a fault and this is far away from the present area and then followed the devoted work of Crookshank (1938b) and Ghosh (1941). They have mapped the area between the Bailadilla range and Eastern Ghat including the present area. Gupta (1938) and Chatterjee (1949) mapped the northern parts of Bastar Craton and correlated these rocks with older metamorphics, Dharwars and Iron Ore Group. Dutt (1963) classified the Indravati sedimentaries and correlated them with the rocks of Chhattisgarh Group.

The earlier works were confined mostly to brief description of the rock types of the area, and were documented in the Records and General Reports of the Geological Survey of India. Crookshank (1963) published ^{for} the first time the detailed account of his work done in the form of a Memoir (Geological survey of India, Memoir No. 87 published in 1963). He classified the metasediments and volcanic rocks into Sukma, Bengpal and Bailadila Suits in the ascending order. Recently it is established that sedimentary rocks with unmetamorphosed basic intrusives belong to the younger sequence (Abujhmar Group). Crookshank tried to separate the various metasedimentary enclaves occurring within the gneissic complex into the Sukma and Bengpal Series.

Ramakrishnan (1969) discovered that high grade metasedimentary rocks having similar lithology occur in both Bengpal and Sukma Groups providing compelling evidences to group them into one composite group i.e. Bengpal Group. Ramakrishnan's composite Bengpal Group includes gneissic complex hosting metasedimentary and meta-igneous enclaves. Ramakrishnan's classification is more tenable and is being followed by the later workers of Geological Survey of India. The crucial point is the status of conglomerates, grits and shales of Dantewara stage, which have been reported to overlie the gneissic rocks (Crookshank, 1963). The rocks of Dantewara stage were also grouped under the Bengpal Group by Ramakrishnan (1969). Dutta *et al.*, (1981) suggested that the Sukma and Bengpal Groups represent different facies of the same suite.

The Bengpal metasediments occur as enclaves within the unclassified basement gneisses and migmatites (here with referred to as granite gneiss). The granites occur as discrete units within the gneisses and also in close spatial association with the supracrustal rocks. In the north of Sukma, a fine to medium-grained, non-foliated biotite granite (Paliyam granite similar to as Darba granite) appears responsible for generation of pegmatitic activity and pneumatolytic cassiterite mineralisation (Ramaswami *et al.*, 1981).

In Bastar (Dantewada), lithium and tin mineralisations were also documented by Bose (1899, 1900), Deshpande (1979), Suryanarayana *et al.*, (1979), Murthi *et al.*, (1979), Babu, (1979), Guha and Raychowdhury (1979) etc. The contributions of Mukerjee (1975), Mukerjee and Rai (1978) and Singh (1980) also carry the useful information on various aspects of the deposit in Bastar area.

Exploration of tin and associated mineralisation in Bastar was carried out by the Geological Survey of India with an integrated multi-disciplinary approach from 1973 to 1991. In 1975 and 1979-1980 U.N.D.P. (New York) agency was associated with the exploration activity (Beus; 1976, Kanasiewicz *et al.*, 1980). During 1988-89 B.R.G.M. (France) collaborated with the exploration activity in Bastar. The state Governments of Geology and Mines of Madhya Pradesh and Orissa, and Atomic Mineral Division, Department of Atomic energy, Government of India, have also carried out minerals investigations in the Bastar area.

In the study area, several phases of rare metal mineralisation viz., magmatic, pegmatitic, pneumatolytic and hydrothermal phases have been recognized in and around Katekalyan by Babu (1983). The magmatic phase has been attributed to the granitic intrusions into the pre-existing granite gneiss and migmatite. The tin mineralisation can be attributed also to as ²⁸² granitic apophyses intruded into the basic and Bengpal metasediments. The soda-rich fine-grained (aplitic) biotite granite at Lakharas contains 50 ppm Sn and the porphyritic leucogranite near Katekalyan area ^{showed} analysed Sn as high as 100 ppm (Murti *et al.*, 1982). This indicates the stanniferous nature of the granite with the enrichment of Sn in the younger granitic phase exposed at Paliam and Darba (including Katekalyan) areas.

The gneissosity of the granite gneiss shows NNW-SSE trend, with steep northerly dip. Pegmatites of different phases are found emplaced into the granites along fracture planes trending N-S, NNW-SSE and E-W, at places, cutting across each other at Benglur, Katekalyan and Parcheli areas. Younger basic dykes are also found intruding the granite. Three phases of deformation related to granitic activity have been noticed (Murti *et al.*, 1982).

The first phase F_1 is along ENE-WSW to E-W, followed by F_2 along NNW-SSE to NW-SE and the last F_3 along N-S to NNE-SSW.

1.7. Nature and scope of the present investigation

A very little about geology has been persuaded in India because of the absence of commercial deposits. There is an urgent need to discover more deposits of tin, niobium and tantalum. There is a scope for fulfilling the need as the Indian Peninsula offers possible locales in the different areas that are conditioned by favorable geological set-ups for mineralisation. With the increasing understanding of the different petrogenetic and tectonic regimes of the different geological periods, it should be possible for research personals to aid in the search for these rare metals in the country.

The Bastar (Dantewada) and Koraput occurrences of lithium-tin mineralisation on an appreciable scale have generated a hopeful situation now. The structure, mineralogy, petrology, geochemistry, genesis and economics of these deposits will be the main consideration of geoscientists from different organizations and academic institutions. It has to be accepted that still there exists several gaps in our knowledge regarding these interesting occurrences.

Recently discovered tin, niobium, tantalum, beryllium bearing pegmatites of Bastar (Dantewada) district in Madhya Pradesh (Chhattisgarh), where intensive exploration is being conducted by the Geological Survey of India and other departments. Since last few years, the Geological Survey of India has launched a national time-bound priority investigation for tin in the Bastar (Dantewada), where tin bearing granites and pegmatites associated with W, Nb, Ta, Mo etc. have been identified.

Cassiterite along with allied rare metal mineralisation in the host rock (pegmatite) exhibits a complex picture in the study area regarding their occurrence, distribution pattern and genesis. Several pegmatites emplaced within granite in and around Katekalyan areas are also tin bearing. In this context tin mineralisation genetically associated with acid magmatism needs a detailed investigation for the following reasons.

- [a] A detailed petrological and geochemical study of the source rocks to know their genetic behaviour. *its*
- [b] To study and to decipher the evolution of parent magma with ~~their~~ late stage emanative differentiates.

In order to evaluate the nature of granitoids as a source rock, their emplacement history including tectonic regime. The detailed mineralogy of the granitic rocks is quite significant. Accessory minerals viz. tourmaline, fluorite, topaz and zircon etc. will also give an ideas of the temperature of formation and stage of hyperfusible enrichment. Alteration phenomena like microclinisation (potash-metasomatism), albitisation (soda-metasomatism), greisenisation, silicification and sericitisation have played an important role. In order to understand their evaluation, the true nature of acidic magmatism must be known. As water vapor, boron, fluorine and other volatiles with their respective components of partial pressures (fugacities) in a late phase of acid residuum affect the fixation of mineral phases therefore it is necessary to correctly assess the role of such hyperfusibles as mineralisers. *.....?*

The interpretation of the ore forming processes, comprising their favorable geological environments, may be a powerful tool in evaluating the resource potential of an area. The nature of the granitic plutons favorable geological setting and composition of host rocks can be used as important factors to assess the degree of ore potential more clearly to focus attention on particular areas. Keeping in the view of above presumption, the areas in and around Katekalyan of Dantewada (Chhattisgarh) have been chosen to document and to bring a detailed and unified picture of the tin mineralisations. */2)*

Methodology: A brief account of the works carried out under present study in the field as well as in the laboratory is summarized herewith: *.....?*

- (i) A detailed geological mapping of the mineralized area of Katekalyan has been performed for appreciating the relation between the country rocks and the emplaced pegmatite veins to prove the mineralisation phase of the granitic activity.
- (ii) Collection of minerals and rocks (n=280) was carried out to cover the different litho-units of the Katekalyan area.

- (iii) Petrographic study of the ore and host rocks of the Katekalyan area has been carried out with the help of high resolution polarizing and ore-microscopes. Further identification of guide minerals viz. quartz, feldspar, beryl, tourmaline, fluorite, apatite, lepidolite and biotite (both magascopy and microscopy) was also carried out.
- (iv) Fluid inclusion study was carried out to infer the microthermometry of ore-fluids forming the cassiterite.
- (v) Chemical analysis of the granitoids and pegmatites as well as cassiterite was performed to determine the major, trace including the rare earth elements and ^{were wh:sd} utilization of these data to infer the petrogenesis and tectonic environment.

On the basis of the data thus obtained both in the field and in the laboratory, the finally attempt has been made to suggest a genetic model of tin mineralisation and its relation with granitoids of the Katekalyan area.

GEOLOGICAL SETTING

2.1. Introduction

The Precambrian in central India is divided into two distinct crustal provinces, namely the Northern Crustal Province (NCP) and the Southern Crustal province (SCP), separated by a crustal scale shear zone (Ramachandra *et al.*, 1998; Ramachandra and Roy, 1998) referred to as the Central Indian Suture (CIS) by Yedekar *et al.* (1990). Recent work (Acharya and Roy, 2000; Ramachandra, 1999; Bhowmick *et al.*, 1999) has shown that this zone in fact represents the southern part of the Sausar Mobile Belts including dismembered granulite belts, gneiss and supracrustals. The terrain to the south of this mobile belt (the SCP) includes the Bastar craton and that to the north (NCP), the Bundelkhand Craton. The Sausar Mobile Belt (SMB) probably includes components of both these cratons. The different cratonic components in the SCP are given in table 2.1.

Bastar craton exposes the well-developed sequence of rocks ranging from Archaean to Neo-Proterozoic age. It is one of the oldest crustal segments within the Peninsular Indian Shield occupying an area of 40,000 sq. km and is flanked to the northeast by Mahanadi graben, to the southwest by Godavari graben, to the northwest by Satpura mobile belt and to the southeast by Eastern Ghat mobile belt (Fig. 2.1). The craton consists of three major supracrustal belts viz; Sausar-Chilpi belt, Bailadila-Dongargarh belt and Sukma-Bengpal belt.

The Sukma-Bengpal belt and southern part of Bailadila belt constitute a larger part of southern Bastar Craton. Ball (1877), King (1881), Bose (1899, 1900) and Walker (1900) are the pioneers of Bastar geology, followed by the classical work of Crookshank (1938a, 1938b and 1963) and Ghose (1941).

Table 2.1. Generalised Tectonostratigraphy of the Southern Crustal Province (SCP) in the Precambrian of Central India (Ramachandra *et al*, 1998)

Age	Super group/Group
Meso to Neoproterozoic	Cover sequences of the Chattisgarh Suprgroup and Indravati, Khariar, Albaka, Pakhal, Sullavai Groups
Palaeo to Mesoproterozoic	Sakoli Group (younger supracrustal), Cover sequences of Khairagarh Group and Abujhmar Group
Palaeoproterozoic	Dongargarh and Malanjkhanda granitoids
Neoarchaeal to Palaeoproterozoic	Younger Supracrustals of the Chilpi Group, Nandgaon Group, Sonakhan Group, Bengpal Group, Bailadila Group and equivalents; older intrusive granitoids
Neoarchaeal	Bhopalpatnam granulites, Kondagaon granulites (Older granulites belts)
Palaeo (?) - and Mesoarchaeal	Older Supracrustals of the Sukma Group and Equivalents (e.g. Amgaon Group) including unclassified gneissic complexes with relic TTG enclaves

Crookshank (1963) published the detailed account of his work in the form of a Memoir and classified the metasediments and volcanics into Sukma, Bengpal and Bailadila Series stratigraphically in the ascending order, which gives an overview of regional geology. The tin mineralisation of the Dantewada (Bastar district) is then genetically associated primarily with granitic intrusive, which^{was} emplaced into the pelitic and psammopelitic metasediments rocks of the Bengpal Series of Proterozoic age. Basic igneous activity as sills, dykes and sub-aqueous lava flows preceded the granitic phase. Pegmatites and quartz veins with metasomatic and pneumatolytic imprints succeeded the granitic phase hosting the tin and associated rare metal mineralisation. Occurrence of tin in Dantewada district was first recorded by Fermor and Kellerschön (1909). The discovery of tin and associated rare metal deposits has made the Bastar craton a very significant unit for detailed geological investigations using modern methods.

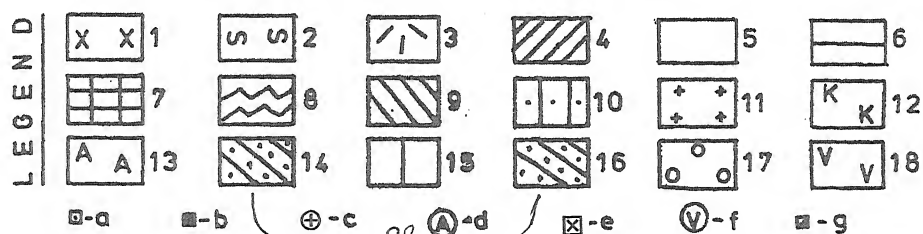
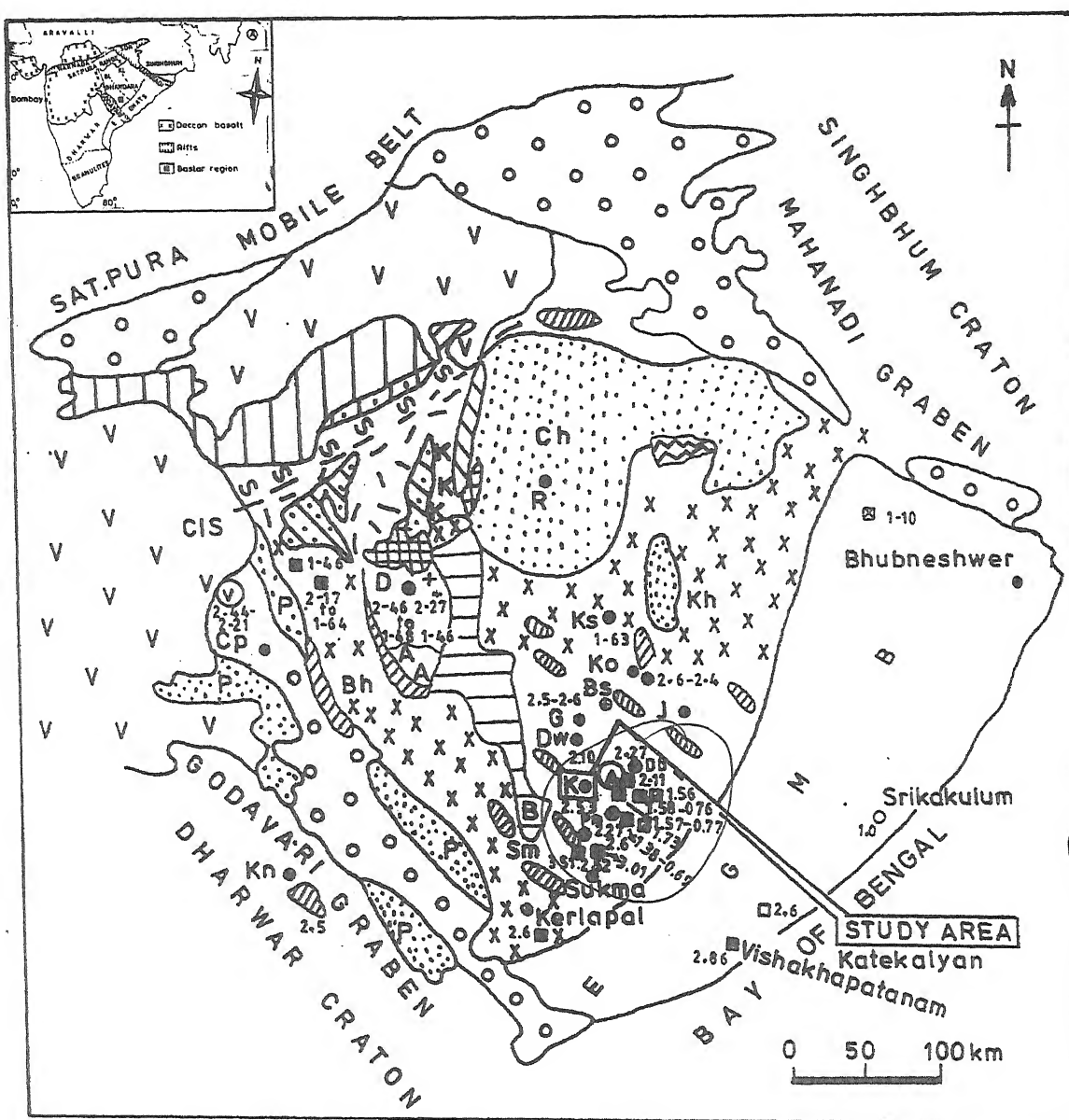
2.2. Regional geology

The Bastar Craton (part of SCP) is dominated by granite and gneisses with belts of supracrustal suits showing variable rock association and metamorphic grade. In the western part, the supracrustals are represented by (a) Sakoli, Dongargarh and Sausar Groups, while in the southeastern part they are recognized as (b) Sukma Suite, Bengpal and Bailadilla Groups. ⁱⁿ The western part, C/S separates the widespread granite gneiss, known as the Amgaon gneiss ^{from} and Tirodi gneisses in south and north respectively. However the stratigraphic correlation between the supracrustal belts is still uncertain (Sarkar *et al*; 1990).

On the basis of the regional geological works, the Baster craton may be considered into four following belts (Fig 2.1).

- (A) Sukma-Bengpal Belt (Sukma metamorphic suite and Bengpal Group)
- (B) Granulite Belts (Bhopalpatnam and Kondagaon Granulite Belts)
- (C) Bailadilla Belt (Bailadilla Group)
- (D) Sausar-Sakoli-Dongargarh Belt (Kotri Super Groups or Dongargarh Super Group)

The Litho-succession (Table 2.2) of the Bastar Craton is given by Ramachandra *et al* (1998) and has shown that the Sukma group including ^{es} the gneiss-granite and the granulite belts below the Bengpal Group. ^{es} The Bhopalpatnam granulite belt was considered to be a mobile belt involving the Sukma supracrustals during its evolution. This belt has been correlated with the Karimnagar granulite belt occurring across the Godavari graben to southwest in the Dharwar Craton (Rajesham *et al*; 1993).



1. Migmatite-Granite Gneisses; 2. Tirodi Gneisses; 3. Amgaon Gneisses; 4. Granulite Belt; 5. Metasediments (Bengal) with Metabasic Intrusives & Extrusives; 6. Bailadilla Belt; 7. Nandgaon Group; 8. Sonakhan Group; 9. Chilpi Group; 10. Bharweli Group; 11. Dongardarh Granitoids; 12. Khairagrh Group; 13. Abujhmar Group; 14. Sakoli Group; 15. Sausar Group; 16. Purana Basins (Indravati, Pakhal, Albaka); 17. Gondwana Basin; 18. Deccan trap. CIS = Central Indian Suture

Rocks used for radiometric age:

a. Migmatite Gneiss, b. Granitic Gneiss, c. Granite, d. Amphibolite, e. Granulite, f. Metavolcanics, g. Mineralised Pegmatite.

B = Bailadilla, Bs = Barsur, G = Gidam, Dw = Dantewada, K = Katekalyan, Db = Darba, Ko = Kondagaon, Bh = Bhopalpatnam, P = Pakhal Basin, Sm = Sukma belt, Ks = Keskali, Ch = Chhattisgarh, Cp = Chandrapur, R = Raipur.

Fig 2.1. Generalised regional geological map of the Southern Crustal Province (SCP) in the Central Indian Peninsular Shield (CIPS). The inset shows the major structural features of Peninsular India (KL= Kondagaon Lineament, BL= Bhomargarh Lineament).

Table 2.2. Lithosuccession in the Bastar Craton (Ramachandra *et al.*, 1998)

Cover Sequence	Chhattisgarh, Indravati, Albaka, Abujhmar
	-----Unconformity-----
	Dongargarh Supergroup(=Kotri) including Chilpi Supergroup
	Sonakhan schist belt
	-----Unconformity-----
	Bailadila Group
	-----Tectonic contact / unconformity -----
	Bengpal Group (Chandenar-Tulsidongar, mobile Belt: CTMB)
	-----Tectonic contact / unconformity -----
	Sukma Group / TTG and other gneisses / granite including granulite mobile belts

The Konta granulite belt (Fig. 2.1) has been interpreted to involve parts of the Bhopalpatnam belt and the Sukma supracrustals during the EGMB orogeny characterised by alkaline magmatism. Younger supracrustals in the Bastar craton include the N-S trending BIF dominated belts of the Bailadilla Group (and equivalents; Crookshank, 1963; Mishra *et al.*; 1984) and those of the Dongargarh Super group (Sarkar, 1957-58). This Super group comprises a sequence of volcano-sedimentary rocks and younger granite, occurring in a N-S trending linear belt. The Chilpi Group in parts of Madhya Pradesh has been shown to be an equivalent of the Dongargarh Group (Rao, 1981; Tripathi *et al.*; 1981; Chaudhari *et al.*, 1994). The Sakoli Group of rocks occurs in the western part of the Bastar Craton. Roy *et al.* (1995) have given a detailed structural framework, lithostratigraphy and metallogenetic characters of the Group. Crookshank (1963) has classified the rocks of the southern part of Bastar craton into Sukma, Bengpal and Bailadilla series (table-2.3).

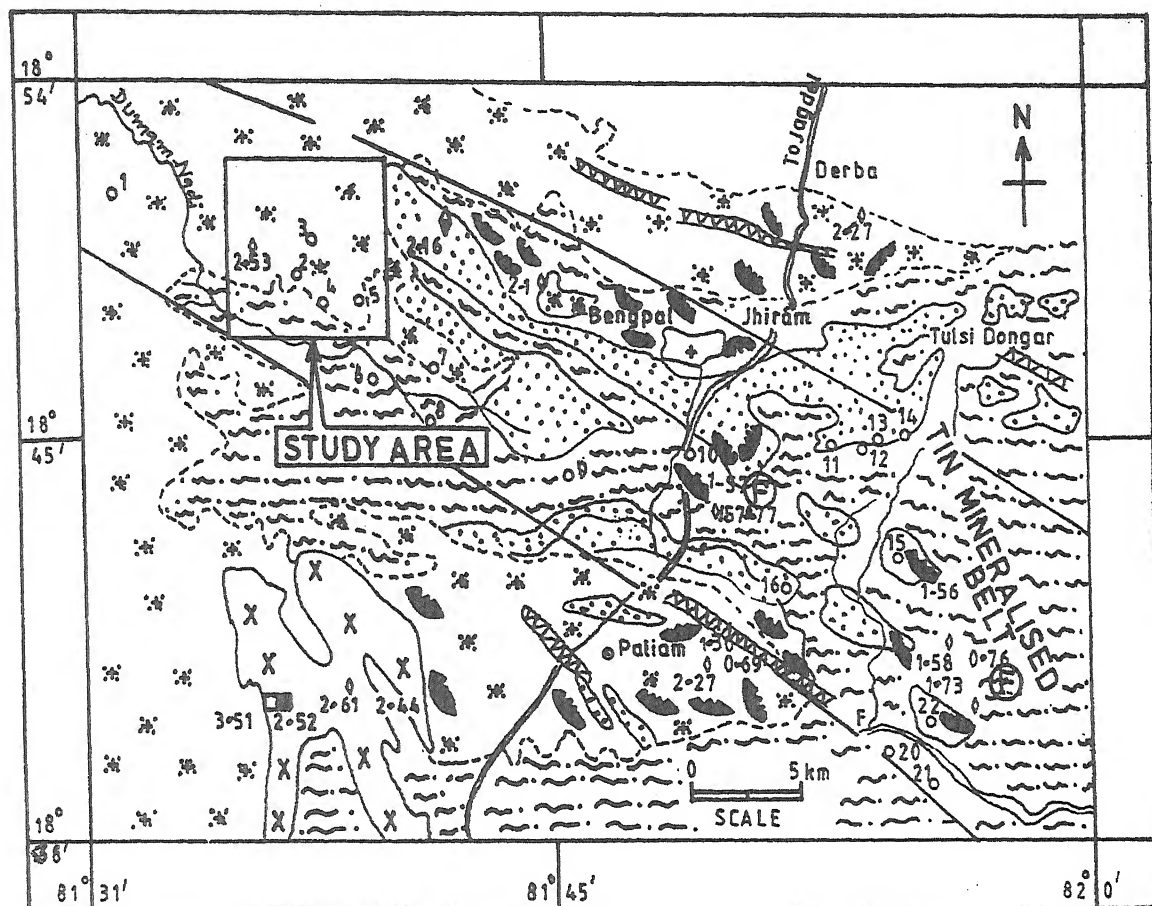
Table-2.3. Lithostratigraphy in the southern part of Bastar Craton (Crookshank, 1963)

	Dolerite, pegmatite
	Charnockitic series
	Granite
	Greenstone
	Granite-gneiss, pegmatite
Bailadila Series	<div> <div>BHQ, Grunerite quartzite, chlorite Fe- phyllite, carb shale, white quartzite</div> <div>— ?.</div> </div>
	— Unconformity —
Bengpal Series	<div> <div>Ferruginous schist, schistose conglomerate, basalt and tuff</div> <div>Andalusite phyllite, schist, gneiss, quartzite</div> <div>Grunerite-garnet schist, BHQ, quartzite</div> <div>Sericite quartzite and sandstone</div> </div>
	— No clear dividing line —
Sukma Series	<div> <div>Sillimanite quartzite/ magnetite quartzite, grunerite hornblende schist, cordierite biotite gneiss, cordierite- anthophyllite rocks</div> </div>

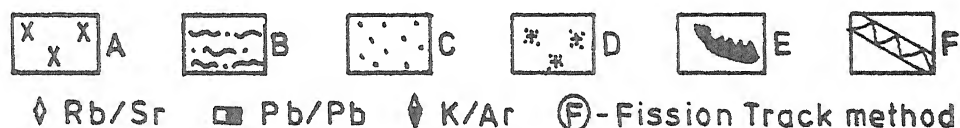
Table 2.4. Regional stratigraphy of southern Bastar (After Ramakrishnan, 1990).

Basic dykes	Dolerite and meta-dolerite Greenstone dykes and sills Amphibolite dykes
Granites	(Undifferentiated)
Bailadilla Group (Ca 2100 Ma)	Banded Iron Formation Phyllites with cherts and local conglomerates (Loa) Feldspathic quartzite
~~~~~Unconformity~~~~~	
Bengpal Group (Ca 2300 Ma)	Gneissic granites (undifferentiated) Andalusite quartzites and conglomerates. Andalusite and chiasolite schists and nodular sillimanite schist intercalated with amygdular metabasalts, sericite quartzites (local)
~~~~~Unconformity~~~~~	
Sukma Metamorphic (Supracrustal) Suite (Ca 2500 Ma)	Charnockites. Granites, gneisses and migmatites (TTG suite) Banded Iron Formation Cordierite-biotite-sillimanite-andalusite-garnet schist, gneisses and quartzites. Cordierite-anthophyllite rocks. Amphibolites and ultramafic schists. Diopsidic-calc-silicate gneisses and quartzites. Sillimanite quartzites.
-----Basement gneisses (Ca 3000 and 3400 Ma) -----	

Regional geological map with radiometric dates of the tin mineralized belt in parts of Bastar Craton are given in Fig. 2.2. Since the Bastar area has proved as one of a potential zone of metallic and non-metallic deposits therefore significant works with special attention to deposits have taken into account by many geologist/ of GSI in different part. The Kondagaon and Bhopalpatnam areas were studied by Mishra and Coworkers (1984 and 1988). Sukma-Konta-Dantewada area was studied in detailed by M. Ramakrishnan (1969). Besides these, many workers T.M. Babu (1985) and Ramesh Babu *et al*; (1984,1993) also carried the detailed geological, structural and petrological works.



LEGEND



- A. Sukma Supracrustal Suite B. Bengpal Metasediments C. Metabasic Intrusives
D. Stanniferous Granitic complex E. Mineralised Pegmatites F. Silicified Shear Zone.

Locality:

1. Metapal 2. Katekalyan 3. Kopanar 4. Kondaras Dongri 5. Pinjupara 6. Parcheli 7. Koapal
8. Bothapara 9. Marjun 10. Tongpal 11. Chidpal 12. Chuirwada 13. Bedanpal 14. Bodawada
15. Govindpal 16. Kudripal 17. Jongarpal 18. Mundwal 19. Pushpal 20. Kikripal 21. Bondey
22. Mundaguda.

Fig. 2.2. Regional geological map with radiometric dates (billion of years) of the primary tin mineralised belt in the southeastern part of Bastar Craton.

Granulite-gneiss complex of Kondagaon area has been described in detail by Mishra *et al*; (1984), Sukma-Bengpal belt by Crookshank (1963) and discussed the Pakhanjur belt by Mishra *et al*; (1981).

Because of limited geochronological data and detailed works in small sector could not prove the regional geologic of the Bastar. Mishra *et al*; (1988) compiled the works on Bastar craton and suggested the following succession.

The succession shows three group⁸ i.e. Bengpal group (Archaean), Bailadilla Group (Lower Proterozoic) and Indravati Group (Upper Proterozoic), whereas Middle Proterozoic is represented by Kotri Super Group.

Following observation⁸ were made by Mishra *et al* (1988) in his proposed stratigraphy of Bastar Craton:

- 1- Rocks of Chandanar valley unconformably overlie the gneissic complex of the Bengpal Group.
- 2- Quartz-sericite-andalusite schist/grits and sandstone of Bhodhghat area actually belong to the Abujhmar Group.
- 3- The unmetamorphosed sandstone (with detrital andalusite) of Tulsi Dongar Group appears to be equivalent of Abujhmar Group and does not constitute a part of the Bengpal Group as envisaged by Murti *et al* (1977). There was confusion in Crookshank²⁵ (1963) classification of the rocks because of profuse andalusite (detrital) occurrence in the sandstone, which had been derived from the underlying Bengpal rocks (Mishra *et al*; 1984c). — (C) 25
- 4- Intrusive relation of post –Bailadilla granite and its tectonic significant.

Nearly at the same time another geologist of GSI (Mr.)[?] M. Ramakrishnan (1990) also compiled his works on southern part and proposed the following stratigraphic sequences (Table 2.4) for Precambrian of Bastar. However, the most significant feature of the Sukma-Bengpal relationship was a angular unconformity between these two in the Chandanar

basin (Ramakrishnan, 1990). The geological maps of Crookshank (1963) and Ramakrishnan (1969) clearly show that the Sukma enclaves striking N-S and dipping steeply eastward/^{which} are abruptly truncated near Gadmiri and Renganar and are overlain by the Bengpal metabasalts striking E-W and dipping northward on Pesal Dongri and Epiya Dongri Hills.

The detailed works in southern parts of Bastar also reveal that Bengpal Group trending E-W comprises low grade metamorphic/along with metabasalt /s and granitic intrusive while the Sukma Group of rocks comprises TTG, granite-gneisses, medium-to-high grade metamorphic/^{s which} are characterised by NW-SE trend. The Bailadilla Group dominated by Iron Ore Formation has distinct N-S trend in southern Bastar.

2.2.1. Regional structure

Bastar craton exhibits complex structural history due to polyphase deformation and metamorphism during the Bengpal and Bailadilla orogenies. The polyphase deformations are reflected by varying trends in the outcrop pattern of Bengpal Group. Since the Bengpal Group comprises metasedimentary and metabasaltic rocks and ^{constituents} constituents the older metasediments of the Bastar craton, ~~So~~ their structural elements primary and secondary structures may be useful to understand the early regional structural history of the craton. Primary structure is recorded as color banding in BMQ (Banded Magnetite Quartzite) and lithological contacts between the various metasedimentary bands (S₀), which are obliterated due to different phases of deformations. The litho contacts appear to be more reliable and they ~~vary~~ ^{trend} from NW-SE ~~trending~~ in the southeastern margin of the craton.

Secondary structural elements are well preserved in the form of schistosity / gneissosity (S₁) and mineral/^s banding. The first phase of deformation^s is represented by earliest planar fabric (S₁) preserves/^{ed} in the metasediments particularly in BMQ at Bijapur-Bhopalpatnam and Sukma Bengpal belts. They show NNW-SSE to NW-SE trends and dip steeply in

either direction. In the gneissic rocks, S_1 is preserved^d as alternate bands of mafic and quartzo-feldspathic layers. The second phase of deformation developed axial planar fabric (S_2), which is the most dominant in whole of Bastar Craton. The important regional folds interpreted from the available data are described as follows: -

- (i) **Jagargonda fold (South Bastar):** - A N-S trending major synformal fold is recorded in north of Jagargonda i.e. in the southern foothills of Bailadilla range, plunging 30° - 40° northerly. Chatterjee (1970) suggested that in the Bailadilla range, horizontal shearing has produced NNE, plungingⁿ overturned fold with axial planes dipping ENE resulted from flexural slip folding. The fold geometry changes to N-S trending non-plunging fold, as seen in the west of Bailadilla.
- (ii) **Bijapur fold:** - Mishra *et al* (1984 d) described the presence of major NW-SE trending synformal fold, south of the Bijapur Ghat sections, plunging 25° - 30° towards southeast. This synformal fold is formed^{ed} by a band of Grunerite magnetite Quartzite (GMQ), which extends further southeast. East of this fold, closure another ~~sympathetic~~ synformal structure is still preservedⁱⁿ by BMQ, plunging southeasterly. The intervening area between the two synclines is a peneplained country indicating that anticlinal structure present in between has been eroded away.
- (iii) **Toynar fold:** - North-South trending synformal fold with culminations and depressions formed by a calc-quartzite and BMQ in the north of Toynar yield 15° - 25° plunge toward south.
- (iv) **Pamed fold:** - In the southeastern extension of Bhopalpatnam granulite belt particularly southeast of Pamed ($18^\circ 12'$: $80^\circ 54'$), metasedimentary rocks, ~~so~~^{show} a ~~swerve~~^{swing} in strike from NNW-SSE to E-W to NE-SW indicating a major fold closures^s. Similar fold closures are seen in the southern extreme of Bastar craton bordering Andhra Pradesh.

Beside these above folds, some others structural data on Sukma and Bengal belt are recorded. The Sukma enclaves of north Bastar show WNW-trending first fold, (F_1) associated with the main foliation and overprinted by NNE-trending (F_2) folds. The third phase deformation (F_3) developed crenulation cleavages and NW-trending shear zones (Datta, *et al*; 1981). Bengal belt is described as a major SSE-plunging synclorium (Ramakrishnan, 1973) and Bailadilla belt as asynclorium with two synclines and intervening anticline plunging north (Crookshank, 1963).

To sum up, the structural analysis with the mineralized area, Babu (1994) ^{found} ~~find~~ out four phases of folding.

- | | | |
|------------------|----------------------|---|
| F1: E-W, WNW-ESE | : Indravati trend | : affected the older Bengal metasediments |
| F2: N-S | : Bailadilla trend | : affected the schistosity planes parallel to F_1 and F_3 |
| F3: NE-SW | : Eastern Ghat trend | : appears to be due to cross-folding in initiation of granitic orogeny |
| F4: NW-SE | : Godavari trend | : is the most predominant related to the younger phases of granitic and pegmatitic activity. Most of the cassiterite bearing complex pegmatites have preferred this trend indicating structural control of mineralisation. show |

The mafic dykes are intruded mainly into the granite gneisses. The greatest concentration of dykes may be seen around the villages of Bastanar Dantawara, Pondum, Kaklur and Katekalayan. The dykes trend predominantly in NW-SE to WNW-ESE ^{cutting the} foliation of the granite gneisses and the major ~~regional~~ structural trend. ~~To~~ Mega-lineaments viz; Kondagaon and Bhamragarh and a number of intermediate and small lineaments, related to the Godavari rift system occur in the Bastar area with a ~~preferred~~ NW-SE orientation, as recognized on the basis of LANDSAT imagery (Rajurkar *et al*; 1990).

The detailed structure ^{anal} ~~analysis~~ suggested that the structure and tectonics of southern Bastar has ^a ~~dominating~~ role for the mineral deposit of tin and associated ~~other~~ mineral ^{is} and played a dominant role in mobilization and

deposition of the minearlisation especially in the last culminating dominant phase along NW-SE trend. Most of the tin ⁱⁿ an associated rare metal bearing Pegmatites was emplaced along ~~trend~~ NW-SE which was in turn genetically related to granitic orogeny.

The dominant NW-SE trend appears to have resulted due to late-to post-kinematics^s granitic activity. Criss-crossing of several Silicified shear zones, fault planes, major fractures, major joint patterns, lineation and foliation of the rocks type project a complex structural framework of the area with several reactivations and superimpositions of the later events on the earlier trends.

2.2.2. Geochronology

Recent geochronology studies in Peninsular India reviewed by various workers, ^{from} at time to time which indicates that, Bastar Craton is one of the oldest Archaean nucleuses^s like Dharwar, Bundelkhand and Singhbhum Cratons (Radhakrishnan and Naqvi, 1986). Attempts have been made by many to date and understand the various geological events in and around Bastar. The geochronological data and reviews of several worker like Sarkar, *et al.* (1967), Balakrishna and Naqvi (1986), Babu (1986), Sarkar, *et al.* (1980 and 1990), Radhakrishnan (1989), Radhakrishnan and Naqvi (1986), Babu (1990), Bandyopadhyay *et al.* (1990) and Rogers (1993) ^{ve} has been compiled in table 2.5. An appraisal of the isotopic age data reveals several major tectonothermal magmatic events in the processes of crustal evolutionary continental growth history of the area. These events have been summarized in table 2.5.

The oldest age (3310 ± 336 Ma) has been obtained from the deformed banded gneisses of high alumina trondhjemitic affinity of Markampara area of Bastar by Sarkar and Gupta (1990). This age is comparable to the other tonalitic-trondhjemitic gnisses reported from the south Indian and Eastern Indian Craton (Beckinsole *et al.*; 1980). Moor bath *et*

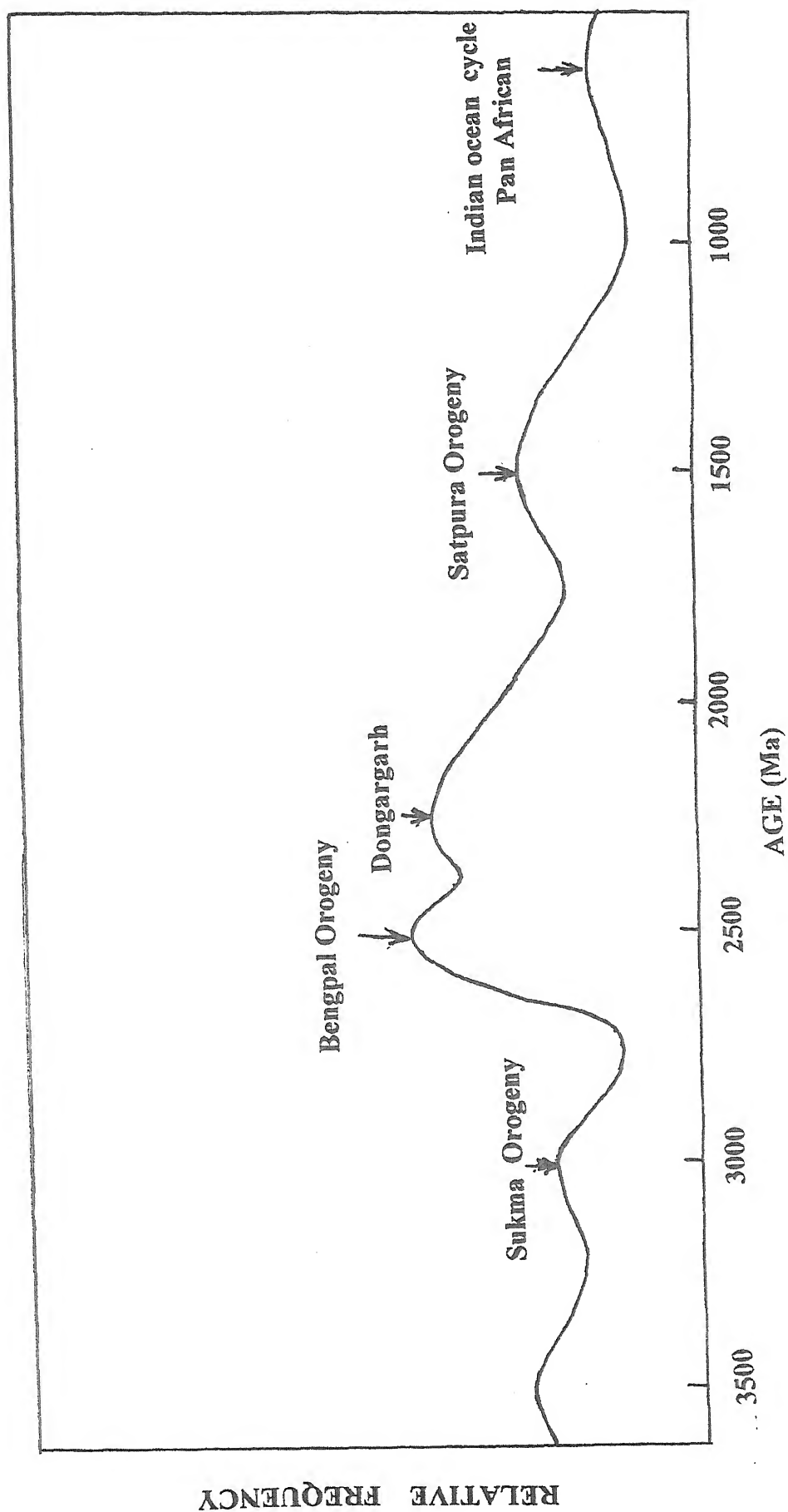


Fig. 2.3. Tectono-thermal events in Bastar Craton.

al; 1986, Dhoundial *et al*; 1987, and Bundelkhand complex (Sarkar, *et al*; 1990). The petrological study suggests that Markampara trondhjemitic gneiss ^{has} have mantle isotopic signature (initial $^{87}\text{Sr}/^{86}\text{Sr}$ ratio or $I_{\text{Sr}} = 0.70104 \pm 260$), represent ^{is a} juvenile sialic crust.

Pb/Pb isotopic age data ^{on} whole rock samples of migmatite gneiss and granite gneiss of south Bastar yield isochron age of 3511 ± 155 Ma, ^{table} – 2.5, S. No. 2 (Beckinsole *et al*; 1980) to 3018 ± 61 Ma, ⁱⁿ Table- 2.5, S.No. 3 (Sarkar, *et al*; 1990) respectively. This isotopic age data establishes that the gneissic rocks of Bastar Craton are comparable in age to the oldest rocks in Singhbhum Craton and to the Gorur-Hassan gneisses of Dharwar craton (Beckinsole *et al*; 1980). These data further confirm that there were older components in granitic crust prior to deposition of Sukma Suite.

Sarkar *et al*. (1990) interpret ^{ed} the Pb-Pb age of 3000 Ma as the emplacement age and the 2600 Ma Rb-Sr ^{iso} errorchron age ^{as} reflecting a secondary metamorphic event. The 3000 Ma event presumably marks a period of granite plutonism in Bastar region. The gneisses around Sukma represent a typical tonalite-trondhjemitic-granodiorite (TTG) suite (Karkare and Srivastava, 1985). The Sukma gneisses show great deal of scatter and define an ^{iso} errorchron of 2636 ± 489 Ma, table 2.5, S.No. 5, (Sarkar *et al*; 1990). Pb isotopic data on fine-grained granite near Sukma also suggest an age of around 2610 ± 143 Ma (Table 2.5, S.No. 6) and an intrusive leucogranite into the migmatites near Barsur gives Pb-Pb age of 2573 ± 139 Ma with $M = 9.24 \pm 0.32$ (Table 2.5, S.No. 7) whereas the Rb-Sr data yields 2101 ± 323 Ma with Sr initial ratio of 0.750 ± 0.042 (Table 2.5, S. No. 20). This probably suggests a strong orogeny (Bengpal orogeny) 2600-2500 Ma. The migmatitic gneisses near Sukma define an eight-point Rb-Sr isochron of 2528 ± 110 Ma (Table 2.5, S. No. 9) with Sr initial ratio of 0.707030 ± 30 (Sarkar ^a and Gupta, 1989).

The isotopic composition of leucosomes of migmatitic gneiss exposed near Katekalyan yielded an age of 2530 ± 89 Ma (Table 2.5, S.No.

8) with an initial Sr ratio of 0.70305. The low ratio possibly indicates a Rb depleted source or Rb removal at late stage.

Intrusive granitic activity at 2600 Ma is supported by the Pb-Pb whole rock errorchron age of 2573 Ma from the Sukma granitoid of Bastar. The granite has U^{238}/Pb^{204} ratio implying involvement of crustal component (Sarkar *et al* 1990). In addition, a host of Rb-Sr whole rock errorchrons of migmatitic gneiss (Sukma) and granite gneiss (Kerlapal) from Bastar area show errorchron age ranging from 2528 to 2659 Ma. The highly disturbed Rb-Sr isotopic systematics of the migmatitic gneiss and granite gneiss suggest incomplete isotopic equilibration at 2600 Ma or different diffused thermal impression. The late Archaean (2600 ± 50 Ma) event hence appears to represent a period of deformation, metamorphism, syntectonic granitic activity involving limited anatexis and related migmatization of pre-existing rocks. This is corroborated by (i) Rb-Sr isotopic resetting of 3000 Ma gneisses at 2600 Ma (Table-2.5, S.No. 4); (ii) deformed gneissic nature of most of the granitic rocks yielding errorchrons and (iii) relatively high initial value of Sr (0.707-0.708) in these granitic rocks.

Several diapiric suites of anatectically derived granitoids evolved almost synchronously. These are represented by the granites of Sukma (Sarkar and Gupta, 1989), Paliam-Darba, Burugudam in Bastar, Pujariguda and Cholanguda in Koraput district, Orissa (Pandey *et al*; 1989).

The available whole rock Rb-Sr ages and petrological studies of granitic plutons from different part of Bastar craton viz; Paliam, Darba: 2275 ± 80 Ma; Burugudam 2237 ± 70 Ma; Pujariguda: 2110 ± 47 Ma; Cholanguda: 2301 ± 53 Ma (Pandey *et al*; 1989) suggest another strong phase of thermal activity in which remobilization of sialic crust by an anatectic melt resulted in the emplacements of granitic magma into Sukma and Bengpal Group of rocks. The wide geographic distribution of acid magmatism may possibly take place during the period 2300-2200 Ma.

These granitic rocks belong to $2200 \text{ Ma} \pm 0.1 \text{ Ma}$ age level and possess typical crustal isotopic signatures ($Sr_i = 0.7125-0.7430$). Sn-W

mineralisation is said to characterize S-type granitoids (Pitcher, 1983) and indeed, pegmatoidal phases associated with the S-type granites of 2200 ± 100 Ma age ^{level} in Bastar host Sn-W mineralisation (Murti *et al.*; 1979). It is also important that this granite contain^{ed} various phases of Sn-bearing pegmatites.

The presences of highly altered andalusite taboids (1-4 cm) in the schists bordering the granites point to the contact metamorphic effect, and the emplacement of granites at shallow depth (Lamba and Agarkar, 1988). However, younger K-Ar age of 1345 ± 22 Ma (Table- 2.5, S.No. 33) for biotite from granitic rocks exposed in the vicinity of village Paliyam (Anonymous, 1978a) may be due to the effect of loss of a Ar during some late geological event.

The stanniferous pegmatites of Bastar yield ~~is~~ ages varying from 2112 (K/Ar) to 697 ± 60 Ma (Fission Track ages). The muscovite of pegmatite ^{with} ~~elapsed~~ with in granite near Tongpal ^{gave} an age of 1573 Ma (Rb/Sr, Table- 2.5, S.No. 24) and that of pegmatites near Mundval ^{are} ~~is~~ 1528 Ma ^{in 1971} (Rb/Sr, Table- 2.5, S.No. 25). The fission track ages of the micas of pegmatites exposed around Paliyam, Tongpal and Mundval are younger~~er~~ ranging from 775 to 697 Ma. These geochronological data indicate different phases of cooling or thermal signatures in pegmatite and granitic suite.

^{ed} The thermal imprint of the early Proterozoic granitic activity is manifest^{ed} in the K-Ar muscovite age of pegmatoidal gneiss intruding the Bengpal sequence, K-Ar ages of metalava from the Bengpal, Rb-Sr whole rock isochron age Amgaon gneiss and the K-Ar age of Maspur metalava of the Abujhmar Groups (Table 2.5, S No. 16, 17, 18, 19). - ??
??

The absolute whole rock isochron Rb/Sr age data indicated 1639 Ma interpreted as the age of emplacement for Kaskal granite in Bastar Craton. The Tirodi gneiss (near Dongribuzurg, Bhandara, M.P.) occurring at the basal zones of the Sausar Group (Table 2.5, S No. 26) and the Kaskal granite of Bastar (Table 2.5, S No. 22) yield Rb/Sr isochron ages in the range 1700-1500 Ma. Sarkar *et al.*; (1981) consider^{ed} the Tirodi gneiss ^{as} ~~is~~ a product of synkinematic granitisation during the tectonometamorphic event of the Sausar

Group. High ^{values} Sr_i (0.7148 – 0.7632) of these granitic rocks ^{indicate} is consistent with their derivation from crustal sources.

The Dongargarh granite massif appears to be composed of at least two phase^s of granitic activity at 2470 Ma and 2220 Ma (Krishnamurthy *et al*; 1988, Sarkar S. N. *et al*; 1981; table 2.5, S No. 11,14). Each of these intrusive phases has left its thermal imprint in rhyolite of the Nandgaon group (Bijli rhyolite 2462 ± 25 with $Sr_i = 0.7054 \pm 14$, Krishnamurthy *et al*; 1988; 2180 ± 25 with $Sr_i = 0.7057 \pm 15$, Sarkar, S. N. *et al*; 1981). Unlike the Bundelkhand complex, the Dongargarh granite shows Proterozoic thermal imprint around 1500 Ma (Table 2.5, S No. 27, 29, 31).

Fine-grained granites are presents^d in the many parts of the Sukma and the Kondagaon areas. In the Kondagaon area, however, the fine-grained granite occurs in close association with the pegmatoidal granite (granodiorite-granite composition) as marginal variants. The age of this pegmatoidal granite is ^{obtained} 2409 ± 148 Ma (Table 2.5, S No. 12). A pegmatoidal granite near Sukma has also ^{yielded} a similar Rb- Sr age of 2409 ± 148 Ma with $Sr_i = 0.72216 \pm 0.02175$ (Sarkar and Gupta, 1989).

A regime of crustal extension leading to the developement of intracratonic rift systems appear^s to have closely followed initial Archean cratonisation after the 2600 Ma compressional tectanometamorphic event. The acadeimic effusives^{of} Nandgaon Group with a minimum age of 2462 Ma and mafic volcanics of the Abujhmar group with a Rb- Sr whole rock isochron age of 2490 (Table 2.5, S No. 10) suggest repeated effusion of acidic / mafic lavas along the Kotri rift (Mishra *et al*.; 1988).

1200 Ma event is marked by a tectonic mafic dyke activity in the Bastar craton. Unmetamorphosed mafic dykes intruding the Abujhmar supracrustal sequence and the granitoid of Bastar have yielded K- Ar ages in the range 1259 – 1228 Ma (Table 2.5, S No. 34,35, 36).

Along with the age determination by Pb/ Pb, Rb/ Sr, K/ Ar and fission track method, thermo chronometric studies to indicate the cooling of

granitic rock was very slow from 500–200°C with an average rate of cooling about 1.6°C per million year. From thermal history, it is inferred that the region was not reheated above 200°C during the period between 1345 Ma and 770 Ma, with distinct thermal impulse around 770 Ma (Ray Burman *et al*; 1982).

It is evident from the data, the Rb- Sr isochron age for granite of Bastar – Koraput area and nearby areas of Bastar craton, define an important event around 2250 ± 150 Ma, which in all probability represents the emplacement event of these granites. The significant feature in all these isochron ^{data} is the higher 0.71 to 0.75 initial $^{87}\text{Sr} / ^{86}\text{Sr}$ ratios, which indicate that all these granites in the Bastar craton are crustal ^{derivative} ~~derived~~. The nature of such precursor crustal rock, which on anatexis gave rise to the melt leading to the crystallization of the Paliam and Darba granites and their associated pegmatites, could be most probably metasedimentary in nature (Ramesh Babu, 1990).

Combined regression line with all twelve samples (eleven granite samples from Darba and one from Paliam) yields an isochron age of 2308 ± 48 Ma with initial $^{87}\text{Sr} / ^{86}\text{Sr}$ ratios 0.7354 ± 0.0097 and decreases M.S.W.D. to 1.41 (Ramesh Babu *et al*; 1993). This whole rock isochron age for the Paliam and Darba granites indicates the time of their emplacement. ~ ??

Thus the published available geochronological data indicate that Bastar craton ^{is a} ~~in~~ crustal ^{active} ~~derived~~ part of one of the oldest Archaean Supercontinent. The cratonisation has taken place between 3500 to 3000 Ma. There are several phases of igneous and thermal activities. The major acid igneous plutonic activities appear to have occurred mainly around 2600 Ma, 2200 Ma, 1500 Ma and 700 Ma. Different granitic phases ^{were} ~~are~~ predominant before 2200 Ma, whereas pegmatitic activity dominated around 1500 Ma with reactivation and thermal imprints continuing till 700 Ma.

To conclude the above available geochronological data, the tectonothermal events in Basar craton are shown in fig 2.2.

2.3. Geology of the study area

The present area under investigation covers the southeastern part of the Bastar Craton in Peninsular India. The regions in and around Katekalyan ^{consists of} tin and rare metal deposits covering an area of about 81 sq. km ^{it was} ~~has been~~ mapped for recording the lithological and structural details. For the identification of several encouraging occurrences of both primary and secondary tin mineralisation, the granitoids and pegmatites as well as colluvial and alluvial areas of Dumam nadi drainage respectively around Katekalyan village ^{were} ~~have been~~ systematically examined. This was done during three field sessions, ^{during} ~~covering within~~ a period of about three months. The geological map of the mineralized study area is shown in Figure 2.4, where the width of pegmatites and quartz reefs has been shown ^{as} ~~exaggerated~~. . . . why??

The area in and around Katekalyan constitutes of metasediments, which are considered to be a part to Tulsi Dongar Formation Stage of Bengpal Group (Crookshank, 1963) of Lower Proterozoic age. They are mostly argillaceous and ferruginous metasediments represented mainly by andalusite-sericite schist (A.S.S.), quartz-sericite schist (Q.S.S.), banded magnetite quartzite (B.M.Q.), and grunerite magnetite quartzite (G.M.Q.). Metabasics are extrusive. Metadolerite and gabbro were found emplaced within the Bengpal metasediments and also in granite gneiss. The succeeding granite ^{ic} and pegmatitic activities have led to the formation of tin and associated rare metals mineralisation. Tin as discrete crystals of cassiterite along with columbite and tantalite, are found mainly in the pegmatites emplaced into the metabasic intrusives and in the granitoids (granite and granite gneiss).

The area under study has experienced several phases of activities viz; magmatic, pegmatitic and pneumatolytic and rare metal mineralisation.



INDEX

	Meta-Gabbro/Amphibolite (MBI)		Meta-Dolerite Dyke		Dip of Foliation
	Meta-Basalt (MBE)		Barren Pegmatite		Fault
	Banded Ferruginous Quartzite (BMQ/GMQ)		Mineralised Pegmatite		Location of Analysed sample
	Quartz Sericite Schist (QSS)		Granite (KBG/KHG/KTG) (KG)		Alluvium
	Andalusite Sericite Schist (ASS)		Granite Gneiss (KGG)		Quartz Reef

Fig. 2.4. Geological map of the Katekalyan area, district Dantewada, Chhattisgarh (Modified after T.M. Babu 1985).

The magmatic phase attributed to the granitic intrusions into pre-existing granite gneiss. The granitic apophyses intruded into the metabasics and Bengpal metasediments ~~are also appear~~^{were} responsible for tin-bearing ore fluids. Biotite granites (KBG) are ~~found as~~^{are} medium-to fine-grained and some times as porphyritic (light coloured). Granite-gneiss bodies belonging to Sukma Suite at several places, exhibit distinct domal shape, which is characterised by leucocratic bands of quartz and feldspar and melanocratic bands of biotite and other ferro-magnesian minerals. The mineralising stanniferous nature of the granite with tin as ^{an} enriched component in the younger granitic phase is exposed at Paliam, Katekalyan and Darba areas. Structurally, the metasedimentary rocks in the area form a major synform, flanked by granites on the north (Darba granite) and south (Paliam granite) ^{which} ~~that~~ were emplaced in the antiformal regions (Murti *et al.*, 1979).

Different types of pegmatites such as simple unzoned, greisenised, albitised and graphic in nature are found emplaced into the metabasic intrusives, granites and Bengpal metasediments of the area. Emplacement of mineralised pegmatites is more frequent in metabasic intrusives (MBI), granite (KG) and granite gneiss (KGG) than the Bengpal metasediments. The dolerite dykes are traversed and cut across all the earlier formations and subsequently metamorphosed into metadolerites of variable length and width. Pegmatites emplaced in Bengpal metasediments are generally unzoned, simple albitic to graphic and practically devoid of noticeable cassiterite mineralisation in the study area. Cassiterite along with columbite and tantalite mineralisation has been encountered in the greisenised pegmatites emplaced in the granites at Kondaras Dongri, Benglur and Lakras area in and around Katekalyan village. Quartz veins indicate the last phase of acid magmatic activity succeeding the pegmatites and have traversed all the older formations. Silicified shear zone or quartz reef (upto 40 m wide and about 2

km long) has been found at the contact of granite and Bengpal schist, between Gatam and Benglur villages.

2.3.1. Topography and drainage

The area under investigation is characterised by NW-SE trending chains of hills. The altitude of the hills varies from 605 m to 877 m. The central part of the area along the Dumam nadi and its tributaries is having low altitude and ~~tends to be~~^{has} nearly flat to undulated topography surrounded by [?] patches of alluvium. Geologically the investigated area has been divided into granitic terrain and metabasaltic terrain. These two contrasting lithounits ~~has~~^{have} been separated by E-W flowing Dumam river in the investigated area. The former usually ~~have~~^{has} low topographic level mountain 629 m, near Kondaras Dongri, whereas later terrain has high altitude mountains up to 850 m. (toposheet No. 65 F/9).

The hard and resistant acid and basic rocks form the hills while the comparatively softer schistose rocks have given rise to undulating plains. Since tin and associated rare metal mineralisation are often related to acid igneous intrusions with different phases of magmatic, pegmatitic and pneumatolytic activities, the arched up portions of the hills appear to be the high spots in the roof part of the igneous intrusives. The area is drained by ~~the~~^a number of streams and their tributaries. The stream ~~shows~~^{has} radial and dendritic drainage patterns. Dumam nadi is the only major stream of the region and it flows in the SE direction. The drainage pattern in the entire area is quite significant and is also responsible for the colluvial, eluvial and alluvial concentrations of tin and associated rare metal minerals. They originate in the ^{??} hilly region of the study area and are seasonal in nature, having water only during the rainy season (July to September).

2.3.2. Succession of the rocks of the area

The generalized geological succession of the study area as evident from field studies is given below.

Table 2.7. Succession of the rocks of the Katekalyan area.

Recent	Alluvium
P R O T E R O Z O I C B E N G P A L G R O U P	Younger meta-dolerite dykes
	Silicified Shear Zones (Quartz reef) (Last phase of acid magmatic activity).
	Pegmatites (KP) : Simple non-greisenised, greisenised unzoned, graphic, albitised and associated with mineralised and non-mineralised pegmatites.
	Granite (KG) : Medium grained, non-foliated mica granite, porphyritic and leucocratic at places (<u>KBG</u> , <u>KHG</u> and <u>KTG</u>). ??
	Metabasic Intrusives (MBI) : Meta-gabbroic to amphibolitic in composition emplaced as sills and dykes into the Bengpal schistose rocks.
	Metabasic Extrusives : Meta-basaltic and spilitic composition with pillow lava structures (rarely).
	Bengpal Metasediments : Andalusite sericite schist (ASS), quartz sericite schist (QSS), ferruginous quartzite (BMQ/GMQ) etc.
	Granite-gneiss and migmatite (KGG) Sukma gneisses ?

The area under investigation comprises of the Precambrian metasedimentaries represented by some units of the Bengpal Group. These are found both in the hilly and valley regions. The metasediments are intruded by igneous rocks of different ages. Acidic intrusive exposed in the area are granitoids (granite and granite gneiss) and pegmatites. In some part of the

area, the metasediments and the igneous rocks are found to be covered by recent alluvium.

2.3.3. Lithology, field relationships and structure

The field ^{of occurrence} ~~distributions~~ of different lithounits found within the study area along with their structural characteristics have been described in the following pages.

2.3.3.1. Metasediments

2.3.3.1.1. Andalusite sericite schist

The andalusite sericite schist (A.S.S.) constitutes the oldest lithounit and belongs to the Tulsi Dongar Formation of the Bengpal Group. It has been observed in two patches mainly in the central part of the study area along the Dumam nadi sections and also southwestern part between the Tumakpal and Talem villages (Fig. 2.2). These rocks are medium-to fine-grained, yellowish to buff coloured and well laminated. Highly altered andalusite tabloids ranging in size from 1 to 5 cm with shapes varying from ellipsoidal, nodular and prismatic. *incomplete*. = ??

The andalusite tabloids are mostly trending parallel to the foliation planes of the schistose rocks striking NW-SE, dipping northeasterly with an amounts ^{??} varying from 50° to 70° . At places, ~~quite~~ ^{have} near to the metabasic extrusives and granitic intrusion, the steep dips ($>70^{\circ}$) ^{have} been observed towards NW of Gatam on the eastern side of Dumam nadi. *Direction ??* ??

2.3.3.1.2. Quartz sericite schist

Quartz sericite schist (Q.S.S.) is exposed near Gudse over a large surface in the southeastern part of the study area (Fig. 2.2). It can be observed in southeastern portion of the valley of Dumam nadi. The general dip and strike of Q.S.S. is in agreement with the same of the other rock types namely A.S.S., B.M.Q. and G.M.Q. etc., of the Bengpal Group.

2.3.3.1.3. Banded ferruginous quartzite

Banded ferruginous quartzite (BFQ) ^{has a} ~~appears to have~~ restricted occurrence in the study area (Fig.2.2). This rock-type has distinctly variable ~~in~~ band thickness of the magnetite, grunerite and quartz association. These bands represent the primary bedding of the sedimentary rock which is more or less parallel to the secondary (foliation) plane. It is exposed at the Pinjupara, SW of Kondaras Dongri, Tumakpal, Nayanar and Talem. The banded magnetite quartzite (B.M.Q.) and grunerite magnetite quartzite (G.M.Q.) have similar strike to the A.S.S. and Q.S.S., but at places they have gentler dip (20° to 30°).

2.3.3.2. Metabasic extrusive

The metabasic extrusives of basaltic compositions trending WNW-ESE is exposed mainly in the southern part of the area especially along with Dumam Nadi. These metabasalts occur as flow of average 600m. thickness. These extrusives are nearly homogenous in nature but at many places amygdales were noticed in certain flows. The sinistral strike-slip fault has been also observed at near Tumakpal village. Metabasalt is also exposed in the northeastern part of the area near the Kondaras Dongri hill where basalt showing pillow structures. These pillow basalts are ~~recorded as~~ rounded to kidney shaped ^{with} of 30 to 70 cm in diameter. Similar feature has been also described by Babu (1983). This sequence is further intruded by metabasic intrusive (metagabbro / amphibolite).

2.3.3.3. Metabasic intrusives (metagabbro and amphibolite)

The metabasic intrusives are observed as mounds or hillocks in different parts of the area under investigation. These metabasics also occur as linear ridges within granite-gneiss. Some of the metabasic outcrops are fringing the gneissic rocks in such a way that ~~they are~~ ^{these} intermittent exposures

show (a) more or less parallelism with the marginal boundaries. These metabasics covers a large surface in the northeastern part of the area and have a more or less north-south extension. But in the southwestern part of the Lakharas, metabasics (metagabbro/amphibolite) are ~~introduced~~ ^{intruded} by the younger metadolerite dykes.

The special features about these metabasics are that they are ~~are~~ ^{occur} present as concordant and occasionally discordant bodies with respect to the granite gneiss. The concordant relation is observed in the metabasics cropping out in the south of Kondaras Dongri hill. The discordant relation of the outcrop is recorded near Kusapal village.

2.3.3.4. Granitoids (granite and granite gneiss)

The present study is mostly concerned with the ^{sp} behavior, mode of occurrence and mutual relationships of the intrusive rocks of this region in view of its genetic connotation with tin and rare metal mineralisation.

With reference to their possible mineralisation episode, the acid magmatic rocks namely granite (KG) and granite gneiss (KGG) are of special significance. It has been observed by several authors (Deshpande and Bose, 1979; Suryanarayana *et al.*, 1979; Babu, 1979; Mahapatra, 1979) that two distinct granite plutons; viz; Darba and Paliyam are mainly responsible for the tin mineralisation in southern Bastar Craton. One of them is exposed north of the area known as Darba granite and other is to the south known as the Paliyam granite.

In the investigated area granitoids (granite and granite gneiss) comprises more than 50% of total area. The detail investigation suggests that there were multiphase of magmatic activity. On the basis of field relationship, texture, structure and mineralogy, they have been named as biotite granite, hornblende granite, tourmaline granite, and granite gneiss. Some times it ~~can~~ ^{is} also ~~are~~ characterized by foliated and non-foliated and porphyritic ~~in nature~~ containing phenocrysts of quartz and feldspar. The hornblende granite is

mostly restricted to the western part near Kondaras Dongri, whereas tourmaline granites ^{seen} were noted in the south-western part of the area near Talem village. The biotite granite intrusives are generally coarse-to medium-grained, non-foliated, leucocratic ~~rock~~ and ~~occur throughout~~ ^{intruding} the granite gneiss as mounds like hillocks in the study area. These mounds like ~~bodies~~ are seen prominently near Sentapara, Gatam, Naynar and Tumakpal. These granites are pink to grey white, ^{in colour}, hard and compact and mainly consist of quartz, feldspar, biotite and muscovite.

In the northwestern part of the Kusapal village, conspicuous foliated biotite granite (Plate II, Fig. A) is ^{well} best exposed; it may be the part of Darba granite. At several places, ^{it} this exhibits distinct domal shape characterised by leucocratic bands of quartz and feldspar and melanocratic bands of biotite (Plate I, Fig. D). The enclaves of metasediments hosted in the granite-gneiss have been also recorded at Benglur village. At some places, porphyritic granite exposures ~~appear to an~~ (younger phase) ^{well} were found emplaced into the foliation planes of older granite gneiss around Benglur, Tumakpal and Naynar areas. Such field relationship suggests that younger granitic (KG) emplacement as discrete plutons within the granite gneisses (KGG) exposed near Pinjupara and Nayanar village within nala cuttings ^{shows} gives the intrusive relationships between the granite (KG) and granite gneiss (KGG).

The gneissosity of the granite shows NNW-SSE trends, with steep northerly dip. The granite gneiss is coarse-to medium grained and characterized by leucocratic and melanocratic bands giving rise to migmatite like structures. The quartzo-feldspathic leucosomes and biotite-rich bands of melanosomes seldom have well defined margins of two phases and vary in thickness from a few millimeters to tens of centimeters probably due to the advanced stage of migmatisation showing lit-par-lit injections. The typical foliated granite gneiss (KGG) was found to the east of Lakharas. Pegmatites of the different phases were found to be emplaced into the granitoids (granite and granite gneiss) along fracture planes trending N-S, NNW-SSE and E-W, at places, cutting across each other at Katekalyan and Benglur villages.

The presence of minerals like tourmaline, muscovite, sericite and chlorite indicate that the granite has been subjected near solidus and subsolidus alterations particularly prevailing in the mineralised area. The different metasomatic activities leading to the formation of rare metal mineralisation have been ^{observed} ~~recognized~~ in the Katekalyan and adjoining area. However, distinct zones of formation of cassiterite with niobium (Nb) and tantalum (Ta) in varying compositions can be demarcated, starting from microclinisation (potash-metasomatism), albitisation (soda-metasomatism) and zones of pneumatolytic activity (greisenisation). Greisenisation is the common alteration process in the northern part of the Katekalyan mineralised area. However, un-greisenised granitic exposures are also found in the southern part near the Tumakpal. 11 Jan 27.

2.3.3.5. Pegmatites (mineralised and non-mineralised)

In the study area, on the basis of mode of occurrences, mineral assemblage and their mineralisation characteristics, three types of pegmatite ^s viz; unzoned simple pegmatites, recrystallised granite pegmatites and metasomatic pegmatites can be recognized. These pegmatites of the different ^{types} ~~nature~~ were found emplaced into the metabasic, granite, granite gneiss and Bengpal metasediments. The field relationship suggests that the emplacement of pegmatites might have occurred due to the post-tectonic activity subsequent to the emplacement of major phase of acidic magmatism. It is also noticed that tin-bearing pegmatites appear to have emplaced more within metabasics and granites than the Bengpal metasediments. This may be due to the prevailing joints and fractures in metabasics and granitic rocks compared to those of Bengpal schistose (impermeable) rocks. It is also notice ^d that pegmatites are older than the newer dolerites, amphibolites and gabbros.

The widespread occurrence, extreme variation in size, shape, mineralogy and structural trends make the pegmatites of the area highly complex. Pegmatites are generally 10 m to 100 m long but rarely exceed 100 m, the width varying from less than a metre to 10 metres. They show

trend mainly along NNW-SSE, N-S and NE-SW directions with steep northeasterly and easterly dips.

Type I

The pegmatites emplaced in Bengal metasediments are unzoned and non-greisenised in nature. At places, graphic intergrowth of quartz and K-feldspar has been noticed indicating eutectic crystallisation of its formation. Pegmatites are mainly composed of quartz, microcline, plagioclase (albite to oligoclase), muscovite and occasional garnet ^{are} and practically devoid of noticeable cassiterite and rare metal mineralisation. This may be due to the dissipation of rare metal bearing pneumatolytic gases into the weak ~~permeable~~ foliation planes of Bengal schistose rocks, ~~thereby not leading to~~ the concentration of cassiterite and allied mineralisation and even no marked wall-rock alteration effects were ^{also} noted. These types of pegmatites are also observed in the southwestern part of the Gatam, and northeastern part of the Kondaras Dongri of the study area.

Type II

The second type of pegmatites ^{are} are recrystallised and ~~is~~ emplaced into the granites only and are found at Benglur, Kondaras Dongri and Lakharas areas. These are inequigranular coarse-grained and ^{are} composed mainly of quartz, feldspar and muscovite as thin-ribbon type bands. They have gradational contact with granite and are generally unzoned but at their fringes development of mica is predominant. The mineralogy of the pegmatites is similar to that of parent granite but the proportion of minerals differ. Graphic intergrowths are not present in the recrystallised granitic pegmatites. This type of pegmatite appears to have ^{been} ~~been~~ emplaced along the shear and fracture planes in granites during the late stage of the crystallisation of granite and is moderately mineralised.

Type III

This type of pegmatites appears to be metasomatically altered *due to* ~~probably~~ by tin and associated rare metal bearing pneumatolytic fluids, which were chemically not in equilibrium with the primary pegmatite mineral mass. The different alteration zones developed by the metasomatic activity leading to the formation of cassiterite and associated rare metal mineralisation have been ~~observed~~ ^{to be observed} ~~recognized~~. At several places, potash-metasomatism, soda-metasomatism, and pneumatolytic activities appear to be responsible for the tin and associated rare metal mineralisation of the study area. These pegmatites can be further classified into greisenised pegmatites, microclinised pegmatites and albitised pegmatites. The cross-cutting relationships of these pegmatites in the area indicate that there were different phases of pegmatitic activities in space and time. The greisenised (unzoned type) pegmatites are relatively wider than the non-greisenised (unzoned) pegmatites. ~~are~~ (comprised of randomly oriented muscovite, quartz and feldspar). The coarse-grained uneven texture of quartz and muscovite ~~are~~ ^{is} associated with tin-bearing minerals, lepidolite, cassiterite, columbite, tantalite, fluorite, tourmaline and beryl. They ~~are~~ ^{are} developed ~~most~~ ^{present} probably by the action of pneumatolytic activity and are ~~pronounced~~ ^{present} in the north of ^{in a zone which} Katekalyan, Kondaras Dongri and Lakharas. They ^{They} are generally exposed 1 to 3 metres wide and 25 to 100 metres in length, ~~and~~ ^{are} more abundant in granites and metabasics.

In the field, albitised pegmatite can be identified by its monomineralic nature, predominantly feldspathic in composition with subordinate quartz and incipient mica. Feldspar is mostly present as albite or cleavelandite variety replacing the microcline, which indicates the prevalence of albitisation due to soda-metasomatism. In this pegmatite, the ore minerals are encountered predominantly cassiterite rich with minor or rare columbite and tantalite minerals. It is also noted that the albitised pegmatites have been encountered in granite and metabasic rocks. Albitisation has played a major role in lithium mineralisation. The contact of the pegmatite with host rock is sharp and slightly curvilinear, unlike the straight one as observed in the

previous types. The prominent minerals are potash and soda feldspars, quartz, garnet, lepidolite, beryl, cleavelandite, fluorite, and apatite.

2.3.3.6 Quartz reef

Quartz reef being the last phase of acid magmatic activity succeeded the pegmatites and traverses^d all the older Formations. On the basis of colour, texture, structure and mineral associations, at least three of quartz reef were identified (Fig.) prominently exposed. Minor quartz veins of less than 1 cm wide were noticed in Bengpal schist, meta-basic intrusives and extrusives in criss-cross pattern mainly along joint planes trending NW-SE, NNW-SSE and E-W due to the closed-spaced fracturing. / ?

The fault and shear planes in most of the cases have been silicified striking almost parallel to the regional structural trend (NW-SE direction). But the one remarkable occurrence of the quartz reef in the shear zone extends up to 40 m wide and 3 kms long trending E-W direction, which is found between the Benglur and Gatam villages.

2.3.3.7. Younger metadolerite dykes

The dolerite dykes are found to be present randomly in different parts of the area. These intrusives are very large tabular bodies traversing and cutting across all the earlier Formations, which have been subsequently metamorphosed into metadolerites having variable length between 400 metres to 5 kilometres and width varies ^{from} between 10 to 20 metres. Regional alignment of these bodies exhibit NW-SE trend. Though, the dykes are widespread which are seen more prominently to the north of the Benglur and Gatam villages of the study area.

2.3.3.8. Alluvium

Thick deposits of silt, sand and gravel cover the study area, along the bank of the Dummam nadi section. Although the alluvium together with

the sand and gravel appear to be not of any geological importance, yet these have economic significance. It may be pointed out that the placer deposits of cassiterite, columbite, tantalite, and other heavy mineral concentrations are a helpful ~~guide~~ to prospectors.

2.3.4. Mineralisation potential of the area

The cassiterite exists in and around the Katekalyan area in appreciable quantity and its exploitation is worth undertaking. The evolution differentiating granitic magma shows enrichment of tin in the residual melt and fluids. Tin-bearing felsic residual end products ^{were} intruded as pegmatites into the uplifted and fractured rocks. Close association of cassiterite mainly with columbite, tantalite, lepidolite, beryl and fluorite may point out that niobium, tantalum, lithium, beryllium, fluorine and rare earths were intimately involved in the transportation of tin from magmatic stage to the main pneumatolytic stage. Several phases of rare metal mineralisation such as magmatic, pegmatitic and pneumatolytic phases ^{were} ~~have been~~ recognized in the study area.

The Sn bearing pegmatite of third type ~~phase~~ can be attributed to the younger intrusive type of coarse-grained non-foliated porphyritic biotite granite, which includes the pre-existing granitic gneiss, and also the granitic apophyses, which intruded into the metabasic and Bengpal metasediments. The soda-rich fine-grained (aplitic) biotite granite at Lokharas area contains 50 ppm Sn and the porphyritic leucogranite near Katekalyan village measures as high as 100 ppm of Sn (Murti *et al.*, 1982). This indicates that stanniferous nature of the granite with tin ^{was predominant} as ~~enriched component~~ in the younger granitic phase. Occurrence of discrete cassiterite crystals especially in the unzoned pegmatites can be related to the pegmatitic phase of acid magmatism. Tin-bearing pegmatites are found mostly in meta-basic rocks. However, for the first time pegmatite with discrete crystals of cassiterite have been reported emplaced within granite at Kondaras Dongri and Benglur areas.

Cassiterite along with niobium and tantalum bearing rare metal minerals is found in the greisenised portion of the pegmatites. This is evident from the appearance of extensive greisenised pockets, ^{characterised by} tourmaline (boron-metasomatism), and fluorite in pegmatites. ^{was} During ~~the course of~~ ^{the} post-magmatic metasomatic process ^{was} caused by actions of chemically active aqueous solutions forming the pegmatites. ^{was} The tin has ~~been~~ fixed in the lattice of rock forming minerals which subsequently ^{was} ~~might~~ have remobilized and reconcentrated by the volatiles leading to the formation of tin ore minerals.

Table 2.5. Geochronological data on Precambrian rocks of Bastar Craton (compiled by author from G.S.I. records and publications)

A S. No.	B Location	C Rock type	D Method used	E Age (in Ma)	F Source	G Remark
1	Markampara (Bastar)	Trondjemite gneiss	Rb/Sr	3610 ± 336 (0.70104 ± 260)	Sarkar G. and Gupta (1990)	*
2	Sukma (Bastar)	Migmatite Gneiss	Pb/Pb	3511 ± 155	Beckinsole <i>et al</i> ; (1990)	*
3	Sukma (Bastar)	Granite gneiss	Pb/Pb	3018 ± 61 (E) ($M=9.00 \pm 0.09$)	Sarkar G. and Gupta (1989) Sarkar <i>et al</i> ; (1990)	*
4	Kerlpal	Granite gneiss	Rb/Sr	2659 ± 310 (E) (0.707)	Sarkar G and Gupta (1990)	Thermotectonic impress
5	Sukma	Granite gneiss	Rb/ Sr	2636 ± 489 (E)	Sarkar, G <i>et al</i> . (1990)	Thermotectonic impress Empl. Age 3018 Ma (S. No. 3)
6	Sukma - Kondagaon (Bastar)	Granite	Pb/Pb	2610 ± 143 (E)	-do-	Empl.
7	Barsur (Part of Sukma)	Leuco granite	Pb/Pb	2573 ± 139 (E) ($M= 9.24 \pm 0.32$)	-do-	*
8	Katekalyan	Migmatite (leucosome)	Rb/Sr	2530 ± 89 (0.70305)	Bandhyopadhyay <i>etal</i> ; (1990)	*
9	Sukma	Migmatite gneiss	Rb/Sr	2528 ± 110 (E) (0.70703 ± 30)	Sarkar G and Gupta (1989)	*
10	Masapur (Bastar)	Masapur trap, Abujhmar basin	Rb/Sr	2490 ± 48 (0.70362 ± 8)	Sarkar G and Gupta (1989)	Eff.
11	Dongargarh	Granite	Rb/Sr	2466 ± 22 (0.7010 ± 42)	Krishnamurti <i>et al</i> ; (1988)	Empl. (phase -I)
12	Kondagaon and Sukma	Pegmatoidal granite	Rb/Sr	2409 ± 148 (0.722 ± 0.022)	*	*
13	Paliarn Darba	Granitic rock	Rb/Sr	2275 ± 80	Pandey <i>et al</i> ; (1989)	*
14	Dongargarh	Granite	Rb/Sr	2270 ± 90 (2222) (0.7092 ± 54)	Sarkar S. N. <i>et al</i> ; (1981)	Empl. (phase II)
15	Barugudam (Bastar)	Granitic rock	Rb/Sr	2237 ± 70 (0.7318 ± 0.0049)	Pandey <i>et al</i> ; (1989)	Empl

A S. No.	B Location	C Rock type	D Method used	E Age (in Ma)	F Source	G Remark
16	Maspur (Bastar)	Maspur metalava WR Abujhmar Group	K/Ar	2217	*	Thermal impress
17	Amgaon	Biotite gneiss, WR isochron age (Amgaon belt)	Rb/Sr	2170 \pm 60 (2124)	Sarkar S. N. <i>et al</i> ; (1981)	Thermal impress
18	Bastar	Metalava (amphibolite) WR, Bengpal Group	K/Ar	2167	Sarkar S. N. <i>et al</i> ; (1967)	Empl.
19	Bailadilla and Bengpal	Muscovite pegmatoidal gneiss intruding Bengpal group, Bailadilla	K/Ar	2112 (2043)	Sarkar S. N. <i>et al</i> ; (1967)	Empl.
20	Barsur	Granite plutons in the migmatitic gneiss	Rb/Sr	2101 \pm 323 (0.750 \pm 0.042)	Sarkar, A <i>et al</i> ; (1990)	*
21	Amgaon	Biotitic gneiss (biotite)	Rb/Sr (mineral age)	1640 (1605)	Sarkar S. N. <i>et al</i> ; (1981)	Thermotectonic impress
22	Keskal	Granite	Rb/Sr	1639 \pm 40 (0.7632)	*	Empl.
23	Amgaon	Biotitic gneiss (biotite)	Rb/Sr	1590 (1556)	Sarkar S. N. <i>et al</i> ; (1981)	Thermotectonic impress
24	Tongpal	Stanniferous pegmatite (muscovite)	Rb/Sr	1573 \pm 35	*	Thermotectonic impress
25	Mundval	Stanniferous pegmatite (muscovite)	Rb/Sr	1528 \pm 57	*	Thermotectonic impress
26	Dongribuzurg	Tirodi gneiss Dongribuzurg, Bhandara (MP)	Rb/Sr	1525 \pm 70 (0.7148 \pm 0.033)	Sarkar S. N. <i>et al</i> ; (1986)	Age of formation by granitisation
27	Dongargarh	Granite (WR+Mineral)	Rb/Sr	1480 \pm 40 (1499) (0.7641 \pm 0.025)	Sarkar S. N. <i>et al</i> ; (1981)	Thermotectonic impress
28	1-6 km WNW of Amgaon	Biotite gneiss (biotite)	Rb/Sr	1460 (1429)	Sarkar S.N. <i>et al</i> ; (1981)	Thermotectonic impress

A S. No.	B Location	C Rock type	D Method used	E Age (in Ma)	F Source	G Remark
29	Dongargarh	Granite (WR + Mineral)	Rb/Sr	1460 \pm 60 (1429) (0.7753 \pm 0.05)	-do-	-do-
30	Maspur (Bastar)	Maspur metalava WR, Abujhmar group	K/Ar	1456	*	*
31	Dongargarh	Granite (WR + Mineral)	Rb/Sr	1450 \pm 50 (1419) (0.7753 \pm 27)	Sarkar, S. N. <i>et al</i> ; (1981)	Thermotectonic impress
32	NE of Paliam	Stanniferous pegmatite (biotite)	Rb/Sr	1385 \pm 26	*	-do-
33	Paliam	Granitic rock (biotite)	K/Ar	1345 \pm 22	Anon (1978a)	Thermal impress
34	Bastar (Abujhmar group)	Dolerite dyke, Wr intruding Abujhmar group	K/Ar	1259	*	*
35	Bastar (Abujhmar group)	Plagioclase, dolerite dyke intruding Abujhmar Group	K/Ar	1243	*	*
36	Bastar (Abujhmar group)	Dolerite dyke WR intruding Abujhmar group	K/Ar	1228	Sarkar, G <i>et al</i> ; (1986)	*
37	Amgaon	Amphibolite WR, Amgaon group		1220 (1178)	*	*
38	Amgaon	-do-		1150 (1105)	*	*
39	Tongpal	Pegmatite (mica)	Fission track	775 \pm 67	*	*
40	Mundval	Pegmatite (muscovite)	-do-	769 \pm 65	*	*
41	Paliam	Stanniferous pegmatite (biotite)	-do-	697 \pm 60	*	*

Note:- (Col. E) age data in Ma in the first line. Bracketed number indicate ages recalculated following new decay constants recommended by IUGS. In the second line initial $^{87}\text{Sr}/^{86}\text{Sr}$ ratio for Rb/Sr isochron ages. Errorchron ages (MSWD>5) are indicated by (E)

Col. G) Primary events- age of crystallization (Xn) / emplacement (empl.) / effusion (Eff.).

Secondary events- age of secondary thermal / thermotectonic (deformation / regional metamorphism) event

Table 2.6. Geochronostratigraphy of Southern Bastar (compiled from Published Geochronological Data)

	Age (Ma)	Rock types and its locality	Remarks
Pegmatite	697 ± 60	Biotite, Stanniferous pegmatite in the Paliam	Fission track method
	769 ± 65	Muscovite, pegmatite in the Mundval	Fission track method
	775 ± 67	Mica, pegmatite in the Tongpal (Bastar)	Fission track method
Dolerite	1259 – 1228	Dolerite dyke, WR, intruded into the Abujhmar Group – K/Ar	
Pegmatite	1385 ± 26	Biotite, stanniferous pegmatite in the Ne of Paliam - Rb/Sr	Thermotectonic impress
	1573 ± 35	Muscovite, stanniferous pegmatite in the Tongpal - Rb/Sr	Thermotectonic impress
	1528 ± 57	Muscovite, stanniferous pegmatite in the Mundval - Rb/Sr	Thermotectonic impress
	1560 ± 35	Muscovite, mineralised pegmatite (Sn, Nb, Ta, Be - Rb/Sr and Li) intruded into metabasic in the Govindpal	Av. Muscovite age=1622 Ma (Ramesh Babu 1990)
	1588 ± 35	Muscovite, mineralised pegmatite (Sn, Nb, Ta, Be) - Rb/Sr intruded into metabasic in the Mundval	
	1732 ± 40	Muscovite, mineralised pegmatite (Sn, Nb, Ta, Be) - Rb/Sr intruded into metabasic in the Mundaguda	
Granite and pegmatoidal gneiss	2101 ± 323	Granite pluton in the migmatitic gneiss, Barsur	- Rb/Sr
	2112 (2043)	Muscovite, pegmatoidal gneiss intruding Bengpal Group and Bailadilla	- K/Ar Emplacement
Metabasic intrusive	2167	Amphibolite(metalava, WR, Bengpal Group)	- K/Ar
Metabasalt	2217	Metalava (Maspur, WR, Abujhmar Group)	- K/Ar Thermal impress
Bengpal	2275 ± 80	Granitic rock (Paliam and Darba)	- Rb/Sr
	2530 ± 89	Leucosome from migmatite (Katekalyan)	- Rb/Sr
	2409 ± 148	Pegmatoidal granite intrusive into gneisses (Sukma-Kondagaon)	- Rb/Sr
	2528 ± 110 (E)	Migmatite gneiss	- Rb/Sr
	2610 ± 143 (E)	Granite (Sukma – Kondagaon)	- Rb/Sr Emplacement
	2636 ± 489 (E)	Granite gneiss	- Rb/Sr Thermotectonic impress
Sukma	3018 ± 61 (E)	Granite gneiss	- Pb/Pb
	3511 ± 155	Migmatite gneiss	- Pb/Pb
	3610 ± 336	Trondjemite gneiss	- Rb/Sr

PETROGRAPHY

3.1. Introduction

The present chapter deals with the petrographic description (megascopic and microscopic studies) of the different rock types present in the study area.

3.2. Metasediments

3.2.1. Andalusite sericite schist (A.S.S.)

Megascopically, this rock type is ~~usually present as~~ medium to fine-grained ~~texture~~ in which prismatic and nodular crystals of andalusite tabloids are embedded (Plate IV, Fig. A). The colour varies from light yellow to greyish, but at places, it becomes light coloured mainly due to the development of porphyroblasts of andalusite and sericite. The andalusite tabloids are mainly chiasolite and are of variable shape and size (Plate IV, Fig. B).

In thin section, this rock unit shows the following mineral compositions (in the order of ~~decreasing~~ abundance) viz; muscovite, biotite, quartz, andalusite, sericite, opaques and apatite. The rock shows well-developed schistose structure, where schistosity is mainly defined by the preferred orientation of the mica minerals.

Muscovite is ~~present as medium to fine-grained~~, colourless and mostly aligned along the preferred orientation. In few thin sections, the muscovite flakes are microfolded in nature particularly when it is associated with large porphyroblasts of andalusite (Plate IX, Fig. B).

Biotite is usually medium-to fine-grained, characterised by one set of cleavage in prismatic sections. It shows strong pleochroism i.e., light brown to dark brown. The petrographic studies point the different stages of alteration of the biotite, which develop secondary chlorite, and fine dusty aggregate of opaque iron oxides.

Quartz is represented by medium-to fine-grained subhedral to anhedral shape. The presence of undulose extinction in quartz indicates the strain effect due to the post-tectonic deformation.

Andalusite is present usually as large porphyroblasts sometimes-symmetrical rhombic crystals. In few andalusite, the inclusions of carbonaceous materials as well as small needle-shaped grains of sericite were noticed. Inclusions in porphyroblasts of andalusite and groundmass within the same matrix point the incomplete growth and continuation of replacement processes of metamorphism. (Plate IX, Fig. A). The andalusite tabloids were also altered to sericite to some extent (Plate IX, Fig. B). Most of the tabloids trend parallel to the foliation planes of schistose rock. Andalusite shows high relief, low birefringence and first order grey colour.

Opagues are fine-grained, usually present as aggregate clusters of magnetite. This is supported by the presence of brownish yellow ~~patches of~~ limonitic material in and around the magnetite grains. The leached opaques usually show the sieved structure.

Apatite is quite restricted in this rock type. It ^{occurs in} ~~is represented as~~ small, colourless grains having more or less anhedral shape. It is characterized by low relief and first order interference colour. At times, the hexagonal cross-sections of the apatite mineral are observed to be isotropic.

The textural study and its metamorphic assemblage of andalusite-sericite-biotite-chlorite-quartz indicate its development under low-grade metamorphic facies conditions.

3.2.2. Quartz sericite schist (Q.S.S.)

It is grey to dirty white and is characterised by medium-to fine-grained minerals of quartz and mica. Tiny, flaky and shining mica are frequently present as thin alternate bands with quartz (Plate IV, Fig. C) along the schistosity plane.

The microscopic characters of this rock depict the preferred orientation of quartz and mica, which imparts the clear schistosity. Quartz being the most dominant (35 to 70%) constituent the other minerals is sericite, biotite and iron oxides.

Quartz is highly strained which is defined by intense wavy extinction. It also occurs as mixed quartz grains ranging in size from tiny particles to coarse-grained. The tiny flakes of sericitic mica are present as inclusions in the quartz.

Sericite is the next abundant mineral to quartz and shows preferred orientation (Plate IX, Fig. C). Its textural analysis indicates that sericite is crystallized under low-grade metamorphism through alteration of feldspars originally present in the sediments.

Biotite is medium-to fine-grained and it is characterised by flaky orientation (Plate IX, Fig. D) along the schistosity planes.

Opaque constituents apparently seem to be of two types; one is subhedral to anhedral fine-grained magnetite, whereas another is occurring as material of brownish colour along the margin of the magnetite.

3.2.3. Banded ferruginous quartzite (BFQ)

Megascopically, the BFQ shows the wide variation in characters like colour and thickness of bands. It shows variation in bands from dark green (grunerite) to brownish black (magnetite) colour. Banded magnetite quartzite

(B.M.Q) and grunerite magnetite quartzite (G.M.Q) show the alternate variation colour bands ranging from 1.0 mm to 5.0 mm in thickness (Plate IV, Fig. D). The magnetite bands are very thin in comparison to grunerite bands. At times, the thickness of grunerite bands is exceeded to the thickness of the quartzite bands.

Microscopically, the minerals recorded in the order of decreasing abundance; grunerite, quartz, magnetite, hornblende, mica and epidote etc.

Grunerite crystals show the prismatic, bladed forms, but sometimes occur as acicular to fibrous in nature. It is colourless with high relief in ordinary light (Plate X, Fig. B) but shows high interference colours ranging from upper second order to low third order in cross nicol (Plate X, Fig. C). Prismatic crystals show low first order colours. The extinction angle of grunerite varies from 10° to 15° . The polysynthetic twinning is characteristic feature of grunerites. It also contains inclusions of iron oxide.

Quartz shows coarse-to fine-grained and subhedral to anhedral form. The quartz grains boundaries are somewhat fractured which are filled by mica and quartz (Plate X, Fig. D). Quartz also shows corrosive structure.

Magnetite is present as coarse-to fine-grained and black in colour. It exhibits banded nature (Plate X, Fig. B). Magnetite inclusions are found in the amphiboles, but could not be recorded in the grains of quartz. The other types of iron oxide such as limonite, is characterised by brownish yellow to pale brownish colour as a patchy occurrence (Plate X, Fig. A).

Hornblende shows prismatic to needle shape crystals. It shows various shades of green colour (Plate X, Fig. B). The scheme of pleochroism and pleochroism formula can be denoted by:

X-pale green; Y-yellowish green; and Z-bluish green, hence

Absorption formula is $X < Y < Z$.

It is noted that the hornblende is found as rims of the grunerite grains (Plate X, Fig. C).

Chlorite is pale brownish to green in colour. It shows the retrograded texture in and around the amphiboles.

3.3. Metabasic extrusives (MBE)

Megascopically, this rock is characterised by very fine-grained, massive form and dark gray colour, with the presence of amygdules (Plate V, Fig. A). The vesicular structures were also noticed which are rounded to ellipsoidal in shape. The vesicles present in the rock, which are filled with some secondary minerals like quartz and other minerals.

In thin sections, the rock shows green mass of fibrous amphibole. Sometimes the amphibole shows alteration into chlorite, zoisite and iron oxides. Amygdules of metabasalts are filled with aggregates of quartz, zoisite, epidote and also cluster of the fibrous amphibole.

The following mineral constituents are observed in order of decreasing abundance; amphiboles, plagioclase feldspars, chlorite, quartz, epidote, iron oxide and leucoxene.

Two types of hornblende in the rock represent amphibole. The first type of hornblende showing light pale yellow with clear two set of cleavages and it is found as inclusion in light green variety of amphibole. At places, the light pale yellow variety of hornblende has been noticed replacing the second type light green hornblende. Thus, these two types of amphiboles are present in vice-versa relation (Plate XI, Fig. D). The pyroxenes (augite) are changed into amphibole (actinolite). The actinolite variety of amphibole is represented by the strong pleochroism from pale green to green. (Plate XI, Fig. B). Hornblende also contains the aggregate of fine inclusions of the sericitised

plagioclase. The chloritisation of amphiboles is observed at the periphery and at times along the parallel to the parting and cleavage traces.

Plagioclase feldspars are mostly altered to sericite. At places, the small needles of plagioclase are also observed in the rock (Plate XI, Fig. A).

Chlorite occurs as small patches, sporadically distributed and has appeared due to the alteration of amphiboles. It shows berlin blue interference colours.

Quartz is found as accessory with very small anhedral grains in the rock. The quartz is present in the vesicles as secondary fillings (Plate XI, Fig. C).

Epidote is present as granular aggregates. In polarised light, epidote shows colourless and high relief, but in cross nicol, it shows variegated violet, blue and pink colours. It occurs mainly as alteration product of plagioclase feldspars. At places, epidote as secondary mineral filled the vesicles of the rock (Plate XI, Fig. A, B and C).

Iron Oxides are noticed as a leached product along the cleavage traces of the amphiboles. Occasionally, the magnetites show the sieved structure.

Leucoxene occurs as alteration product of ilmenite. At times, complete pseudomorphs of ilmenite are observed. The skeleton crystals of leucoxenes are filled by the quartz and epidote.

3.4. Metabasic intrusive (MBI)

Megascopically, metabasics are usually medium-to fine-grained, mostly dark in colour and compact. In some places, the grain size becomes coarse which can be termed as metagabbro, while the fine-grained variety

may be designated amphibolite (Plate V, Fig. B). Sometimes the metabasics were intruded by the pegmatite veins with cassiterite grains. (Plate V, Fig. C).

In thin sections, the metabasic of the coarse-grained variety is characterised by porphyroblastic to blasto-ophitic texture. The metabasics are mainly composed of hornblende and plagioclase feldspars together with other accessories. The proportion of mafic to felsic minerals is about 2:1.

The petrographic studies of these rock units yield amphiboles as major constituents followed by plagioclase, biotite, quartz, epidote as subordinate minerals. At places augite, zircon, sericite, chlorite and iron oxides were also noticed:

Hornblende is present as the most abundant mineral and shows wide variation in grain size. Usually, it is medium-grained, although small prismatic needles of the amphiboles are also present. In the nearly unaltered coarse metagabbroic rocks, the pyroxene crystals seem to have quite large size. (Plate XII, Fig. C).

The hornblende pleochroism shows following characters;

X (pale green) < Y (yellowish green) < Z (bluish green).

The amphibole shows typical second order interference colour and oblique extinction of about 16° . The small inclusions of biotite, sphene, zircon and fine-grained opaques are enclosed within the hornblende (Plate XII, Fig. A). Alteration of hornblende into chlorite is also recorded in many thin sections. The actinolite is present in acicular form and sometimes as crudely radiating pattern (Plate XII, Fig. A). It shows weak pleochroism in shades of green.

Plagioclase feldspars are present as laths from small to large in size. Calcic plagioclase completely becomes saussuritised, giving rise to albite and small granular epidote and sericite (Plate XII, Fig. D). The myrmekitic intergrowths of quartz (myrmekite) and plagioclase (oligoclase)

are also recorded in the rock (Plate XII, Fig. C), due to the replacement of K-feldspar by plagioclase with release of silica. Such type of texture may be possibly related to the presence of hot hydrothermal fluid enriched with Na_2O solution during the later stage of cooling.

Biotite occurs in close association with hornblende. The colour of the biotite is pale brown and its pleochroism varies from pale to deep shades of brown.

Quartz is present as small inclusions in hornblende and biotite and also shows myrmekite intergrowth with feldspar.

Epidote is colourless with high relief. The interference colour of epidote is pinkish to pale green. It represents the granular aggregates of anhedral grains.

Sphene is medium-to fine-grained and shows high relief with dark outlines (Plate XII, Fig. C). Sometimes, the clustering of fine-grained sphene at one place gives a rhombic crystal outline, mainly associated with amphibole.

Augite is present as coarse-grained. It is surrounded by hornblende and epidote and rarely by tremolite-actinolite. The presence of relict augite indicates that pyroxenes have not been completely altered to form amphiboles under the influence of metamorphism (Plate XII, Fig. B).

Zircon is found as inclusions in hornblende forming the halos.

Sericite is present as tiny flakes in plagioclase feldspars. The abundant sericites were occurred due to strong hydrothermal activity.

Chlorite has been recognised as two types in origin. One is derived from the alteration of biotite, showing the pseudomorphic occurrence, which retain of pleochroic halos, while other type of chlorite occurs as patches around hornblende (Plate XII, Fig. A) with pale brownish green colour.

Clinozoisite shows medium-to fine-grained aggregate. It shows the abnormal polarization colours around the leucoxene.

Opaques are present within amphiboles and sphene. Limonite material is also observed as yellowish brown to reddish brown in colours due to the alteration of biotite.

3.5. Granitoids [granite (KG) and granite gneiss (KGG)]

Megascopically, the granites (KG) appear to be medium-to fine-grained leucocratic to mesocratic rocks. The coarse-grained variety is observed at certain places. In a few samples, fractures were also observed. Such fractured and sheared granite is usually coarse-grained in which mylonite patches of different sizes were noticed. Along the contact, linear arrangement of flaky minerals with developed folded bandings of quartzofeldspathic masses is seen in rocks (Plate V, Fig. D). At some places, granite gneiss (KGG) show the development of linear and straight alternate banding of leucocratic and melanocratic minerals as lit-par-lit relation thereby appearing somewhat gneissic (Plate VI, Fig. A). Dome-like hillocks are quite common in the study area.

Based on textural, structural and mineral compositional, the granitoids can be classified into two broad groups viz. non-foliated and foliated types. The non-foliated granites (KG) are medium-to coarse-grained and leucocratic in nature. However, at places fine-grained variety appears aplitic in character (Plate VII, Fig. A). Large feldspathic patches are found to lie in a fine-grained groundmass containing quartz, mica and iron oxides (Plate VII, Fig. B). Feldspathic augens measuring up to 3 c.m. \times 1.5 c.m across are also encountered. The minerals identifiable in hand specimens are quartz, feldspars and biotite. But some samples of granite near or at contact with pegmatites, contain tourmaline (Plate VI, Fig. C) and also hornblende (Plate VI, Fig. D). Among the ferromagnesian minerals, hornblende is

subordinate to biotite but occasionally can be noted as an important constituent in some varieties.

The foliated granite is present in the foliation plane that contains quartzo-feldspathic bands showing more or less preferred orientation with alternate micaceous bands. In biotite-rich variety, the mica bands are often continuous as waning and waxing patterns along the direction of foliation planes and the quartzo-feldspathic portions form small lenticular patches along these planes. In some varieties, pegmatite veins, consisting of quartz and feldspar cut-across the gneissic foliation at an angle confirming later origin of pegmatite.

Microscopically, the texture is typically igneous i.e. hollocrystalline, hypidiomorphic, allotriomorphic, fine-to medium-grained and equigranular. Both preferred (Plate XIII, Fig. A, B) and non-preferred orientation (Plate XIII, Fig. C) are also recorded in the flaky minerals. Porphyritic texture is however shown by quartz and feldspars (Plate XIII, Fig. D). These phenocrysts appear to be formed prior to the quartzo-feldspathic constituents of the granite. Subsequently these phenocrysts might have introduced along the contact of the granite and have attained the large size with subsequent pegmatitic emplacement. There is wide range of variation in the grain-size of constituent minerals in such cases. Thus very tiny grains of quartz and feldspars are also found to occur along with coarse-grained quartzo-feldspathic mass, which has resemblance with mylonitic structure (Plate XIV, Fig. A). At the contact of granite and pegmatite, highly crushed, fine-grained quartzo-feldspathic mass is accompanied with tiny greenish biotite crystals often associated with cassiterite. Such greenish variety of biotite is indicative of pneumatolytic action (Plate XIV, Fig. B).

The granite gneiss (older lithounit referred to as KGG) is characterised by development of foliation and the flaky minerals like biotite together with quartz and feldspars showing distinct preferred orientation. It shows foliated structure and large augens. These augens are made up of

quartz or quartzo-feldspathic constituents. The textural relation indicates that the augens have been emplaced within the gneissic rocks along their bandings.

The microstructural features of individual mineral constituents of granitoids are described below:

Orthoclase, microcline and plagioclase feldspars represent feldspars in the KG and KGG. The feldspars show intense alteration to sericite and as such it may be presumed that it was originally orthoclase and/or a little microcline (Plate XIV, Fig. C). At places, sericitic altered grains of untwined to twinned nature of orthoclase and occasionally Carlsbad twinned crystals (Plate XIV, Fig. D) are also recognized. Most of the microcline observed in the KG and KGG is fresh and coarse-grained and shows well developed crosshatched twinning after the albite and pericline laws. Microcline-perthite (Plate XV, Fig. A) appears to be medium-to coarse-grained. The host mineral is fresh microcline whereas the sodic intergrowths within the later are of albite or oligoclase composition and they are somewhat altered. The sodic intergrowths within microcline (Plate XV, Fig. B) might have subsequently under-gone alteration through the process of metasomatism. In bigger microcline, patchy intergrowth of albite shows lamellar twinning. The plagioclase feldspar is mainly albite composition. Sometimes albitic twin lamellae show distinct zoning, tapering and bundle shaped (Plate XV, Fig. C) and others are present as bent (Plate XV, Fig. D) with the development of minute microcline grains also.

Some grains of microcline are devoid of perthite intergrowth showing distinct crosshatched twinning. In plagioclase feldspar, the saussuritisation phenomenon is quite predominant, responsible for the formation of epidote. At some places, the perthitic texture (Plate XVI, Fig. B) is developed, because, albite lamellae are present within the large grain of altered orthoclase. The fine albite lamellae are observed as a microfaulted (Plate XVI, Fig. C) The hair perthite (Plate XVIII, Fig. D) texture also

observed. All the feldspars except the fresh microcline of shear zone show crushing recrystallisation and alteration. In such cases they are criss-crossed by veins and veinlets of irregularly running secondary silica (Plate XVII, Fig. A).

Quartz is the predominant mineral varying in grain size from medium-to fine-grained and belong to the granite proper whereas the large grains of quartz are found from pegmatites near the granite contact. Quartz grains show crushing at places and formation of different grain sizes varying from very fine grains to megacrysts. It shows undulose extinction (Plate XIV, Fig. B) due to strain effect. Thin veinlets and cracks are noted in quartz grains, which are later filled with secondary silica and feldspathic solutions. The phenocrysts of quartz contains many tiny inclusions of other minerals namely, biotite, tourmaline, apatite, zircon and dot-like inclusions of opaques.

Biotite is predominating mineral among the accessory and occurs as medium-to coarse-grained prismatic crystals with brownish green to yellowish brown in colour (Plate XVI, Fig. A) and having strongly pleochroic. In the vicinity of mineralisation, biotite is found to be distinctly of brownish green colour (Plate XVII, Fig. B), which probably indicates the release of tin from the lattice of biotite. This tin subsequently gets oxidised to form as the ore mineral. Often patchy biotite, undergoing alteration, gives rise to dark green chlorite around the feldspathic mass, which is non-pleochroic (Plate XVII, Fig. C, D). In fracture zones, elongated biotite are found to be highly altered by vapour and gases. Apatite, epidote, quartz and sphene are poikilitically enclosed in biotite.

Muscovite often the same crystal of biotite is found to show continuation into muscovite having the same orientation. Such a case appears to be the replacement of biotite by muscovite particularly at border of the biotite grains (Plate XVII, Fig. B, C).

Cassiterite grains show random fractures and pleochroism from pale brown to deep brown. High order interference colours, particularly pink

(Plate XVI, Fig. B) and green are quite prominent. These cassiterite grains are intimately associated with altering biotite and also highly fractured rounded grains of brownish green biotite (Plate XVII, Fig. B).

Sphene is present usually as four-sided lozenge shaped grains with deep body colour showing weak but distinct pleochroism. Often it has been found that the mineral is developed as subhedral to anhedral grains with very dark margins and its associate with altered brownish green biotite.

Hornblende is present as large grains, which are leached into the iron-oxide ore in the same crystal outline (Plate XVIII, Fig. A). At places, hornblende is also changing into biotite along the periphery (Plate XVIII, Fig. B).

Apatite is quite frequent. This shows usual character of being colourless (silvery white) in thin sections and is represented mostly by more or less needles, small-six sided prismatic crystals with low relief hosted in biotite. Its basal sections are isotropic but less commonly elongated prismatic grains show first order gray colour. Apatite is also occurring as inclusions within quartz, feldspar, mica and hornblende (Plate XVIII, Fig. B,C). Abundant apatite proves the presence of phosphorous saturated volatile phase at the time of emplacement of leucogranite. Hence, apatite particularly the prismatic one is crystallized late in the sequence whereas the needle shaped apatite might have formed early in the sequence but relatively undercooled at the initial stage of felsic magmatism.

Zircon is mostly observed as inclusions within the nucleus of the pleochroic halos in hornblende granite (Plate XVIII, Fig. B and C). It also shows circular, colorless in the bleached portion of the prismatic flakes of biotite. Sometimes, elongated prismatic crystals having pyramidal faces are present within hornblende and feldspars. Zircon is distinguished from apatite by higher relief and stronger birefringence.

Tourmaline is found as comparatively rare accessory mineral in granitic rocks. At places, clusters of radiated needles of greenish tourmaline are observed giving an appearance like "tourmaline Sun" (Plate XIX, Fig. A, B). These needles of tourmaline on an intensive scale are suggestive of sustained pneumatolytic action through the introduction of boron.

Opaque (Magnetite/Ilmenite) is found abundantly either as patchy, irregular masses or rarely as subhedral crystals in the granitic rocks. It is also found as inclusions in quartz, feldspars, biotite, hornblende etc.

Sericite is the most predominant of all the secondary minerals noted in the granite/granite gneiss. The intense alterations of the potash and sodic feldspars through the process of the sericitisation have yielded tiny, flaky mineral in haphazard and random fashion and this alteration is taking place along the twin lamellae (Plate XIX, Fig. D). The intensity of sericitisation is increasing along the zones of fracture present in the granite body. It may be recorded that extensive activity of the volatiles during the late magmatic stage was mainly responsible for the widespread alteration of the feldspar. At places, the development of sericite is so intense that the original structure of the feldspars is difficult to be recognized.

Epidote grain is colourless, non-pleochroic with high relief the inference colour of epidote are pink, pale yellow, violet, blue etc. It is found to be usually an aggregate of anhedral grains occurring randomly in associate with quartz, hornblende and altered plagioclase feldspars (Plate XVIII, Fig. A,C). Its occurrence is notable around zones fracture, where it develops in appreciable quantity along with quartz. Hence it appears that the formation of epidote has been pronounced by the breakdown of the plagioclase feldspar, which has supplied the required calcium and aluminum during the course of fluid activity and alteration.

Chlorite is found as pale dirty greenish to brownish in colour mostly derived by the hydrothermal alteration of biotite (Plate XVII, Fig. A,D). Such chlorite patches are weakly pleochroic.

Limonite is present as patchy, skeletal and interstitial yellowish brown material in the KBG particularly around the altering biotite as well as iron oxides (Plate XIV, Fig. C).

3.6. Pegmatites (mineralised and non-mineralised)

Megascopically, three types of pegmatite viz., simple unzoned, recrystallised and metasomatic pegmatites are found emplaced with the Bengpal metasediments, granites, granite gneiss and metabasic intrusives.

The examination of mineralised pegmatite veins of the study area reveals that it is coarse to very coarse-grained rock, the individual mineral constituent, however, varying widely in grain-size from one specimen to another. The size of the mineral grains varies from few mm to >5cm. Large crystals of different minerals like quartz, feldspar, mica, beryl and cassiterite are found. In the mineralised pegmatites, feldspars are very coarse-grained and they occur usually with quartz, micas, cassiterite, beryl and fluorite etc. Both potash feldspars and plagioclase are usually slightly greyish white or milky white in colour.

Quartz is usually dirtied white in colour or colourless and transparent. Some other quartz-type i.e., smoky variety of massive quartz, which is locally developed within the dirty-white variety of quartz was particularly observed in the pegmatitic body in and around Katekalyan. Muscovite shows bright greenish-white colour, occurring as well developed books (Plate VII, Fig. C) and somewhat bleached. This may be due to the action of volatiles present during pegmatitic intrusions. Sometimes, specimens of lepidolite made up of fine-to medium-grained shows pale violet colour. It is usually occurring intimately associated with altering feldspars.

At some places, crude graphic texture (Plate VII, Fig. D) is noticeable in pegmatites, where quartz and feldspars are intergrown, having step-like relation shown by both the minerals. Cassiterite represented mostly

by discrete bipyramidal crystals and also by irregular masses in handspecimens (Plate VIII, Fig. A). Cassiterite shows brownish black to blackish gray colour. Sometimes crystals apparently show penetration twin in such a way that two individual crystals grow parallel to c-axis, one being partially within the other (Plate VIII, Fig. B). The common associations with cassiterite crystals are quartz, feldspar and mica. Columbite-tantalite shows black colour, sub-metallic to sub-resinous lustre. The fresh broken surface of crystal shows very brilliant lustre and uneven fracture. Streak of the mineral is black. Beryl occurs in hexagonal crystal forms, shows shining pale to whitish green colour, stained by pale yellowish brown colour. The garnet crystals along c-axis measures more than 1 to 4 cm have been noted in pegmatites. Fluorite occurs as small dot-like clusters of violet colour. They are found to be intimately associated with the mica zone of the pegmatites.

- (i) Essential minerals: Feldspar and quartz.
- (ii) Accessory minerals: Micas, cassiterite, columbite, tantalite, beryl, garnet, fluorite and sphene.

Microscopic characters

Feldspar is dominant mineral in pegmatites and is found as microcline, microcline-perthite, and orthoclase and then followed by albite-oligoclase and cleavelandite. Microcline is medium-to coarse-grained, euhedral to subhedral in shape. The grains are commonly fresh showing typical two sets of lamellar twinning on albite and pericline laws and characteristic cross-hatched (Plate XIX, Fig. C). Sometimes, spindle-shaped twinning as crosshatched in two sets nearly at right angles is also notable in microcline. The intergrowth of albite is confined to the twinned portions of microcline and this is particularly noted in such sections where some broad untwined bands alternate with fine cross-hatching bands. It is very interesting to note that the sericitisation has taken place along the crosshatched lamellae

of the microcline. Orthoclase is present in large rectangular crystals showing common simple twinning on Carlsbad law. Margins of orthoclase have altered to sericite. Sericite has also developed along the cleavage planes of the mineral. At places, these feldspars are being replaced by lithium mica. Feldspars often show the inclusions of quartz, mica and fine opaque. Microcline-perthite (Plate XIX, Fig. D) is found to be the intergrowth of microcline with subordinate albite. The fine vein lets or stringers of albite appear to be diffused unevenly in microcline.

Cleavelandite variety of albite shows well-developed twinning. Due to fracturing, its twin lamellae are not only micro-faulted but they become non-continuous (Plate XX, Fig. A). Cleavelandite consisting of large aggregate of laths is transversely cracked showing slightly bend and micro-faulting (Plate XX, Fig. B). Parallel to sub-parallel laths of cleavelandite show lamellar twinning after albite law. The twin lamellae are often varying in width and may be irregularly running with tapering ends, which ultimately makes them discontinuous. When cleavelandite encloses cassiterite its contact is often sharp and sometimes-small grains of cleavelandite are enclosed as inclusion within the peripheral region of cassiterite. Cleavelandite is believed to be formed due to metasomatic activity of sodium bearing vapors during the emplacement of the pegmatites. Therefore, the presence of cleavelandite strongly supports dominance of soda-metasomatism in the pegmatite.

Quartz of varying sizes encloses the minerals muscovite, feldspars, garnet and dust of the opaque as inclusions, which confirm that the quartz is the last mineral in the crystallizing sequence of pegmatites. At places, myrmeckitic texture (Plate XX, Fig. B) is developed by the intergrowth with plagioclase and vermicular quartz.

Mica is another important and dominant constituent and is represented by muscovite, sericite, lepidolite and biotite in the forms of books and also as small flakes associated with other minerals in the pegmatites. Primary muscovite occurs in thick tabular crystals and is perfectly fresh (Plate

XIX, Fig. C). The small flaks of muscovite (sericite) are present in the direction of cleavage planes in the feldspars (Plate XIX, Fig. D). The muscovite is of secondary origin and is an alteration product of feldspars. Lepidolite (Plate XX, Fig. C) appears to be micro-folded and usually show inclusions of cassiterite and other tiny opaque minerals. It is important to note that lepidolite occurs as inclusions as well as along the fractures of feldspars (perthite and plagioclase). Lepidolite is distinguished from muscovite in thin sections by its lower refractive index and characteristic body colour. Biotite shows variable colours from yellowish brown to brownish black. The brownish black variety of biotite shows feeble pleochroism and is invariably associated with opaque. Alteration of biotite gave rise to muscovite and also limonitic secondary minerals (Plate XX, Fig. D).

Cassiterite is brown to dark brown in colour and sometimes shows yellowish gray in polarised light. It shows pleochroism from colourless to dark brown. Its refractive index is very high and can be distinguished from other minerals by its straight extinction, high order interference colour. The presence of lithium mica within the fractures of cassiterite (Plate XX, Fig. C) indicates that while its crystallization the deformational forces were also acting upon them. During the regime of vapour stage, lepidolite got deposited within such irregular cracks and fissures. In some large twinned cassiterite crystals (Plate XXI, Fig. A) showing discrete zoning and different portions give rise to different shades of colour. Cassiterite is shown by both free and full of inclusions. Inclusions free cassiterite shows the colourless and brownish shades, whereas inclusion-bearing variety of cassiterite shows the dark red to brown red colour, which may be due to the intergrowth with Sn-Ta. The deep brownish-zoned portion shows the internal reflection, which is intense reddish brown. Such dark coloured portions of zoned cassiterite crystals usually have the composition of columbite $\{(\text{Fe}, \text{Mn})\text{Nb}_2\text{O}_6\}$ and tantalite $\{(\text{Fe}, \text{Mn})\text{Ta}_2\text{O}_6\}$ which form unlimited solid solution series. The columbite-tantalite is orthorhombic and the tantalum content is usually much higher than the niobium content.

Beryl is colourless, having very weak pleochroism noticeable only in thick section. Commonly criss-crossed fractures and cracks are present in the mineral. Fine opaque is present as inclusions.

Garnet is present as euhedral to subhedral shape, rhombododecahedral form, high relief, high refractive index and isotropic character (Plate XIX, Fig. C). Along its boundary, irregular cracks are found. Sometimes fine grains of opaque, muscovite and anhedral quartz grains as inclusions are noted within garnet.

Fluorite shows bluish colour patchy occurrence in the greisenised pegmatite (Plate XXI, Fig. C). At times, it is present as veins within fractured cleavelandite variety of albite (Plate XXI, Fig. D).

Sphene is found in a number of small aggregate grains in and around the mica flakes.

3.7. Quartz reef

Megascopically, the quartz reef appears to be of dirty white or grayish white and reddish brown in colour (Plate VIII, Fig. D).

Microscopically, it shows the rich clustering of opaque minerals.

3.8. Younger metadolerite dykes

Megascopically, these rocks appear as melanocratic, hard and compact in hand specimens. Granular, black crystals of pyroxenes with white or grayish white interstitial feldspars can be recognized (Plate VIII, Fig. C). Some specimens show schiller structure and often show alteration of greenish material, appearing as hornblende. Sometimes, bronzy biotite flakes are associated with pyroxene crystals.

Pyroxenes are the main mineral constituents of the rock but the major portion of the original mineral has altered. The pyroxene is dominantly

augite, which is nearly colourless, non-pleochroic, having low birefringence, fine parting lines and straight extinction. Often the core region of enstatite crystals might have been originally composed of pleochroic hypersthene which on alteration has given rise to schiller structure containing dusty titaniferous magnetite in the central portion of the pyroxene (Plate XXII Fig. A).

Plagioclase feldspars are present as long laths of labradorite. The maximum-recorded extinction angle is 32° , which identifies it as labradorites (Plate XXII, Fig. B), which are slightly cloudy showing the initial stage of alteration.

Magnetite is present as black opaque coarse grains along the cleavage planes of pyroxene (Plate XXII, Fig. A, B, C). Sometimes, biotite flakes showing the inclusion of more or less subhedral magnetite, which may be usually along the cleavage planes or rarely across it.

Uralite includes fibrous, yellowish brown amphibole and is found as alteration of pyroxene. Sometimes, relicts of the original pyroxene may be found embedded within uralite (Plate, XXII, Fig. B). The pleochroism of uralite is not intense but distinct from pale yellow to yellowish brown.

Biotite is usually occurring in clusters of flakes showing pleochroism from pale yellow to dark reddish brown (Plate XXII, Fig. D). Sometimes, it surrounds the uralite and formed along cleavage planes of pyroxene.

the study
ing in NW

er (ASS)
el group
an area

they stop

the band
ite rich
m distal

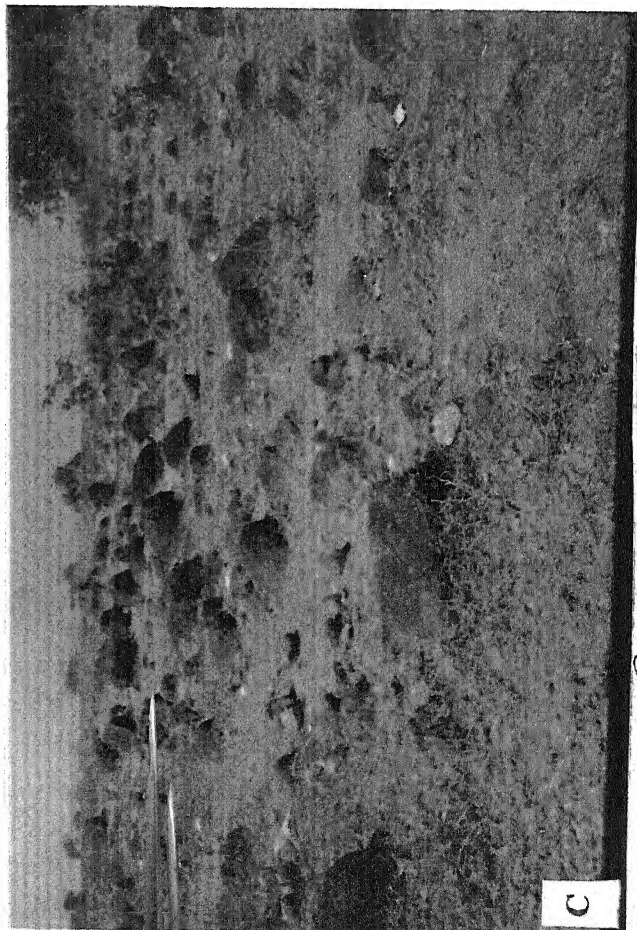
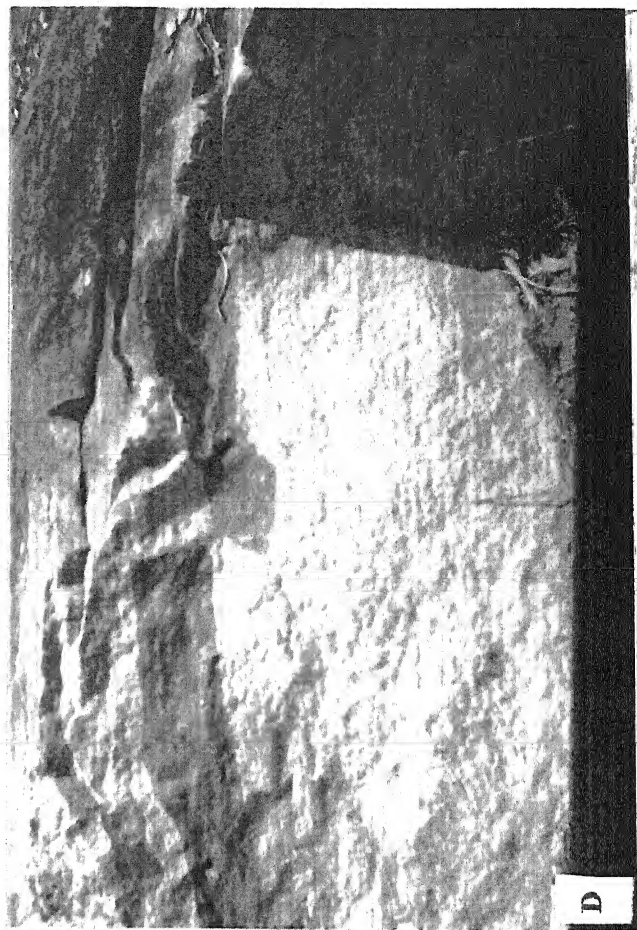
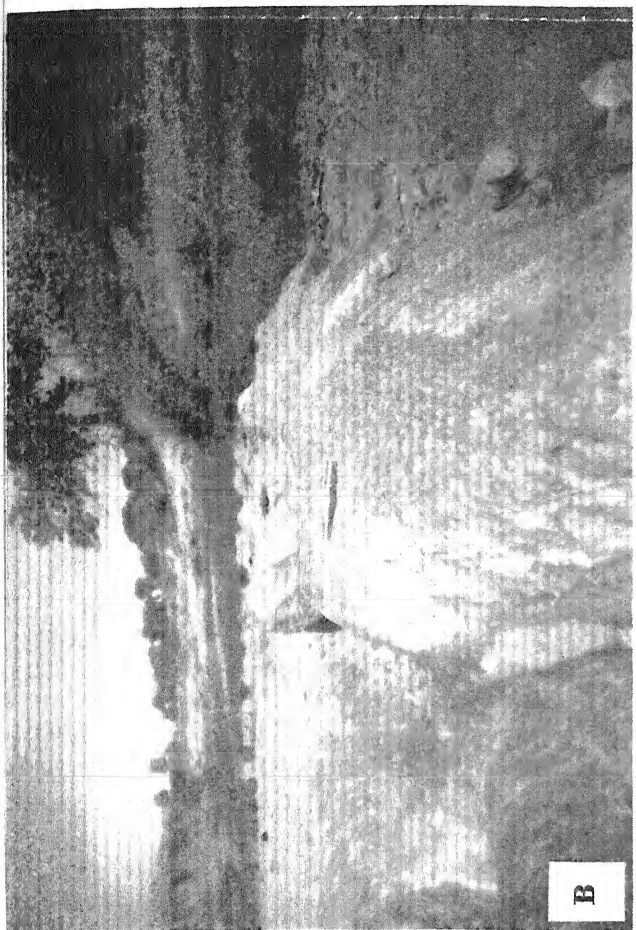


PLATE - I

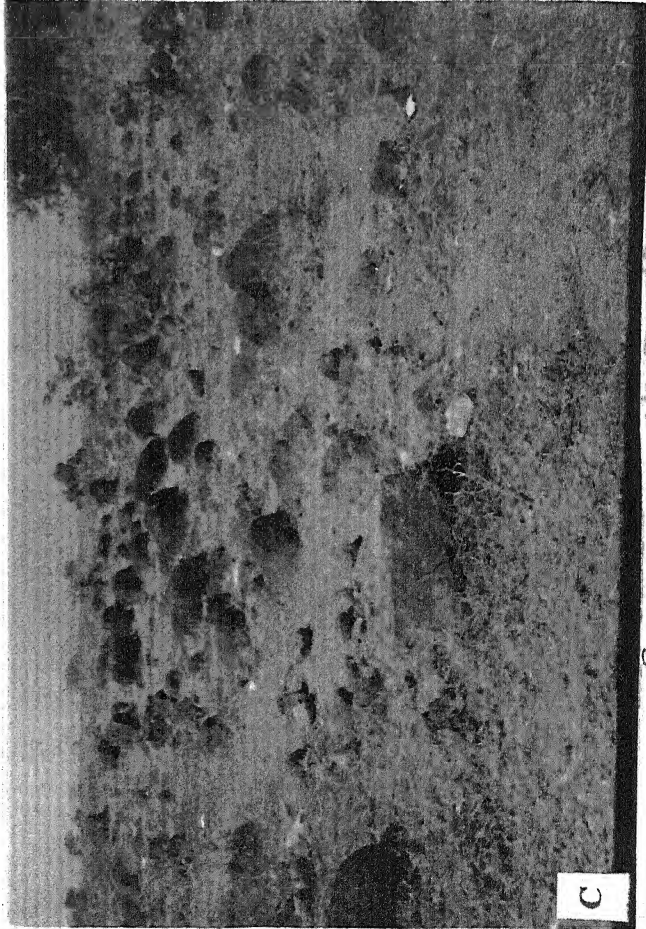
- Fig (A): Field photograph showing the panoramic view of the study area. In the distance background different hillocks are trending in NW-SE in the south of mineralized belt.
- Fig (B): Field photograph shows the andalusite-sericite schist (ASS). This litho unit shows the older metasediment of the Bengpal group and mainly exposed along the Dumam nadi of the Katekalyan area.
- Fig (C): Field photographs show the pillow basalt (rounded to kidney shaped of 30 -70 cm in diameter) exposed near Tumakpal.
- Fig (D): Field photograph shows the granite gneiss (KGG). The bands of leucocratic (quartzo-feldspathic) and melanocratic (biotite rich) in granite gneisses (KGG) exposed at Benglur village, 1.5 km distance in west from Katekalyan town.



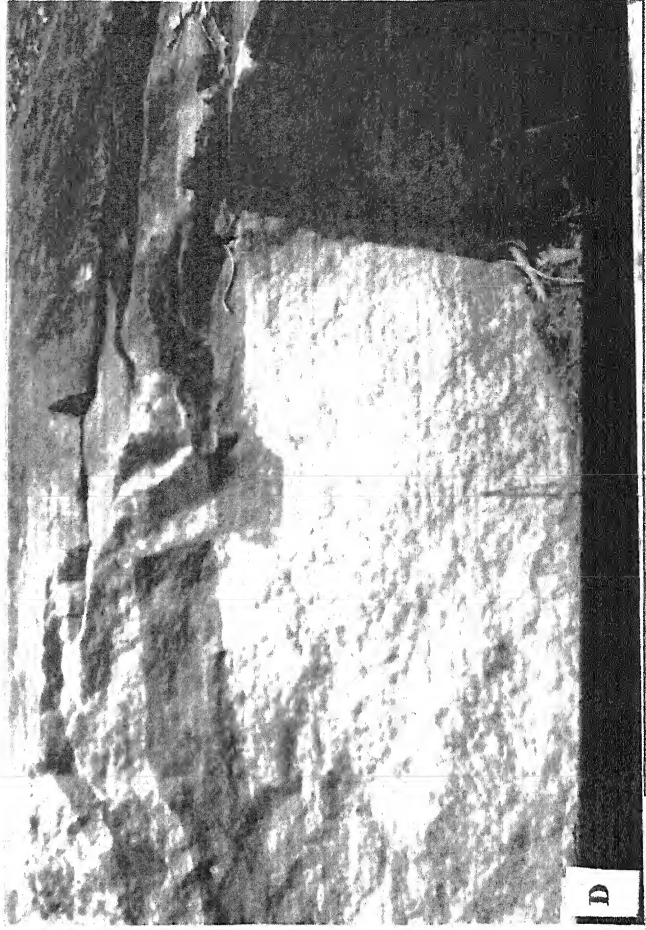
A



B



C



D

PLATE - II

- Fig (A): Field photograph of granite gneiss (KGG) exposures (western part of Kusapal village) trending mostly along the NNW-SSE direction as dome shaped hillock, in which flow of magma of quartzo-feldspathic compositions are clearly seen.
- Fig (B): Field photograph shows the contact of older foliated granite gneiss (KGG) terrain and younger non-foliated granite (KG) as intrusive near Tumakpal village. The pegmatite vein is only traversed in the foliated granite gneiss terrain (KGG)
- Fig (C): A field photograph of minerlised pegmatite vein intruded into the metabasic rock near Kondaras Dongri.
- Fig (D): Field photograph of large dimension of the minerlised pegmatite vein traversed in the granite rocks (KG) along the nala. It is exposed at the distance of 1 km. south from the Pinjupara village.

PLATE-II

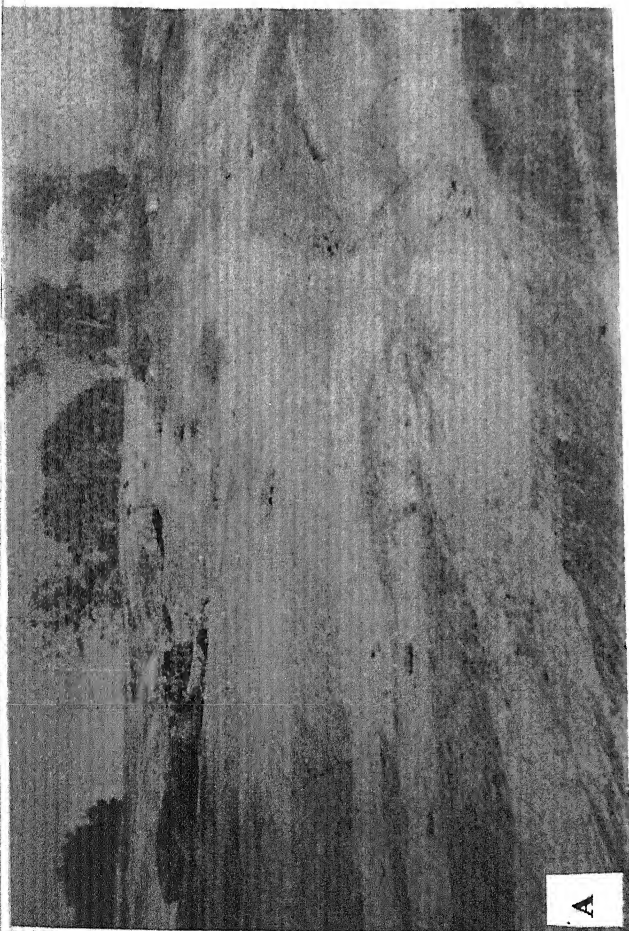


PLATE - III

- Fig (A): Field photograph shows the mineralised pegmatite vein in large dimensions where exploratory work like dug and picking of cassiterite is going on near Kondaras Dongri.
- Fig (B): Field photograph in the giant metadolerite dyke, trending NW-SE direction exposed at near Kusapal village.
- Fig (C): Field photograph of the quartz reef in shear zone. This reef runs 3 km. long from Benglur to Gatam village.
- Fig (D): Field photograph shows the mining of placer deposit of cassiterite with the help of sieving and panning method by the tribes of Kondaras Dongri.

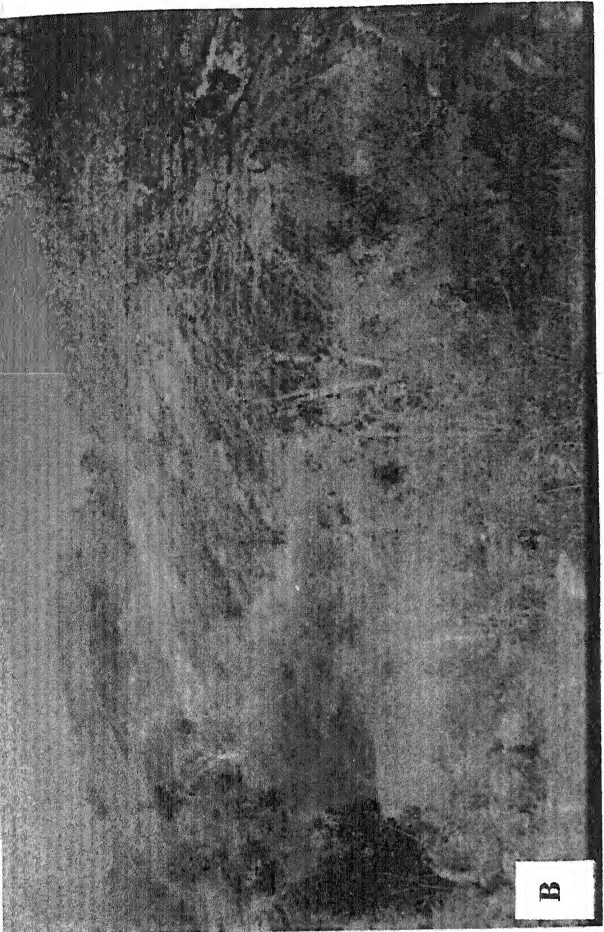


PLATE - IV

Fig (A): Hand specimens photograph of the andalusite sericite schist (ASS). The andalusite tabloids are embedded very conspicuously in the rock.

[Ref. No. F/92, A and F/106,c]

Fig (B): Hand specimen (polished portion) of the ASS. The chiasolite varieties of the andalusite tabloids are present as prismatic to nodular forms.

[Ref. No. F/116, B]

Fig (C): Hand specimens photograph of quartz-sericite schist (QSS), where laminations are clearly seen.

[Ref. No. F/106, A and F/79]

Fig (D): Hand specimens photograph of the banded magnetite quartzite (BMQ) and grunerite-magnetite-quartzite (GMQ). It shows the displaced alternate bands of brownish black to dark green of 1 mm. to 5 mm. in thickness. The magnetite (brownish black) bands are very thin in comparison to grunerite (dark green) bands and also vice-versa.

[Ref. No. R89/503 NY6]

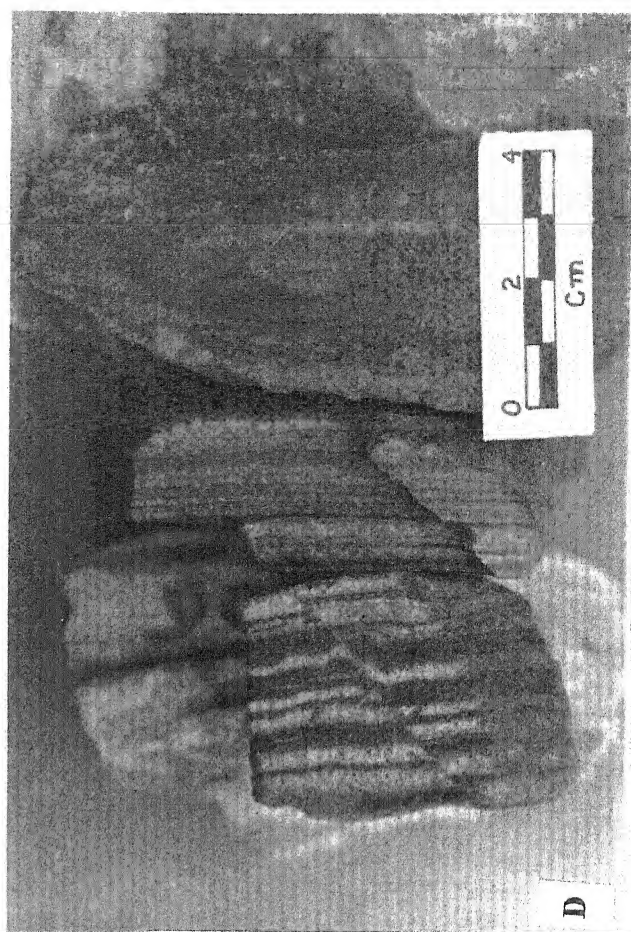
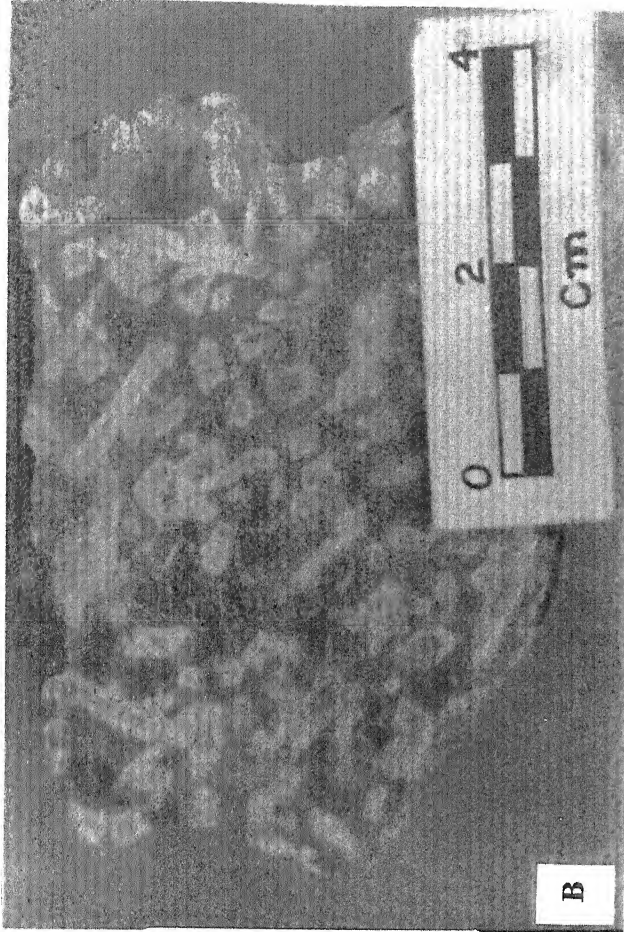
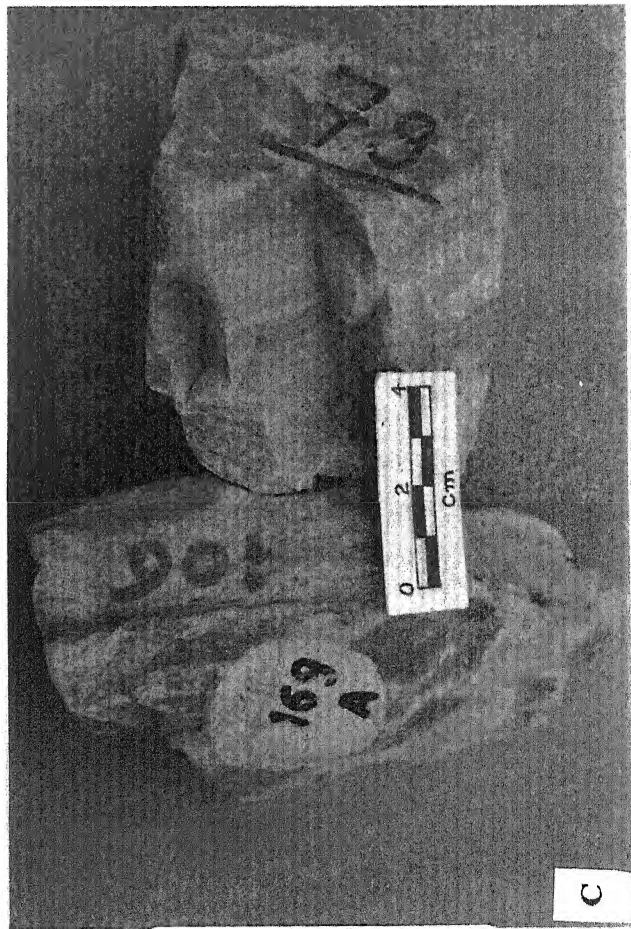
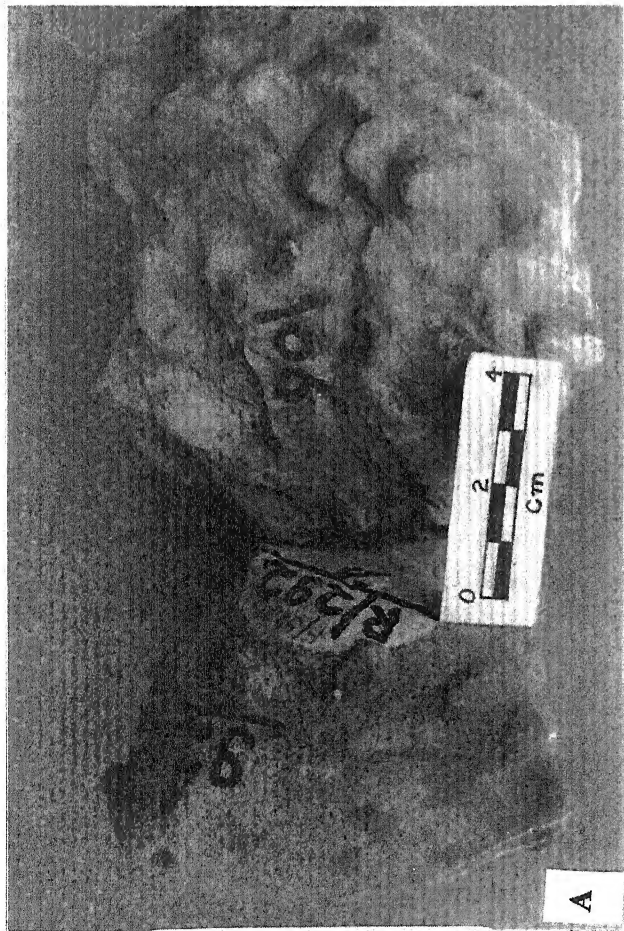
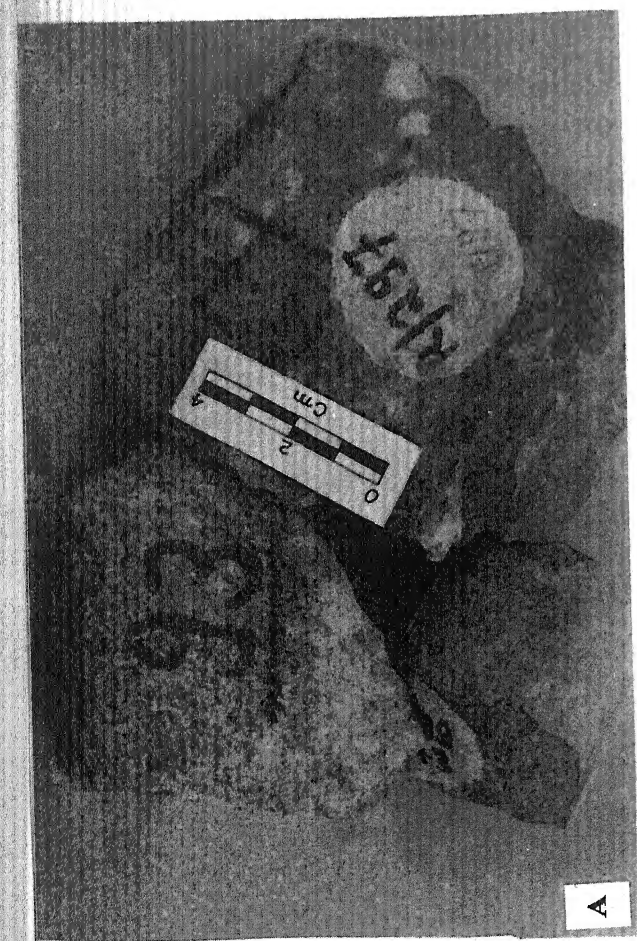


PLATE - V

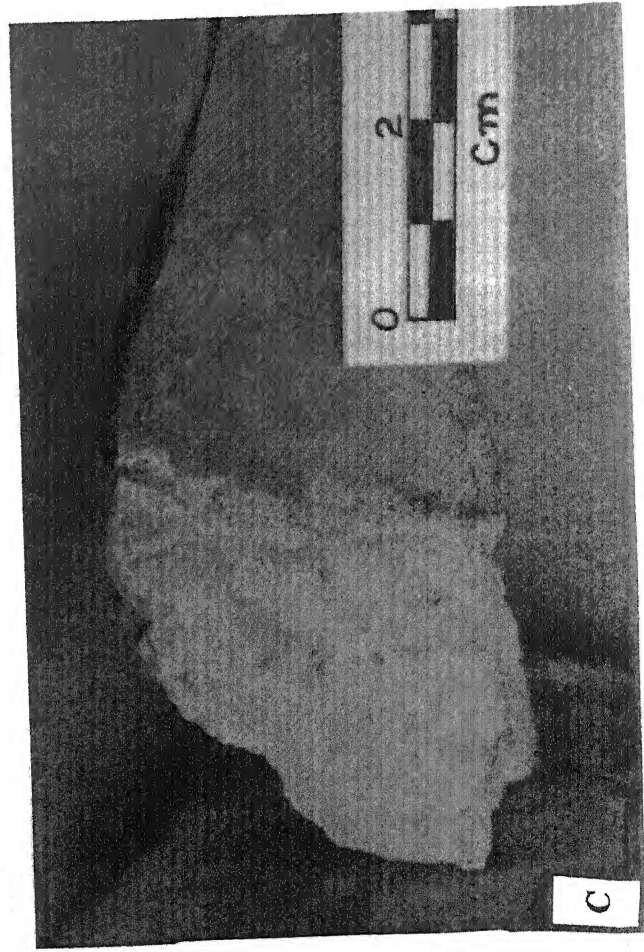
- Fig (A): Hand specimens photograph of matabasalts (MBE) show the very fine grained and dark coloured and present of amygdules (vesicles). These vesicles are often filled with some secondary minerals like quartz and other minerals.
[Ref. No. F/93, LB6 and F/97]
- Fig (B): Hand specimens photograph of metagabbro (=amphibolite) showing coarse-grained texture. The dark coloured minerals are pyroxene and magnetite while the light coloured minerals are mainly feldspars.
[Ref. No. F/16 and F/70]
- Fig (C): Hand specimen photograph of the contact zone, where the pegmatite vein is intruded in the metabasic (MBI). The cassiterite was found as minute grains in this pegmatite vein.
[Ref. No. L8]
- Fig (D): Hand specimen photograph of granite gneiss (KGG). The folded quartzo-feldspathic mass presents with the melanocratic bands.
[Ref. No. F/1, A]



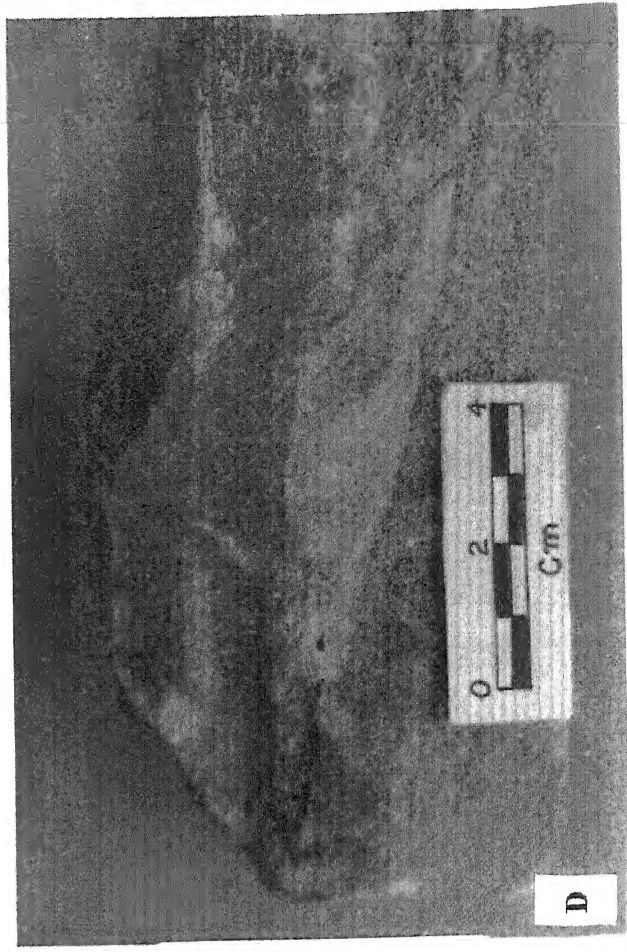
A



B



C



D

PLATE - VI

- Fig (A): Hand specimens photograph of the granite gneiss (KGG) showing the developments of augens of the quartzo-feldspathic masses and also present as the alternate linear and straight bandings by the leucocratic and melanocratic minerals as lit-par-lit injections
[Ref. No. F/15, A and F/1, B]
- Fig (B): Hand specimen photograph of the contact zone, where the foliated granite gneiss (KGG) and non-foliated granite (KG) are present.
[Ref. No. F/42, B]
- Fig (C): Hand specimen photograph of pinkish tourmaline granite (KTG) where the radiating tourmaline is present.
[Ref. No. L3]
- Fig (D): Hand specimen photograph of the hornblende granite (KHG) where the bands of hornblende and augens of quartzo-feldspathic mass are present in the rock.
[Ref. No. F/57, B]

(G) shows
masses of
brings by the
ins
and F/1, B

the foliated
esent.
o. F/42, B

ite (KTG)
f. No. 13

(3) where
ic mass

F/57, B

PLATE - VI

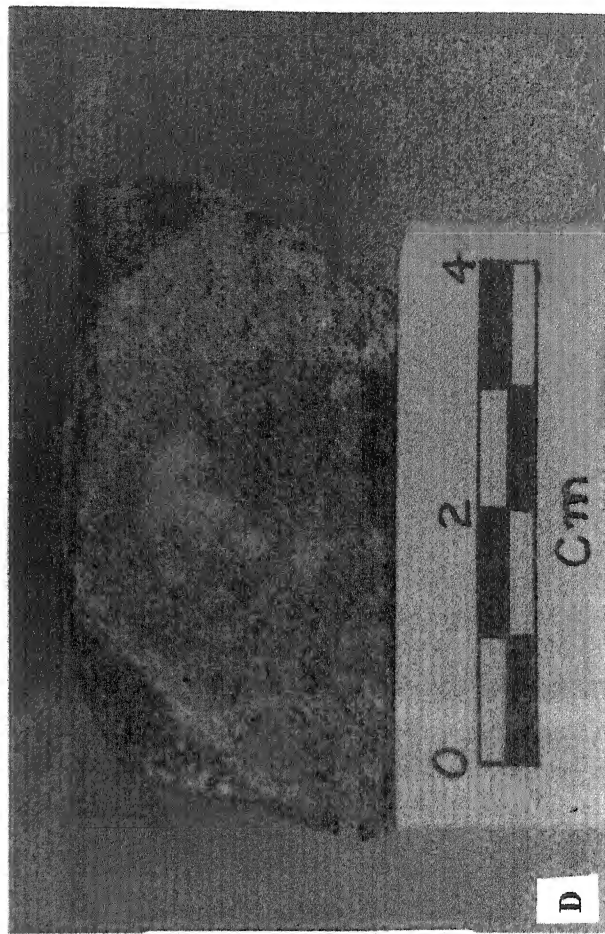
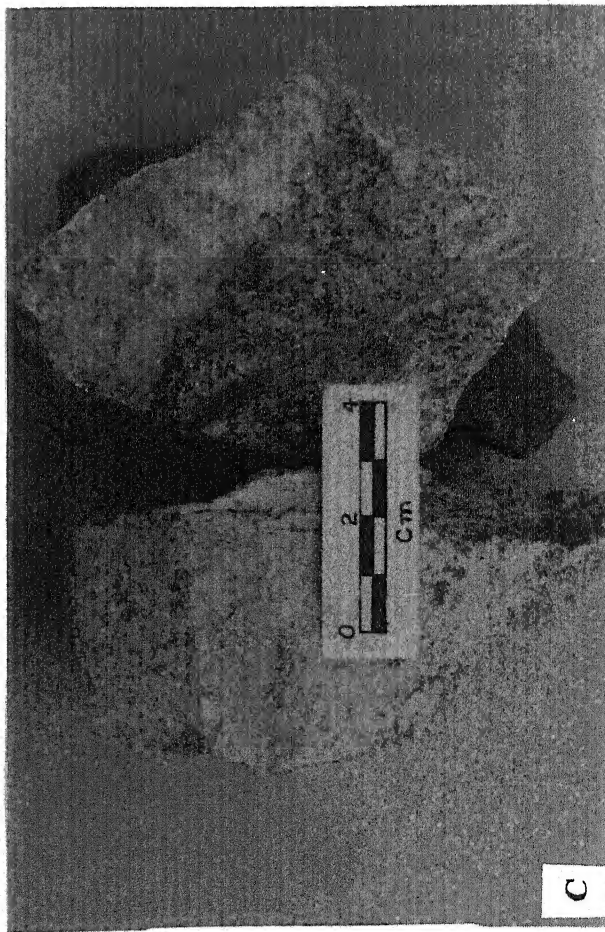
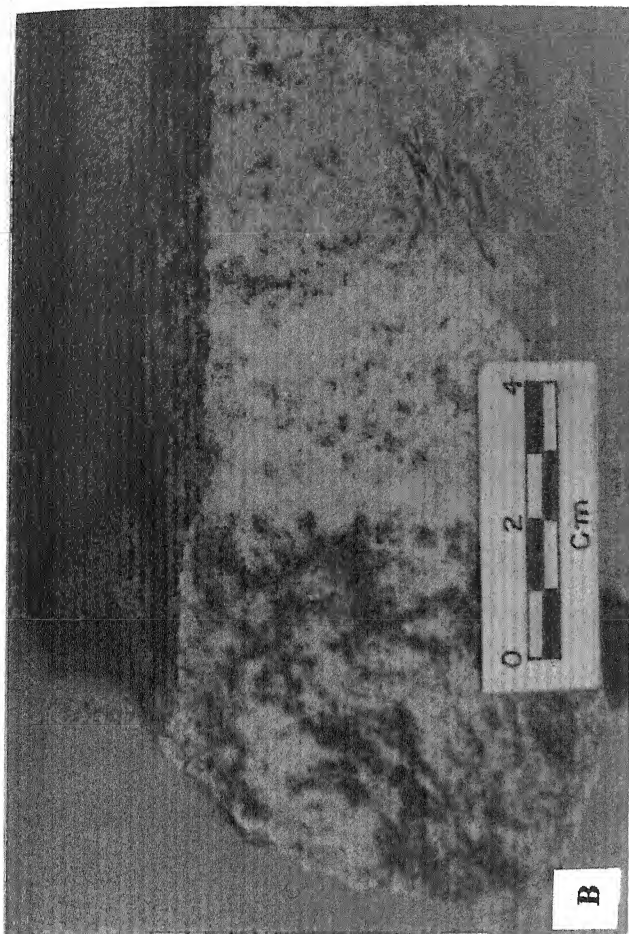
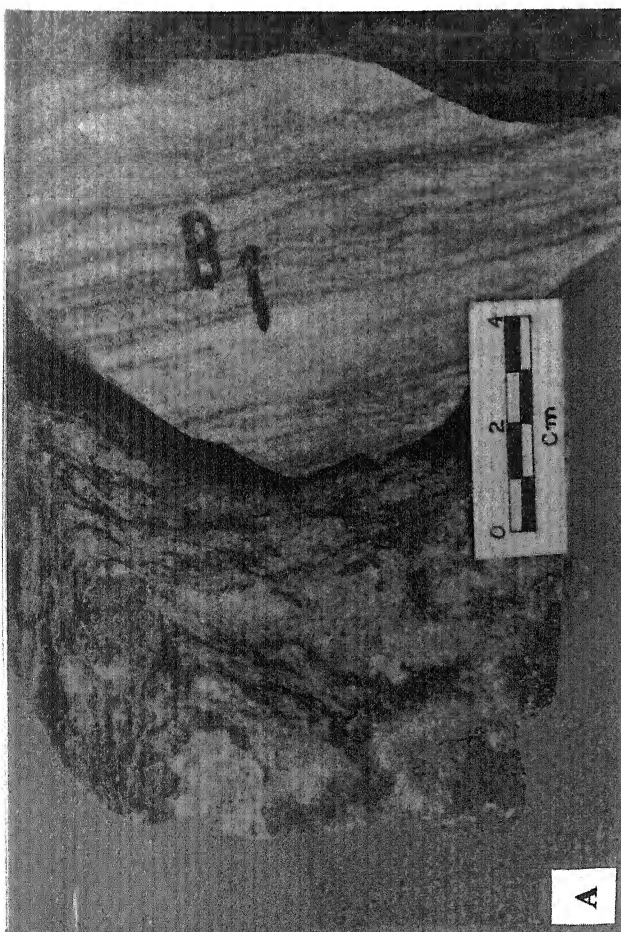


PLATE - VII

Fig (A): Hand specimen photograph of the biotite granite (KBG). The numerous minerals are present as a fine-grained non-foliated and appears aplitic in character.

[Ref. No. F/127 and F/39]

Fig (B): Hand specimens photograph of the contact zone, where biotite granite (KBG) and pegmatite (KP) are present. Large feldspathic patches are embedded in a fine-grained groundmass in the granitic portion.

[Ref. No. K/16 and F/37, A]

Fig (C): Hand specimens photograph of the greisenised pegmatite (KP), where the intercalations of quartz and mica are present.

[Ref. No. LB10 and K5]

Fig (D): Hand specimen photograph of the graphic pegmatite (KP), where the intergrowths of quartz and feldspar are present. Cassiterites are also observed in the rock.

[Ref. No. K14]

PLATE -VII

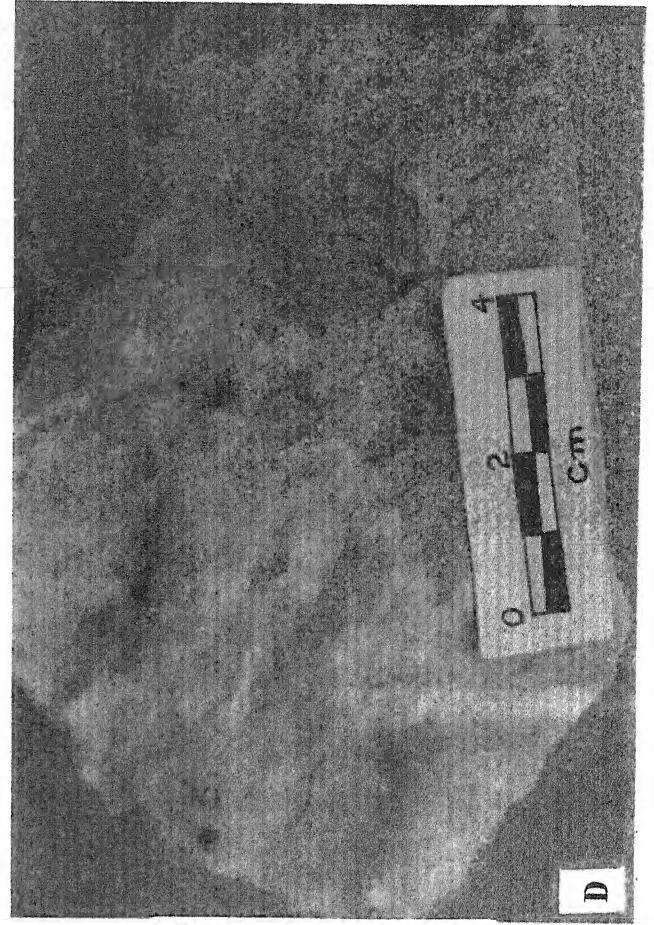
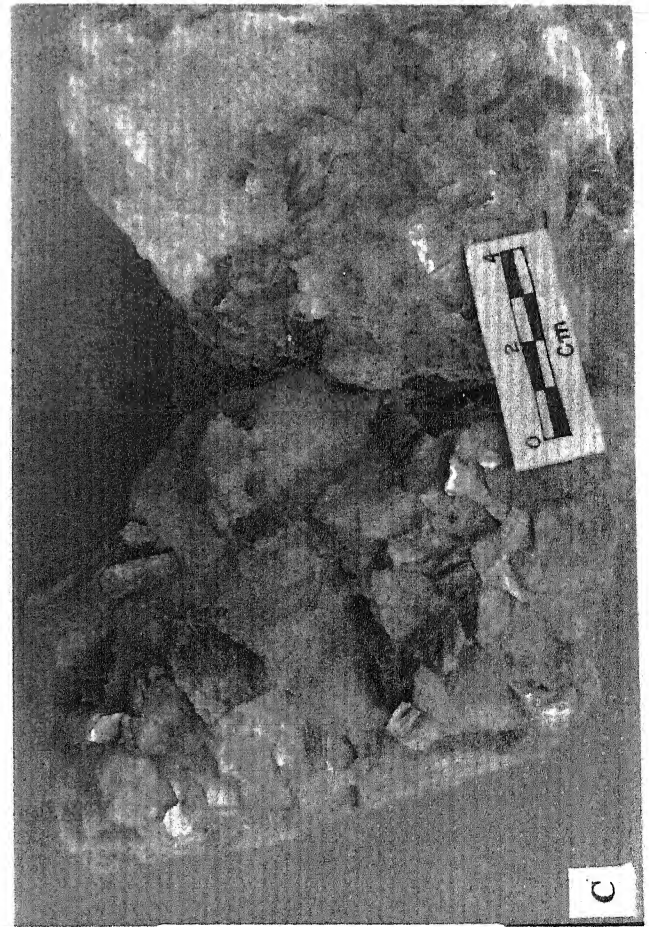
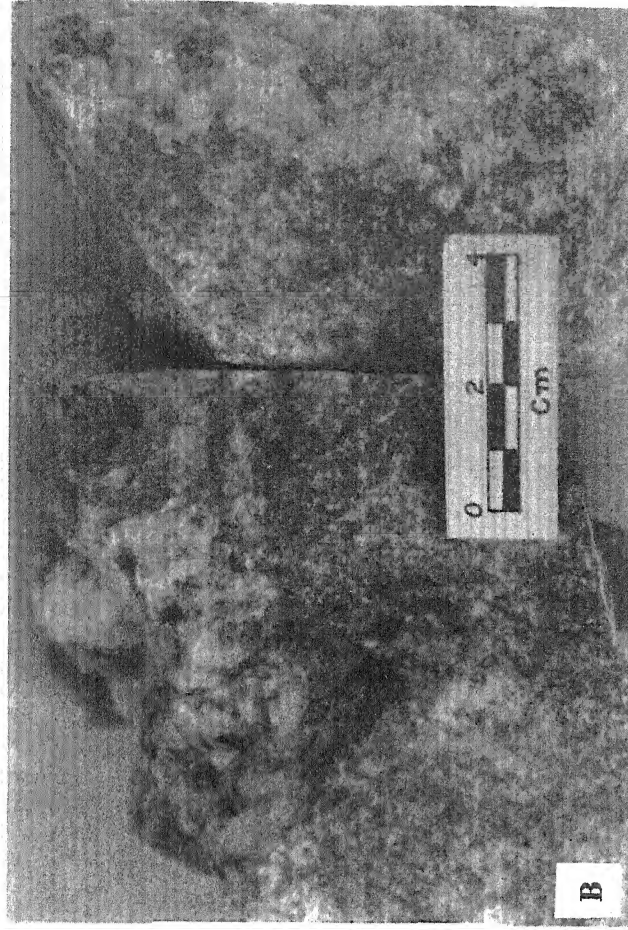
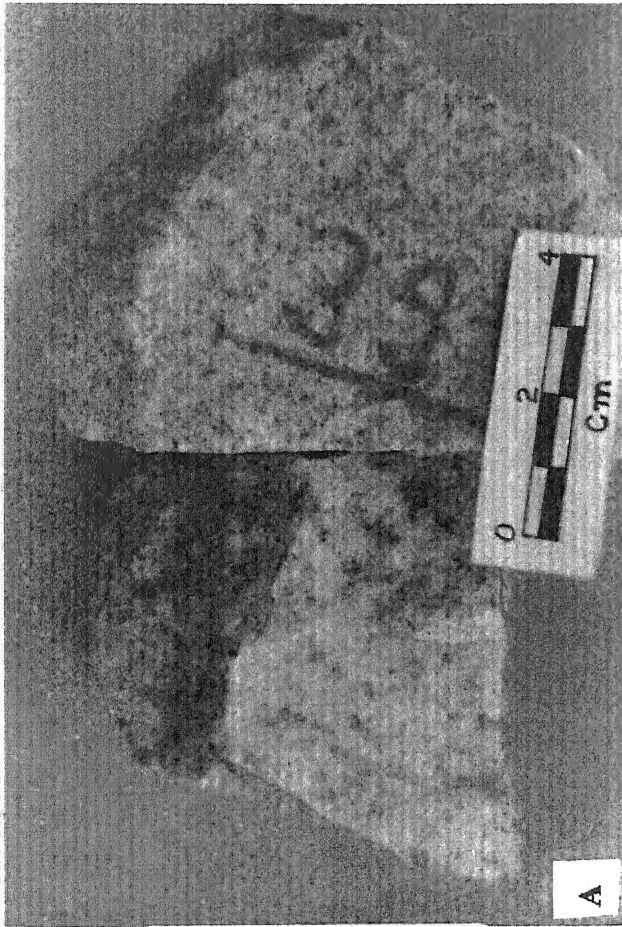


PLATE - VIII

Fig (A): Hand specimens photograph of the pegmatite (KP), where the fluorite and cassiterite crystals are embedded in pegmatite.

[Ref. No. K15 and K6]

Fig (B): Photograph of the cassiterite crystals. The twinned, prismatic, bipyramidal forms are obtained from primary and secondary deposits of the investigated area.

[Ref. No. C301]

Fig (C): Hand specimen photograph of the metadolerite, where the feldspar (white) and pyroxene (green) are present.

[Ref. No. F/85, A]

Fig (D): Hand specimen photograph of the quartz reef, where the quartz veins are present as a criss-cross pattern in nature.

[Ref. No. F/8]

PLATE-VIII

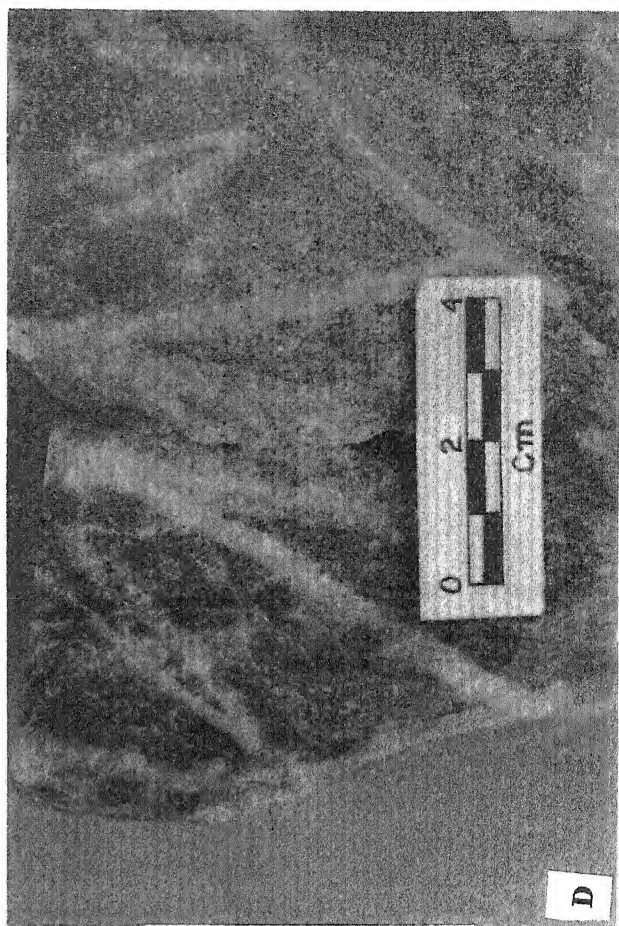
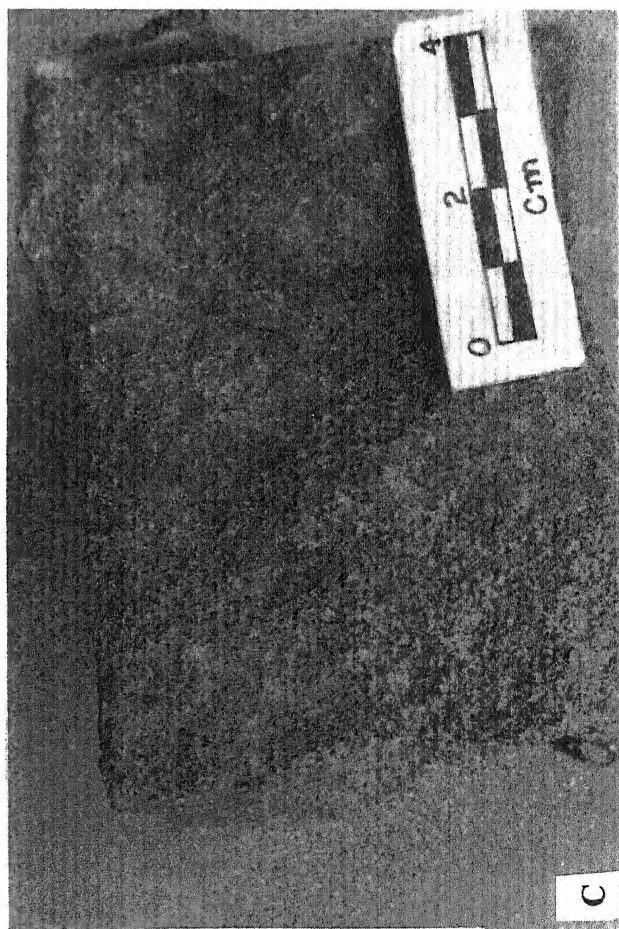
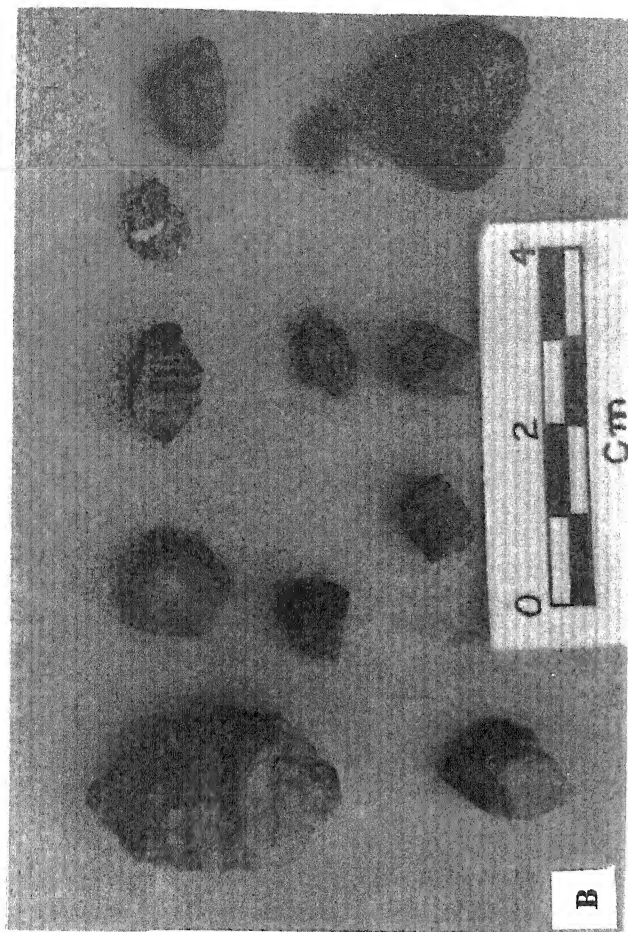
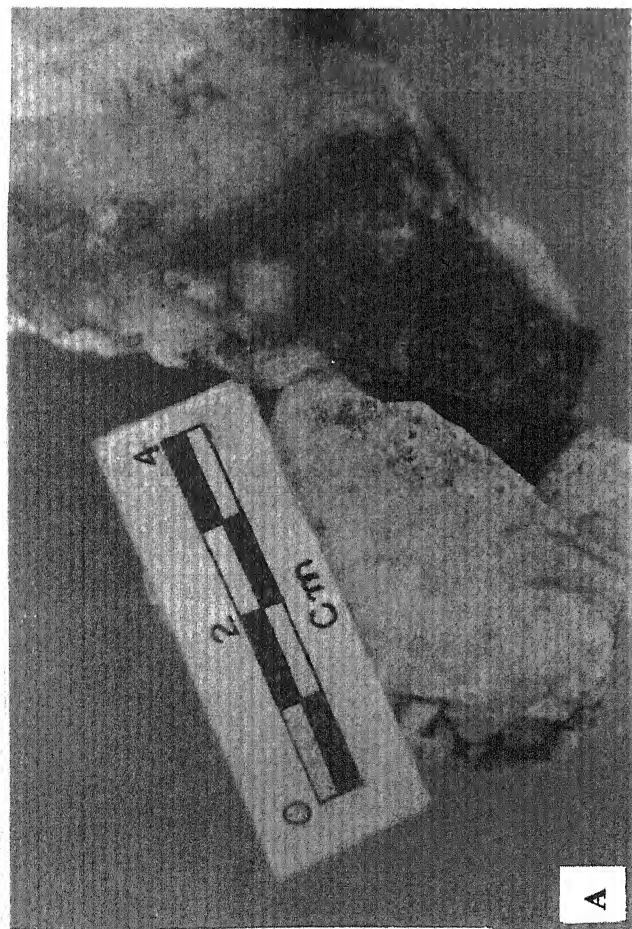


PLATE – IX

Fig (A): Photomicrograph of andalusite-sericite schist (A.S.S.). The symmetrical rhombic chiasmolite variety of andalusite is embedded in the groundmass of sericite needles. The needles of andalusite also recrystallised along the cross-fracture.

(Ref. No. T₁₇)
(Plane Polarized Light, 2.5 × 6]

Fig (B): Photomicrograph of andalusite-sericite schist (A.S.S.). The mica flakes and quartz crystals are aligned in S1 direction around the sericitised andalusite tabloids.

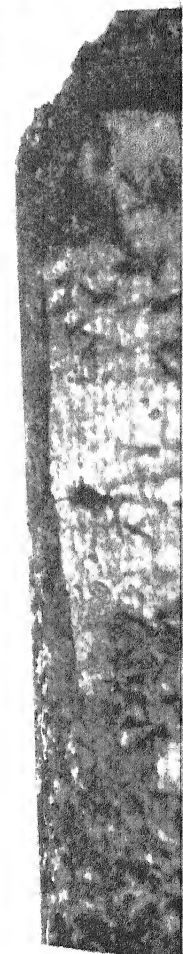
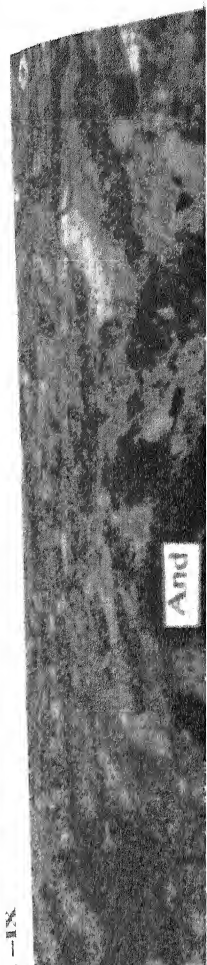
(Ref. No. F/131A)
(Crossed Polars, 4 × 3.3]

Fig (C): Photomicrograph of quartz-sericite schist (Q.S.S.). The tiny flakes of mica and minute grains of quartz are present in the alternate layer. Sericite inclusions are also recorded within quartz grains.

(Ref. No. F/75B)
(Crossed Polars, 4 × 3.3]

Fig (D): Photomicrograph of quartz-sericite schist (Q.S.S.). The mica flakes and quartz grains are showing in preferred orientation as alternate bands.

(Ref. No. F/80A)
(Crossed Polars, 4 × 3.3]



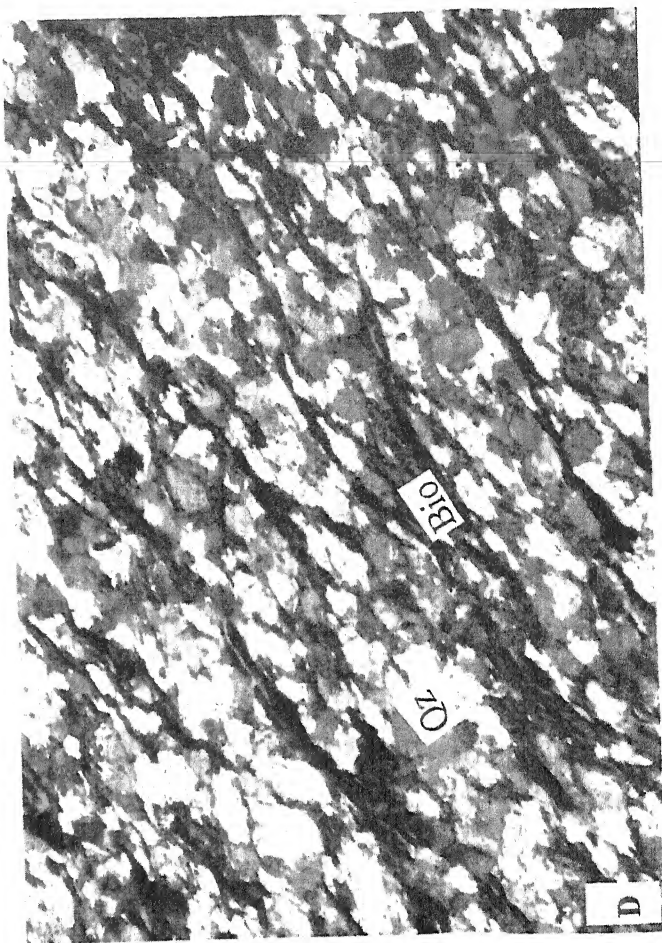
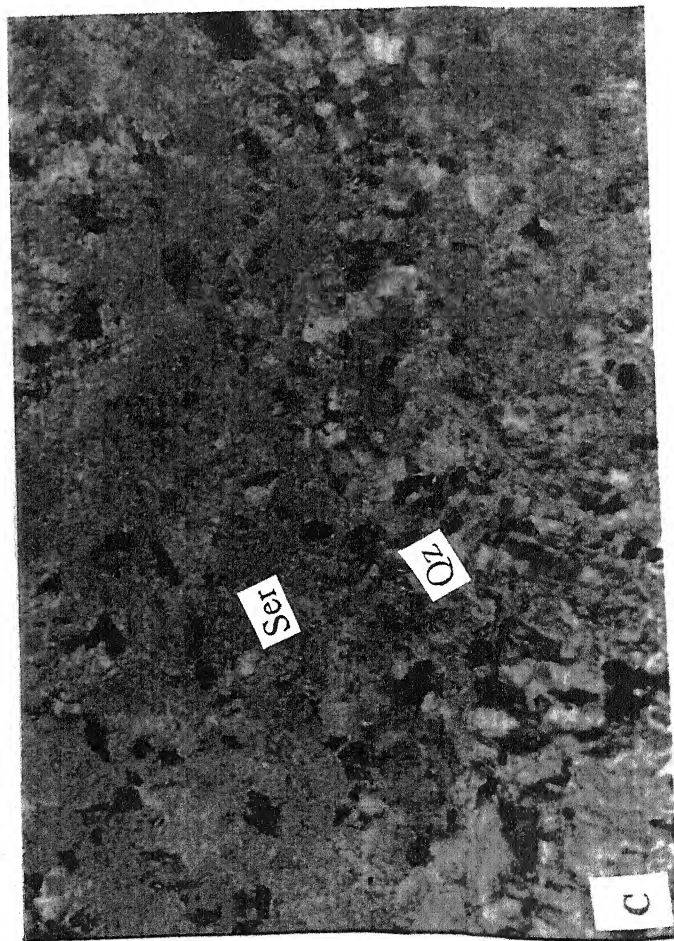
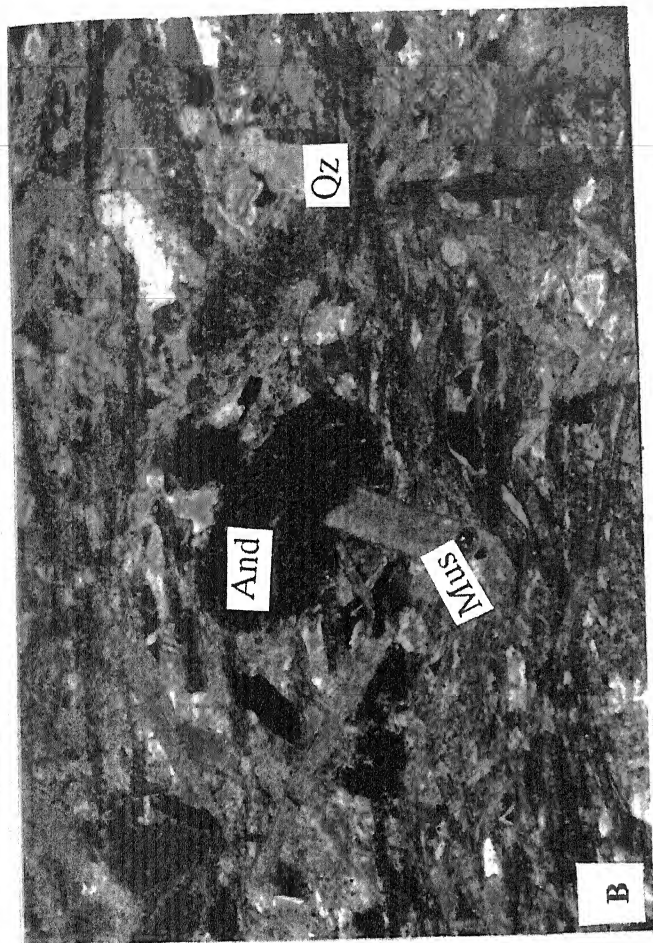
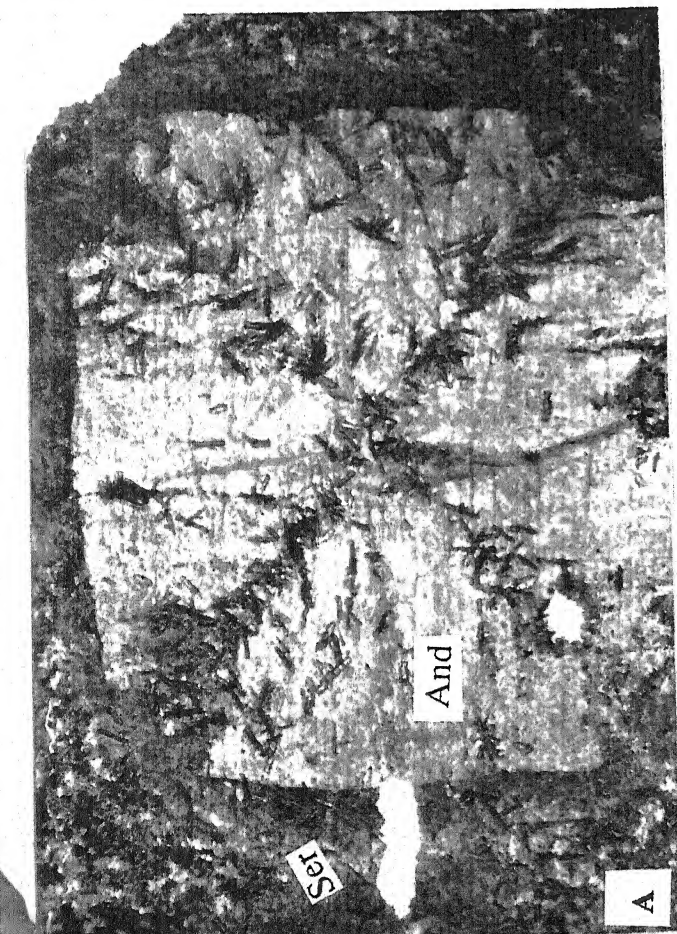


PLATE - X

Fig (A): Photomicrograph of banded ferruginous quartzite (B.F.Q.).
(Ref. No. F/117D)
[Cross Polars, 4×3.3]

Fig (B): Photomicrograph of grunerite magnetite quartzite (G.M.Q.) showing alternate bands of amphiboles (grunerite) and black magnetite.
(Ref. No. Ny6)
[Plane Polarized Light, 2.5×6]

Fig (C): Photomicrograph of grunerite magnetite quartzite (G.M.Q.). The grunerite shows the polysynthetic twinning. Hornblende, magnetite (iron oxide), quartz and chlorite are present.

(Ref. No. F/110)
[Crossed Polars, 4×3.3]

Fig (D): Photomicrograph of quartz-sericite schist (Q.S.S.). The mica flakes and quartz grains are showing in preferred orientation as alternate bands.

(Ref. No. F/80A)
[Crossed Polars, 4×3.3]



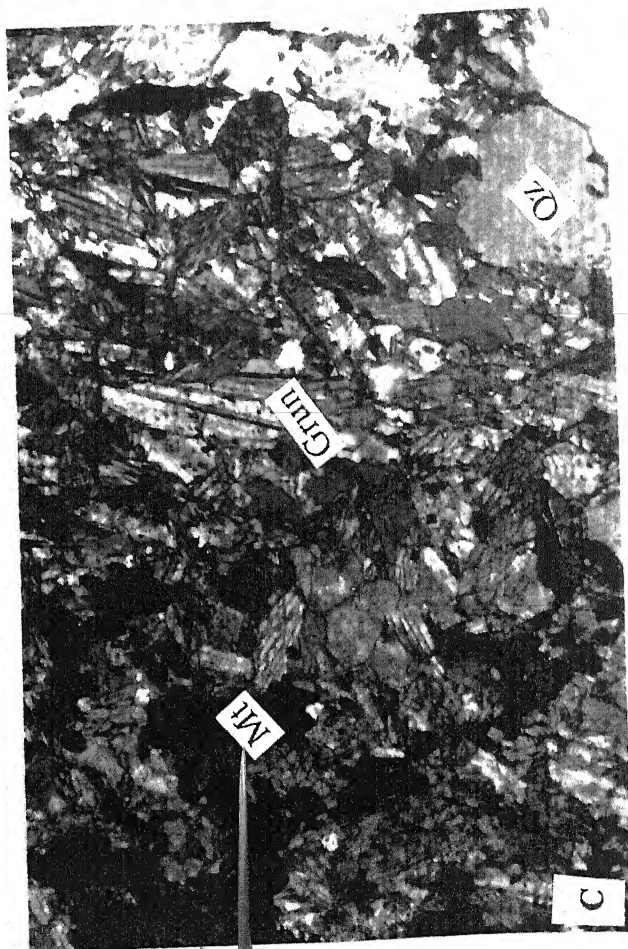
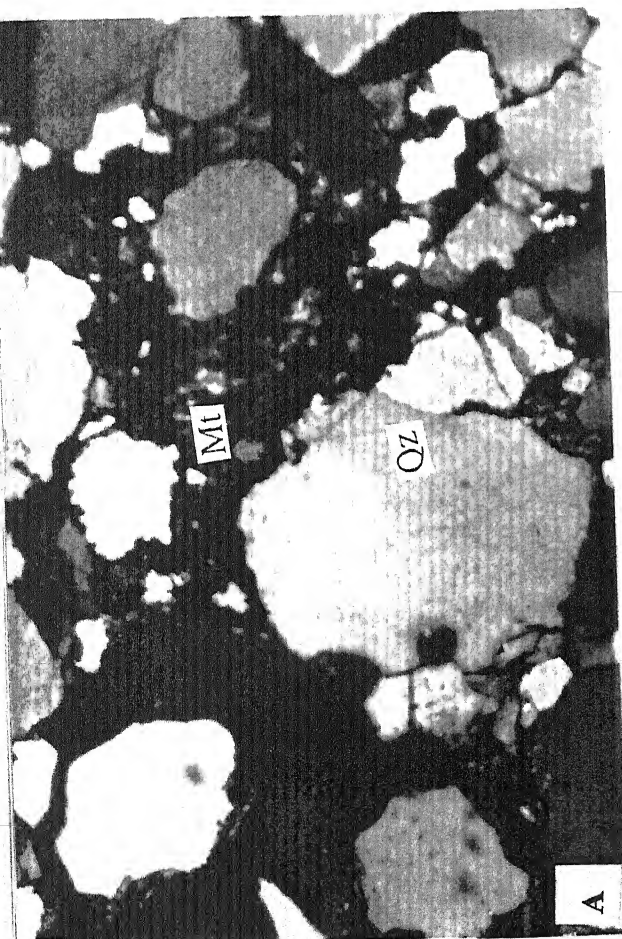
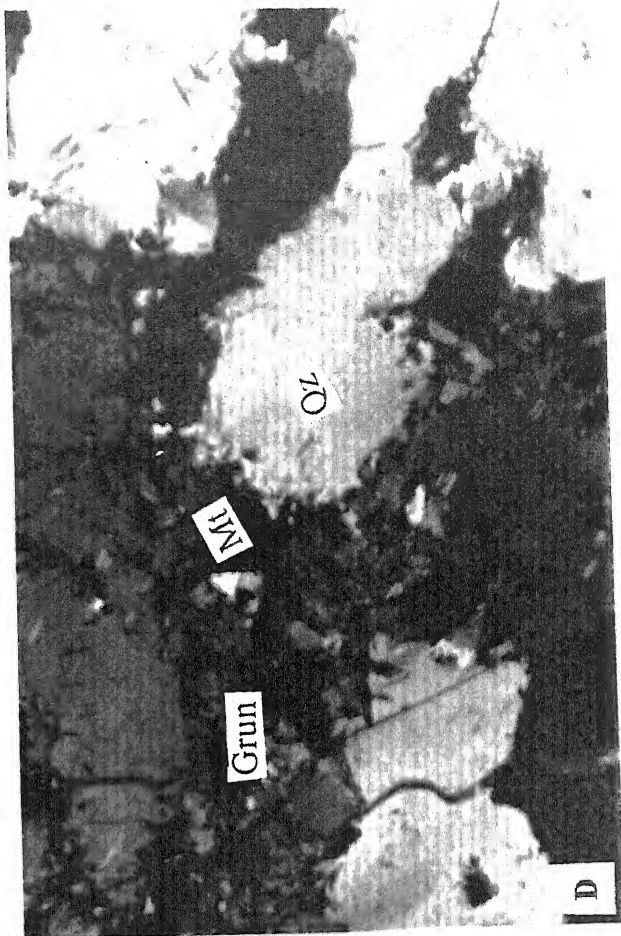
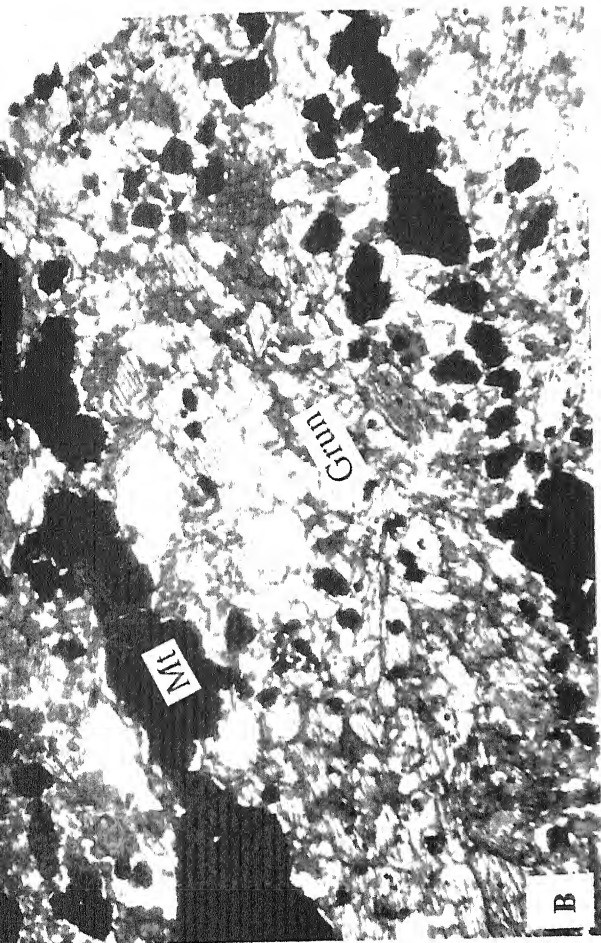


PLATE - XI

Fig (A): Photomicrograph of metapillow basalt (M.B.F.). Laths of plagioclase and altered pyroxenes are present.

(Ref. No. F/L_{B1})
[Crossed Polars, 4 × 3.3]

Fig (B): Same photomicrograph of the above Fig. A shows the sub-ophitic texture. The pyroxenes (augite) are changed into amphiboles (actinolite). The chlorite is present as altered product in patches at many places.

(Crossed Polars, 4 × 3.3)

Fig (C): Photomicrograph of metabasalt (M.B.F.) shows the numerous vesicles filled by the secondary minerals such as quartz, zoisite, epidote and fibrous amphibole.

(Ref. No. F/95)
[Crossed Polars, 4 × 3.3]

Fig (D): Photomicrograph of metabasalt (M.B.E.) showing two types of amphibole. Chlorite, feldspar and iron oxide are also present.

(Ref. No. F/91)
[Crossed Polars, 4 × 3.3]

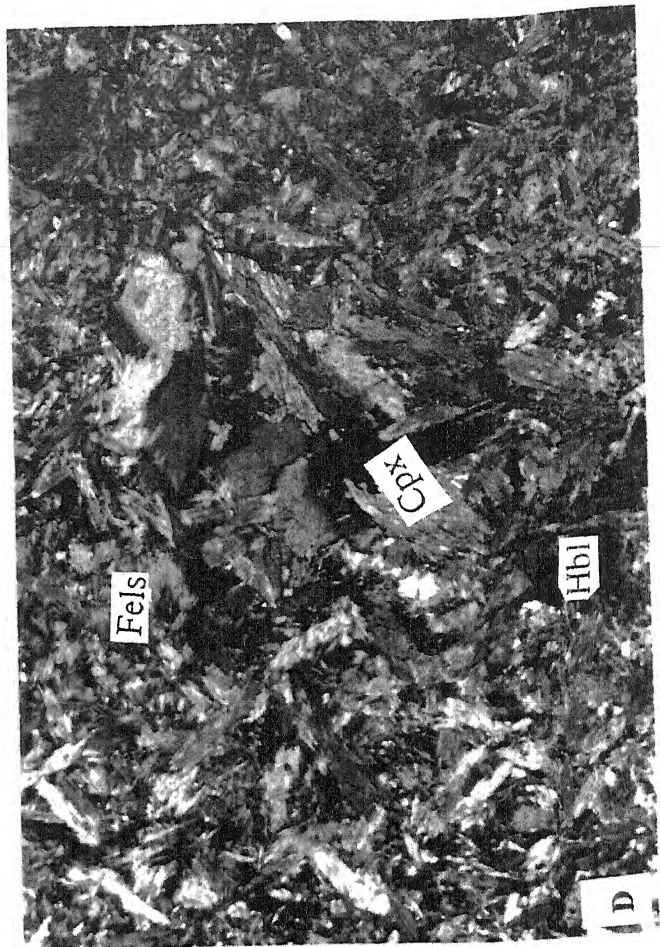
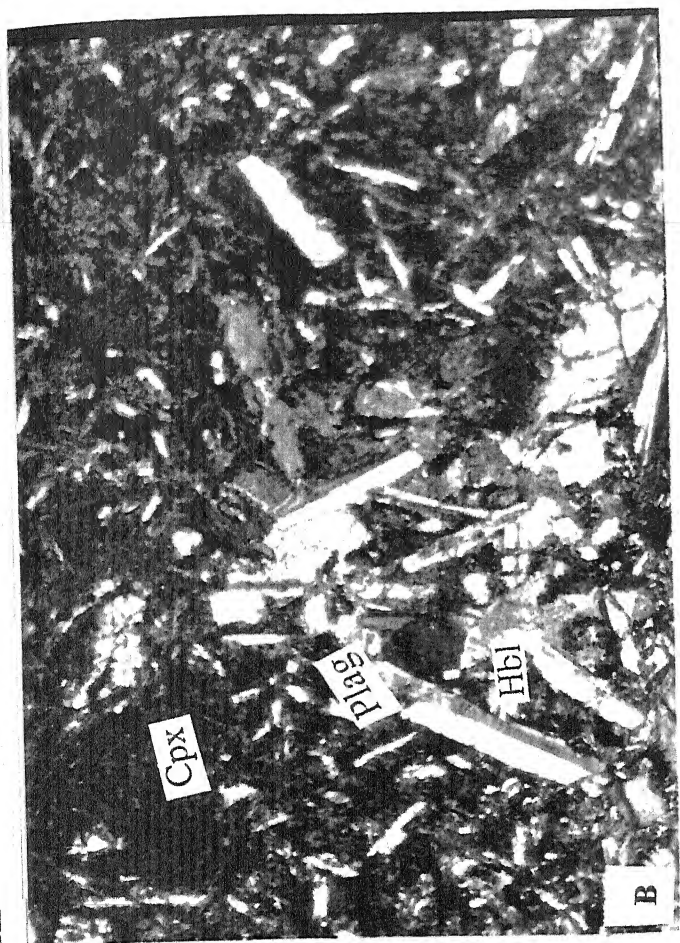
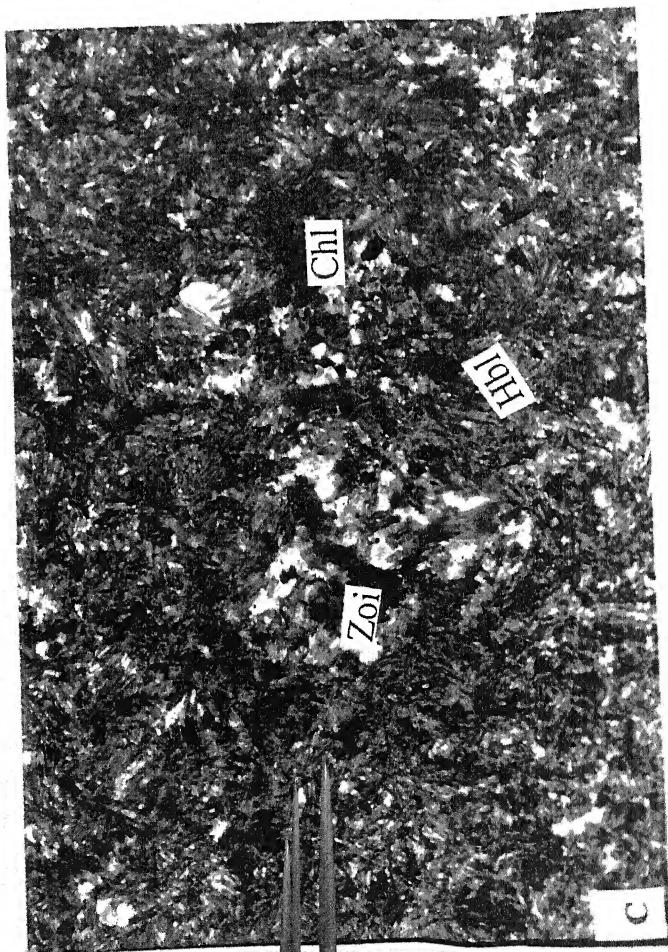
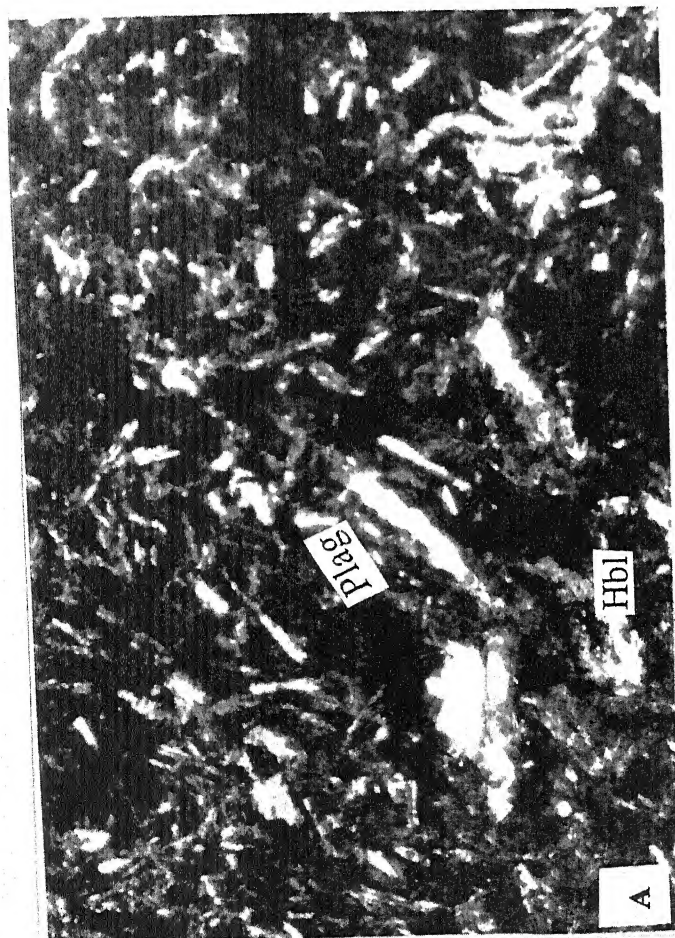


PLATE - XII

Fig (A): Photomicrograph of metagabbroic rock (M.B.I.) shows the small relict ophitic texture by the dominant constituents of hornblende and plagioclase feldspar. Quartz, magnetite, actinolite and zircon are present.

(Ref. No. F/54A)
[Cross Polars, 4×3.3]

Fig (B): Photomicrograph of amphibolite rock (M.B.I.) shows the actinolite and hornblende. Leucoxene variety of sphene is observed around the reddish brown of ilmenite. Inky-blue colour of clino-zoisite and epidote are also present along the periphery of leucoxene.

(Ref. No. F/84C)
(Crossed Polars, 4×3.3)

Fig (C): Photomicrograph of metagabbroic rock (M.B.I.) shows the myrmekitic intergrowth due to later emplacement of hydrothermal solution along the contact of the rock. Deep colour of clinozoisite, sphene, actinolite, hornblende, sericitised feldspar, biotite and iron oxide are occur after metamorphism.

(Ref. No. F/16)
[Crossed Polars, 4×3.3]

Fig (D): Photomicrograph of metagabbroic rock (M.B.I.). The calcic plagioclase is becomes saussuritised and gives rise to aggregate of albite and epidote. Most of the pyroxenes are altered into amphiboles. Sphene, quartz and sericite are also present.

(Ref. No. F/10B)
[Crossed Polars, 4×3.3]

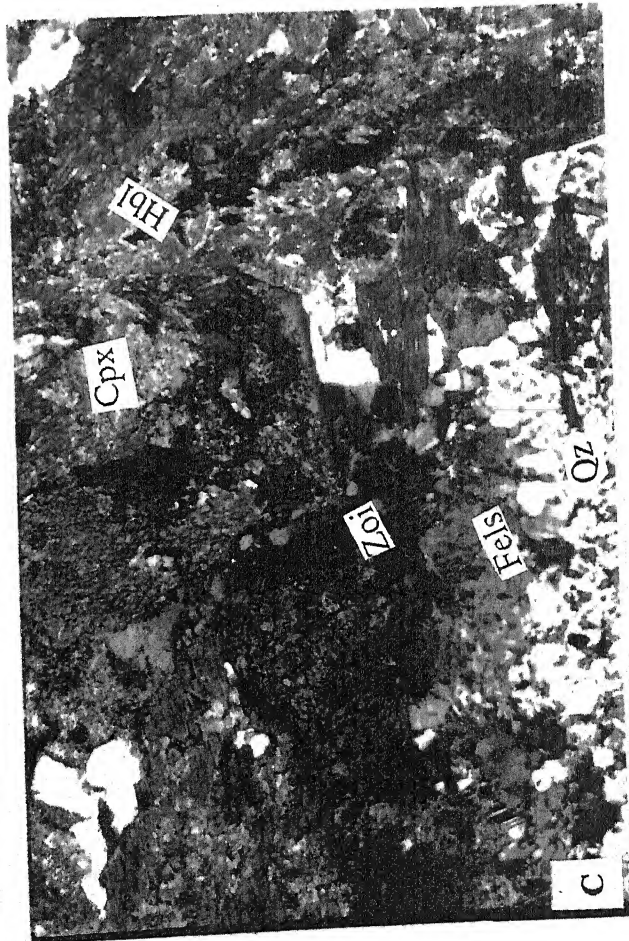
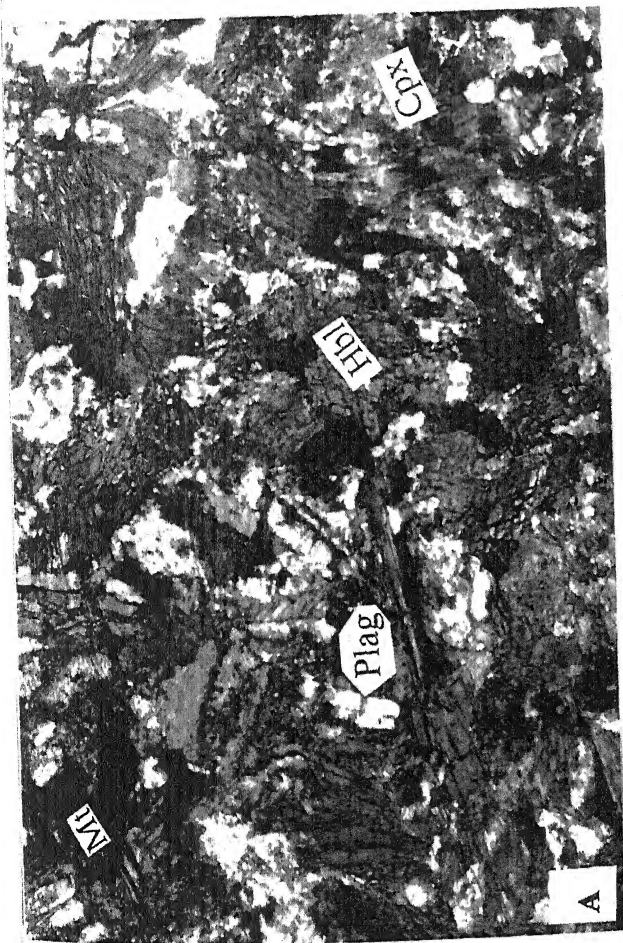
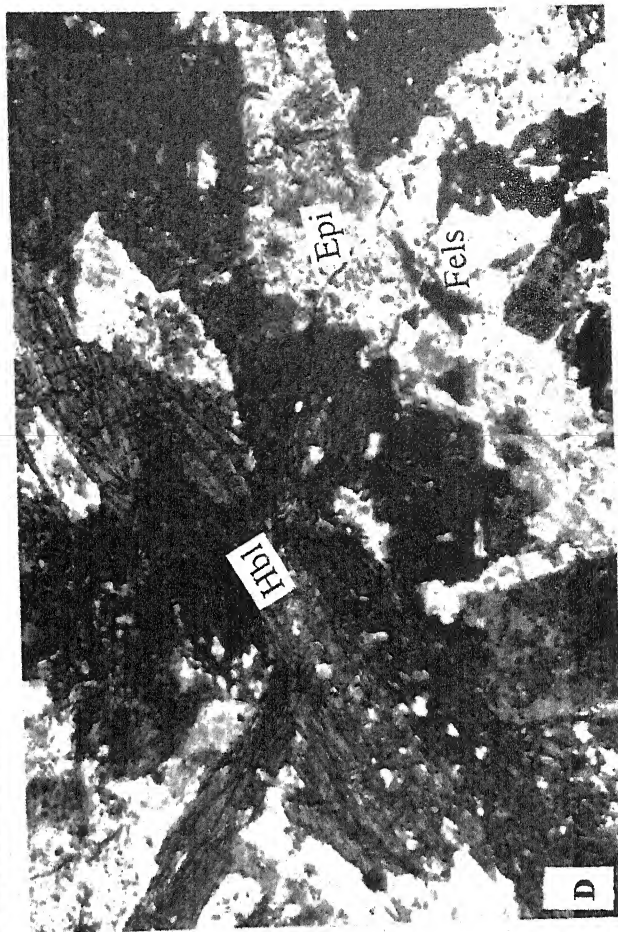
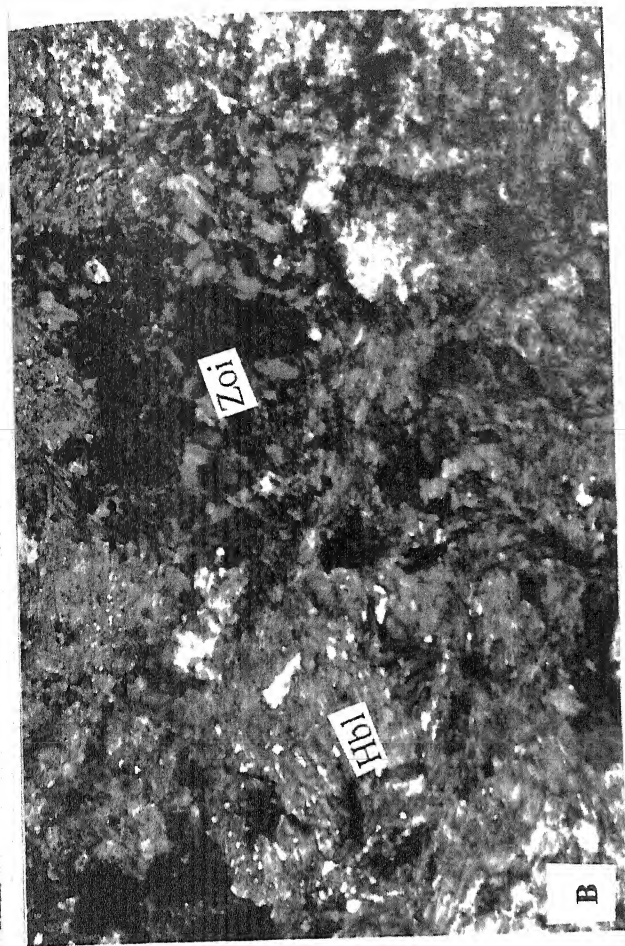


PLATE - XIII

Fig (A): Photomicrograph of granite gneiss (K.G.G.) showing gneissose structure. The large crystals of biotite are undergoing alteration to produce muscovite and dark magnetite. The feldspars are also sericitised in the rock.

(Ref. No. F/50B)
[Cross Polars, 4×3.3]

Fig (B): Photomicrograph of gneiss (K.G.G.) showing the augen structure. In this rock, preferred orientation of biotite flakes around the augen of the sericitised quartzo-feldspathic masses. Brown biotite flakes are also altered into muscovite and leached reddish yellow limonitic material in the rock.

(Ref. No. F/1A)
[Plane Polarized Light, 4×3.3]

Fig (C): Photomicrograph of granite gneiss (K.G.G.), showing the large numbers of microcline. The sericitised orthoclase having the inclusions of microcline and quartz are present. Biotite flakes are altered into chlorite, muscovite and leached limonitic materials.

(Ref. No. F/54,C)
[Crossed Polars, 4×3.3]

Fig (D): Photomicrograph of mylonitised biotite granite (K.B.G.). The large crystals of microcline are highly sericitised. Along the boundary of the microcline, altered biotite and magnetite are present. Quartz and feldspars are present as angular to sub angular grains.

(Ref. No. F/132B)
[Crossed Polars, 4×3.3]

PLATE - XIII



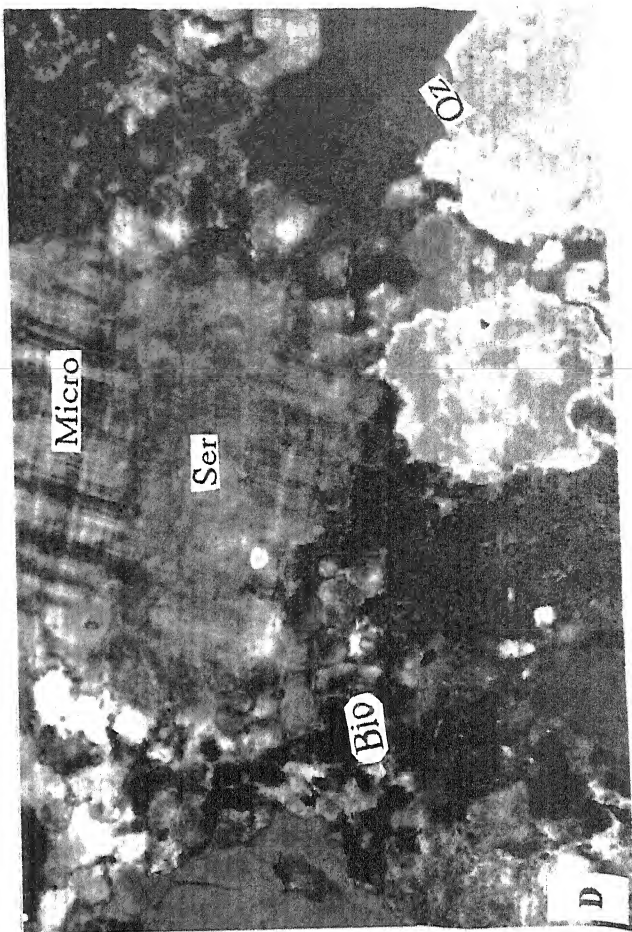
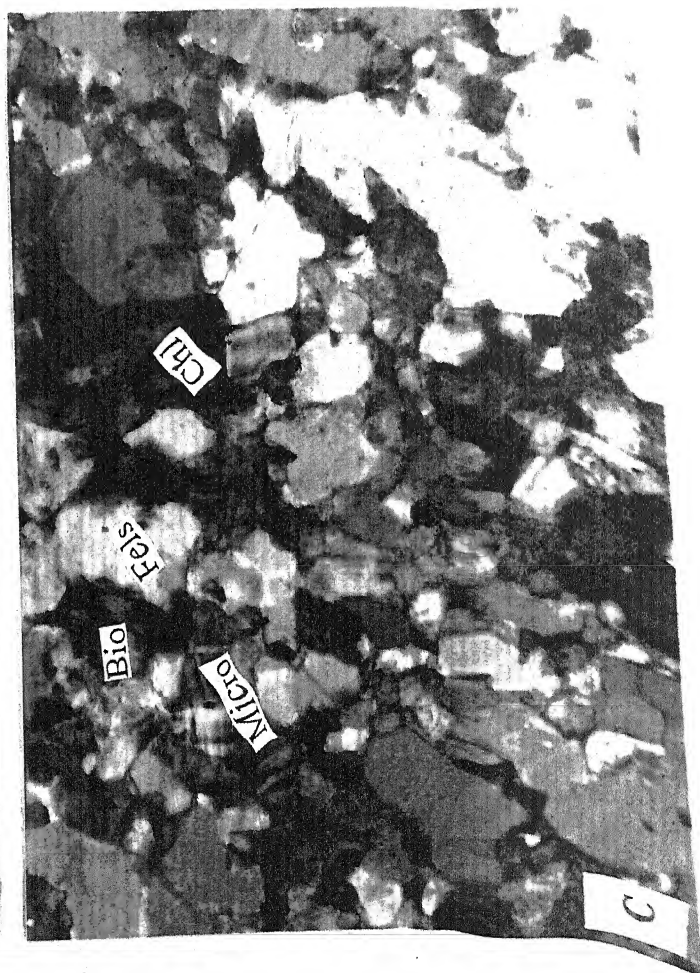
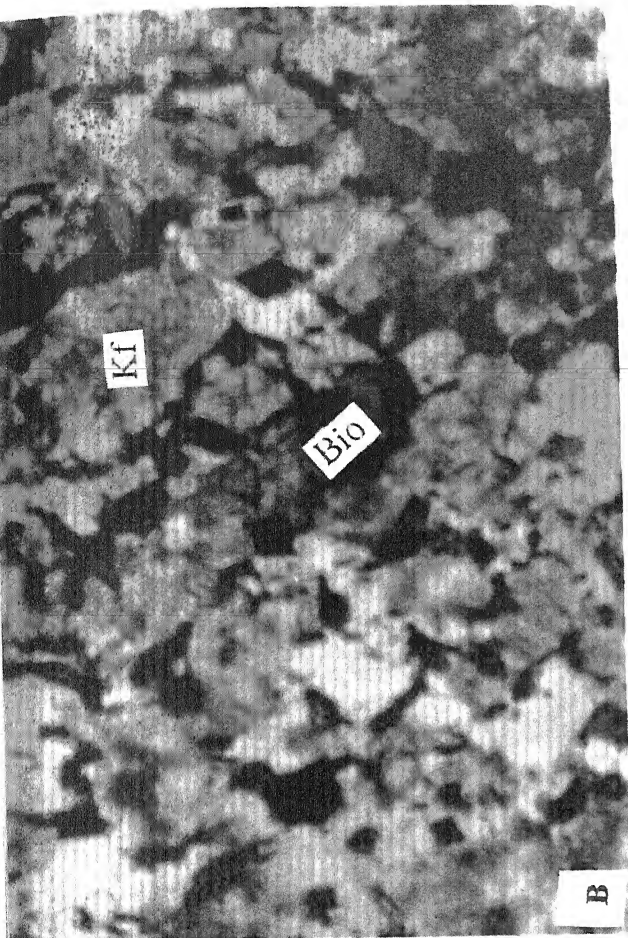
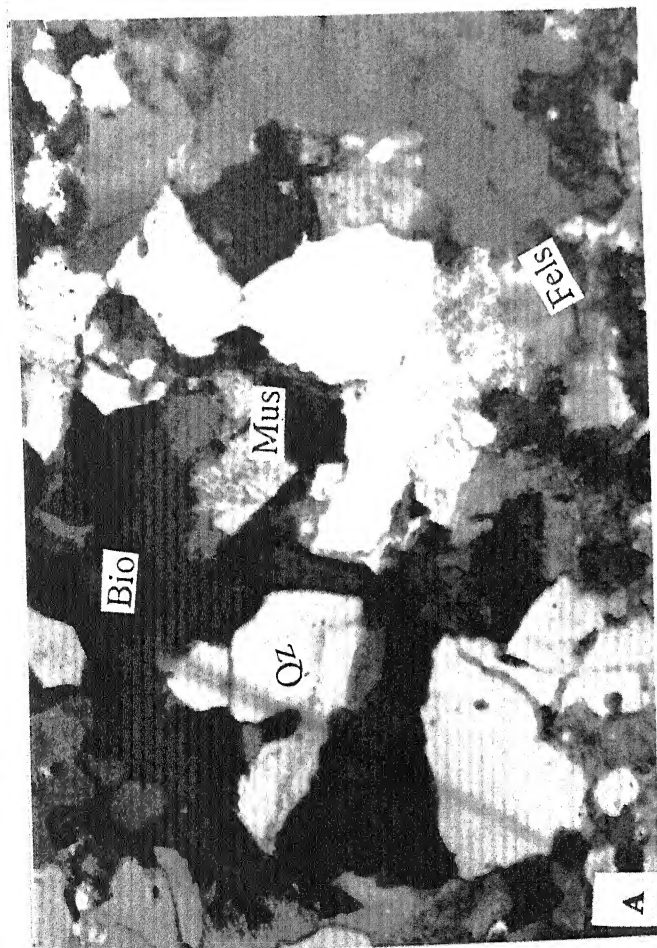


PLATE - XIV

Fig (A): Photomicrograph of mylonitised granite (K.G.). The sericitised feldspars are highly fractured and sheared giving the mosaic appearance. The plagioclase lamellae are micro folding and micro faulting along the fractures. Quartz is also affected by crushing give rise to angular to subangular grains.

(Ref. No. F/24,B)
[Cross Polars, 4 × 3.3]

Fig (B): Photomicrograph of biotite granite (K.B.G.). Quartz, biotite, cassiterite, chlorite, microcline, albite and epidote are present.

(Ref. No. F/57,C)
[Plane Polarized Light, 4 × 3.3]

Fig (C): Photomicrograph of biotite granite (K.B.G.). Both the albitisation and sericitisation in orthoclase are observed. Biotite is altered into the chlorite and magnetite. Microcline is present as a minor quantity.

(Ref. No. F/37,B)
[Crossed Polars, 4 × 3.3]

Fig (D): Photomicrograph of mylonitised granite (K.G.). The perthitic orthoclase are highly sericitised and shows Carlsbad twinning. Muscovite and magnetite are recorded as inclusion within the sericitised orthoclase.

(Ref. No. F/25,B)
[Crossed Polars, 4 × 3.3]

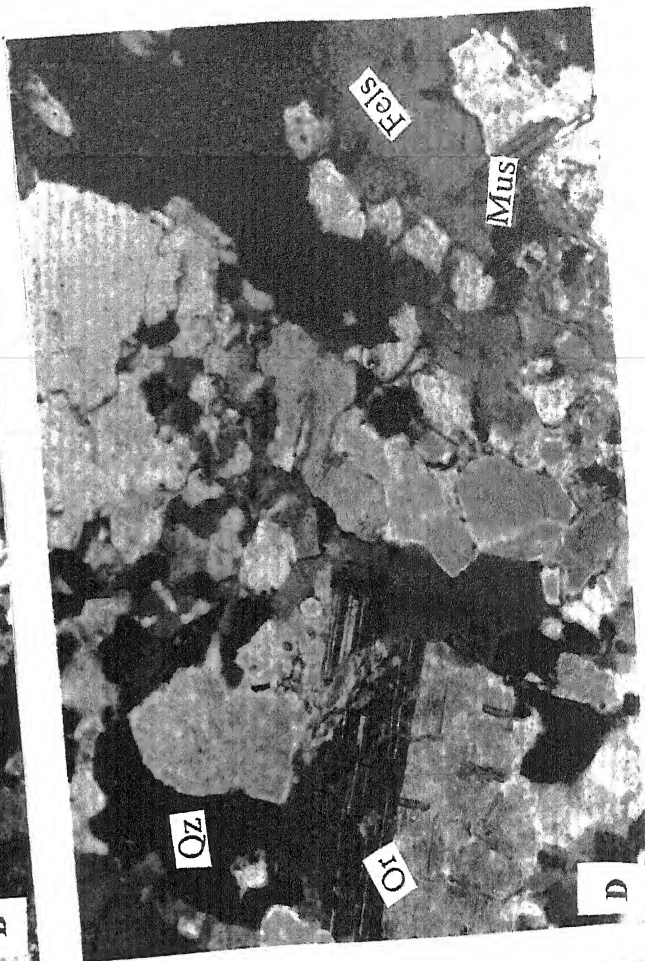


PLATE - XV

Fig (A): Photomicrograph of biotite granite (K.B.G.), showing the microcline perthite texture. Biotite, muscovite, sericitised feldspars, quartz and iron oxide are also present.

(Ref. No. F/101, A)
[Crossed Polars, 4×3.3]

Fig (B): Photomicrograph of biotite granite (K.B.G.). It shows equal visible proportions of microcline and albite. Sericitisation is taken place in the orthoclase and also along the albite lamellae. Biotite, muscovite, quartz and magnetite are present.

(Ref. No. F/32)
[Crossed Polars, 4×3.3]

Fig (C): Photomicrograph of mylonitised biotite granite (K.B.G.). The large microcline is subjected to highly sericitisation. Quartz, biotite and also zoning and bundle shaped of plagioclase are also present.

(Ref. No. F/103)
[Crossed Polars, 4×3.3]

Fig (D): Photomicrograph of biotite granite (K.B.G.), showing the albitisation on large scale. The inclusions of muscovite, microcline and quartz are present in the sericitised albite. The lamellae of the albite are somewhat microfolded in nature. Due to the alteration of biotite, gives the chlorite and iron oxides are formed.

(Ref. No. F/10, A)
[Crossed Polars, 4×3.3]



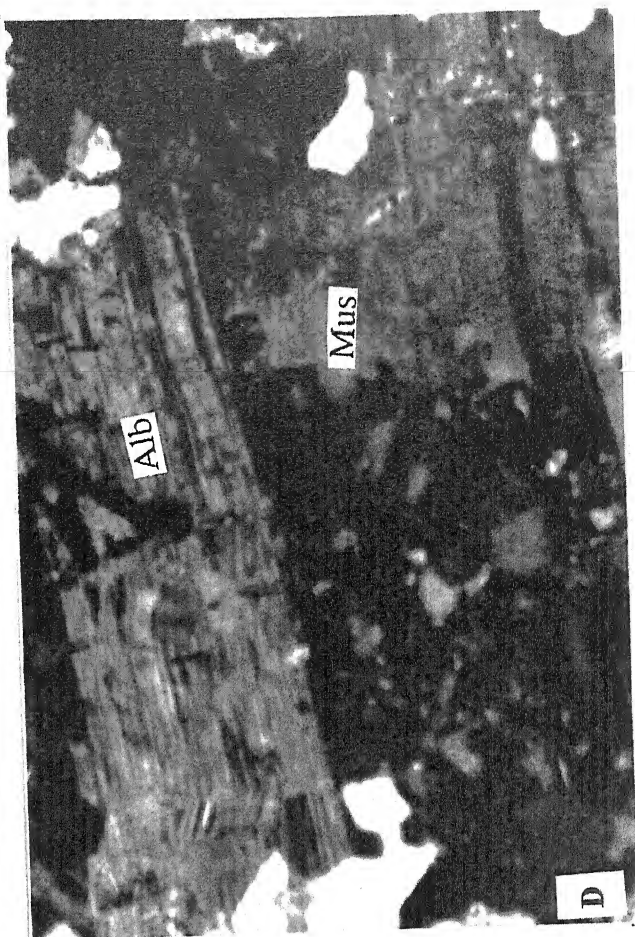
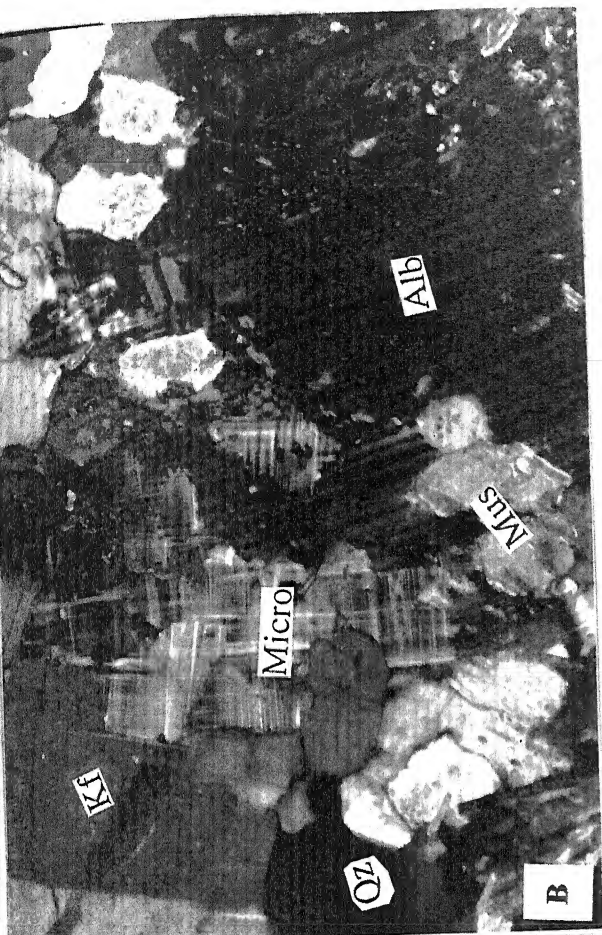
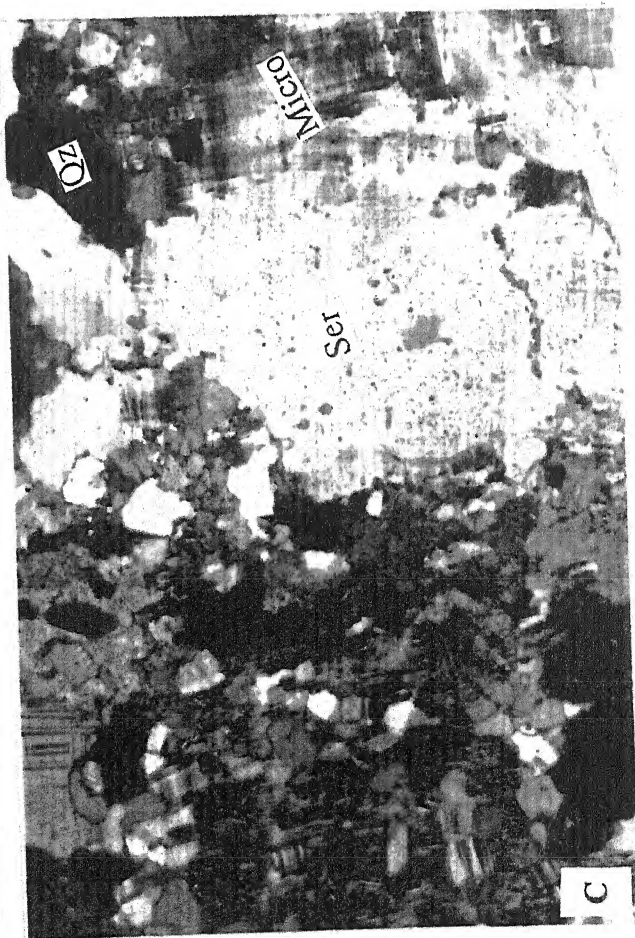
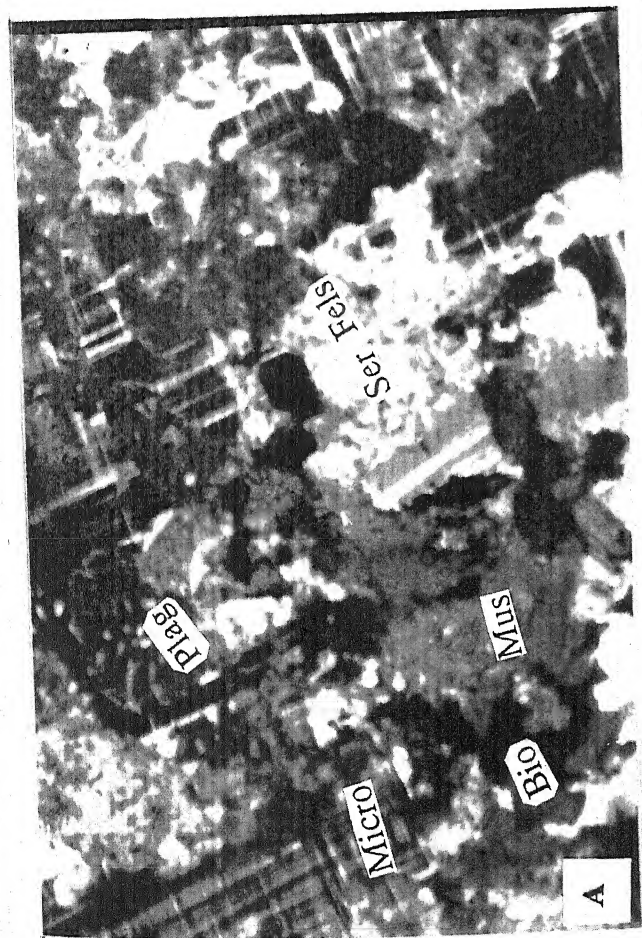


PLATE – XVI

Fig (A): Photomicrograph of the biotite granite (K.B.G.). The cassiterite occurs in the altered biotite. Quartz, feldspars and iron oxides are also present.

(Ref. No. F/57,C)

[Plane Polarized Light, 4 × 3.3]

Fig (B): Photomicrograph of biotite granite (K.B.G.), showing perthitic texture. In the large grains of orthoclase, developed albite lamellae and also having the inclusions of quartz and sericite. Biotite, magnetite and apatite are also present in the rock.

(Ref. No. F/53)

[Crossed Polars, 4 × 3.3]

Fig (C): Photomicrograph of biotite granite (K.B.G.). It shows the perthite texture and their lamellae are in microfaulting. Quartz, biotite and Carlsbad twinning of orthoclase are also present.

(Ref. No. F/2, A)

[Crossed Polars, 4 × 3.3]

Fig (D): Photomicrograph of biotite granite (K.B.G.). The graphic intergrowth of quartz and orthoclase are present. The albite and microcline are highly sericitised in nature. Biotite, chlorite and sphene are also present in the rock.

(Ref. No. F/111)

[Crossed Polars, 4 × 3.3]

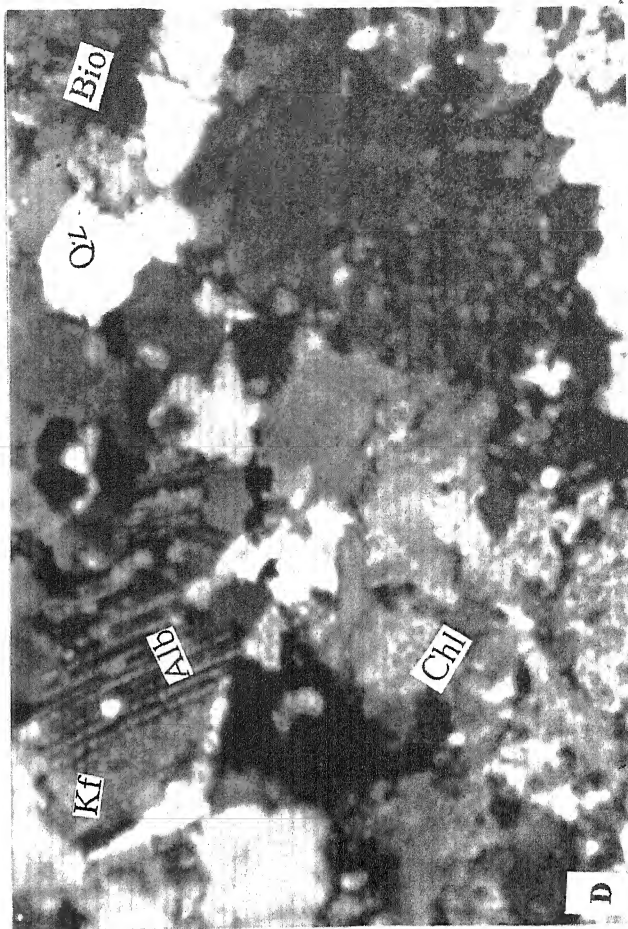
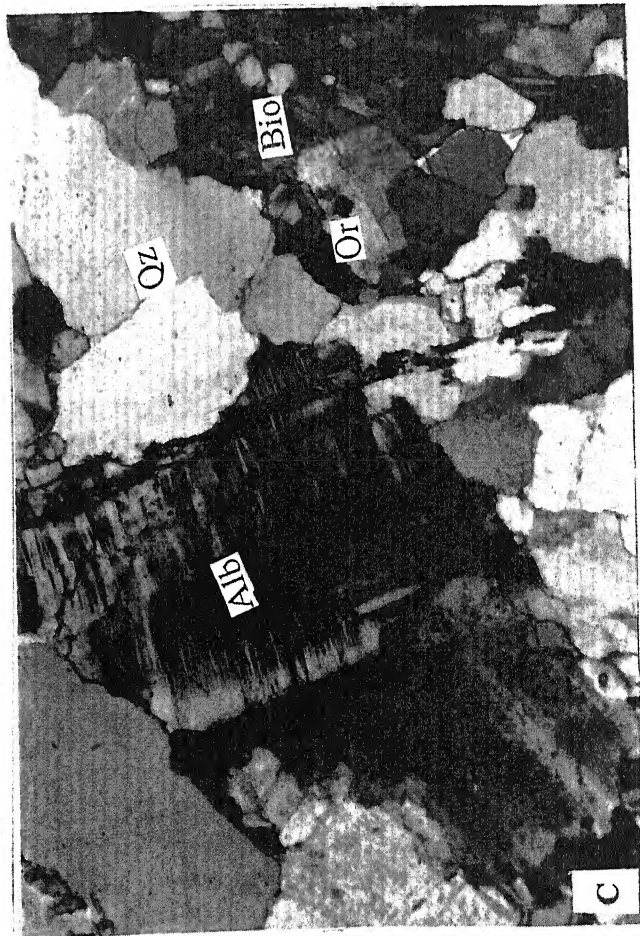
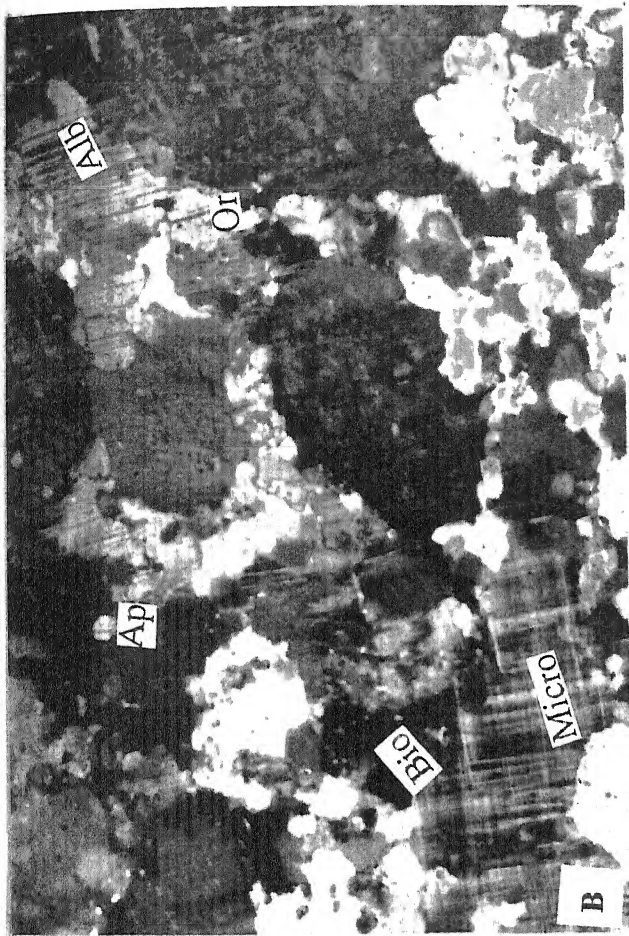
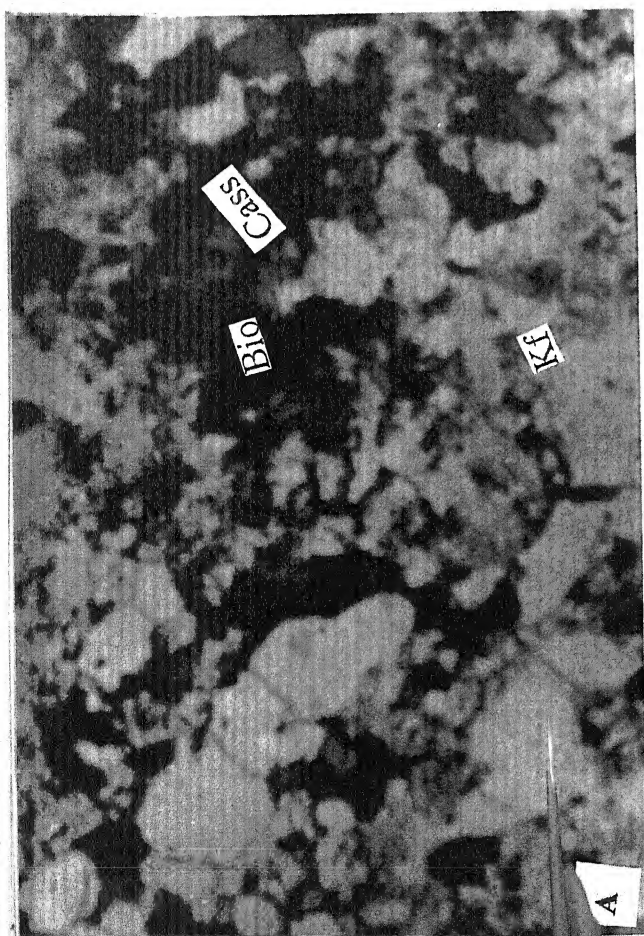


PLATE – XVII

Fig (A): Photomicrograph of granite gneiss (K.G.G.), showing microcline perthite texture. The biotite grains have been altered and also present non-crystallised quartz along the periphery of microcline. Cleavelandite variety of albite and epidote are observed in the rock. Quartz veins are cut-across the microcline.

(Ref. No. F/56, A)
[Crossed Polars, 4×3.3]

Fig (B): Photomicrograph of biotite granite (K.B.G.). Muscovitised biotite, orthoclase, microcline and albite are visible round shape biotite; quartz and iron oxides are present.

(Ref. No. F/23, A)
[Crossed Polars, 4×3.3]

Fig (C): Photomicrograph of biotite granite (K.B.G.). The sericitised orthoclase shows the Carlsbad twinning. The brown biotite has been altered into chlorite to some extent. Quartz, apatite and magnetite are also present.

(Ref. No. F/15, A)
[Crossed Polars, 4×3.3]

Fig (D): Photomicrograph of the contact biotite granite (K.B.G.) with the pegmatite (K.P.). The large grains of albites, which are highly sericitised along its lamellae, have inclusions of quartz and feldspar. Along the boundary of this large grain of albite, the altered greenish biotite and quartz are present.

(Ref. No. K₂)
[Crossed Polars, 4×3.3]

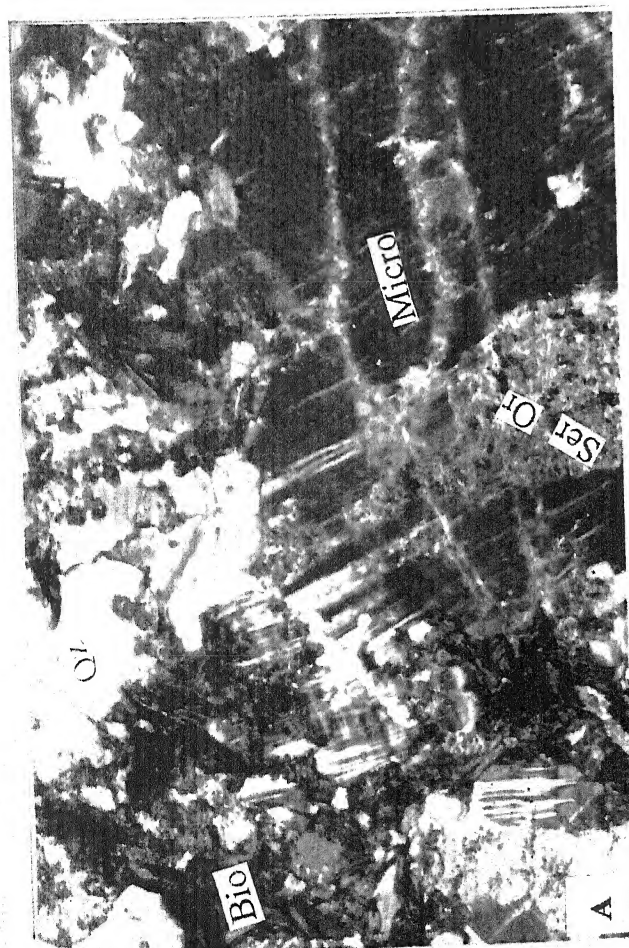


PLATE – XVIII

Fig (A): Photomicrograph of hornblende granite (K.H.G.). Due to alteration of hornblende, large crystals of iron oxide are developed. Sericitised feldspars, quartz, sphene and epidote are also present.

(Ref. No. L₃)

[Crossed Polars, 4 × 3.3]

Fig (B): Photomicrograph of hornblende granite (K.H.G.). Hornblende is changing into biotite along the periphery. Quartz, plagioclase, feldspar, zircon and magnetite are also visible.

(Ref. No. F/57, B)

[Crossed Polars, 4 × 3.3]

Fig (C): Same photomicrograph of the above (Fig. B).

[Crossed Polars, 4 × 3.3]

Fig (D): Photomicrograph of hornblende granite (K.H.G.), shows the plaited hair type perthite. Quartz, microcline and iron oxides are present.

(Ref. No. L₆)

[Crossed Polars, 4 × 3.3]

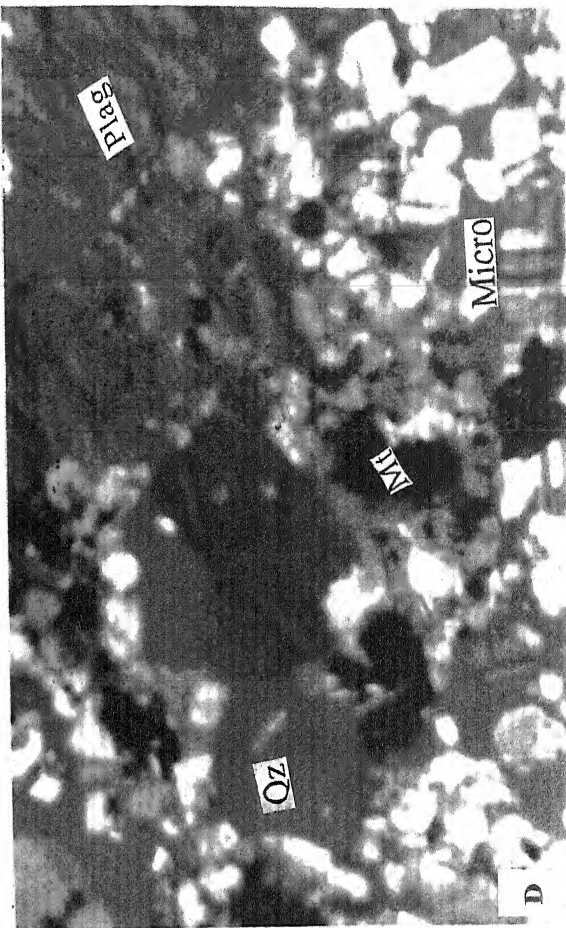
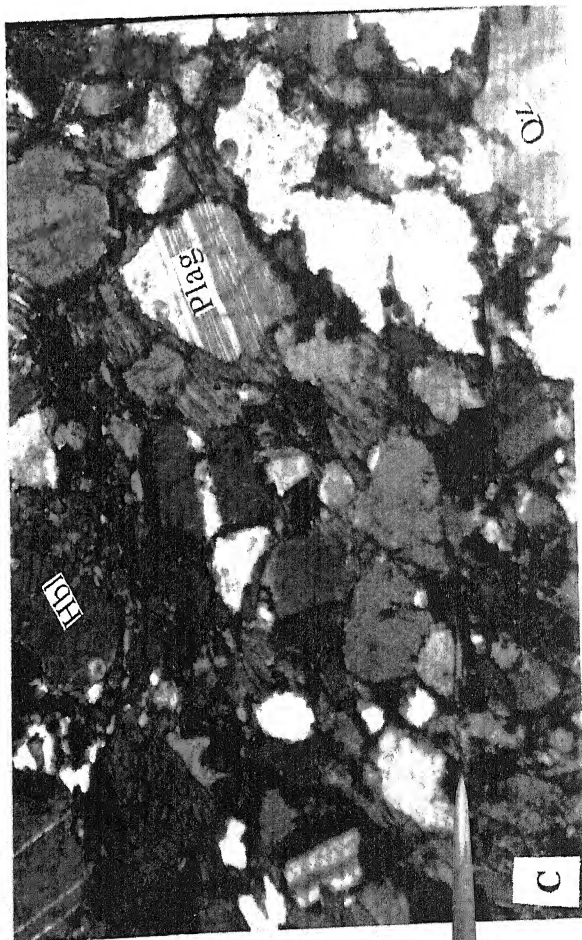
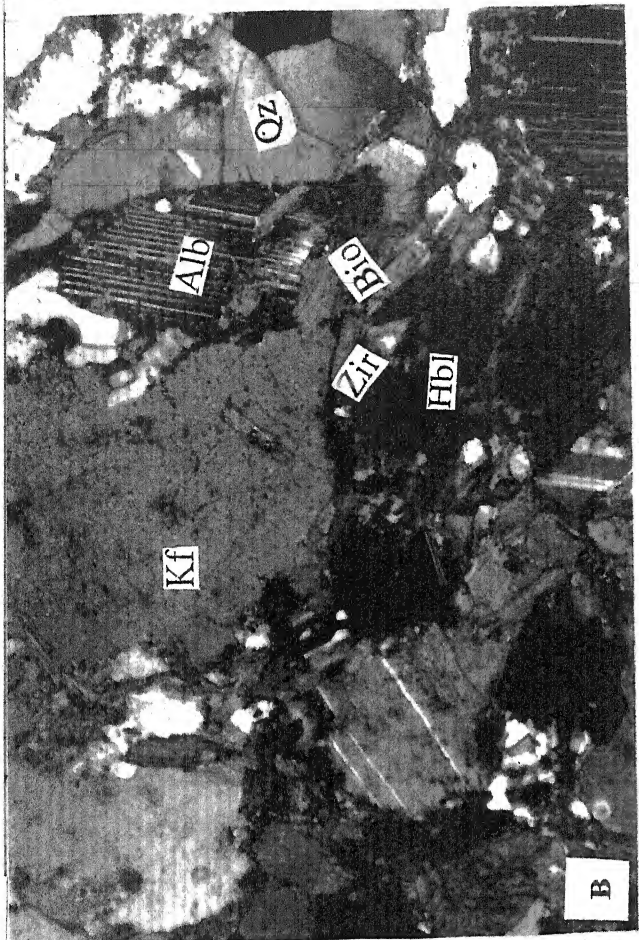
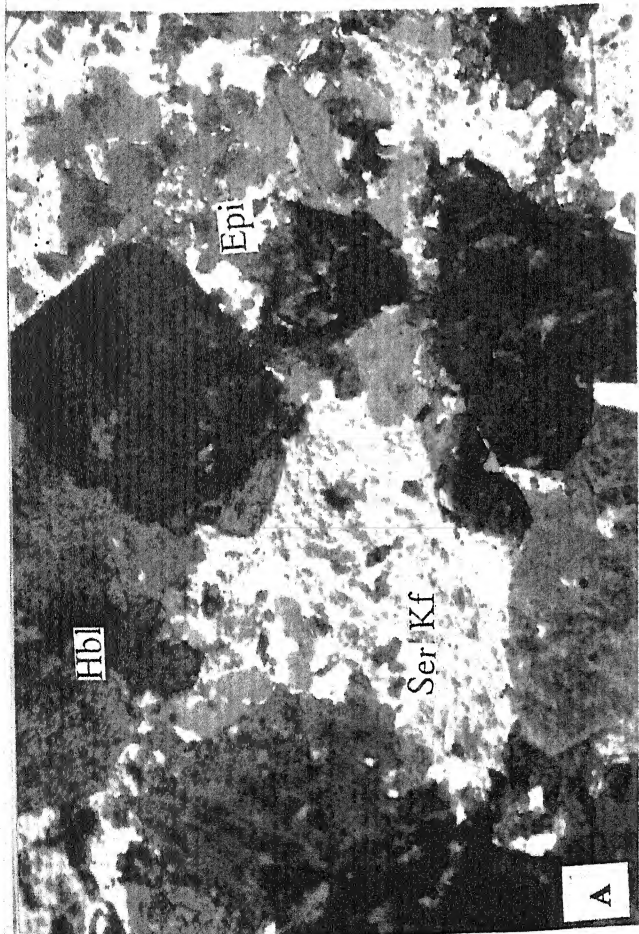


PLATE - XIX

Fig (A): Photomicrograph of tourmaline granite (K.T.G.). It shows clusters of tiny radiating needle grains of tourmaline, which appeared like "tourmaline Sun", due to pneumatolytic action. Feldspars are sericitised and also development of albite in it.

(Ref. No. F/109, A)
[Crossed Polars, 4×3.3]

Fig (B): Same photomicrograph (Fig. A) in high magnification. Quartz shows undulose extinction (strain effect).

(Ref. No. F/109, A)
[Crossed Polars, 4×3.3]

Fig (C): Photomicrograph of pegmatite (K.P.) shows the well-developed crystals of garnet. A number of inclusions such as lithium mica, sericitised orthoclase is present in the large grain of microcline.

(Ref. No. K₂₄)
[Crossed Polars, 4×3.3]

Fig (D): Photomicrograph of contact of granite (K.B.G.) and pegmatite is showing microcline perthite texture. Some part of the thin sections, intergrowth of quartz and microcline has developed to produce graphic in nature. The brownish biotite has been altered to muscovite and iron oxides. Sericitisation phenomenon is also observed in the rock.

(Ref. No. F/42, A)
[Crossed Polars, 4×3.3]

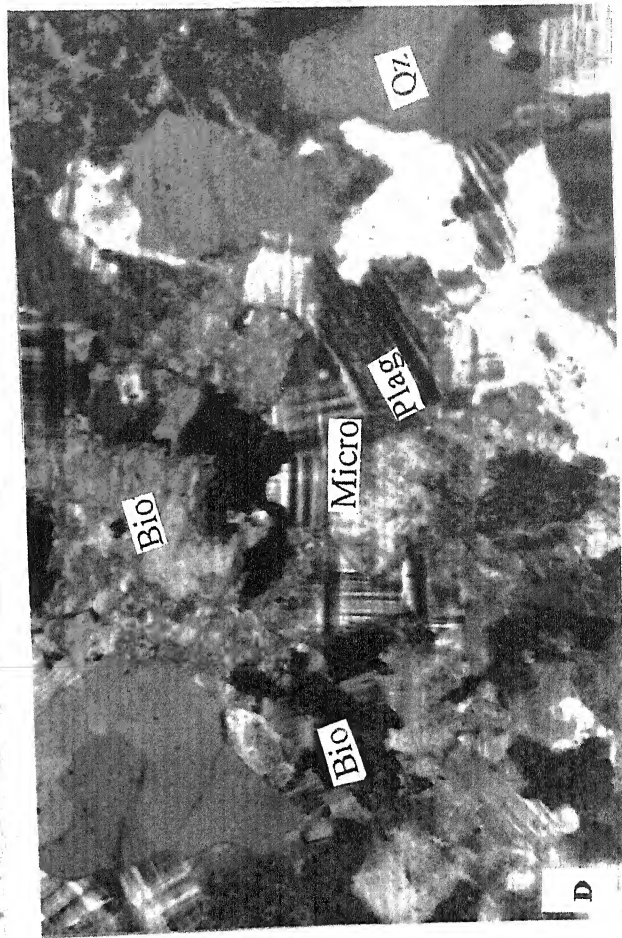
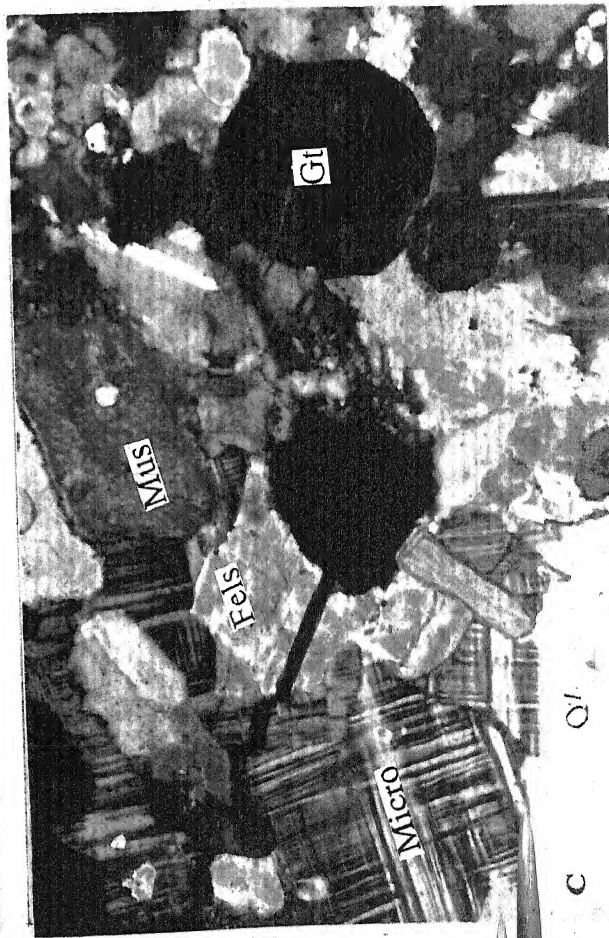
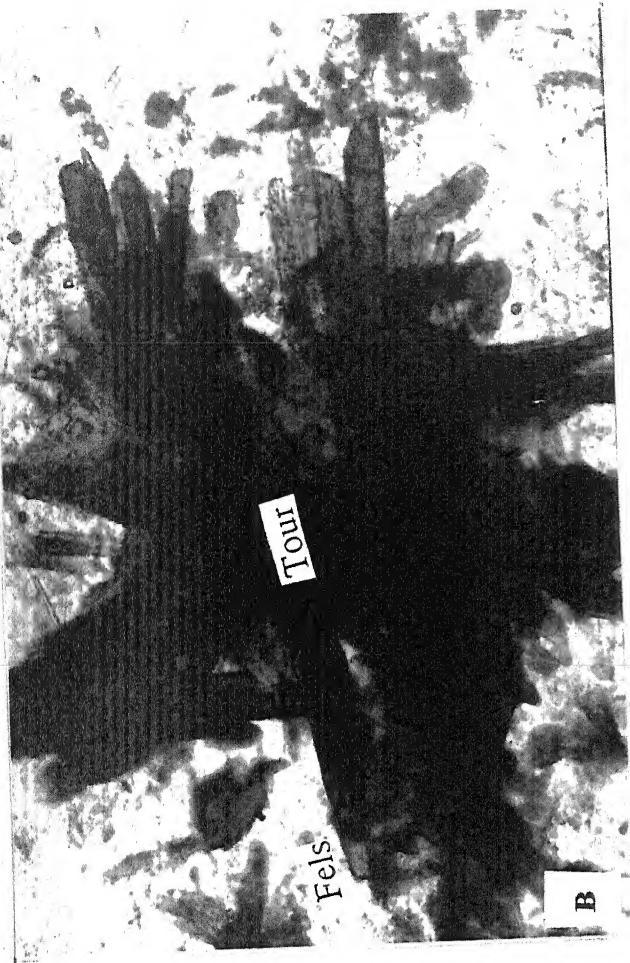


PLATE - XX

Fig (A): Photomicrograph of pegmatite (K.P.), in which original orthoclase has been changed into albite with minute inclusions of quartz and sericite. Large numbers of vein lets of quartz are present as criss-cross pattern in different directions.

(Ref. No. K₉)

[Crossed Polars, 4 × 3.3]

Fig (B): Photomicrograph of pegmatite showing lamellar twinning and its twin lamellae are transversely cracked and becomes non-continuous in nature. The original orthoclase has been changed into cleavelandite of the albite variety. These cleavelandite is believed to have been formed due to metasomatic activity of sodium bearing vapors during or after the emplacement of the pegmatites.

(Ref. No. K₈)

[Crossed Polars, 4 × 3.3]

Fig (C): Photomicrograph of cassiterite bearing pegmatite (K.P.) where minerals such as cassiterite, magnetite, sphene etc., occur at the contact of the altered biotite and orthoclase. The cleavelandite variety of albite is sericitised.

(Ref. No. K₁₄)

[Crossed Polars, 4 × 3.3]

Fig (D): Photomicrograph of greisenised pegmatite (K.P.) showing the muscovitisation of the biotite. Quartz and iron oxides are also present.

(Ref. No. F/57, A)

[Crossed Polars, 4 × 3.3]

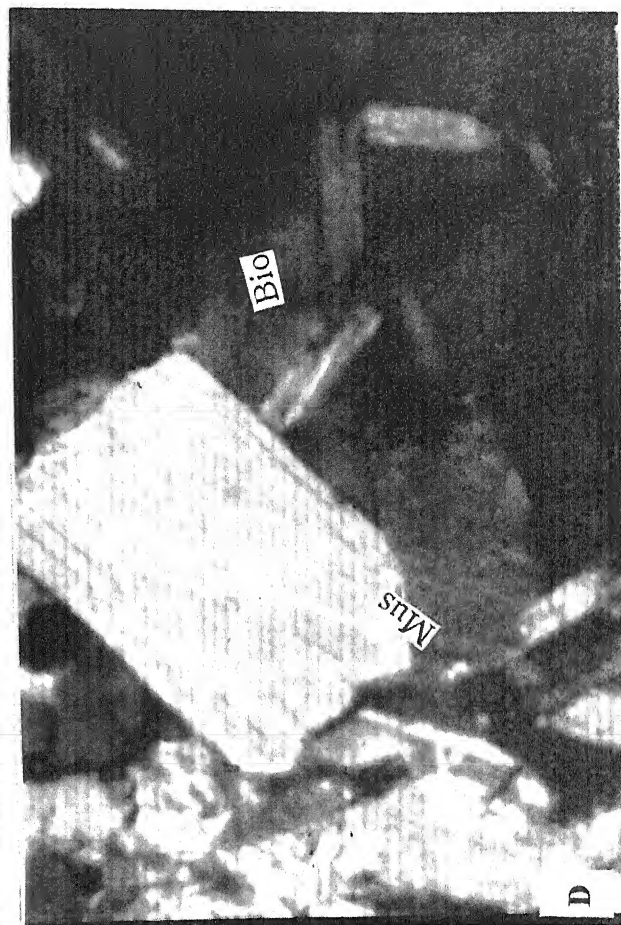
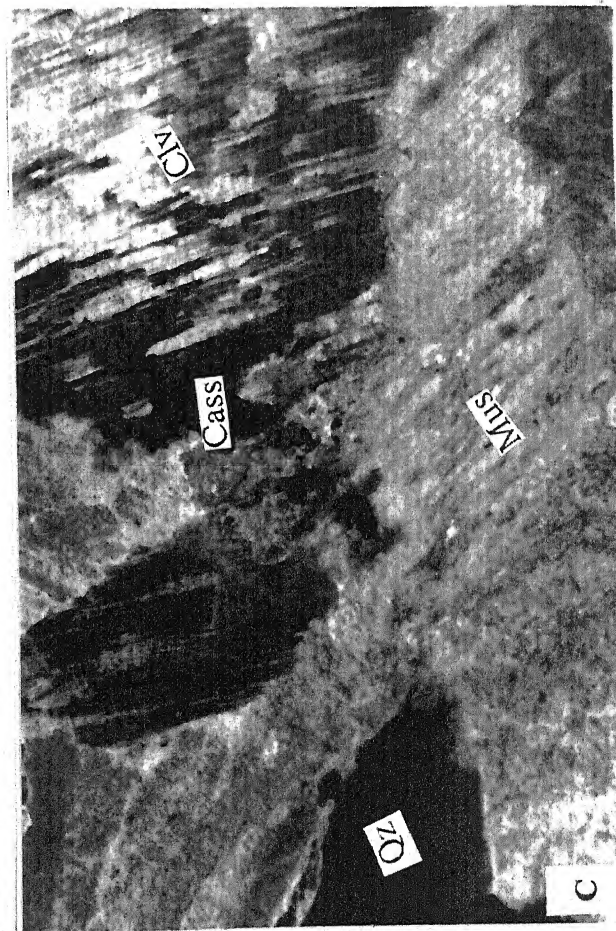


PLATE - XXI

Fig (A): Photomicrograph of pegmatite (K.P.). The zoning of the columbite-tantalite is present in the twinned cassiterite crystal. The quartz, sericitised feldspars and reddish brown limonitic materials are present.

(Ref. No. K₁₂)
[Crossed Polars, 2.5 × 9]

Fig (B): Photomicrograph of pegmatite (K.P.) showing the intergrowths of quartz and originally orthoclase. This orthoclase is altered into the cleavelandite of the albite variety. The minute grains of muscovite, cassiterite and magnetite are also present.

(Ref. No. F/58, C)
[Crossed Polars, 4 × 3.3]

Fig (C): Photomicrograph of greisenised pegmatite (K.P.). The intercalations of quartz and muscovite (lepidolite) are clearly seen in this rock. Leucoxene variety of sphene and cassiterite are also present.

(Ref. No. F/58, B)
[Crossed Polars, 4 × 3.3]

Fig (D): Photomicrograph of pegmatite (K.P.) shows the large crystal of cleavelandite of the albite variety to have the inclusions of fluorite (blue) and quartz. The cleavelandite lamellae are also represent somewhat microfaulted in nature.

(Ref. No. K₁₅)
[Crossed Polars, 4 × 3.3]

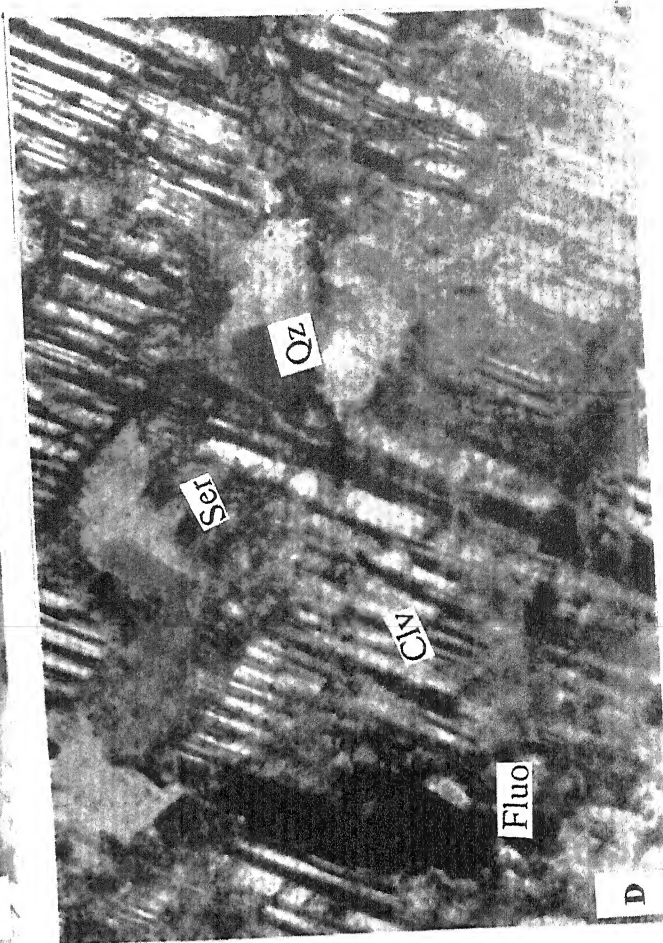
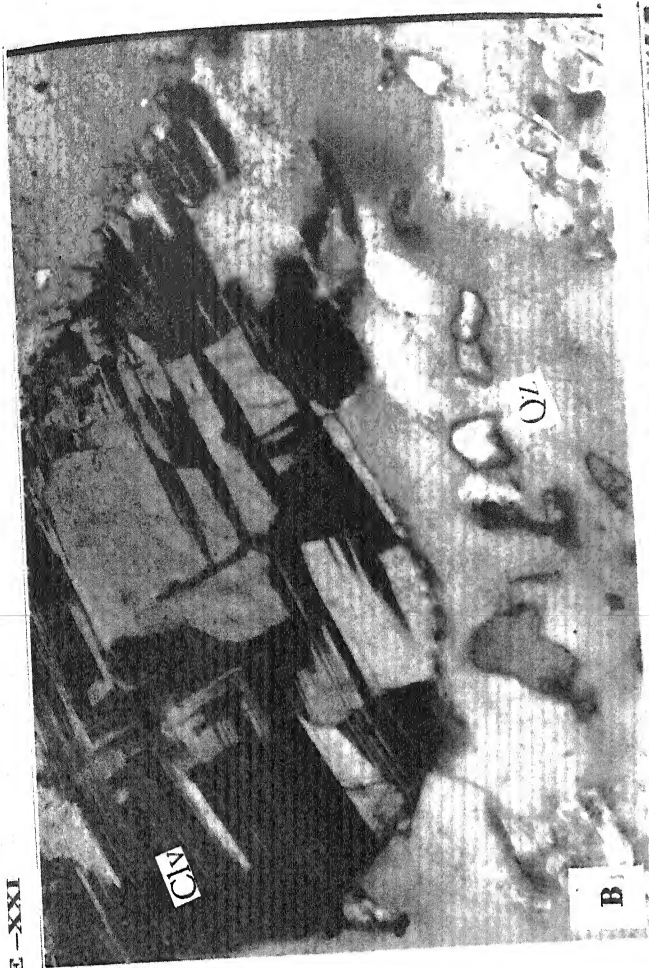
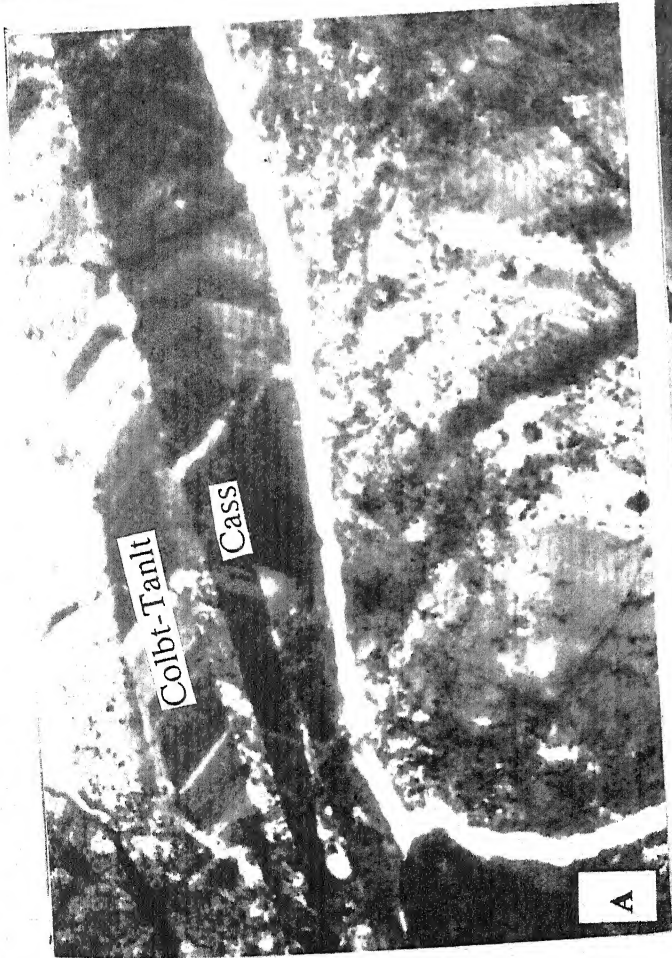


PLATE - XXII

Fig (A): Photomicrograph of the metadolerite. It shows the idiomorphic relict ophitic texture, in which pyroxenes are altered into fibrous amphibole (uralite). The myrmekitic textures are observed in the rock. Plagioclase and magnetite are also present.

(Ref. No. F/59)
[Crossed Polars, 4 × 3.3]

Fig (B): Photomicrograph of the metadolerite. Reaction rims of hornblende surround the augite. On the reaction rims, hornblende is again changes into biotite produces iron oxides. The plagioclase laths are surrounded by pyroxene in the rock.

(Ref. No. F/70)
[Crossed Polars, 4 × 3.3]

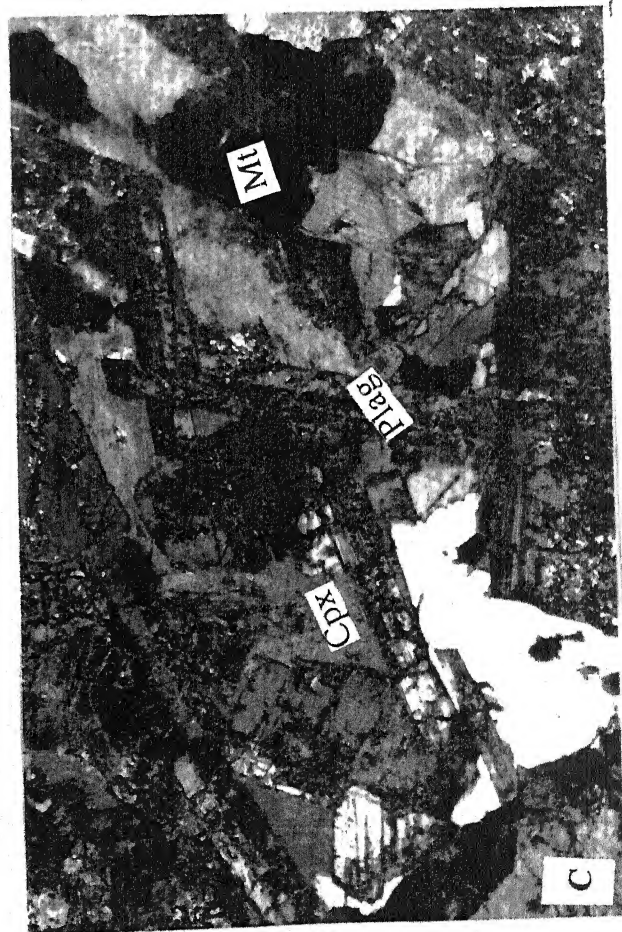
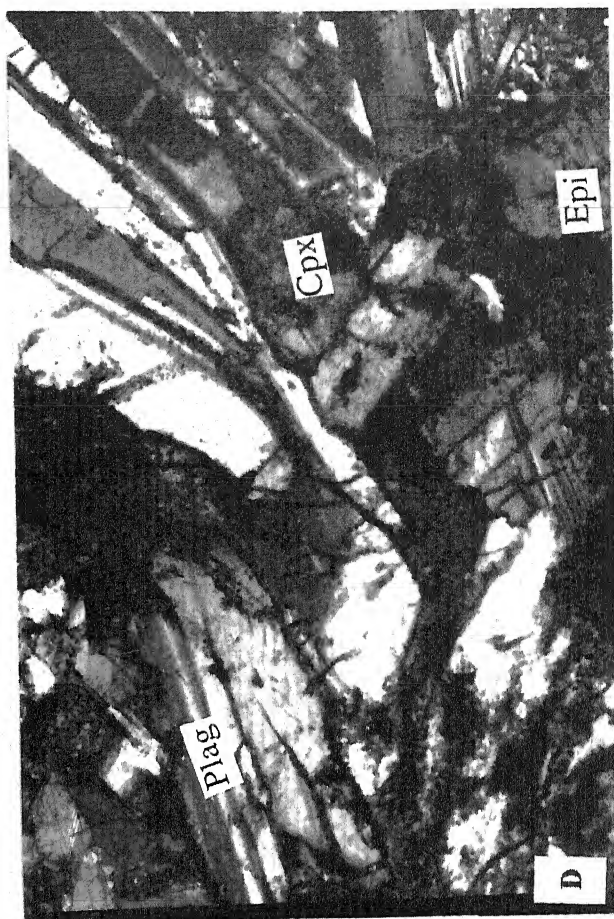
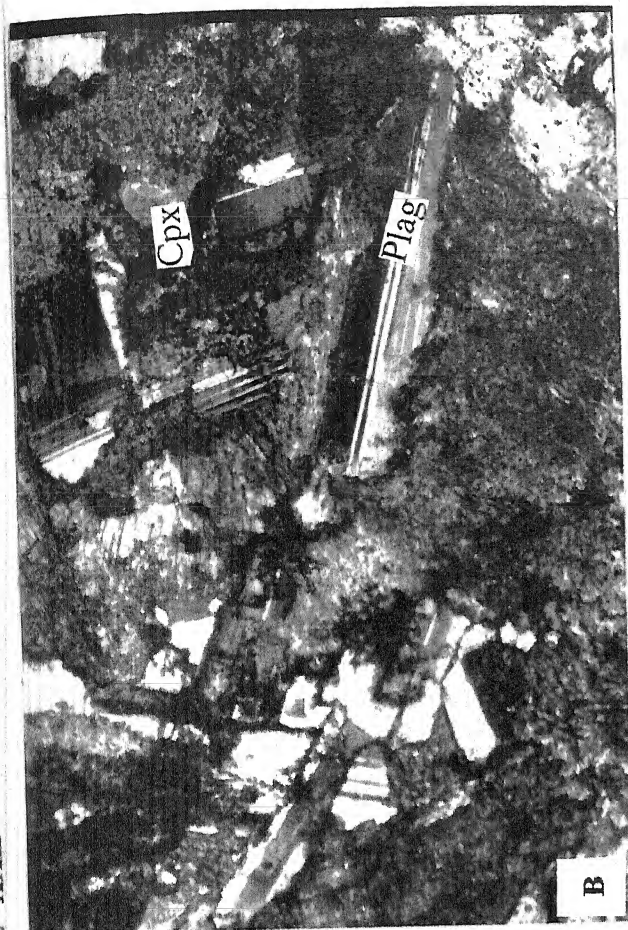
Fig (C): Photomicrograph of metadolerite. The light yellow to colourless enstatite (pyroxene), pinkish colour of hypersthene (pyroxene), hornblende, plagioclase and magnetite and present.

(Ref. No. F/85, C)
[Crossed Polars, 4 × 3.3]

Fig (D): Photomicrograph of metadolerite. The light yellow to colourless enstatite (pyroxene), pinkish colour of hypersthene (pyroxene), hornblende, plagioclase and magnetite and present.

(Ref. No. F/85, C)
[Crossed Polars, 4 × 3.3]

PLATE -XXII



GEOCHEMISTRY

4.1. Introduction

In order to classify the granite (KG) and granite gneiss (KGG) of the study area and further to understand their genetic relation within tin mineralisation, major, trace and rare earth elements geochemistry of representative lithounits of KG and KGG have been carried out. From the field relations and petrographic observation of different lithounits of the area (discussed in preceeding chapter), it appears that the tin mineralisation is primarily associated and genetically related to KG emplaced as the last phases of acidic magmatism of region. Therefore, special emphasis has been given to the genesis of KG and its possible relation with respect to the tin mineralisation. An attempt has also been made to understand the relationships of KGG (equivalent to Sukma granite gneiss as older protolith) with the KG whether or not potential KG melt can be divided by melting of KGG.

4.2 Major element geochemistry

Twenty-five representative samples of KG (N=11), KGG (N=7) and pegmatite (N=7) from Katekalyan area were analysed by X- ray Fluorescence Spectrometer Philips Exam Six and PV 9100 at Wadia Institute of Himalayan Geology, Dehradun. The major elements (wt%) and their calculated CIPW weight norms for the granite (KG), granite gneiss (KGG) and pegmatite (KP) are represented in table 4.1a, 4.1b and 4.1c respectively.

Granitoids [granite (KG) and granite gneiss (KGG)]:

The granites of Katekalyan area is represented by dominant biotite granite (KBG), subordinate hornblende granite (KHG) and tourmaline granite (KTG), collectively referred here with granites (KG).

The major elements data presented in table (4.1 a-c) depicts the following characteristics of the Katekalyan granitoids:

- [i] The KG and KGG are highly silicic, having 57.75 to 72.19-wt% SiO_2 and 65.87 to 75.49-wt% SiO_2 respectively.
- [ii] Alumina in KG and KGG are present as moderate to high ranges from 14.06 to 22.53 wt% and 14.28 to 18.48-wt% Al_2O_3 respectively but have greater than the total alkalies ($\text{Na}_2\text{O} + \text{K}_2\text{O} = 2.23 - 9.76$ wt%).
- [iii] The potash content in KG ($\text{K}_2\text{O} = 2.02 - 7.15$ wt%) and KGG ($1.07 - 8.48$ wt%) is more than the soda content ($\text{Na}_2\text{O} = 0.49 - 3.95$ wt%).
- [iv] The low titania content in KG ($\text{TiO}_2 = 0.02 - 0.75$ wt%) and KGG ($\text{TiO}_2 = 0.05 - 0.71$ wt%).

Thus KG and KGG are characterised by high silica, moderate to high alumina, higher K_2O than Na_2O and low TiO_2 content.

4.2.1. Classification and nomenclature:

These granitoids have been chemically classified on the basis of different oxide, norm and cationic parameters. The classification schemes based on Na_2O vs K_2O (Harpum, 1963), CaO - Na_2O - K_2O (Hunter, 1974), An-Ab-Or (O'Connor, 1965), Q-A-P (Streckeisen, 1967, and Le Maitre, 1989), R_1 - R_2 multicationic (De La Roche *et al*, 1980) and P-Q (Debon and Le Fort, 1983) etc. The Na_2O vs K_2O (Fig. 4.1) and ternary CaO - Na_2O - K_2O (not shown) diagrams for Katekalyan granitoids were plotted where the majority of the samples fall in the field of granite, but few of them are in the adamellite to granodioritic fields. The samples lie in the fields of granite to granodiorite in normative classification, ternary An-Ab-Or (Fig. 4.2) and Q-A-P (Fig. 4.3). However, the hornblende granite (KBG) due to poor potassium content falls in the field of tonalite. An alternative approach based on major element criteria of various granitoids of Katekalyan is proposed using cationic/molecular

values such as R_1 - R_2 multicationic classificatory (after De La Roche *et al.*, 1980) diagram (Fig. 4.4). It includes all major cations derived from a mineralogical network, the degree of silica saturation and the combined changes in $Fe/(Fe + Mg)$ and $(Ab + Or)/a$ ratio which express whole-rock chemistry of the granitoids. $R_1 = [4Si - 11(Na + K) - 2(Fe + Ti)]$ and $R_2 = [6Ca + 2Mg + Al]$ parameters have been calculated from bulk chemical analyses (Table 4.1a and 4.1b) as oxide weight percentage converted to molar proportions. Plotting of samples on this classificatory R_1 - R_2 diagram in figure 4.4 (after De La Roche *et al.*, 1980), the Katekalyan granitoids belong to granite (syenogranite and monzogranite) to granodiorite. But the hornblende granite (KHG) plots in the field of tonalite. The $P = [K - (Na + Ca)]$ and $Q = [Si/3 - (K + Na + 2Ca/3)]$ (Fig. 4.5), proposed by Debon and Le Fort (1983), reveal that majority of the samples are plot in the fields of granite, adamellite and granodiorite.

Greig and Stenprok (1969) proposed a discrimination scheme for tin bearing granitoids in ternary diagram $(SiO_2 - (FeO + CaO + MgO) - (Al_2O_3 + Na_2O + K_2O))$ with the idea that stanniferous granitoid are usually high in silica, Al_2O_3 and Na_2O and depleted in ferro-calc-magnesium constituents. The specified compositional tin field ranges from 75 to 83% for SiO_2 , 17 to 25% for combined $Al_2O_3 + Na_2O + K_2O$ and less than 5% for ferro-calc-magnesium contents. The diagram has been applied (Fig. 4.6) for granitoids (KG and KGG) and pegmatites (KP) of Katekalyan also. Almost all tin-bearing granitoids and pegmatites of the Katekalyan area fall within "tin zone". However, a few of the tin-bearing granitoids represent the excess of FeO and CaO , and slightly away from the field, this perhaps due to partial digested of mafic xenoliths.

The tin-bearing granitoids show low affinity to mafics but high affinity to felsic constituents with preference for moderately to higher K_2O and Na_2O contents (Babu, 1993). Applying the ternary plot (Fig. 4.7) of silica (SiO_2), total mafics ($FeO^* + CaO + MgO + MnO$) and alkalis ($Na_2O + K_2O$) as proposed by T.M. Babu (1993), all the tin-bearing granitoids (KG and

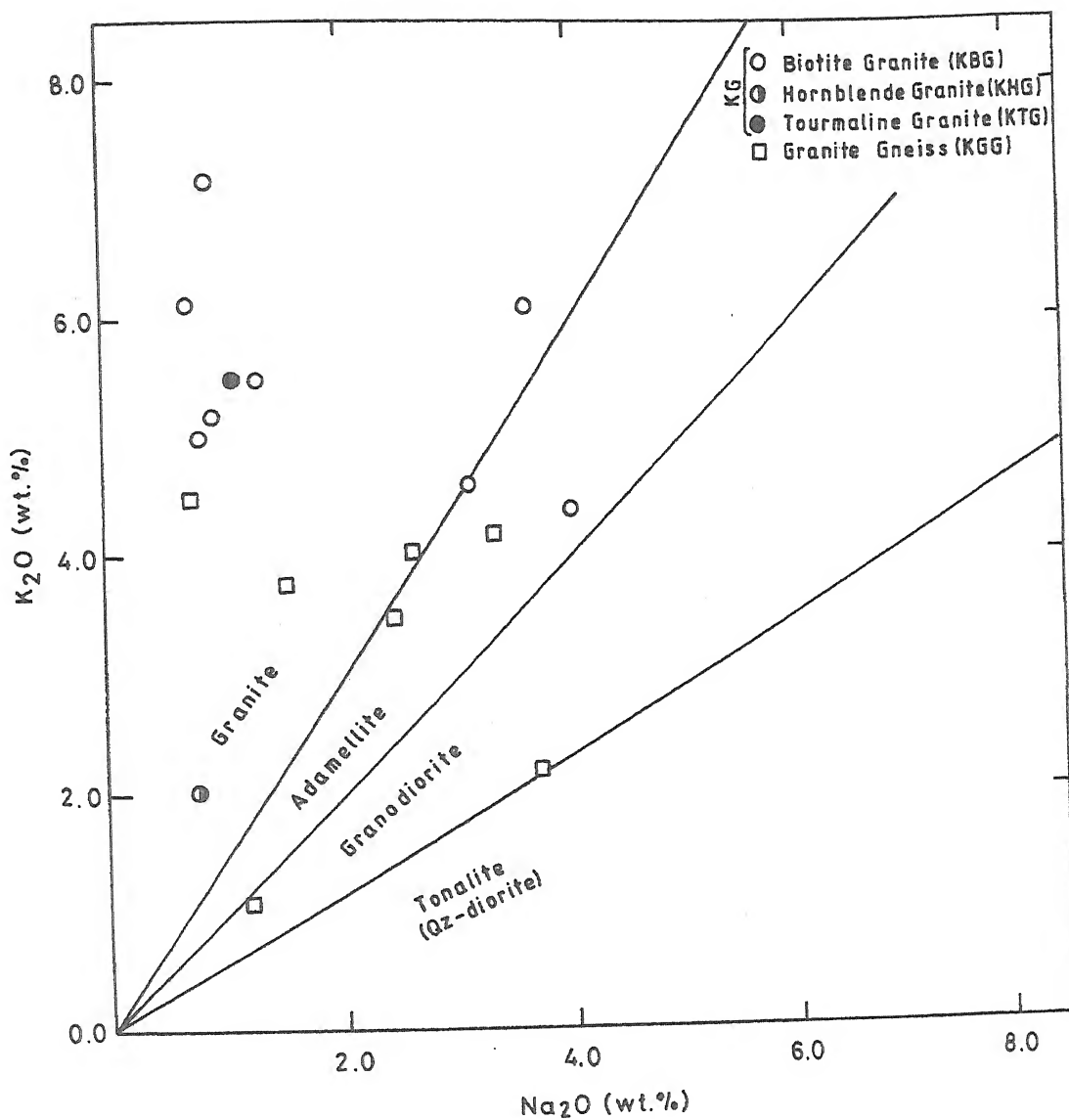


Fig. 4.1. Na_2O vs K_2O (wt.%) plots for the Katekalyan granitoids, district Dantewada, Chhattisgarh (Harpum, 1963).

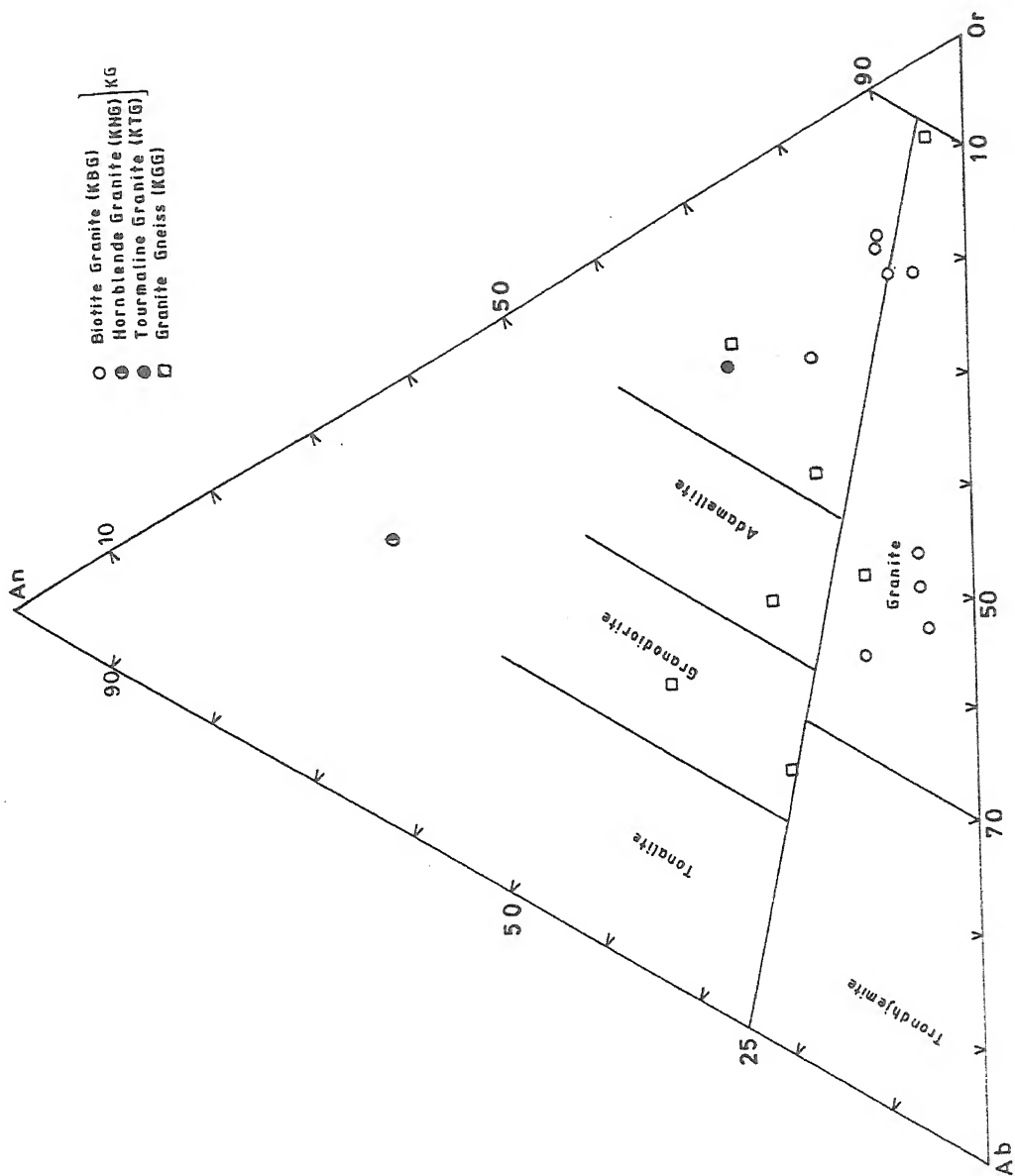


Fig. 4.2. Normative An-Ab-Or plots for Katekalyan granitoids, district Dantewada, Chhattisgarh (After O'Connor, 1965)

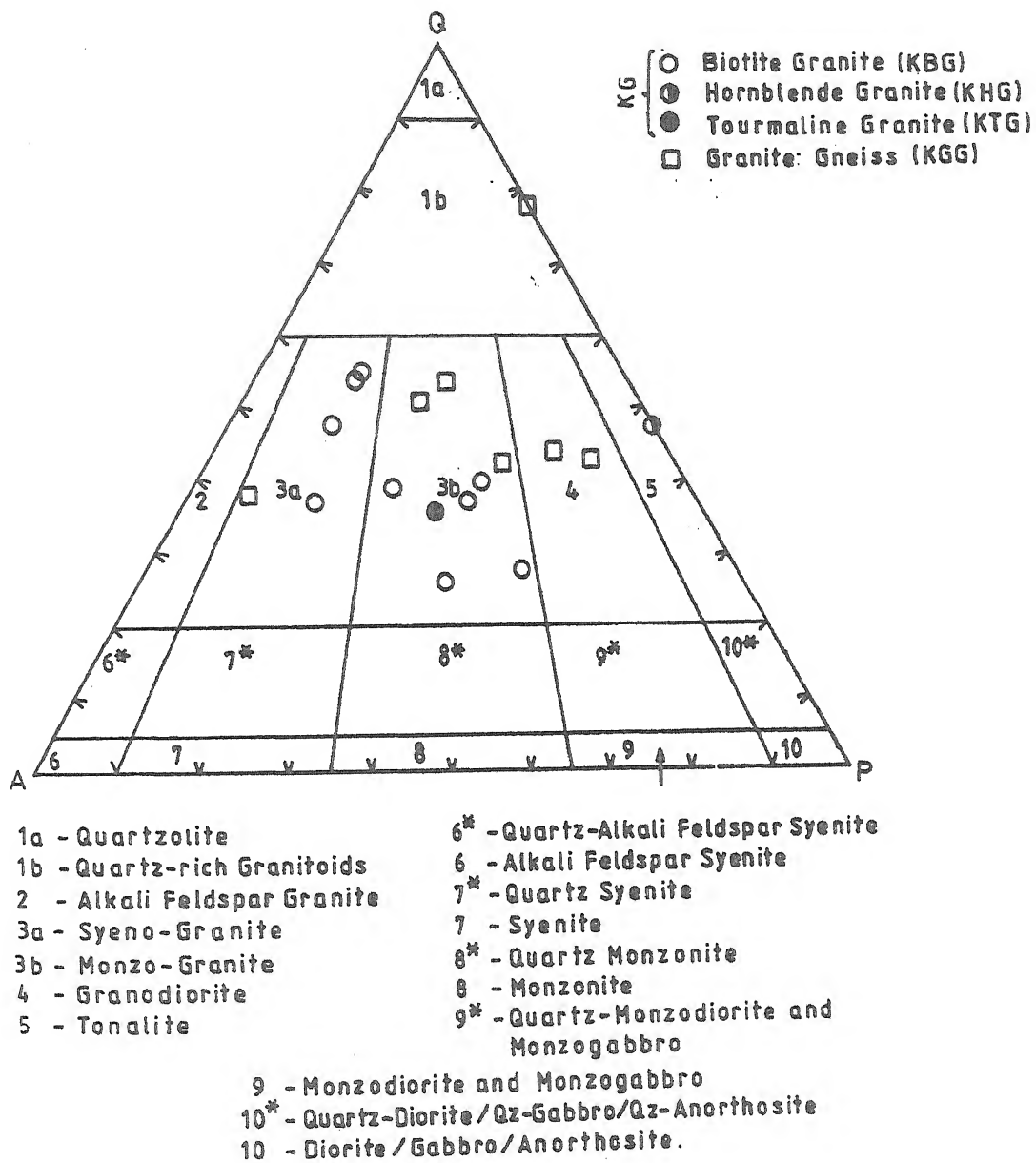


Fig. 4.3. The normative Q-A-P variation diagram after LeMaitre (1989) showing field of variation of the Katekalyan granitoids, district Dantewada (Chhattisgarh).

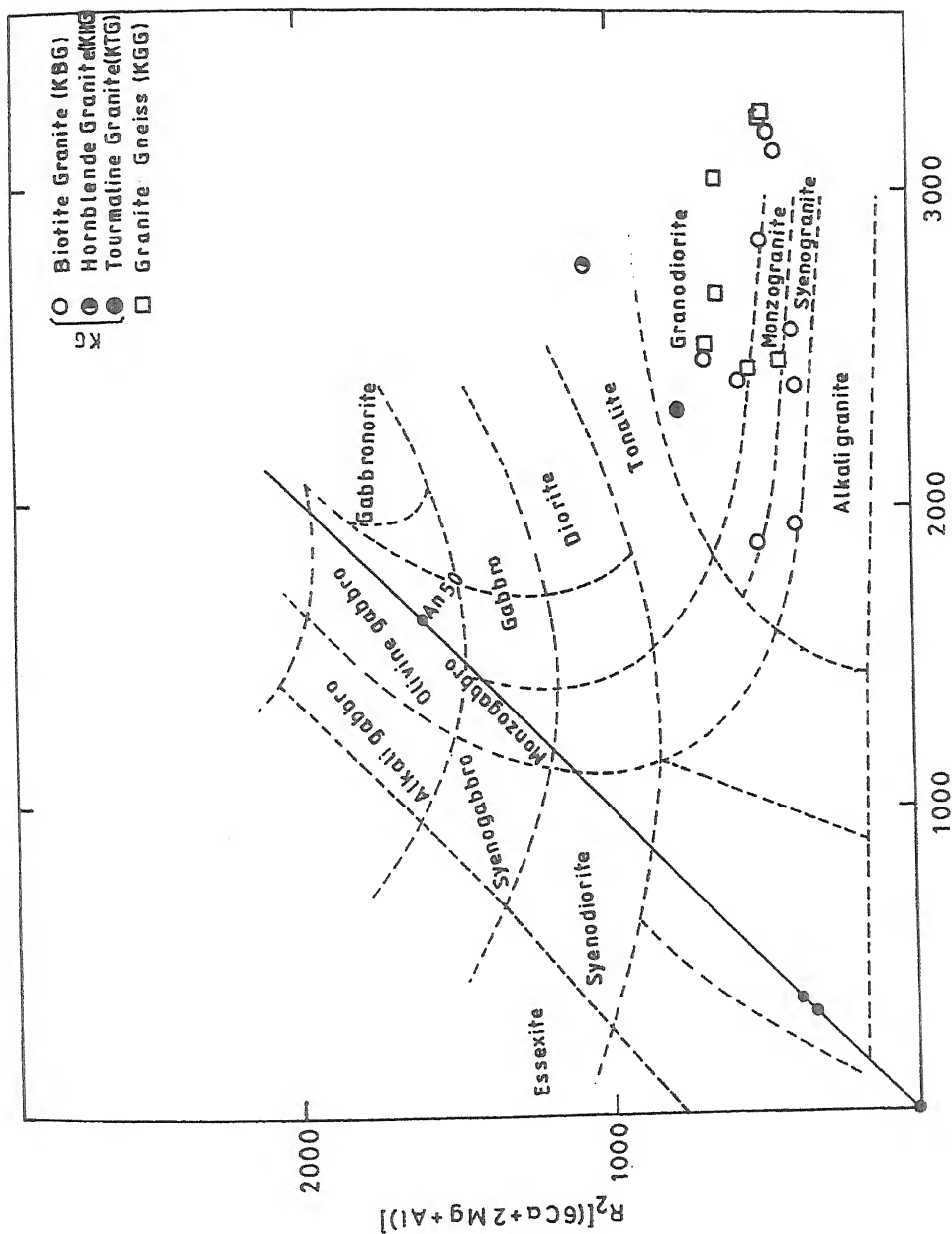
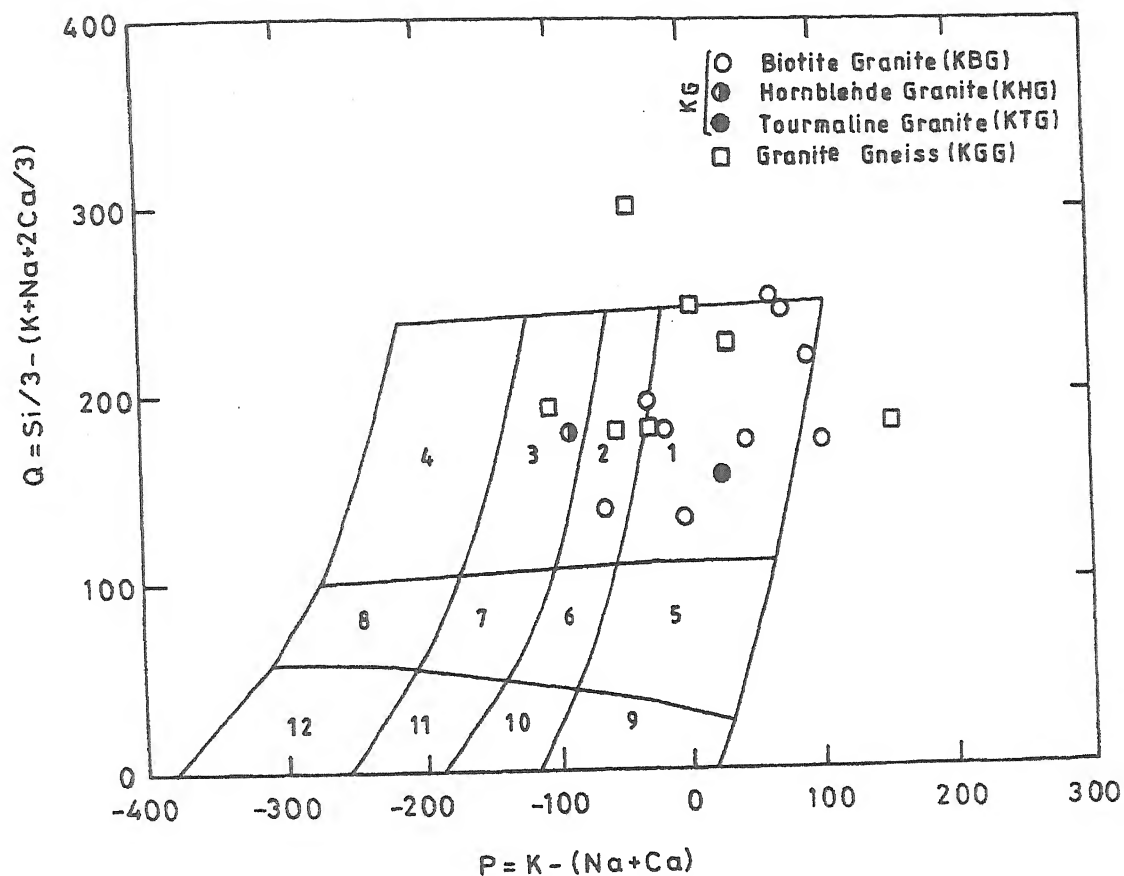


Fig. 4.4. The classification scheme is based on major element criteria of the Katekalyan granitoids using the parameters R_1 and R_2 (After De La Roche *et al.*, 1980), calculated from millication proportions.



1. Granite, 2. Adamellite, 3. Granodiorite, 4. Tonalite, 5. Quartz Syenite, 6. Quartz Monzonite, 7. Quartz Monzodiorite, 8. Quartz Diorite, 9. Syenite, 10. Monzonite, 11. Monzogabbro, 12. Gabbro.

Fig. 4.5. P vs Q diagram for the Katekalyan granitoids based on Debon and LeFort (1982). The parameters are expressed as gram atoms $\times 10^3$ of each element in 100 gm of material. Each pigeon hole of the classification grid corresponds to a petrographical group (1 to 12).

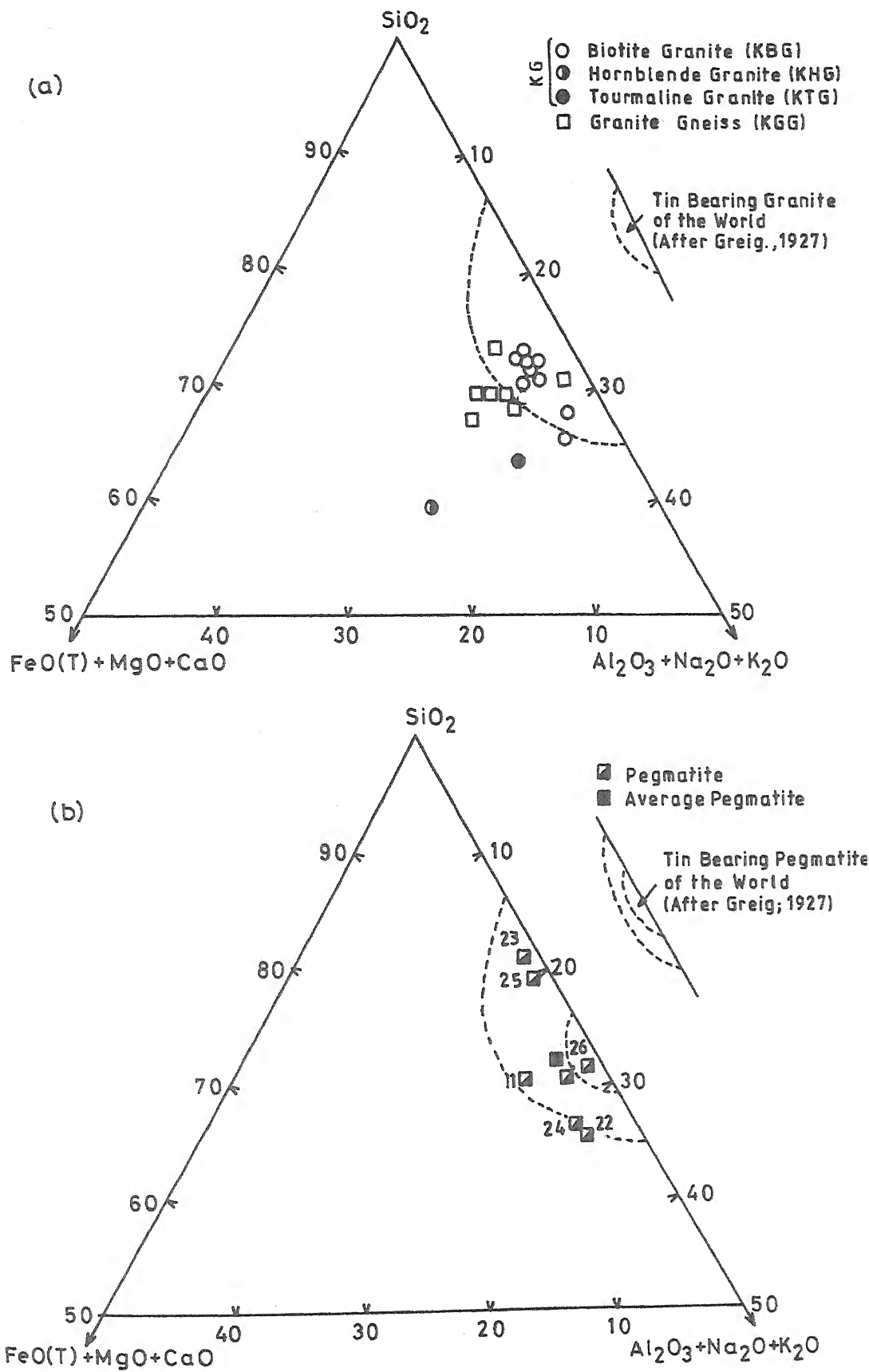


Fig. 4.6. Ternary diagram SiO_2 -($\text{FeO}^* + \text{MgO} + \text{CaO}$) - ($\text{Al}_2\text{O}_3 + \text{Na}_2\text{O} + \text{K}_2\text{O}$) of the tin bearing granitoids (a) and pegmatites (b) of the Katekalyan area, district Dantewada, Chhattisgarh (Greig-Stemprok, 1969).

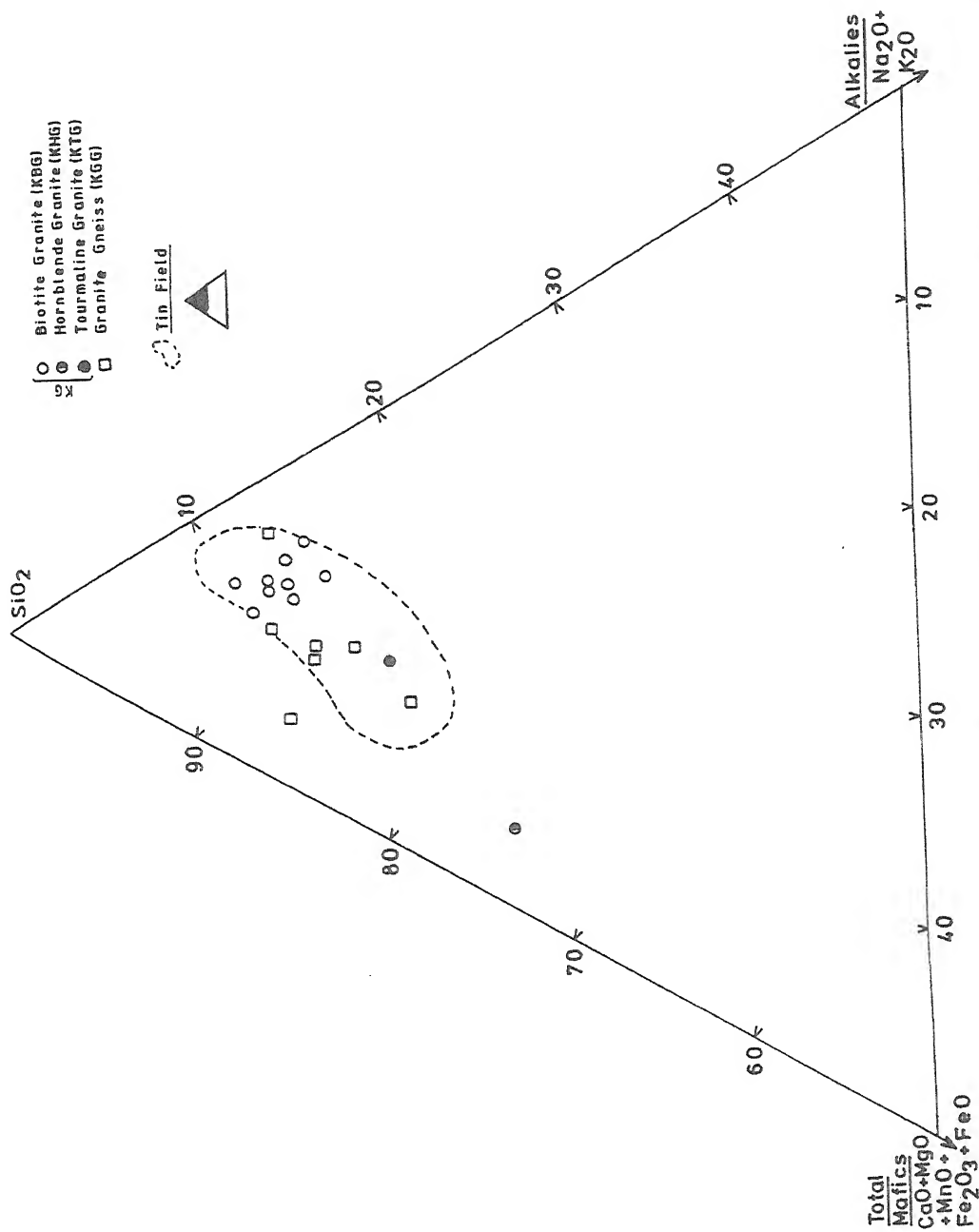


Fig. 4.7. Ternary diagram of Silica-Total Mafics - Alkalies for the Katekalyan granitoids, district Dantewada (Chhattisgarh) along with tin-bearing granites of the world (After T.M. Babu, 1993).

KGG) of Katekalyan plot in the tin field. But the hornblende granite (KHG) and a single KGG plot outside the tin field.

The chemical-mineralogical based on multicationic parameters delineated by Debon and Le-Fort (1982) and Debon *et al.* (1986) define the peraluminous and metaluminous characters depending on its positive and negative values of 'A' respectively. This plot reflects the nature and proportions of their characteristics minerals other than quartz and feldspars. The A-B diagram (Fig. 4.8a), where $A = [Al - (K + Na + 2Ca)]$ versus $B = (Fe + Mg + Ti)$ shows clearly that the most of the Katekalyan granitoids (KG and KGG) occupy the delineated Ist and IInd fields of the peraluminous domain. This indicate that they belong to the association of muscovite > biotite and biotite > muscovite respectively.

The high molar A/CNK i.e., $Al_2O_3/(CaO + Na_2O + K_2O)$ ratios of the analysed granitoids samples are plotted against SiO_2 (Fig. 4.8b). The most of the samples fall in the field of peraluminous composition having molar A/CNK ratio more than 1.1, which suggest that the granitoids though igneous in origin but have some crustal components (Chappel and White, 1974).

Though, it is not possible to assess how much igneous/sedimentary source material was involved in a given granitic rock but it is possible to determine how much a given granitic rock appear an I-type or S-type. Presence of normative corundum and high molar concentration of $Al/(Ca + Na + K) > 1.1$ also suggests the of S-type nature of Katekalyan granitoids (KG and KGG) according to the scheme proposed by Chappel and White (1974).

The criteria used for distinguishing I-type and S-type granites (Chappel and White; 1974 and Takahasi *et al.*, 1980) are given in table, 4.2 and have been compared to Katekalyan granitoids (KG and KGG).

The comperative study reveals that Katekalyan granitoids (KG and KGG) are distinguished as peraluminous S-type granite. They correspond to mica (biotite and muscovite) and presence of garnet, rilit ferromagnisian constituents (metasediment) bzb, relatively high K_2O (with ~ 5 wt% K_2O and <

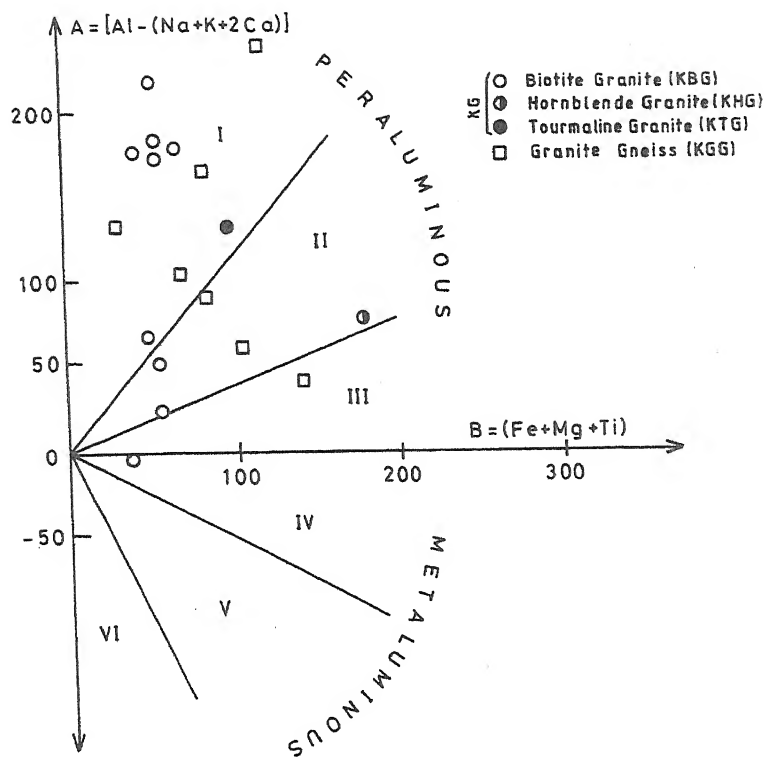


Fig. 4.8a. A vs B diagram of Katekalyan granitoids (After Debon and Lefort; 1982 and Debon *et al.*, 1986). The diagram is divided into six sectors numbered from I to VI. I. $Mu > Bi$, II. $Bi > Mu$, III. $Bi \pm$, IV. $Bi \pm Hbl \pm cpx \pm opx \pm ol \pm$, V. $cpx \pm hbl \pm$, VI. $Di \pm$.

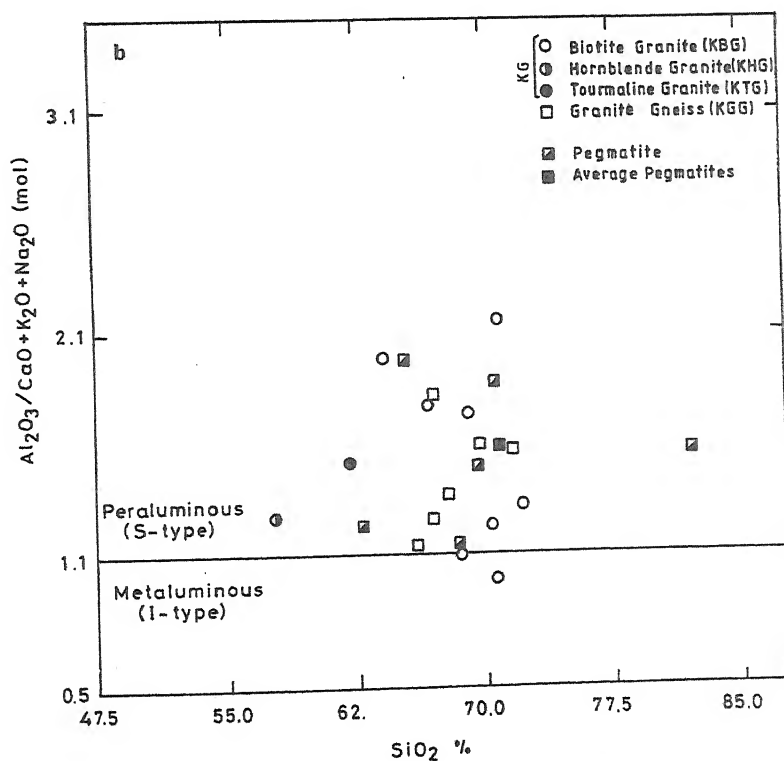


Fig. 4.8b. Mole, $Al_2O_3 / (CaO + K_2O + Na_2O)$ vs SiO_2 plots for the Katekalyan granitoids and pegmatites (Chappel and White, 1974).

3.95 wt% Na_2O), molar $A/(\text{CNK}) > 1.1$, normative corundum > 1 , absence of normative diopside and narrow range of more felsic composition. Leucocratic syeno- and monzo-granite composition predominated with high biotite content are locally important. The other characteristic features viz; presence of ilmenite in place of magnetite and deep brown titanium-rich biotite in place of green biotite indicate that magma was containing relatively low oxygen fugacity and low ferric ferrous ratios.

Total alkalis versus silica (TAS) diagram (not shown) of Middlemost (1985) for classification suggest that most of the Katekalyan granitoids, samples plot in hypoalkalic field and few of them in silica field. It is very clear from this diagram that the Katekalyan granitoids are mostly hypoalkalic in nature and their alkalinity ($\text{Na}_2\text{O} + \text{K}_2\text{O}$) does not exceed more than 10%. This study point out that the local metasomatism may not be ruled out in the study area.

Based on the $\log K_2\text{O}/\text{MgO}$ vs SiO_2 (wt%) diagram (not shown) mentioned in Bhattacharjee (1993), is plotted for the Katekalyan granitoids. The most of the KG and KGG fall in alkali granite field. It is important to mention here that KHG and KGG fall in the field of calc-alkali granite whereas tourmaline granite (KTG) and biotite granites (KBG) fall in the transition zone and alkalic granite fields. These granitoids represent the calc-alkaline differentiation trend, evident from A-F-M diagram (Fig. 4.9) as given by Irvine and Baragar (1971). Though the majority of samples plots in calc-alkaline field but evolved towards alkalis corner.

4.2.2. Tectonic discrimination:

In order to characterise the tectonic environment of the Katekalyan granitoids, the classification scheme proposed by Maniar and Piccoli; 1989 (table 4.3a) demands various steps to be followed in a sequential manner to arrive at the true tectonic environment of the granitoids. Using the different discrimination parameters as proposed by Maniar and Piccoli (1989), it has been noted that the chemical features of KG and KGG granitoids (table 4.3b)

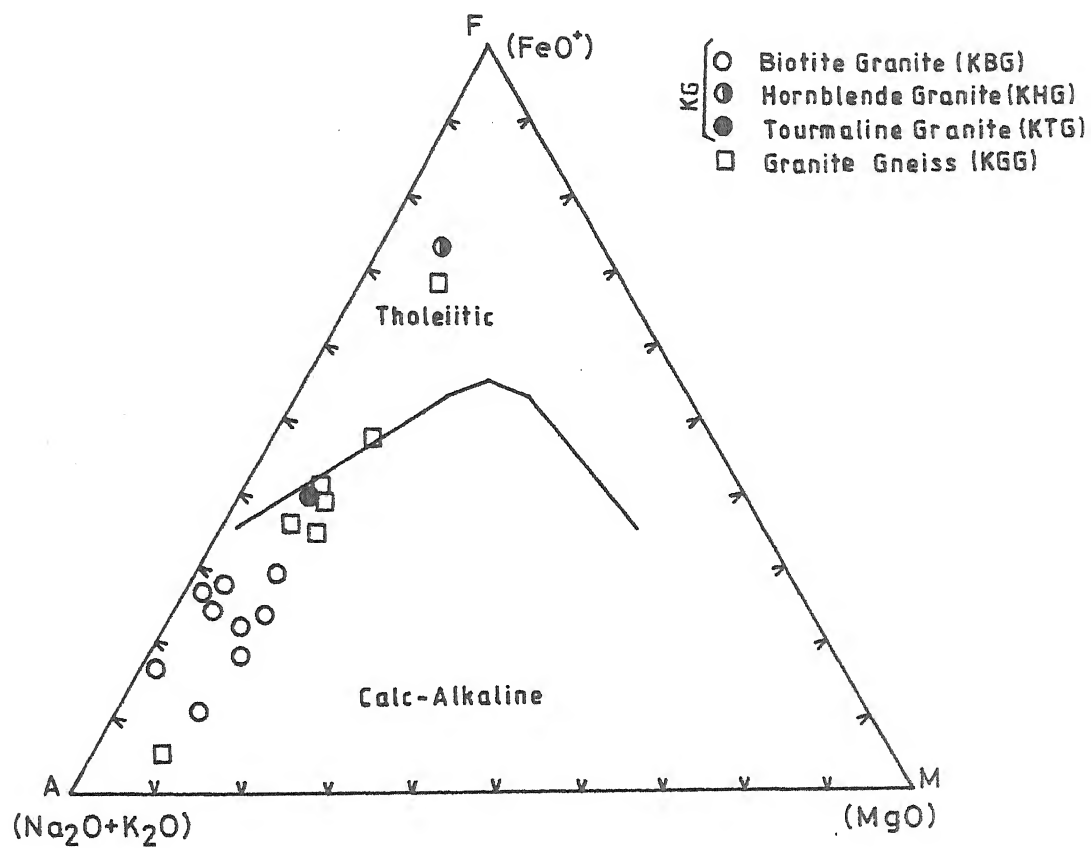


Fig. 4.9. A-F-M diagram plots for the Katekalyan granitoids (after Irvine and Baragar, 1971).

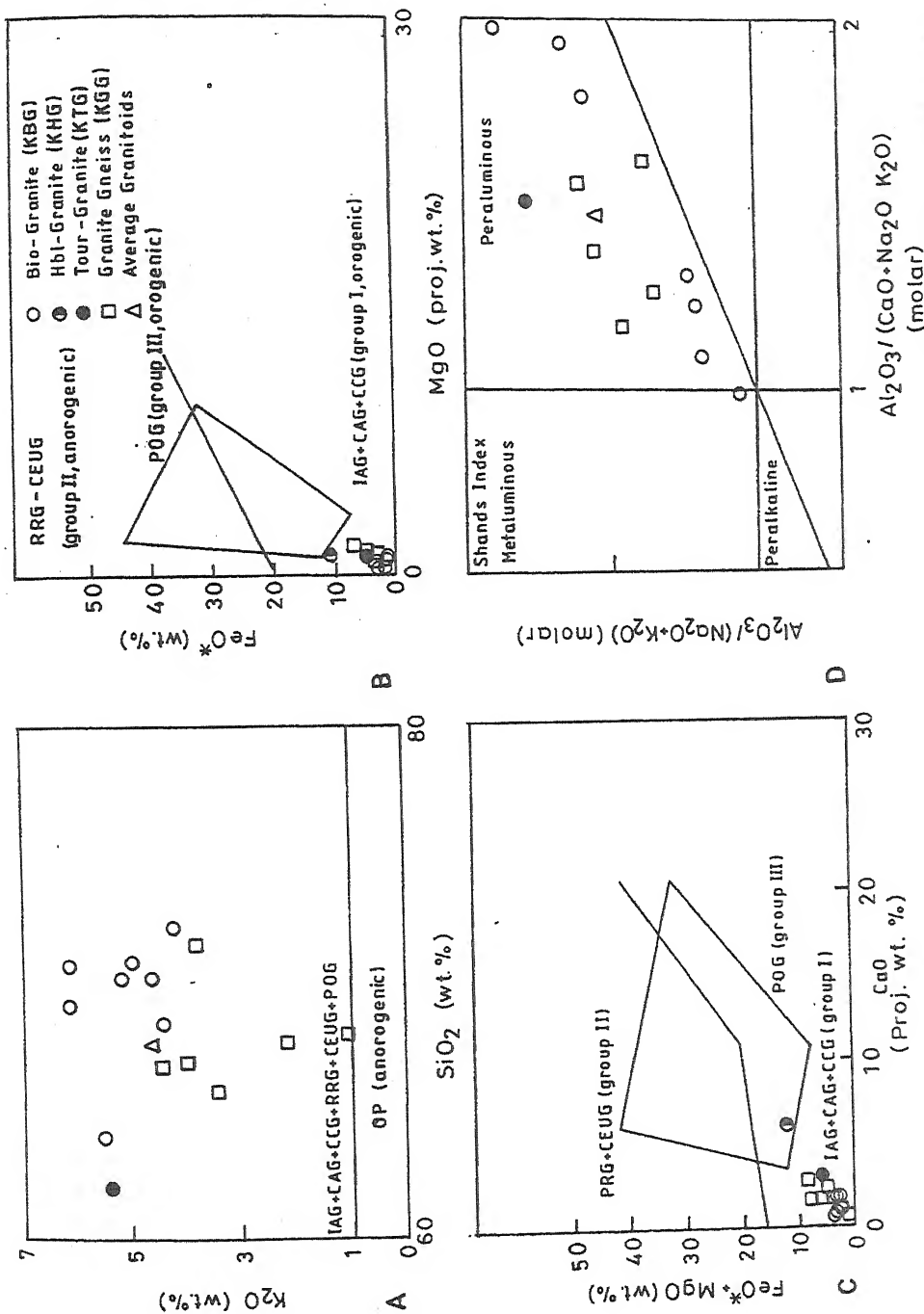


Fig. 4.10. Discrimination diagram for Katekalyan granitoids (Fields after Maniar and Piccoli, 1989).

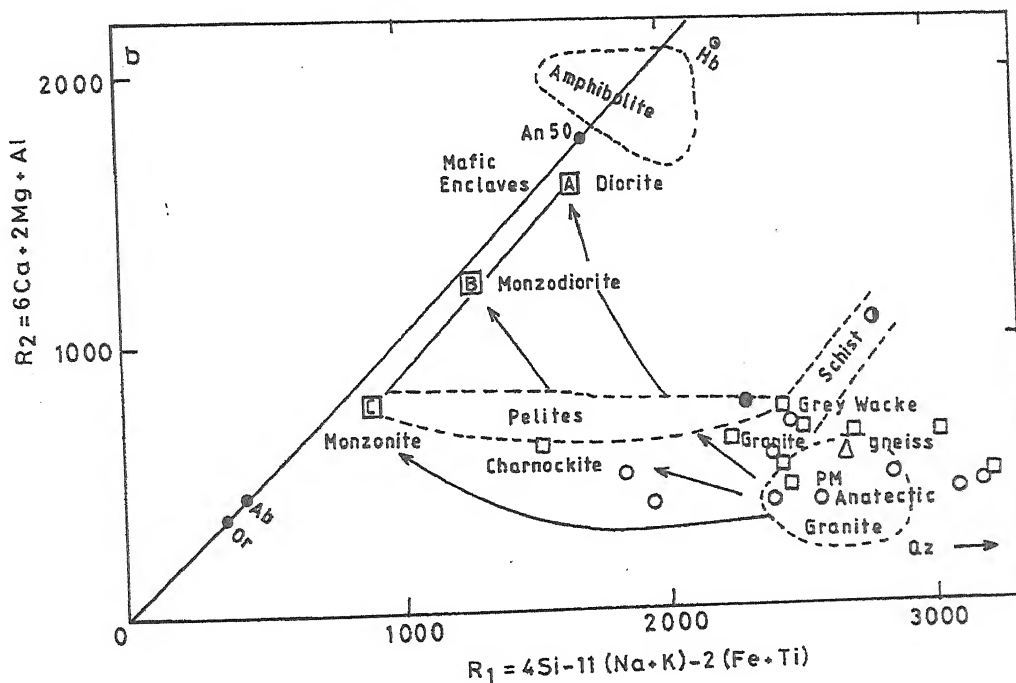
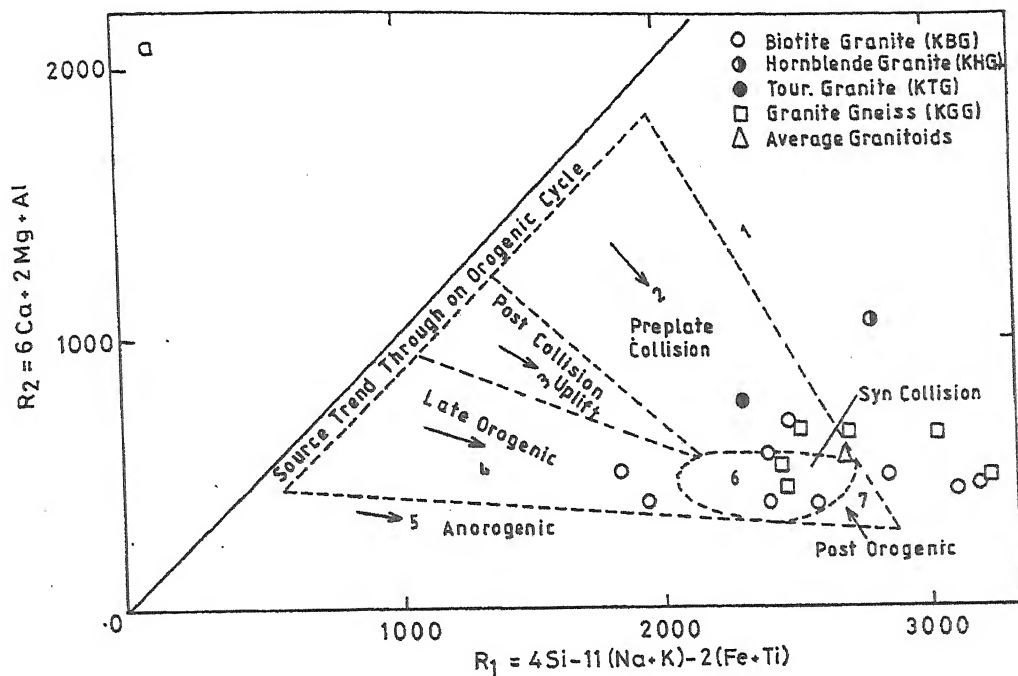
do not follow a single and firm tectonic environment viz; IAG/CAG/CCG/POG in figure, 4.10. The ambiguity involved in this classification scheme cannot be used for tectonic discrimination of granitoids. Nevertheless, C.C.G. appears an appropriate tectonic environment, which has more resemblance with Katekalyan granitoids.

All the Katekalyan granitoids falls in the field of orogenic granites, (Maniar and Piccoli; 1989) distinctly away from the field of anorogenic granites in the discrimination diagram (Fig. 4.10A) and also it does not fall in the field defined for post-orogenic granitoids (POG) (Fig. 4.10B and 4.10C). Discrimination between CCG and IAG + CAG can be made on the basis of molar $A/(CNK)$ ratio (Fig. 4.10D). They suggested that CCG do not have $A/(CNK)$ values less than 1.05; whereas IAG + CAG do not $A/(CNK)$ values greater than 1.15. If the $A/(CNK)$ ratio is between 1.05 and 1.15, it is not possible to discriminate between CCG and IAG+CAG. Considering above constrains, the Katekalyan granitoids represent continental collision. It is therefore suggested that Katekalyan granitoids is peraluminous in nature and resulted from the anatexis of crustal sedimentary rocks during continent collision.

4.2.3. Petrogenesis:

De La Roche's R_1 - R_2 plots, cationic proportion of major oxides (modified by Batchelor and Bowden; 1985) have been used for discrimination of tectonic environments. Most of the Katekalyan granitoid samples plot in the field of pre-to-syn-continental collision in nature (Fig. 4.11a)

For the partial melting vectors and metasedimentary sources, (Batchelor and Bowden; 1985) proposed that the first liquids to get separated from the fusion of felsic crustal source (gneiss, metapelite, intermediate metaigneous rocks) will have compositions equivalent to alkali feldspar and quartz \pm sodic plagioclase. The Katekalyan granitoids plotted in R_1 - R_2 multicationic diagram (Fig. 4.11b) occupied the field of anatectic granite. It indicates that the felsic melt is completely mobilised in the crust and



1. Tholeiitic Group 2. Calc-alkaline and Trondhjemitic Group 3. High-Potassic Calc-alkaline Group 4. Sub-alkaline Monzonitic Group 5. Alkaline and Per-alkaline Group 6. Anatectic Two-Mica Leucogranite.
- PM = Represent the zone of anatectic melt.
- PM-A } indicate the change in the melt composition under progressive
PM-B } equilibrium partial melting of rocks of dioritic, monzodioritic or
PM-C } monzogranitic bulk Composition respectively.

Fig. 4.11. R_1 vs R_2 multicationic plots (a and b) of the Katekalyan granitoids (After De La Roche, 1964) modified by Batchelor and Bowden, 1985).

emplaced at a higher level, its composition will be equivalent to a syenogranite or monzogranite. If it were assumed that lower crustal sources had compositions represented by A, B and C (Fig. 4.11b), then increasing degree of equilibrium, partial melting would generate compositions whose vectors could have represented by PM-A, PM-B and PM-C, respectively.

To identify the nature of the Katekalyan granitoids (KG and KGG), author attempted K_2O/Al_2O_3 vs Na_2O_3/Al_2O_3 (wt%) plot (Fig. 4.12a) which discriminates igneous and sedimentary/metasedimentary protolith as has been outline by Garrels and Mackenzie (1971). The diagram suggests that almost all samples plot in the sedimentary/ metasedimentary field.

4.2.4 Major oxides variation

The felsic ($SiO_2 + Al_2O_3 + Na_2O + K_2O$) vs mafic ($FeO^* + MgO + MnO + CaO$) constituents (Fig. 4.12b) appear to mark inverse relation between Katekalyan tin-bearing granitoids. This antipathic relationship between the silica-alumina-alkalies combination and ferro-calc magnesian of the Katekalyan granitoids indicate the crystallisation differentiation pattern similar to that of the other tin-bearing granites of the magmatic origin (Babu, 1993).

The Katekalyan granitoids (KG and KGG) is leucocratic in nature and have higher weight percentage (average) of SiO_2 (67.74), Al_2O_3 (17.16), K_2O (4.63), Na_2O (1.83), FeO^* (3.91) and lower percentage of CaO (1.73), MgO (0.89) and TiO_2 (0.3). To consider the role of differentiation process in the formation of Katekalyan granitoids, the variation diagrams of Harker (Fig. 4.13) are plotted.

Silica versus other oxides

Calcium and magnesium oxide: CaO and MgO show a sympathetic relationship with one another in Katekalyan granitoids and pegmatites although CaO content is always more than MgO . CaO content in granite and

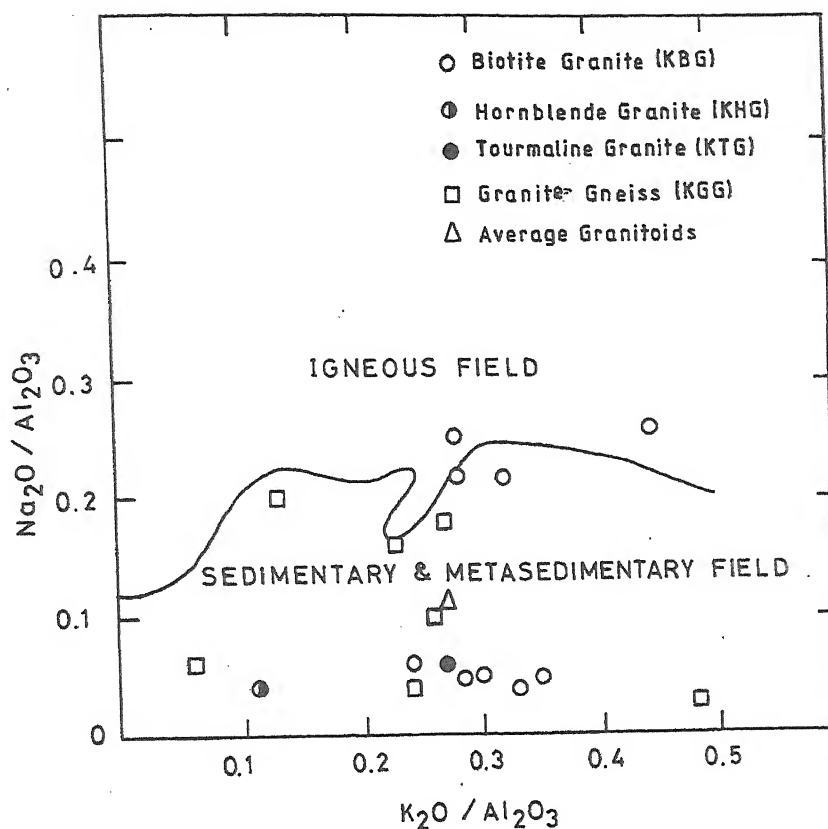


Fig. 4.12a. $\text{K}_2\text{O}/\text{Al}_2\text{O}_3$ vs $\text{Na}_2\text{O}/\text{Al}_2\text{O}_3$ diagram for the Katekalyan granitoids (After Garrels and Mackenzie, 1971).

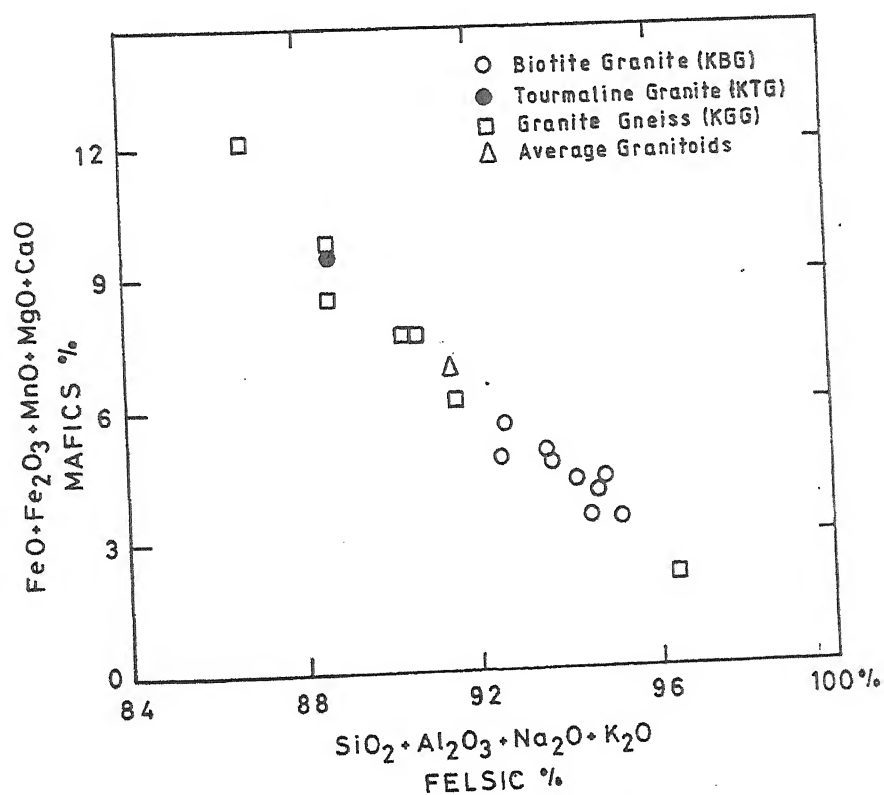


Fig. 4.12b. Binary variation diagram between FELSIC and MAFIC constituents of the Katekalyan granitoids.

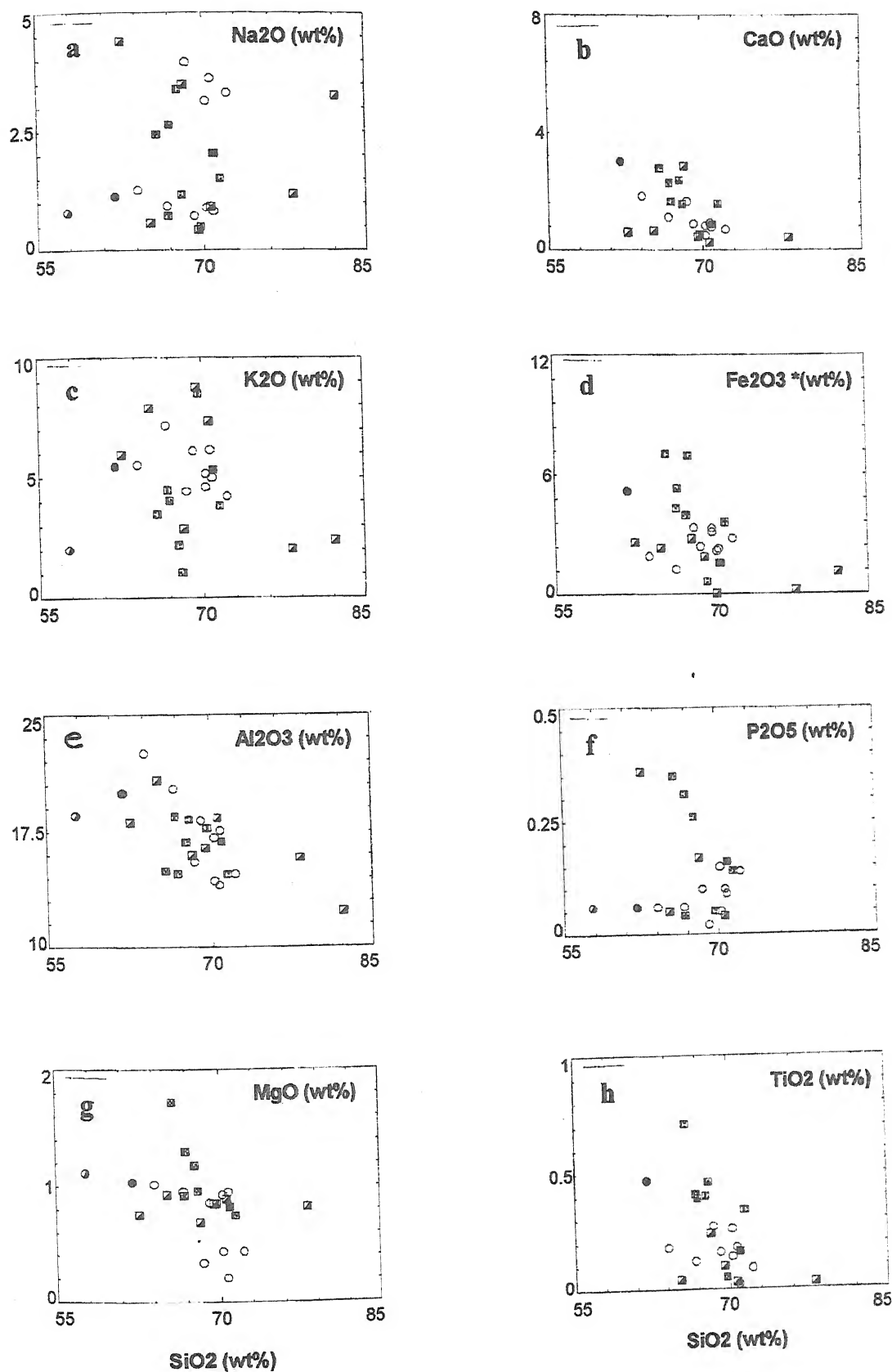


Fig. 4.13a-h. Harker's variation diagrams of SiO₂ vs CaO, MgO, Na₂O, Al₂O₃, Na₂O, K₂O, Al₂O₃, Fe₂O₃*, P₂O₅, and TiO₂, for the granite (KG), granite gneiss (KGG) and pegmatites (KP).

granite gneiss varies from 0.51 to 6.12-wt% and MgO varies from 0.21 to 1.72 wt%. In pegmatites, CaO varies from 0.24 to 2.86-wt% while the MgO varies from 0.69 to 0.93 wt%. The CaO and MgO show antipathetic relationship with SiO₂ (Fig. 4.13).

Alkalies: Na₂O varies from 0.49 to 3.95-wt% and K₂O content varies from 1.07 to 8.48wt% with the maxima and minima for the Katekalyan granitoids. In pegmatites, Na₂O varies from 0.42 to 4.39 wt% and K₂O ranges from 2.03 to 8.75%. The Na₂O and K₂O bear an inverse relationship to each other. Further K₂O/Na₂O ratio varies from 0.65 to 17.31 in granitoids whereas in pegmatites varies from 0.74 to 20.83%. When silica content is plotted against Na₂O and K₂O individually (Fig. 4.13a,c), it is seen that there is a tendency for concentration of SiO₂ around 72 wt% (70 and 72 wt%), Na₂O at 3 wt% (1 and 3 wt%) and K₂O at 5 wt% (4 and 6 wt%), the region where all the tin fertile granitic rocks of the world are normally clustered. Broadly, there is a general trend towards increase in K₂O content with increasing silica. In the binary variation diagram it is found whenever there is enhancement of K₂O, correspondingly there is fall of Na₂O, which indicates the dominance of microclinisation at the expense of albitisation and vice versa. Two stages of microclinisation and albitisation were noted. The concentration of tin is found to be more in the second phase of potassium enrichment, probably during the greisenisation process. K₂O and Na₂O show inverse relationship with each other.

Alumina: In granitoids, Al₂O₃ content varies from 14.06 to 22.53-wt%, whereas in pegmatites it ranges from 12.34 to 20.8 wt%. The alumina content increases with decreasing silica content (Fig, 4.13e). The relationship of Al₂O₃ and SiO₂ in pegmatite is similarly inverse as noted for the Katekalyan granitoids.

Total alkalies and alumina for the granitoids and pegmatites bear a more or less antipathic relationship. There is no definite trend in combined alkalies or alumina though the latter shows a tendency to decrease with increase in silica.

The enrichment of Fe_2O_3 (total) in granite gneiss and its depletion in biotite granite depicts the antipathetic relation of Fe_2O_3 with SiO_2 (Fig. 4.13d).

Thus, the variation and clustering of various oxides, plotted for Katekalyan granitoids in Harker's variation diagrams show more or less similar trend without gap, suggesting the same petrogenetic history for them.

4.3. Trace element geochemistry

For trace element analysis, eighteen powder samples were pelletized and analysed by XRF-ED (X-Ray Fluorescence–Energy Dispersive) for Cu, Zn, Zr, Ga, Y, Rb, Ba, Sr and Nb using Philips Exam Six and PV 9100 spectrometer. Sn and Ba were determined by Atomic Absorption Spectrophotometer (Perkin-Elmer 4000) after total decomposition with an $\text{HF-HClO}_4\text{-HNO}_3$ acid mixture (Word *et al.*, 1969). Analytical results are shown in table 4.4a,b. A clearer picture about the petrogenesis of Katekalyan granitoids and their relation to tin mineralisation may be deciphered by rare-earth elements geochemistry.

There is a wide variation of tin content in Katekalyan granitoids ranging from 22 to 785 ppm. In Katekalyan granitoids, in general, along with tin there appears to be enrichment of several trace elements notably niobium, gallium, rubidium, barium, copper, zinc, nickel and yttrium and conversely depletion in zirconium, cobalt, and strontium. The trace element contents in different granitic and pegmatitic rocks of Katekalyan is shown in table 4.4 a,b, d. There is a broad correlation between Sn and Nb in the granitic rocks indicating that niobium concentration took place along with tin in the granitic magma. Tin also shows positive correlation with rubidium of granite (Fig. 4.18e).

The Katekalyan granitoids, however, when plotted on Rb-Sr log-log variation diagram (Fig. 4.14) of Condie (1973), the most of the samples cluster between the lines defined by $\text{Rb/Sr} = 0.1$ and $\text{Rb/Sr} = 1$, at the depths

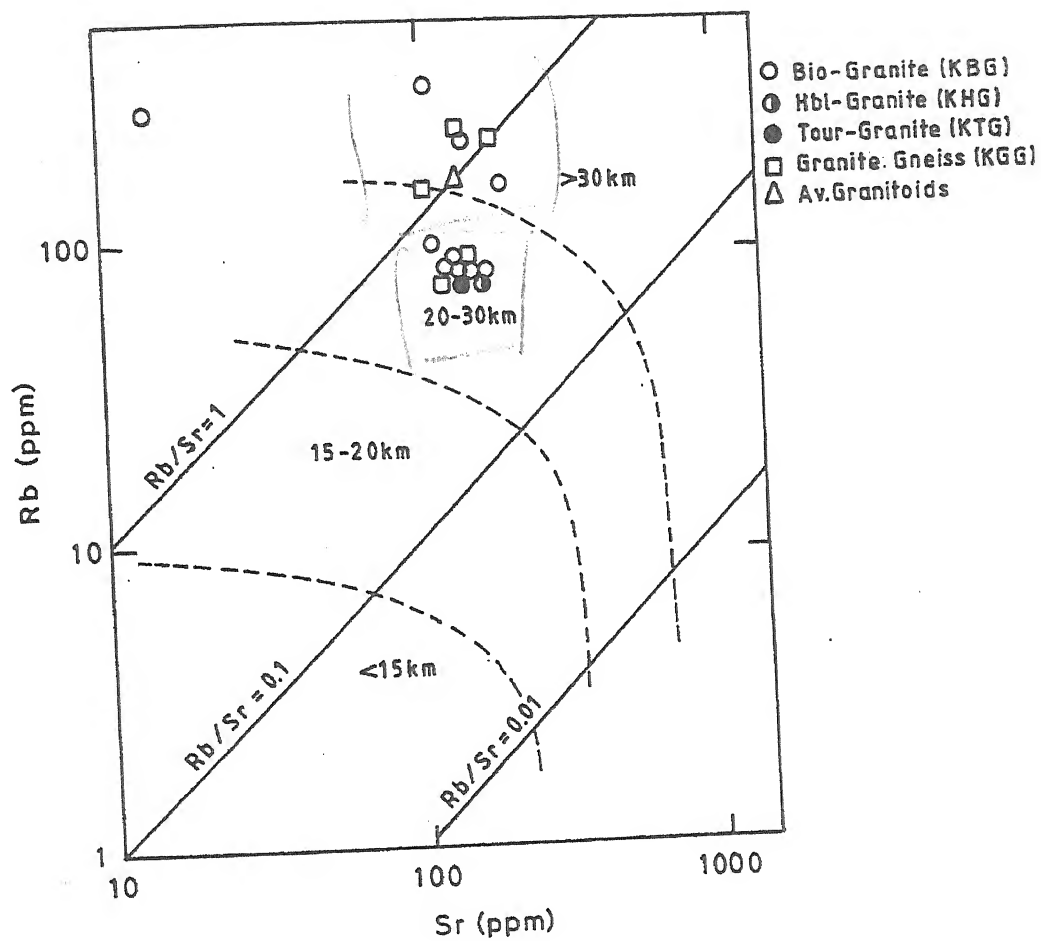


Fig. 4.14. Rb-Sr log-log plot (Fields after Condie, 1973).

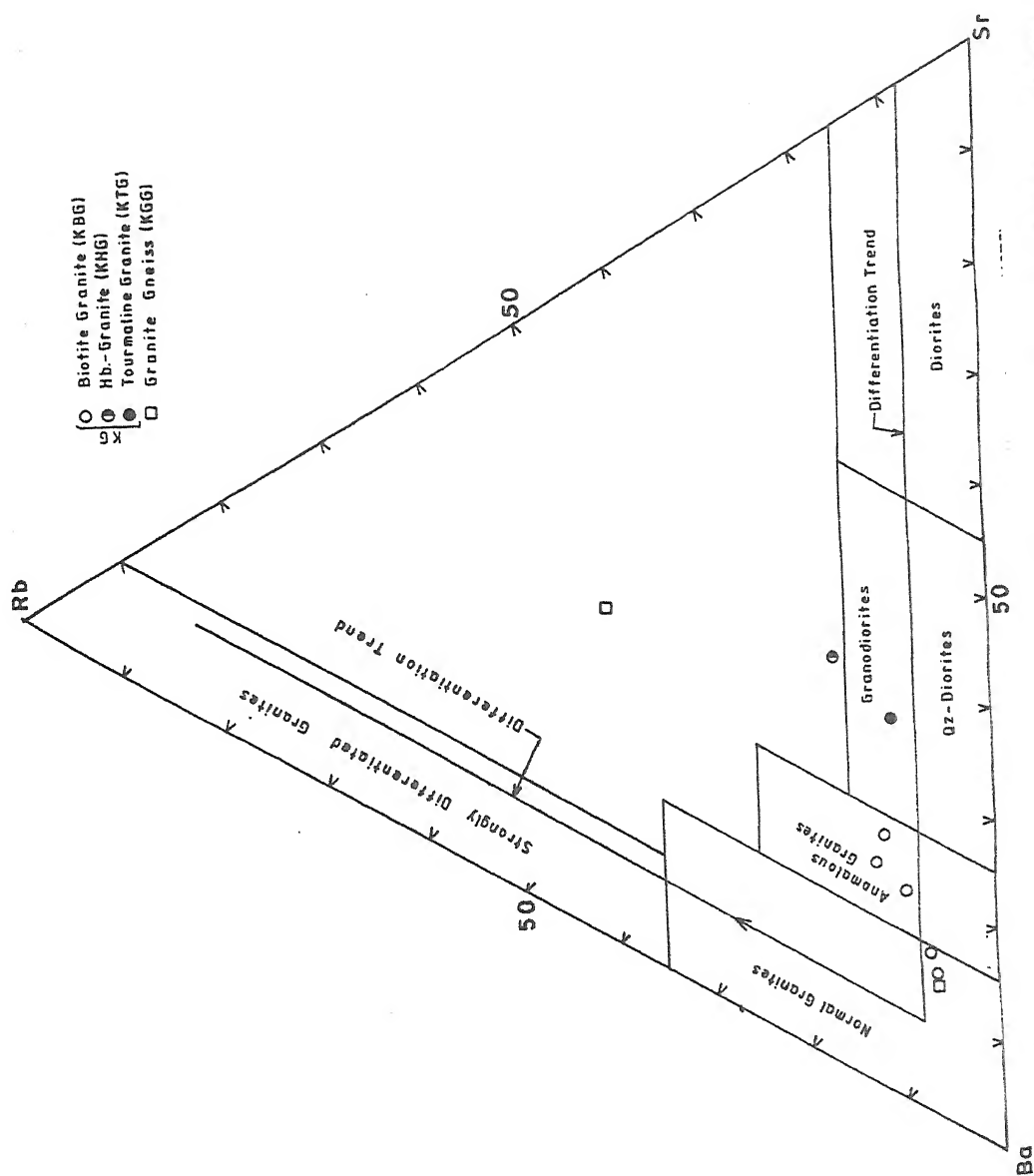


Fig. 4.15. Rb-Ba-Sr ternary diagram after El-Bouseilly and El-Sokkary (1975) with the distribution of Katekalyan granitoids (KG and KGG).

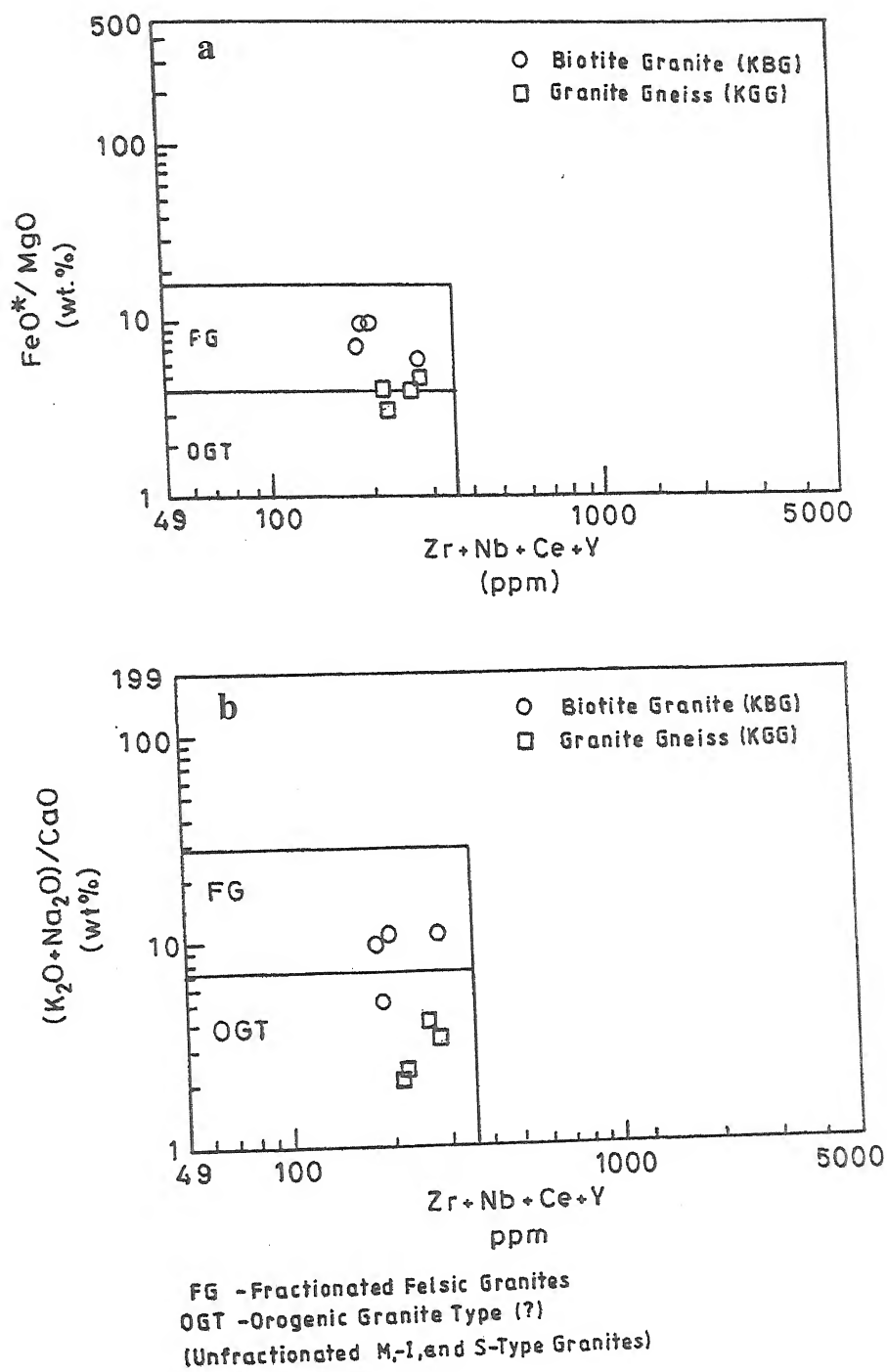
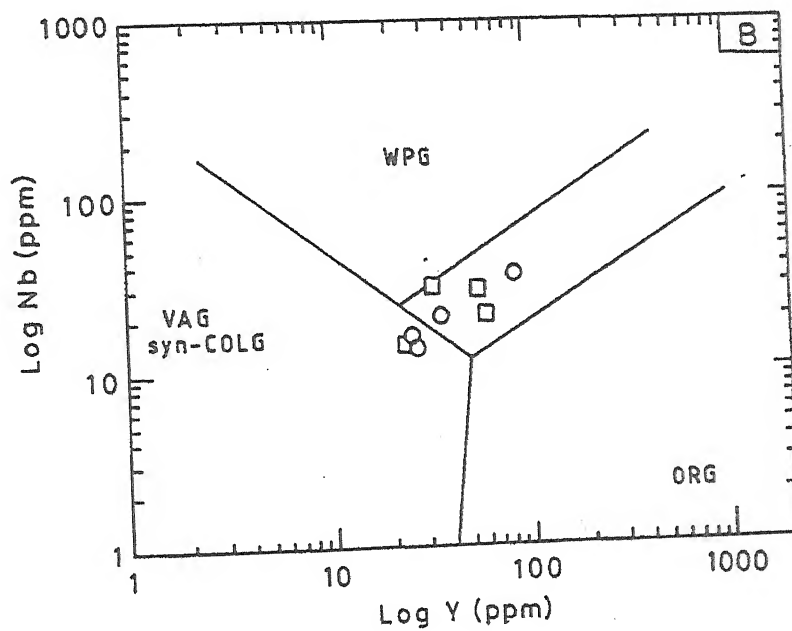
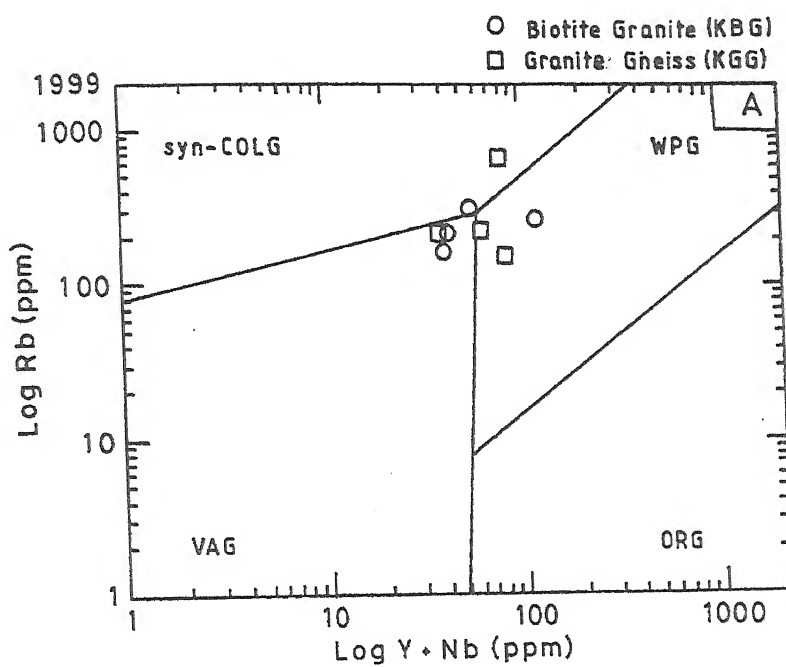


Fig. 4.16. Binary variation Zr + Nb + Ce + Y vs FeO*/MgO (wt.%) and Zr + Nb + Ce + Y (ppm) vs (K₂O + Na₂O)/CaO (wt.%) diagrams (a and b) of the Katekalyan granitoids (After Whalen *et al.*, 1987).



VAG – Volcanic Arc Granites syn. COLG – syn. Collisional Granites
WPG – Within Plate Granites ORG – Oceanic Ridge Granites

Fig. 4.17. Discrimination diagrams for the Katekalyan granitoids (After Pearce *et al.*, 1984).

relevant to 20 to 30 kms. But a few samples are emplaced at depths greater than 30 kms.

El Bouseilly and El Sokkary (1975) pointed out the usefulness of an Rb-Ba-Sr ternary diagram in tracing differentiation trends of granitic rocks. This diagram can also be used to classify granites, evaluate fractionation trend and detect specialization of tin bearing nature of the granites. In the Rb-Ba-Sr ternary diagram (Fig. 4.15), the analyses of the Katekalyan granitoid rocks are plotted showing considerable variation from granodiorite to normal granite through anomalous granite fields. The tourmaline granite falls in the granodiorites field, whereas granitic gneisses fall in the normal granites field. The biotite granites fall in the anomalous granite field chiefly due to its relatively lower Rb levels as compared to that of the normal granites. This is possibly brought by late residual aplitic liquid whereby Rb may be fractionated (El Bouseilly and El Sokkary 1975).

Based on Whalen *et al.*, (1987), the diagrams (Fig. 4.16a,b) $Zr + Nb + Ce + Y$ (ppm) vs FeO^*/MgO (wt%) and $Zr + Nb + Ce + Y$ (ppm) vs $(K_2O + Na_2O)/CaO$ (wt%) show the nature of biotite granite (KBG) as fractionated felsic granites (FG) whereas granite (KBG) gneiss represent the orogenic granite type (OGT) of the unfractionated S-type granites.

The selective trace elements characteristics of the Katekalyan granitoids can not be assigned collectively of any one tectonic regime when plotted on $Y + Nb$ vs Rb log-log (ppm) and Y vs Nb log-log (ppm) diagrams (Fig. 4.17a,b) based on Pearce *et al.*, (1984). The samples cluster near the tripple junction demarcating lines of volcanic arc granitoids (VAG), syn-collisional granitoids (syn-COLG) and within plate granitoids (WPG) fields.

4.3.1. Trace element variation

Table (4.4a,b) shows the average distribution of trace elements of Katekalyan granitoids of the study area. The granitoids have higher Rb

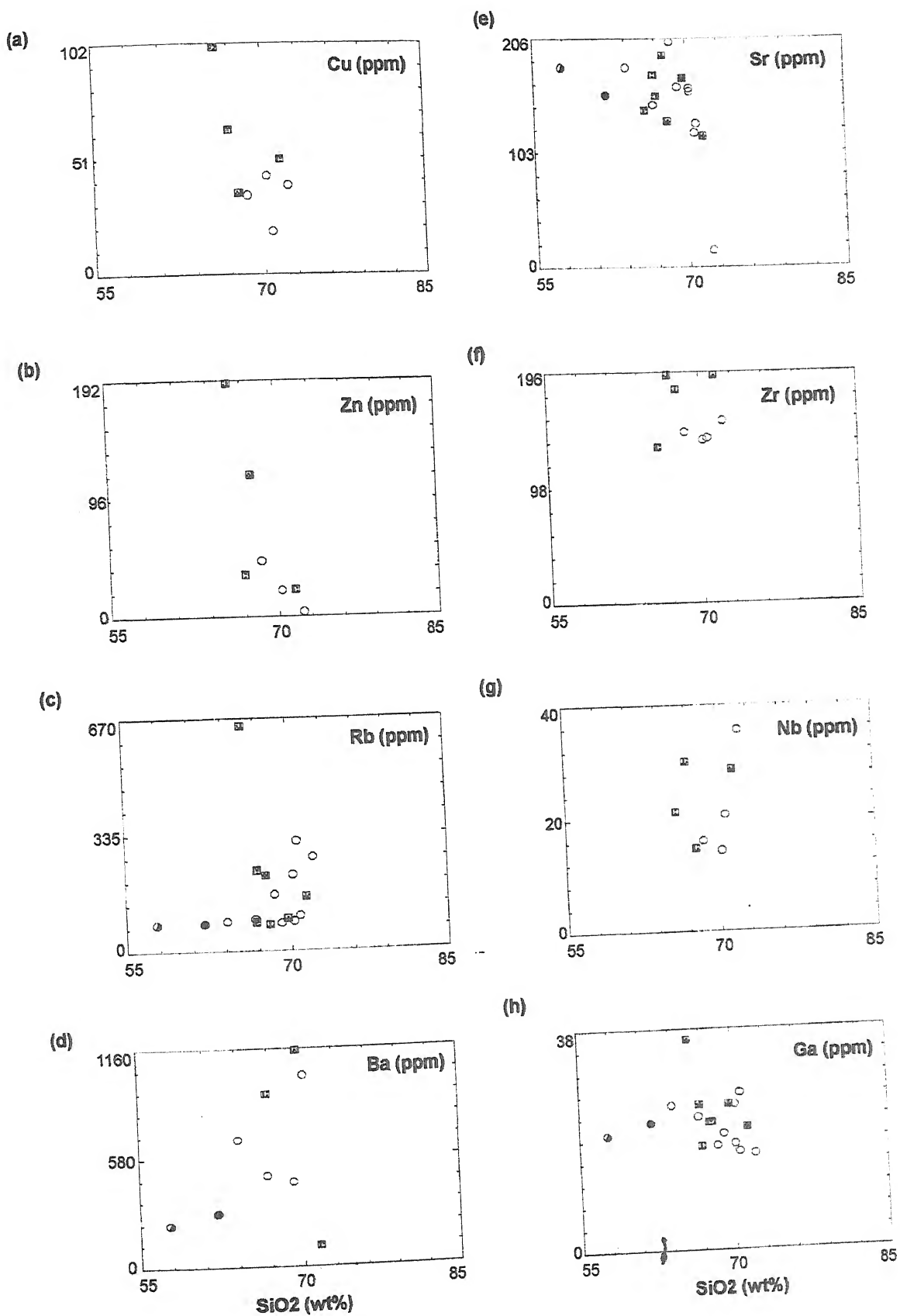


Fig. 4.18. Harker variation diagrams of SiO_2 vs Cu, Zn, Rb, Ba, Sr, Zr, Nb and Ga

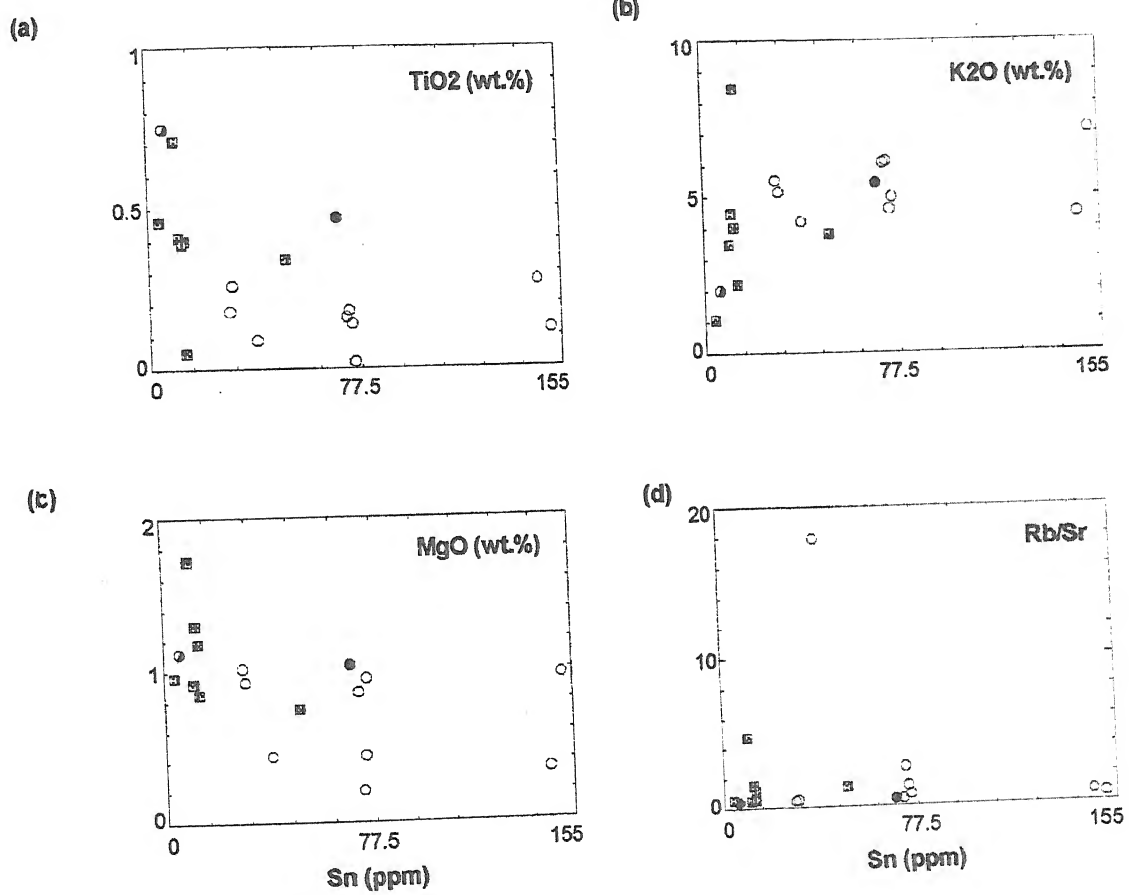


Fig. 4.19. Harkers variation diagrams of Sn vs TiO₂, K₂ O, MgO and Rb/Sr.

(171.66 ppm), Ba (593.11 ppm), Zr (159.99 ppm), Nb (22.65 ppm), Sn (66.61 ppm) and W (21.21 ppm) contents and lower Cu (48.21 ppm), Sr (149.24 ppm), Zn (71.35 ppm), Th (36.27 ppm), Co (6.14 ppm), Ni (23.37 ppm), Ga (22.24 ppm) and Y (42.48 ppm). The increase in Rb, Ba, Sn, W and Nb and decrease in Sr and Zr with increase in SiO_2 content of the Katekalyan granitoids, suggest the role of differentiation in the formation of these granitic rocks.

However, when the trace elements for Katekalyan granitoids are plotted against SiO_2 in Harker's variation diagrams (Fig. 4.18), they show some genetic features. Rb, Ba, Sn W and Nb increase with increasing SiO_2 showing the similar differentiation trend. This supports the view that these granitoids were of the same in nature and possibly have got same petrogenetic history. Cu and Sr show inverse relation with SiO_2 and decrease from granite to granite gneiss rocks. Ga and Y do not show any marked variation with increasing SiO_2 , but form it clusters for the granites and granite gneisses, which also support their same nature. From the tin distribution pattern, as seen from the table (4.4a,b) one can realise that though it is highly fluctuating in character, which were concentrated in two distinct phases, one in the gneissic stage with average tin content of 16.14 ppm and the second in the intrusive granites with average values of 76.55 ppm. Thus, at the initial stage of granitic activity, the concentration factor is around 4 or 6 (considering mean of 3 ppm Sn in any normal granitic melt as starting point). In the late differentiation granites, the concentration factor is more than 20. Thus, there is marked enrichment of tin content in the end phase of granitic activity. There is a broad correlation between Sn and Nb in the granitic rocks indicating that Nb concentration took place along with tin in the granitic magma. Tin also shows positive correlation with lithium and rubidium in intrusive phase of granitoids at places. There is a tendency for rise in tin content with increasing silica at the initial stage up to 50 ppm.

4.4. Rare earth elements (REE)

4.4.1. Introduction

Rare earth elements are progressively becoming an important and useful tool in petrogenetic studies because they are geochemically very similar to those of its nearest atomic neighbour, but differing from Ce and Eu which have tendency of change REE with greater or smaller atomic valency state depending upon the geological environment.

Rare earth elements (REE's) are a group of 15 (trace) elements with atomic number from 57lanthanum (La) to 71lutetium (Lu), 14 of these elements (except promethium-Pm) occur naturally. For convenience the REEs are divided into two sub-group: (I) from La to Sm (i.e., lower atomic numbers and masses) are referred to as the light rare earth elements (LREE) and (II) from Gd to Lu (higher atomic numbers and masses) are referred to as the heavy rare earth elements (HREE). Very occasionally the term middle rare earth elements (MREE) is loosely applied to the elements from about Sm to Ho (Handerson; 1984). In nature all of the rare earth elements exhibit a 3^+ oxidation state (trivalent), except Ce^{4+} (oxidised) and Eu^{2+} (reduced) under most geological conditions.

The ionic radii of the REE are all approximately 1\AA . There is a regular decrease in the ionic radii (for the trivalent REE from 1.03 for La to 0.86\AA for Lu) with increasing atomic number (The Lanthanide Contraction). Eu is both divalent and trivalent in igneous system, the Eu^{2+}/Eu^{3+} ratio depending on the fugacity of oxygen (fO_2). Divalent Eu is geochemically very similar to strontium ionic radius: $Eu^{2+} = 1.17\text{\AA}$, $Sr^{2+} = 1.18\text{\AA}$, thus it is strongly partitioned into feldspars. Ce may be tetravalent under highly oxidizing conditions such as during weathering or hydrothermal alteration (Hanson, 1980).

The procedure described for the determination of REE's by ICP-AES gives very good precision and accuracy and is suitable for the petrogenetic purpose.

4.4.2. Methodology of REE determination

1. ICP-AES instrumentation

(A) **Equipment:** Jobin Yvon, model JY 70 plus. 1m focal length, Czerny-Turner monochromator, Holographic grating 3600 gr/mm.

(B) **RF generator:** 40.68 MHz, single phase, and power stability 0.01%.

(C) **Gas flow rates:** Outer (coolant): 12 l/min; intermediate auxiliary): 0.0 l/min and central (carrier + sheath): 0.55 l/min.

(D) **Nebulizer:** Meinhard concentric glass nebulizer type C'.

(E) **Wavelengths used (nm):** La (398.852); Ce (413.765); Nd (430.358); Eu (381.967); Dy (353.171); Yb (328.937); Sm (359.260); Gd (342.246); Er (326.478); Lu (261.542).

2. Reagents and standards

Synthetic standard solutions of rare earth elements were prepared from their high purity oxides or other suitable salts. All used acids (HCl-35.4%; HNO₃-69.71%; HF-48%; and HClO₄ 70%) were of Ar/Gr grade. Deionised water was distilled before use. For carrying out the separation of REEs analytical grade Blb-Rad AG 50 W-X 8,200-400 mesh cation exchange resin was used. Rock standards used in the present studies are granite (G-2, Source: U.SGS, USA) and metabasic (MB-H, Source: WIHG, India) are listed in table 4.5. The consensus values for the rock standards of metabasic (MB-H) used in this study are taken from Govindaraju (1989) and Rathi *et al.*, (1994).

3. Sample preparation

Dried samples (1.00 gm) were digested with hydro fluoric-perchloric acid mixture in open PTFE crucibles on a hot plate. In order to ensure

complete dissolution the digestion was repeated 4-5 times with evaporation to perchloric acid fumes after each treatment and finally to incipient dryness. The final volume was made up to 100 ml in dilute HCl. Depending upon the expected concentration of rare earth elements; 50 to 100 ml of this solution was used for carrying out the separation.

4. REE separation

Ion exchange chromatography has been widely used to separate rare earth elements in geological samples using different approach by different workers, viz., Crock *et al.*, (1986), Church (1981), Jarvis and Jarvis (1988), Govindaraju and Mevelle (1987) and Walsh *et al.*, (1981). The basic principle in these methods is the same. Our technique is comparable to that of Walsh *et al.*, (1981).

Analytical grade cation exchange resin AG 50 W-x8 (200-400 mesh, H form) is filled in glass columns (inner dia: 20 mm; height-40 cm; fitted with a sintered filter disc at the bottom) up to a level of about 15 cm. The resin is then washed with 250 ml of 4 N HCl followed by 250 ml of 1 N HCl. The liquid level is never allowed to drop below 2-3 cm above the top of the resin bed. Before starting a new batch the resin within the column is swirled with the help of a glass rod in order to avoid lump formation.

The rock solution free from any residue is loaded on to the column along with the washings of the container with ddH₂O. After the passage of the solution 450 ml of 1.7 N HCl is passed to elute the majority of the ions other than REEs. This effluent was discarded. Now 600 ml of 4 N HCl was passed through the column to elute REEs and this effluent was collected carefully in one-liter glass beakers (which have stood overnight filled with 10% HNO₃ and washed with dd H₂O). The process is completed when 2-3 cm of solution remains above the top of the resin bed. The solution collected is evaporated to dryness by slow heating on a hot plate. The whole process takes approximately 2-3 days (8hrs of working day). The dried residue of REEs is

dissolved in exact 10 ml of 10% HNO_3 and filtered to discard any resin particles that might percolate through the disc of column. The REEs are measured in the filtrate. A set of six columns is in use in this laboratory to run a batch of 4 unknown samples, 1 standard sample and 1 blank at a time. The resin is regenerated with 250 ml of 4 N HCl followed by 250 ml of 1 N HCl in order to take up REE separation for a fresh batch of samples.

4.4.3. REE data presentation

Rare earth element concentrations in rocks are usually normalised to a common reference standard, which most commonly comprises the values for chondritic meteorites. Chondritic meteorites were chosen because they are thought to be relatively unfractionated samples of the solar system dating from the original nucleosynthesis. The REE data (ppm) and their chondrite normalised value of analyzed samples are given in table (4.5). In order to compare graphically rare earth elements (REEs) are represented by the spider diagram for the Katekalyan granitoids. The concentrations for the individual rare earth element is generally normalized to their abundance in chondrite by dividing the concentration of a given element in the rock by the concentration of the same element in chondritic meteorites.

The ratio Eu/Eu^* is a measure of the europium (Eu) anomaly and a value of greater than 1.0 indicates a positive anomaly whilst a value of less than 1.0 is a negative anomaly. The Eu/Eu^* ratio in the Katekalyan granitoids varies from 0.38 to 0.57, which indicates negative Eu-anomalies. Taylor and McLennan (1985) recommend using the geometric mean in this case $\text{Eu}/\text{Eu}^* = \text{Eu}_N / \sqrt{(\text{Sm}_N \cdot \text{Gd}_N)}$. Europium anomalies may be quantified by comparing the measured concentration (Eu) with an expected concentration obtained by interpolating between the normalized values of Sm and Gd (Eu^*). The variation of Eu/Eu^* is also limited (0.38 to 0.57) suggesting a source signature rather than feldspar fractionation (Norman *et al.*, 1992).

4.4.4. Interpretation

Rare earth elements of seven selected samples of the Katekalyan granites and granite gneisses were analysed and chondrite normalised patterns by Taylor and McLennan, 1985 (1.5 x values of Evensen *et al*; 1978) are shown in figure 4.20. All the suites exhibit enriched LREE patterns relative to HREE along with variable negative Eu anomalies. In figure 4.20, the most of the granitoid samples show steep by inclined pattern and are highly fractionated. They are enriched in LREE and depleted in HREE showing moderate and large negative Eu-anomalies.

One sample of granite gneiss (Ref. No. F/15A) shows almost flat LREE pattern with pronounced negative Eu-anomaly but shows enriched HREE, most probably due to presence of accessories such as zircon and heavy tin-niobium-tantalum mineralisation. The flat HREE pattern might have resulted due to presence of ample amount of apatite, which is mostly entrapped within large feldspar grains. The strong negative Eu-anomalies indicate that this rock is highly evolved during differentiation processes.

The other granite gneiss (Ref. No. F/1A) contain abundant plagioclase dominating over alkali feldspar. Presence or absence of the Eu-anomaly usually is related to the presence or absence of feldspar in the magma. This may be controlled by the fractionation of feldspar during the differentiation or melting of either feldspar bearing or depleted protolith (s). Small negative Eu anomaly indicate the removal of Calcic-plagioclase from the magma (i.e. probably at initial stage) and the increasing size of negative Eu-anomalies indicate the gradual increase in the removal of relatively more Calcic-plagioclase attaining the last stage i.e., the magma is more evolved.

The degree of fractionation of a REE pattern can be expressed by the concentration of LREE (La or Ce) rationed to the concentration of HREE (Yb or Y). The Katekalyan granitoids is characterized by high LREE abundances (chondrite normalised La = 84.47 – 264.30). The HREE (as Yb) abundances vary between 1.37 – 23.79. All the LREE show positive

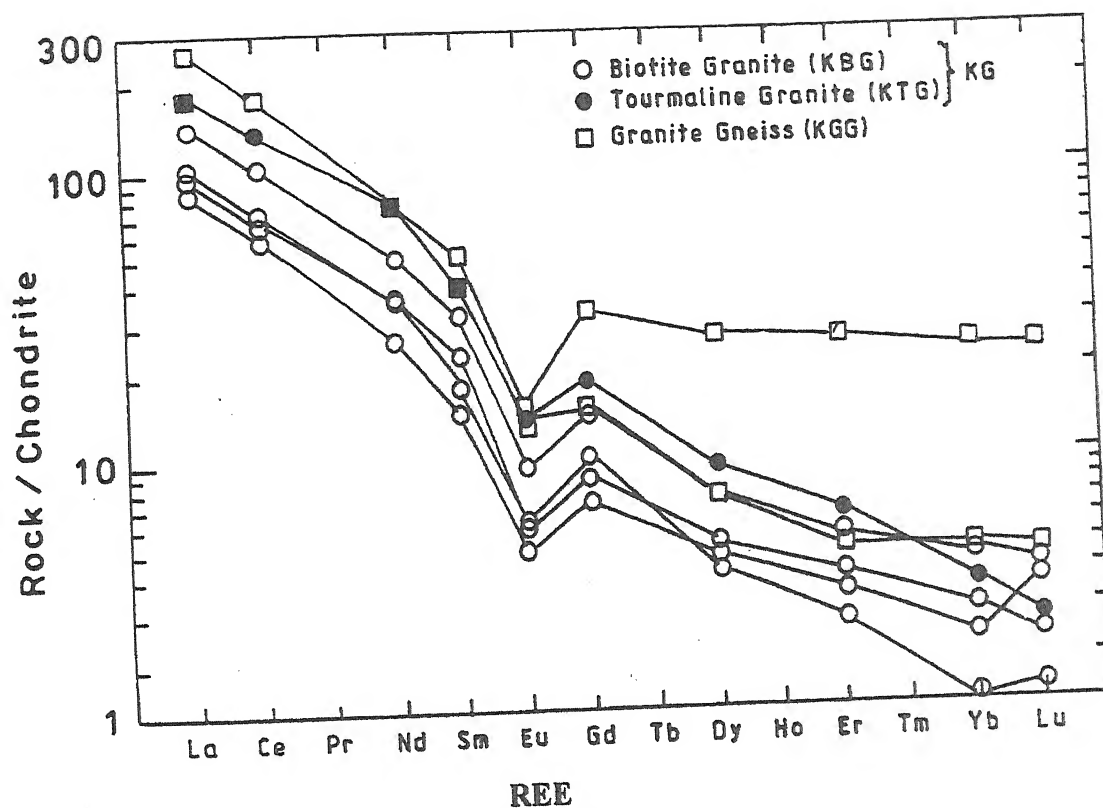


Fig. 4.20. Chondrite-normalized REE patterns for selected samples of the Katekalyan area. Open circles: biotite granite (KBG), closed circle: tourmaline granite (KTG) and opened squares: granite gneiss (KGG). The data are normalized to chondritic values given by Taylor and Mc Lennan; 1985 (1.5 x values of Evensen *et al*; 1978).

correlation with FeO^* . The most iron-rich sample shows the lowest abundance of SiO_2 and highest abundance of LREE with total REE content (343.71 ppm). The REE patterns of the Katekalyan granitoids are moderately to strongly fractionated characterized by an increase of ΣREE and $(\text{La/Yb})_N$ (7.74-76.17) and a consistent pattern of fractionation $(\text{La/Sm})_N = (3.67-6.78)$, $(\text{Gd/Yb})_N = (1.35-7.54)$.

The observed similarities in REE patterns between all the granitoids of the Katekalyan area and those of average Post Archean Australian Shale (PAAS), North American Shale Composite (NASC), European Shale (ES) and Post Archean greywacke (REE data in Taylor and McLennan; 1985) suggest plausible sedimentary source for these granitoids. The suitable source rock for these granitoids could have been quartzo-feldspathic psammopelitic materials most likely over saturated in Al_2O_3 as indicated by high normative corundum values, which can be comparable well with those of S-type granitoid of White and Chappel (1988).

Table 4.1a. Major Element Analyses (in wt.%) and CIPW Weight Norms of granite (KG) of Katekalyan Area

Sample No.	R93/222	R93/223	R93/253	R93/257	R93/284	R93/164	R93/166	R93/172	R93/174	R93/192	R93/197	Average \bar{X} (N=11)
Ref. No.	F/22	F/23A	F/53	F/57B	F/84B	F/101A	F/103	F/109A	F/111	F/127	F/132B	
SiO ₂	70.70	70.84	64.11	57.75	70.28	68.50	66.72	62.08	69.13	72.19	70.27	67.51
TiO ₂	0.18	0.02	0.18	0.75	0.26	0.27	0.12	0.47	0.16	0.09	0.14	0.24
Al ₂ O ₃	14.06	17.58	22.53	18.55	17.14	15.57	20.27	20.00	18.23	14.78	14.32	17.55
Fe ₂ O ₃ (T)	2.17	2.28	1.92	11.08	3.12	3.35	1.25	5.19	2.39	2.80	3.31	3.53
MnO	0.04	0.02	0.03	0.14	0.02	0.06	ND	0.02	ND	0.05	0.04	0.05
MgO	0.21	0.95	1.02	1.12	0.93	0.34	0.96	1.04	0.86	0.44	0.44	0.75
CaO	0.92	0.78	1.84	6.12	0.51	1.67	1.12	3.02	0.89	0.70	0.83	1.67
Na ₂ O	3.61	0.82	1.26	0.79	0.89	3.95	0.93	1.13	0.72	3.31	3.14	1.87
K ₂ O	6.15	5.00	5.53	2.02	5.17	4.43	7.15	5.45	6.10	4.22	4.61	5.07
P ₂ O ₅	0.10	0.09	0.06	0.06	0.05	0.10	0.06	0.06	0.02	0.14	0.15	0.08

CIPW WEIGHT NORMS

Quartz	24.16	44.03	30.32	24.72	42.68	24.26	30.28	25.18	38.46	34.67	31.64	31.85
Orthoclase	36.25	29.55	32.68	11.94	30.55	26.18	42.25	32.21	36.05	24.94	27.24	29.98
Albite	30.55	6.94	10.66	6.68	7.53	33.42	7.87	9.56	6.09	28.01	26.57	15.81
Anorthite	3.91	3.28	8.74	29.97	2.20	7.63	5.16	14.59	4.28	2.56	3.14	7.76
Corundum	0.03	9.62	11.27	4.08	9.27	1.48	9.11	6.90	8.87	3.83	3.02	6.13
Hypersthene	0.52	2.51	2.54	16.17	2.97	1.95	2.39	6.14	2.14	1.95	2.65	3.81
Magnetite	1.19	2.20	0.35	3.26	2.55	2.57	-	2.86	1.89	2.31	2.38	2.16
Ilmenite	0.34	0.04	0.34	1.42	0.49	0.51	-	0.89	0.30	0.17	0.27	0.48
Hematite	0.86	-	1.44	-	-	-	1.25	-	0.36	-	-	0.98
Apatite	0.23	0.21	0.14	0.14	0.12	0.23	0.14	0.14	0.05	0.32	0.35	0.19
Rutile	-	-	-	-	-	-	0.12	-	-	-	-	0.12

Table 4.1b. Major Element Analyses (wt.%) and CIPW Weight Norms of granite gneiss (KGG) of Katekalyan Area

Sample No.	R93/201	R93/209	R93/215	R93/254	R93/256	R93/265	R93/265	Average \bar{X} (N=7)
Ref. No.	F/1A	F/9	F/15A	F/54CB	F/56A	F/65B	F/65C	
SiO ₂	66.82	69.71	71.49	68.06	66.99	67.77	65.87	68.10
TiO ₂	0.41	0.05	0.34	0.46	0.39	0.40	0.71	0.39
Al ₂ O ₃	18.48	17.72	14.75	18.28	14.80	16.81	14.97	16.54
Fe ₂ O ₃ (T)	4.31	0.63	3.60	6.95	5.29	3.79	7.04	4.51
MnO	0.04	–	0.07	0.07	0.09	0.12	0.19	0.09
MgO	0.92	0.85	0.75	0.96	1.30	1.18	1.72	1.09
CaO	2.28	0.53	1.57	1.56	1.65	2.37	2.77	1.82
Na ₂ O	0.72	0.49	1.51	1.16	2.63	3.37	2.43	1.76
K ₂ O	4.47	8.48	3.82	1.07	4.03	2.20	3.48	3.94
P ₂ O ₅	0.04	0.05	0.14	–	0.31	0.26	0.35	0.19

CIPW WEIGHT NORMS

Quartz	38.37	32.64	43.42	49.29	29.75	32.98	28.07	36.36
Orthoclase	26.42	50.11	22.58	6.32	23.82	13.00	20.57	23.26
Albite	6.09	4.15	12.78	9.82	22.25	28.52	20.56	14.88
Anorthite	11.05	2.30	6.87	7.74	6.16	10.06	11.46	7.95
Corundum	8.41	6.89	5.61	12.38	3.85	5.20	3.01	6.48
Hypersthene	4.52	2.12	3.15	9.31	7.44	4.40	10.51	5.92
Magnetite	2.77	–	2.67	2.84	2.74	2.75	3.20	2.83
Ilmenite	0.78	–	0.65	0.87	0.74	0.76	1.35	0.86
Hematite	–	0.63	–	–	–	–	–	0.63
Apatite	0.09	0.12	0.32	–	0.72	0.60	0.81	0.44
Rutile	–	0.05	–	–	–	–	–	0.05

Table 4.1c. Major Element Analyses (wt.%) and CIPW Weight Norms of Pegmatite (KP) of the Katekalyan Area.

Sample No.	R93/251	R93/258	R89/514	R89/523	R89/525	R93/241	R93/257	Average \bar{X} (N=7)
Field No. Ref. No.	F/51	F/58B	K3	K12	K15	F/41B	F/57C	
SiO ₂	82.19	62.72	78.14	70.63	65.25	69.51	68.26	70.96
TiO ₂	ND	ND	0.01	0.01	0.04	0.10	0.24	0.16
Al ₂ O ₃	12.34	18.11	15.81	18.39	20.80	16.45	15.99	16.84
Fe ₂ O ₃ (T)	1.11	2.60	0.18	0.02	2.32	1.88	2.78	1.56
MnO	0.06	0.23	ND	ND	0.04	0.01	0.04	0.15
MgO	ND	0.76	0.82	0.89	0.93	0.85	0.69	0.82
CaO	ND	0.60	0.41	0.24	0.65	0.45	2.86	0.87
Na ₂ O	3.26	4.39	1.18	0.92	0.57	0.42	3.47	2.03
K ₂ O	2.40	5.94	2.03	7.34	7.88	8.75	2.87	5.32
P ₂ O ₅	ND	0.36	ND	0.04	0.05	ND	0.17	0.16

CIPW WEIGHT NORMS

Quartz	54.04	12.50	61.41	35.46	29.06	31.35	39.34	36.31
Orthoclase	14.18	35.10	12.00	43.38	46.57	51.71	16.96	31.41
Albite	27.59	37.15	9.98	7.78	4.82	3.55	29.36	17.17
Anorthite	–	0.62	2.03	0.93	2.90	2.23	13.08	3.63
Corundum	4.38	4.23	10.93	8.59	10.27	5.47	2.38	7.65
Hypersthene	–	3.10	2.04	2.22	2.48	2.12	1.87	3.30
Magnetite	0.20	2.17	–	–	2.23	0.65	2.52	1.26
Ilmenite	–	–	–	–	0.08	0.19	0.46	0.04
Hematite	0.97	–	0.18	0.02	–	1.16	–	–
Apatite	–	0.83	–	0.09	0.12	–	0.39	0.35
Rutile	–	–	0.01	0.01	–	–	–	–

ND: Not detected

Table 4.1d. Comparison of Average Major Oxide Values (in wt.%) for Katekalyan Granite (KG) and Granite Gneiss (KGG) Compared with Metallogenically Specialised Granite (Tischendorf, 1977) and Average Low - Ca Granites (Turekian and Wedepohl, 1961).

Major Oxides	Average \bar{X}		Metallogenically Specialised Granite Average \bar{X}	Average Low-Ca Granite
	Granite (KG) (N=11)	Granite Gneiss (KGG) (N=7)		
SiO ₂	67.51	68.10	73.38 ± 1.38	74.23
TiO ₂	0.24	0.39	0.16 ± 0.10	0.20
Al ₂ O ₃	17.55	16.54	13.97 ± 1.07	13.60
Fe ₂ O ₃ (T)	3.53	4.52	1.90 ± 0.47	1.83
MnO	0.05	0.10	0.045 ± 0.04	0.05
MgO	0.76	1.10	0.47 ± 0.56	0.27
CaO	1.67	1.82	0.75 ± 0.41	0.71
Na ₂ O	1.87	1.76	3.20 ± 0.61	3.48
K ₂ O	5.08	3.94	4.69 ± 0.68	5.06
P ₂ O ₅	0.08	0.19	-	0.14

Table 4.2. Criteria for distinguishing I and S-type granites (Chappel and White, 1974; Takahashi *et al.*, 1980) applied for granite (KG) and granite gneiss (KGG)

Criteria	I-type	S-type	Inferred type	
Mineralogical Criteria			KG	KGG
Sphene	Present	Absent	I-Type	I-Type
Hornblende	Present	Absent or very Rare	S*-Type	S-Type
Magnetite	Present or Absent	Absent	S-Type	S-Type
Garnet	Absent	Present	S-Type	S-Type
Primary Muscovite/Biotite	Absent	Present	S-Type	S-Type
Geochemical Criteria				
Molar $Al_2O_3/(CaO + Na_2O + K_2O)$	< 1.1	> 1.1	S-Type	S-Type
Molar K_2O/Na_2O	< 1	> 1	S-Type	S-Type
Normative corundum	< 1	> 1	S-Type	S-Type
Initial Sr ratio	< 0.708	> 0.710	S-Type	S-Type
Nature of rocks	Quartz-diorite and Granite	Granite only	S-Type	S-Type

* Present only in one sample

Table 4.3a. Major oxide criteria for tectonic environment. (After Maniar and Piccoli, 1989).

Discriminant Function	Orogenic					Anorogenic			
	IAG	CAG	CCG	POG	RRG	CEUG	OP		
SiO ₂ range wt%	60-68	62-76	70-76	70-78	72-78, 60-63	71-77, 60-62	61-78		
	-----Unimodal-----					-----Bimodal-----	unimodal		
Alkali-lime Index	Calcic to calcalkaline	Calc-alkaline	Calc-alkaline to alkali calcic	Alkali calcic	alkalic	Alkalic	calcic		
Shand's Index	Predominantly metaluminous	Metaluminous Peraluminous	Peraluminous	Peraluminous Metaluminous Peralkaline (minor)	Peraluminous (minor) Metaluminous peralkaline	Peraluminous (minor) Metaluminous Peralkaline	Peraluminous Metaluminous		
Na ₂ O/CaO wt%	~ 1.0	~ <4.0	~2.0 - 10.0	~2.0-18.0	~ 2.0-25.0	~1.0-12.0	~ <4.0		
Na ₂ O/ K ₂ O wt%	0.4 - 3.0	0.4 - 2.0	0.4 - 1.5	0.6 - 1.2	0.7 - 1.0	0.6 - 1.0	0.0 - 50.0		
MgO/FeO (T) wt%	0.3 - 0.85	0.1 - 0.5	0.05 - 0.6	0.02 - 0.3	0.0 - 0.2	0.0 - 0.12	0.0 - 0.7		
MgO/MnO wt%	12-28	2-38	2-45	2-18	0.0-7.5	0.0-7.5	0.0-50		
Al ₂ O ₃ / Na ₂ O+K ₂ O (Molar)	> 1.5	> 1.1	> 1.1	0.9-1.4	< 1.15	< 1.15	> 1.0		

Table 4.3b. Inferred Tectonic Environment for KG and KGG based on discriminant functions given in table 4.3a

Orogenic				
Discriminant Function	Granite (KG)		Granite Gneiss (KGG)	
	Inferred types		Inferred types	
Silica Range (wt%)	57.75-72.19 unimodal	IAG/CAG/CCG/POG	65.87-71.49	IAG/CAG/CCG
Alkali-lime Index	Calc-alkaline to alkali calcic	IAG/CAG/CCG/POG	Calc-alkaline to alkali calcic	CCG
Shand's Index	Peraluminous	CCG	Peraluminous	CAG/CCG
Na ₂ O/CaO (wt%)	0.13-4.73	CAG/CCG	0.32-1.59	CAG/CCG
Na ₂ O/K ₂ O (wt%)	0.12-0.89	CCG	0.06-1.53	CCG
Mgo/FeO (t) (wt%)	0.10-0.77	CAG/CCG	0.14-1.35	CAG/CCG
Mgo/MnO (wt%)	5.25-52.00	CAG/CCG	9.05-23.00	CAG/CCG
Al ₂ O ₃ /Na ₂ O+K ₂ O (molar)	1.14-5.32	IAG/CAG/CCG	1.70-5.95	IAG/CAG/CCG

Table 4.4a. Trace Element Analyses (in ppm) of Katekalyan Granite (KG)

Sample No.	R93/222	R93/223	R93/	R93/257	R93/284	R93/164	R93/166	R93/172	R93/174	R93/192	R93/197	Average
Field No.	F/22	F/23A	F/53	F/57B	F/84B	F/101A	F/103	F/109A	F/111	F/127	F/132B	\bar{X}
Ref. No.												(N=11)
Cu	18.71	NA	NA	NA	NA	34.75	NA	NA	NA	39.07	43.18	33.92
Zn	NA	NA	NA	NA	NA	45.59	NA	NA	NA	NA	21.47	33.53
Co	NA	NA	1.00	16.00	4.00	NA	NA	5.00	NA	NA	NA	6.50
Ni	NA	26.00	26.00	28.00	28.00	NA	25.00	23.00	21.00	NA	NA	25.29
Ga	16.87	27.00	25.00	20.00	25.00	17.95	23.00	22.00	20.00	16.49	18.22	21.05
Rb	316.33	101.00	86.00	78.00	85.00	162.70	91.00	79.00	80.00	269.71	219.11	142.53
Ba	NA	NA	680.00	228.00	1019.00	NA	487.00	288.00	453.00	NA	NA	525.83
Sr	120.69	129.00	180.00	180.00	158.00	202.97	146.00	155.00	162.00	15.06	160.86	146.32
Y	34.95	NA	NA	NA	NA	24.78	NA	NA	NA	84.16	26.18	42.52
Zr	140.54	NA	NA	NA	NA	145.36	NA	NA	NA	155.05	138.69	144.91
Sn	73.00	75.00	29.00	6.00	30.00	146.00	151.00	69	72.00	39.00	74.00	69.45
W	19.43	23.06	24.56	5.78	15.86	19.58	26.76	7.93	28.13	32.69	29.85	21.24
Nb	20.67	NA	NA	NA	NA	16.09	NA	NA	NA	35.64	14.29	21.67
Th	45.14	NA	NA	NA	NA	25.20	NA	NA	NA	31.35	32.24	33.48
A/CNK (Molar)	0.98	2.15	1.97	1.27	3.06	1.09	1.79	1.51	1.93	1.31	1.23	1.66
Molar K ₂ O/Na ₂ O	1.12	4.03	2.89	1.69	3.82	0.74	5.07	3.18	5.59	0.84	0.97	2.72
K/Rb	80.61	204.95	266.28	107.69	252.94	113.09	326.37	286.07	316.25	64.88	87.17	191.48
Rb/Sr	2.62	0.78	0.48	0.43	0.54	0.80	0.62	0.51	0.49	17.91	1.36	2.41
Ba/Rb	-	-	7.91	2.92	11.99	-	5.35	3.64	5.66	-	-	6.24
D.I	90.96	80.52	73.66	43.34	80.76	83.86	80.40	66.95	80.60	87.59	85.45	77.64

D. I. - Differentiation Index

NA - Not Available

Table 4.4b. Trace Element Analyses (in ppm) of Katekalyan Granite Gneiss (KGG)

Sample No.	R93/201	R93/209	R93/215	R93/254	R93/256	R93/265	R93/265	Average \bar{X} (n=7)
Field No. Ref. No.	F/1A	F/9	F/15A	F/54C	F/56A	F/65B	F/65C	
Cu	NA	NA	50.59	NA	63.60	35.70	100.10	62.49
Zn	NA	NA	21.95	NA	34.19	115.54	189.39	90.27
Co	4.00	NA	3.00	10.00	NA	NA	NA	5.67
Ni	24.00	25.00	16.70	25.00	11.77	NA	24.29	21.13
Ga	25.00	25.00	20.99	22.00	17.80	21.94	36.16	24.13
Rb	83.00	93.00	154.92	75.00	231.82	217.44	666.86	217.43
Ba	921.00	1150.00	112.00	NA	NA	NA	NA	727.67
Sr	173.00	170.00	117.43	131.00	153.85	190.53	140.99	153.83
Y	NA	NA	54.53	NA	32.46	23.55	59.21	42.44
Zr	NA	NA	192.72	NA	193.56	181.35	132.72	175.09
Sn	11.00	13.00	50.00	4.00	12.00	13.00	10.00	16.14
W	16.36	21.54	39.65	18.87	27.48	28.68	24.28	25.26
Nb	NA	NA	28.61	NA	30.03	14.67	21.23	23.63
Th	NA	NA	18.64	NA	50.46	27.60	59.53	39.06
A/CNK (Molar)	1.81	1.62	1.56	3.09	1.26	1.37	1.15	17.96
Molar K ₂ O/Na ₂ O	4.10	11.42	1.67	0.61	1.01	0.43	0.94	2.88
K/Rb	222.89	378.49	101.99	58.67	72.04	41.85	21.59	128.22
Rb/Sr	0.48	0.55	1.32	0.57	1.51	1.14	4.73	1.47
Ba/Rb	11.10	12.37	0.72	-	-	-	-	8.06
D.I	70.88	86.90	78.78	65.43	75.82	74.50	69.20	74.50

D. I. – Differentiation Index

NA – Not Available

Table 4.4c. Average of Rb, Ba and Sr of the various granite groups (El Bouseily and El Sakkary, 1975) compared with granite (KG) and granite gneiss (KGG). The values for the High and Low - Ca granites taken from Turekian and Wedepohl (1961)

ROCK TYPE	Rb (ppm)	Ba (ppm)	Sr (ppm)	Rb, Ba and Sr Recalculated to 100		
				Rb %	Ba %	Sr %
Qz-diorite and Granodiorites	140	1170	810	7	55	38
Normal Granites	190	550	70	23	69	8
Strongly Differentiated Granites	260	140	20	62	33	5
Anomalous Granites	210	1030	280	14	68	18
High - Ca Granites	110	420	440	11	43	46
Low - Ca Granites	170	840	100	15	76	9
Granite (KG)	142.53	525.83	146.32	17.49	64.54	17.96
Granite Gneiss (KGG)	217.43	727.67	153.83	19.78	66.22	13.99

Table 4.4d. Trace Element Analyses (in ppm) of pegmatite of the Katekalyan area

Sample No.	R93/251	R93/258	R89/514	R89/523	R89/525	R93/241	R93/257	Average (Pegmatite)
Field No.	F/51	F/58B	K ₃	K ₁₂	K ₁₅	F/41B	F/57C	
Ref. No.			R89/514	R89/523	R89/525			
Cu	45.36	51.00	NA	NA	NA	NA	NA	48.63
Zn	29.91	302.84	NA	NA	NA	NA	24.79	119.18
Ni	NA	10.36	25.00	24.00	25.00	23.00	NA	21.47
Ga	15.82	71.85	26.00	24.00	27.00	24.00	15.21	29.12
Rb	164.73	24.36.70	98.00	162.00	168.00	96.00	106.73	461.74
Ba	NA	NA	NA	NA	NA	285.00	NA	285.00
Sr	70.15	NA	102.00	98.00	134.00	120.00	378.01	150.36
Y	21.94	60.96	NA	NA	NA	NA	11.73	31.54
Zr	16.97	NA	NA	NA	NA	NA	124.73	70.85
Nb	NA	102.18	NA	NA	NA	NA	9.67	55.92
Th	NA	193.33	NA	NA	NA	NA	17.44	105.38
A/CNK (Molar)	1.55	1.23	3.14	1.86	1.95	1.49	1.14	1.76
Molar K ₂ O/Na ₂ O	0.48	0.89	1.14	5.28	9.11	13.69	0.55	4.45
K/Rb	-	-	-	-	-	-	-	-
Rb/Sr	2.35	-	-	1.65	1.25	0.80	0.28	1.27
Ba/Rb	-	-	0.96	-	-	-	-	0.96
D.I	95.81	84.75	83.39	86.62	80.45	86.61	76.66	84.89

D. I. - Differentiation Index

NA - Not Available

Table 4.5. Selected REE Analyses and Normalized Chondrite Values (in ppm) of Katekalyan Granitoids (KG and KGG)

Sample No.	R93/201	R93/209	R93/222	R93/284B	R93/164A	R93/172A	R93/197B	Average REE \bar{X} (N=7)	Chondrite Value Taylor & McLennan (1985)	*2 Granite (G-2)	*1 MB-H	R.V MB-H
Ref./Spot No.	F/1A	F/15A	F/22	F/84B	F/101A	F/109A	F/132B					
La (La _N)	97.00 (264.30)	67.60 (184.19)	31.00 (84.47)	35.00 (95.37)	52.40 (142.78)	65.00 (177.11)	38.30 (104.36)	55.18 (150.35)	0.3670	89.00	37.00	36.00
Ce (Ce _N)	172.00 (179.73)	130.00 (135.84)	55.50 (57.99)	64.30 (67.19)	97.00 (101.36)	136.00 (142.11)	68.30 (71.37)	103.30 (107.94)	0.9570	160.00	73.20	73.60
Nd (Nd _N)	54.50 (76.65)	54.50 (76.65)	18.40 (25.88)	25.90 (36.43)	35.10 (49.37)	54.50 (76.65)	25.00 (35.16)	38.70 (54.43)	0.7110	55.00	42.00	39.40
Sm (Sm _N)	9.00 (38.96)	11.60 (50.22)	3.32 (14.37)	4.10 (17.75)	7.15 (30.95)	9.60 (41.56)	5.20 (22.51)	7.14 (30.91)	0.2310	7.20	9.61	9.69
Eu (Eu _N)	1.20 (13.79)	1.33 (15.29)	0.42 (4.83)	0.51 (5.86)	0.81 (9.31)	1.18 (13.56)	0.53 (6.09)	0.85 (9.77)	0.0870	1.40	2.51	2.77
Gd (Gd _N)	4.62 (15.09)	9.80 (32.03)	2.22 (7.25)	2.26 (8.69)	4.40 (14.38)	5.65 (18.46)	3.16 (10.33)	4.64 (15.16)	0.3060	4.30	8.30	9.28
Dy (Dy _N)	2.81 (7.37)	9.94 (26.09)	1.79 (4.69)	1.90 (4.99)	2.90 (7.61)	3.50 (9.19)	1.60 (4.20)	3.49 (9.16)	0.3810	2.40	8.45	9.35
Er (Er _N)	1.20 (4.82)	6.40 (25.70)	0.87 (3.49)	1.00 (4.02)	1.32 (5.30)	1.55 (6.22)	0.68 (2.73)	1.86 (7.47)	0.2490	0.92	5.37	5.23
Yb (Yb _N)	1.20 (4.84)	5.90 (23.79)	0.59 (2.38)	0.73 (2.94)	1.13 (4.56)	0.91 (3.67)	0.34 (1.37)	1.54 (6.21)	0.2480	0.80	5.00	5.02
Lu (Lu _N)	0.18 (4.72)	0.89 (23.36)	0.14 (3.67)	0.09 (2.36)	0.16 (4.20)	0.10 (2.62)	0.06 (1.57)	0.23 (6.04)	0.0381	0.11	0.61	0.67
Y	-	54.53 (25.97)	34.95 (16.64)	-	24.78 (11.9)	-	26.18 (12.47)	35.11 (16.72)	2.1000			
(Y _N)												
ΣLREE	333.70	265.03	108.64	129.81	192.46	266.28	137.33	205.17	() Normalised Chondrite value			
ΣHREE	10.01	32.93	5.61	6.38	9.91	11.71	5.84	11.76				
ΣREE	343.71	297.96	114.25	136.19	202.37	277.99	143.17	216.93				
(La/Yb) _N	54.61	7.74	35.49	32.44	31.31	48.26	76.17	24.21				
(La/Sm) _N	6.78	3.67	5.88	5.37	4.61	4.26	4.64	4.86				
(Gd/Yb) _N	3.12	1.35	3.05	2.96	3.15	5.03	7.54	2.44				
(Ce/Yb) _N	37.13	5.71	24.36	22.85	22.23	38.72	52.09	17.38				
Eu/Eu*	0.57	0.38	0.47	0.47	0.44	0.49	0.40	0.45				
(Eu _N /Y _N Sm _N Gd _N)												

() Normalised Chondrite value

1* and 2* Standard Samples of Metabasic (MB-H, Source WHG, India) and Granite (G-2, USGS, USA)

R.V. = Reputed value

ORE PETROGRAPHY, ALTERATION AND GEOCHEMISTRY

5.1. Ore petrography

5.1.1. Introduction

Ore petrography is done best on a very well polished ore section. But for achieving a perfectly polished ore section there are always difficulties mainly due to variation in mineral and ore composition as well as their hardness. The present study is also no exception to it; however, the author has adopted the following procedure for the opaque sections.

First a suitable sized ore samples were selected and put to coarse-grinding on steel plate using 200-400 and 600-mesh carborandum powder followed by fine grinding in similar way on glass plate using 800-mesh powder. In the next stage some finer grinding was done by dry method, using 2/0, 3/0, 4/0 and 5/0 emery polishing papers. After this, the specimens were subjected to polishing by chrome oxide powder followed by alumina or synthetic diamond paste for about 3 hours.

The usual precautionary measures were strictly followed during the final polishing. Special care was taken in case of such samples which appeared altered or having mineral constituents of variable hardness. In such cases, alumina or diamond polishing was done very slowly but with uniform light pressure.

5.1.2. Microscopic observations

Optical characters of the ore minerals in the polished ore sections were studied with the help of a polarising ore microscope (Carl Zeiss, Jena, the then G.D.R.). The standard work of Ramdohr (1969), Schouten (1962) and Utenbogaardt and Burke (1971) were consulted.

The preliminary observations of the ore samples reveal that cassiterite was the most abundant tin ore mineral in Katekalyan area. The other associated ore minerals like columbite, tantalite, tapiolite, microlite and wolframite were also identified in small amount. Limonite (mainly goethite) was the common secondary ore mineral, and was recognised as the alteration products. The gangue minerals associated with the ore are quartz, fluorite, zinnwaldite and K-feldspar. The texture and structure of the ore and their petrography of the Katekalyan have been studied in detail and is divided into two main classes, namely primary and secondary ore minerals with the salient features are given below.

(A) Primary ore minerals

Cassiterite (SnO_2 , Tetragonal):

Cassiterite is most important ore mineral of the study area. The major bulk of this ore mineral is associated with pegmatites. It occurs mainly as coarse disseminated grains ore body with euhedral to subhedral shape and bypyramidal form and massive in nature. The mineral is dark gray to black in colour with grayish to brown streak and greasy to admantine lustre.

Cassiterite is brownish grey to light grey in colour and have pitted (poor polishing) to non-pitted surface in reflected light. The intensity of the colour was lower than that of associated columbite-tantalite. The reflection pleochroism is very weak and varies from brownish grey to orange red. The internal reflection colour (Plate XXIII, Fig.A) shows distinct anisotropism from light grey to dark grey and a brick red to yellow pale brown. The orange red pleochroic colour and the brick red internal reflection may be due to its numerous inclusions and impurities to its high tantalum and iron content in the lattices. Twinning was noted as common feature in many sections but zoning was not distinct, may be because of the strong internal reflection.

Cassiterite is easily distinguished from columbite-tantalite by its micro-hardness, poorly polished sections, cracks and crevices and low reflectivity (brownish gray). Anisotropy and strong internal reflection and high

relief are also additional distinguishing characters for the identification of the cassiterite mineral. In many polished sections of cassiterite two sets of very feeble cleavage traces have been observed only under cross-nicols (Plate XXIII, Fig. A). Ore microscopic studies on the cassiterite samples of the study area reveal the presence of numerous inclusions (or exsolutions) of minerals. These inclusions were observed to contain columbite-tantalite, tapiolite and silicate minerals. Exsolution texture among cassiterite, columbite-tantalite and tapiolite is a common phenomenon and helpful in the understanding the genesis of mineralisation.

The coarse grains of cassiterite are usually fractured which are filled by the quartz and columbite-tantalite minerals (Plate XXIV, Fig. A and B). Cassiterite often occurs with tapiolite where later has no internal reflection. However, their intergrowth is subjected to alteration particularly at the contact. The altered phase shows white internal reflection of microlite whereas tapiolite shows reddish internal reflection (Plate-XXIII, Fig. A).

Few cassiterite samples exhibit zoning from colourless to brown shades (Plate XXIII, Fig. A) indication of multi stage growth. The colourless zone is free from any inclusion whereas the reddish brown and brownish red shade zone contains numerous inclusions possibly of Ta-W-bearing phases. The paragenetic relationship suggest that the bright coloured (unzoned/inclusion free part) that is Ta-free cassiterites were crystallised first which is followed by the dark crystallization of coloured Ta-Sn rich zones during the lowering of temperature.

Columbite-tantalite $\{(\text{Fe,Mn})(\text{Ta,Nb})_2\text{O}_6\}$, Orthorhombic} :

Columbite-tantalite is usually present in minor quantities, as inclusions in cassiterite but occasionally it occurs as separate mineral. The exsolved grains of columbite-tantalite (Plate XXIII, Fig. D) are irregular in shape and vary in size from small globules to large lamellar grains (Plate - XXV, Fig. B). Babu (1994) suggested that columbite-tantalite is the solid

solution series between columbite $(\text{FeMn})\text{Nb}_2\text{O}_6$ and tantalite $(\text{Fe,Mn})\text{Ta}_2\text{O}_6$ and is commonly associated with cassiterite in Katekalyan.

The ore petrography suggests that some of the larger grains of columbite-tantalite are definitely the product of normal intergrowth. The columbite-tantalite minerals are easily identifiable by their moderate reflectivity (whitish grey) than that of cassiterite, and weak but distinct pleochroism. Columbite/tantalite shows very weak anisotropism and straight extinction. In the coarse crystals of columbite-tantalite veinlets of cassiterite have been observed along fractures. Where subhedral cassiterite grains were found to have columbite-tantalite inclusions with the development of radiating cracks. Occasionally columbite-tantalite also occur as fracture fillings in cassiterite (Plate -XXV, Fig. A). The textural study suggest that columbite-tantalite appears replacing cassiterite and vice-versa texture frequently. But columbite-tantalite shows very rare (or some what unusual) inclusions of wolframite and tapiolite.

Tapiolite $[(\text{Fe,Mn})(\text{Ta,Nb})_2\text{O}_6]$ – Tetragonal :

The tapiolite mineral is also present a very minor constituent cassiterite association. Its occurrence as separate phase is expected in the area, but due to similarity in physical properties with other associated ore minerals makes it difficult to distinguish it individually in the field. Tapiolite mostly occurs as very small grains, bluish grey in colour with brownish tint (Plate -XXIV, Fig. D).

In reflected light, its reflectivity is low and it looks bluish grey. Thus it is of slightly higher reflection colour than that of cassiterite. The tapiolite, ore petrography is characterized by weak reflection pleochroism (but very distinct in oil). It shows strong anisotropism but generally it is masked by its internal reflection (Plate -XXIII, Fig. C). It is easily distinguished from cassiterite by its slightly higher reflectivity, better polishing, lower micro-hardness and moderate anisotropism. It is distinguished by its higher anisotropism, low internal reflection and better polish (Plate XXIII, Fig.B) from columbite-

tantalite. In general, the paragenetic relation of this mineral with the other associated ores indicates that it has intergrowth with cassiterite or as replacement type texture with the original tin mineral but very rare textural relationship with columbite-tantalite mineral.

Microlite [(CaNa)₂(Ta₂O₆) (O, OH, F) – Isometric]:

The microlites mostly occur peripheral to the columbite-tantalite and might be secondary product of the latter (Plate XXV, Fig. C).

Wolframite [(Fe,Mn)WO₄ – Monoclinic] :

It is observed as an inclusions in cassiterite, columbite-tantalite and very rarely in tapiolite. Its reflectivity is moderate and similar to that of columbite-tantalite. The tungsten mineral may be distinguish from columbite-tantalite by the difference in the shades, that is, the tungsten mineral is more grayish white than the whitish gray of columbite-tantalite (Plate XXIII, Fig.D). Moreover, it is having much deeper red internal reflection. Sometimes the bladed form having slanting terminations is helpful in distinguishing wolframite from similar looking opaques.

It is also distinguished from cassiterite by higher reflectivity, better polishing and strong anisotropism. Reflection pleochroism in wolframite is quite low and can be seen along grain boundaries. The textural study points the presence of tiny inclusions, which suggest that wolframite should be related with early paragenetic sequence than cassiterite (Plate XXV, Fig.D).

Secondary minerals

Goethite, in many samples of cassiterite intergrowth with other cassiterite bearing minerals like columbite-tantalite and tapiolite. The fine veins and veinlets of goethite (Plate XXIII, Fig.B), were noticed randomly with tin ore. The goethite is present with grayish reflection colour in reflected light. Sometimes varying between dull gray to bright gray with a bluish tint.

Occasionally it reflects the dull gray reflection, which suggest that the iron hydroxide is not fully crystalline.

5.2. Alteration environment

The formation of cassiterite mineral in the study area is mainly associated with the metasomatic replacement of granitic rocks. The granites are recrystallised by hot gaseous, aqueous mineralised solutions will continue to exchange and receive elements from the wall rocks by the several differing alteration effects may occur at different points. The pneumatolytic alteration in the rocks is due to the combined effects of heat and magmatic emanations largely consisting of the halogen elements, water phosphorus and alkali metals.

Different alteration zones associated with tin mineralisations have been identified in the study area based on field evidences and petrographic and geochemical studies of the granitoids. The influence of different zones with the changes of mineralogical and petrochemical variants shows different alteration activity.

The different metasomatic activities leads to the formation of rare metal mineralisation have been recognised in the study area. Four distinct zones of formation of cassiterite along with Nb and Ta mineral compositions have been demarcated viz, microclinisation (potash-metasomatism), albitisation (soda-metasomatism), greisenisation (pneumatolytic activity) and sericitisation in the Katekalyan granites and pegmatites.

It is commonly observed that tin deposits are mainly confined at the contact of metasediments, metabasics & granites/granite gneisses with pegmatites and quartz veins in Katekalyan. The alteration zones in this area are very narrow. The apical zones of tin-bearing granitoids are sites of intense

and complex metasomatic activity with the transporation of tin ions leading to the formation of discrete crystals of cassiterite. Source of the alteration solutions is highly debated. Feldspathisation takes the form of microclinisation or albitisation. The enrichment of K_2O at the expense of Na_2O and change in petrochemical composition indicate by the process of microclinisation, where plagioclase is replaced by the microcline in the granitic rocks. Albitised pegmatites in Katekalyan area were found in granites and metabasic rocks. The albitised pegmatites can be identified by their monomineralic nature, predominant of plagioclase feldspars and sub-ordinate quartz and incipient mica. The feldspar is mostly albite or cleavelandite variety, which were formed by the replacement of microcline indicating the prevalence of albite due to the soda metasomatism. Albitisation seems more frequent than microclinisation and may be accompanied by lithium enrichment. Albite enrichment of this type is difficult to recognise particularly where the rocks are only partially altered. The phenomenon of albite enrichment is accompanied by the presence of disseminated cassiterite rich with minor or rare columbite and tantalite minerals. Greisenisation is represented by the decomposition of feldspars and biotite and by the formation of quartz, mica, topaz and ore minerals in the granite and pegmatite. Geochemically, the import of OH, F, Li, Sn, W, B and the removal alkalies (especially Na, less pronounced K) are the most significant, while Si, Al remain essentially constant. Greisenised pegmatites constituting mainly of quartz and muscovite intercalations with lepidolite, associated with cassiterite, beryl, tourmaline were formed mainly due to the actions of pneumatolytic activity in the marginal areas of the pegmatites. Muscovitisation of K-feldspar is more intense than plagioclase feldspar due to volatile rich fluid activities. Highly sericitisation of feldspar were observed due to metasomatic hydrothermal fluid activity in the pegmatites. Tourmalisation is also intense at the contact of granites and quartz veins. Wall rocks are

composed of tourmaline, muscovite, chlorite, apatite, fluorite and opaques minerals. It has been commonly observed that in Katekalyan area, mineralisation is associated with wall rock alteration and also the intensity of alteration is directly proportional to the intensity of mineralisation.

5.3. Geochemistry of Cassiterite

To study the main ore minerals found in the pegmatites as cassiterite along with columbite and tantalite in varying proportions, eight representative samples of cassiterite have been analysed. Ore samples were selected from six important mineralised pegmatites. Three samples were taken from placer deposits of the different localities.

5.3.1. Samples preparation method

First, cassiterite grains were separated manually from rich clots of ores. Then each samples were washed in water carefully, dried and crushed. Further, samples were powdered in agate mortar and sieved to different fractions. To get finer fragments free from dust, the sieved material was washed in water again and dried. After this the samples were treated with dilute HCl to make it free limonitic impurities and washed again with pure water and dried. The samples were passed through isodynamic separator to get pure concentrates of ores. Finally, the ore concentrates were checked under binocular microscope to remove the composite grains and extraneous mineral particles.

5.3.2. Procedure of XRF analysis

5 to 6 gms – 100 mesh sample is mixed with 1 ml 5% polyvinyl acetate in acetone. The mass is pressed into pellet of 40 mm diameter at 30-kilo newton pressure. The same pellets were analysed for the elements of Sn, Nb, Ta, WO_3 and others using XRF instruments (Philips Make Model PW-1400).

The analytical data are given in table 5.1.

Table 5.1. Element Analyses of Cassiterite from Katekalyan Area

Sample No.	R89/517	R89/612	R89/790	R89/830	R89/915	R89/1305	R89/1399	R89/1405	Average
Ref./Spot No.	CF/1210	CF/1220	CF/1230	CF/1240	CF/1250	CP/5	CP/99	CP/105	
Sn (%)	56.57	61.98	60.12	71.84	70.76	63.68	69.78	62.34	64.63
Nb (%)	0.97	0.52	0.89	0.76	0.96	0.79	0.84	0.75	0.81
Ta (%)	2.11	2.29	2.18	1.99	1.87	2.16	2.05	1.89	2.07
WO ₃ (%)	2.54	2.48	1.83	2.38	2.46	1.95	2.58	2.19	2.30
FeO _T (%)	11.58	11.49	10.99	11.38	11.27	NA	0.01	0.13	8.12
MnO (%)	7.22	5.86	6.78	7.17	6.86	2.16	2.09	2.38	5.06
MgO (%)	2.13	2.34	2.09	1.99	2.19	3.79	3.69	3.56	2.72
TiO ₂ (%)	0.11	0.09	0.14	0.18	0.07	0.45	0.39	0.41	0.23
CaO (%)	1.39	1.28	1.43	1.32	1.16	3.98	3.76	3.57	2.24
Ni (ppm)	16.00	14.00	18.00	13.00	17.00	16.00	15.00	17.00	15.75
Ga (ppm)	42.00	40.00	43.00	41.00	41.00	94.00	89.00	95.00	60.62
Rb (ppm)	53.00	51.00	51.00	54.00	49.00	52.00	51.00	48.00	51.12

5.3.3. Chemistry of Cassiterite

The element analyses of cassiterite given in Table 5.1 indicated the admixture of tin as major constituent with subordinate quantities of niobium, tantalum, tungsten, iron, manganese and other trace, elements. Tin (Sn) content in the cassiterite ranges from 56.57 to 71.84% indicating that basically 70 to 90% is as SnO₂ mineral phase. The niobium metal content ranges from 0.52 to 0.97% whereas tantalum varies from 1.87 to 2.29%. The concentration of tantalum is more than that of niobium content. Thus, on the whole tin, niobium and tantalum concentration constitute more or less 80%. The other major oxides present are WO₃ varying from 1.83 to 2.58%, FeO (t) ranges from 0.01 to 11.58%; MnO content varying from 2.09 to 7.22%; MgO ranges from 1.99 to 3.79%; TiO₂ varying from 0.07 to 0.45% and CaO ranges from 1.16 to 3.98%. Trace elements like Ni, Ga and Rb are present as low in

content. Hence, it is evident that a number of metallic cations are known to enter into the solid solution in cassiterite. It is presumed that the presence of Nb, Ta and W will have no effect on the cell dimension of the cassiterite.

Niobium (Nb) and tantalum (Ta) are characteristically oxyphile forming a number of complex minerals or they enter isomorphously into minerals of iron, manganese, titanium, tin, tungsten, uranium, thorium and rare earths. Niobium (Nb) shows closer relationship with titanium, tungsten, thorium, the rare earths of cerium group and sodium. Tantalum (Ta) shows a closer relationship with zirconium, tin, the rare earths of yttrium group, uranium and lithium. Mineral occurring in sodic alkali granites and syenites are generally niobium rich, whereas those in lithium pegmatites are tantalum rich (Ginzburg, 1972). The high content of Mn and Ti are indicative of the presence of mangano-ilmenite. The average Sn content in cassiterite samples from the study area is 64.63%, which is considered to be of economically importance. Almost all the cassiterite samples contain significant amounts of Sn, Nb, Ta and W. Whether these elements are present in sufficient quantities to render profitable extraction from these cassiterite crystals.

PLATE – XXIII

Fig (A): Photomicrograph of cassiterite shows two sets of very feeble cleavage traces. In the other portions, microlite shows white internal reflection whereas tapiolite gives reddish internal reflection.

(Reflected Light, $1.6 \times 0.32 \times 4$)
[Crossed]

Fig (B): Photomicrograph of cassiterite (dark) is showing intergrowth with tapiolite (bright) present as twin lamellae. On the sides of this intergrowth, columbite-tantalite (yellowish cream) appears to replace it and also show the presence of goethite.

(Reflected Light, 10×7)
[Uncrossed]

Fig (C): Photomicrograph showing the intergrowth of cassiterite and tapiolite (typical colour) with development of criss-cross fractures traversing the body of the crystal. This tapiolite shows strong anisotropism but it is masked its internal reflection.

(Reflected Light, 10×7)
[Uncrossed]

Fig (D): Photomicrograph showing the intergrowth of pitted cassiterite and columbite-tantalite (whitish gray). The wolframite (grayish white) is present at the contact of cassiterite.

(Reflected Light, 10×7)
[Uncrossed]

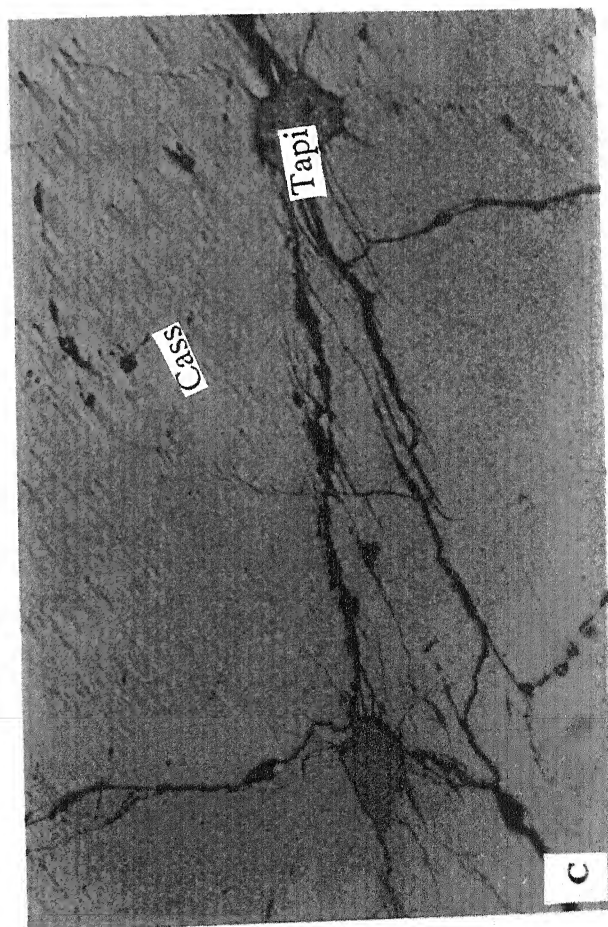
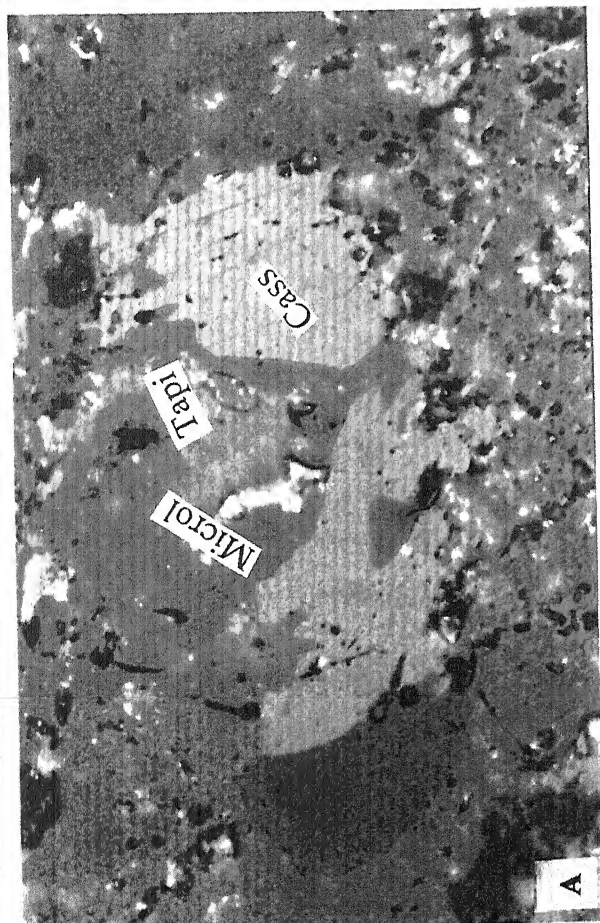
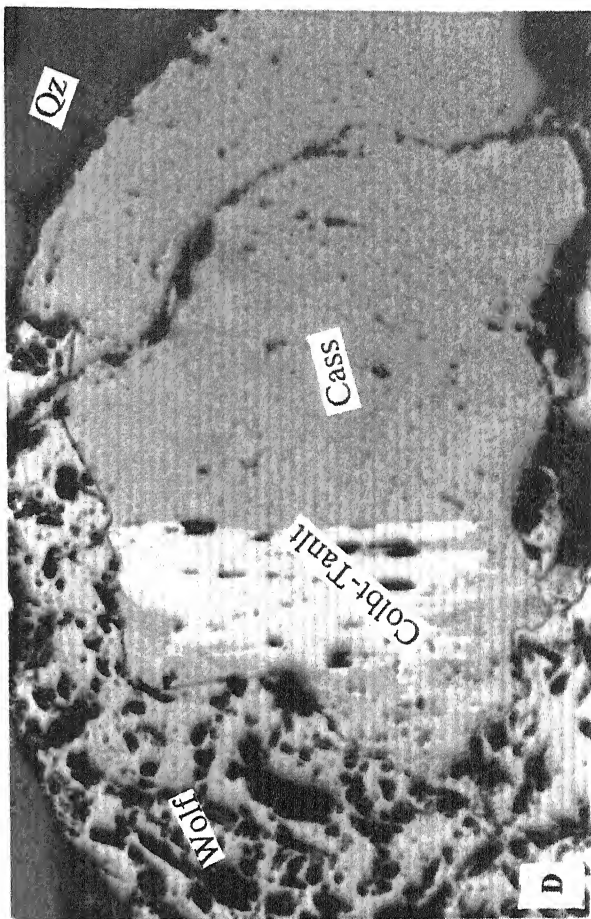
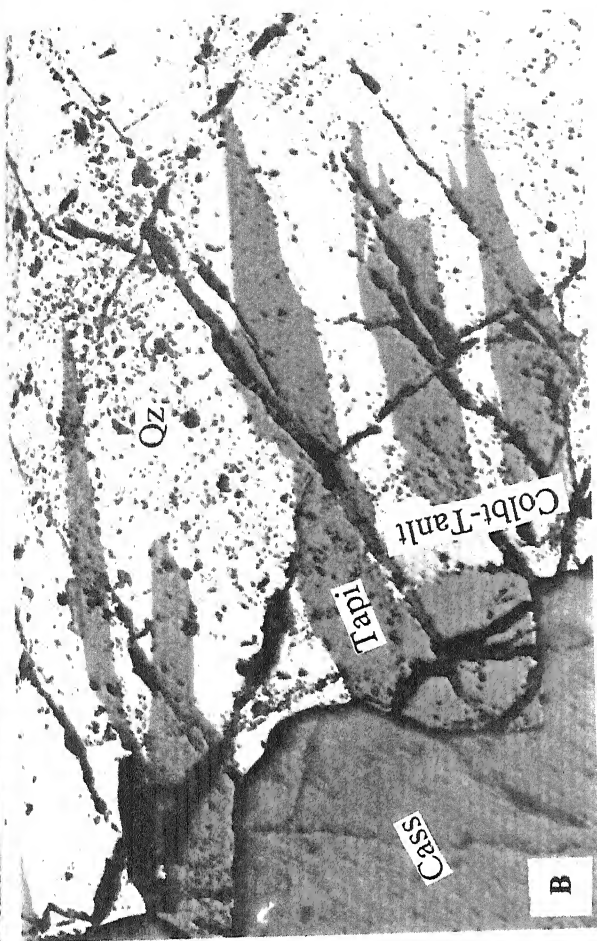


PLATE – XXIV

Fig (A): Photomicrograph of cassiterite crystal (dark brown) shows the intergrowth of columbite-tantalite with varying shape.

(Reflected Light, 10×7)
[Uncrossed]

Fig (B): Same photomicrograph of Fig. (A), in which columbite-tantalite (whitish gray) is present in the highly fractured cassiterite crystal and also observed the veinlets of cassiterite (brownish gray) and quartz (dark gray).

(Reflected Light, 10×7)
[Uncrossed]

Fig (C): Photomicrograph shows the development of cassiterite (light) by the alteration of the lithium bearing mica (brown) within the mass of cassiterite.

(Reflected Light, 10×7)
[Uncrossed]

Fig (D): Photomicrograph shows the exsolution texture among cassiterite (brownish gray), columbite-tantalite (white) and tapiolite (brown gray) within the mass of cassiterite (light gray).

(Reflected Light, 10×7)
[Uncrossed]

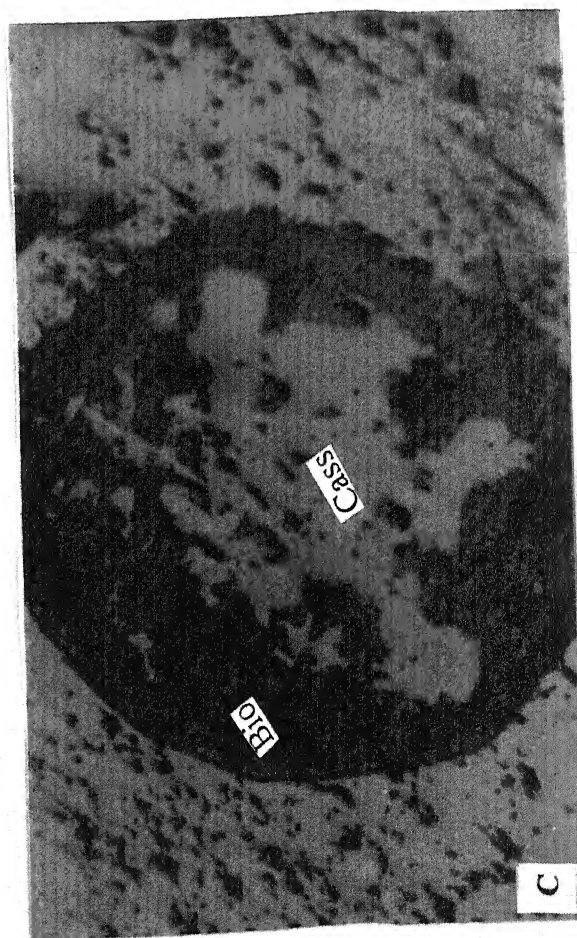
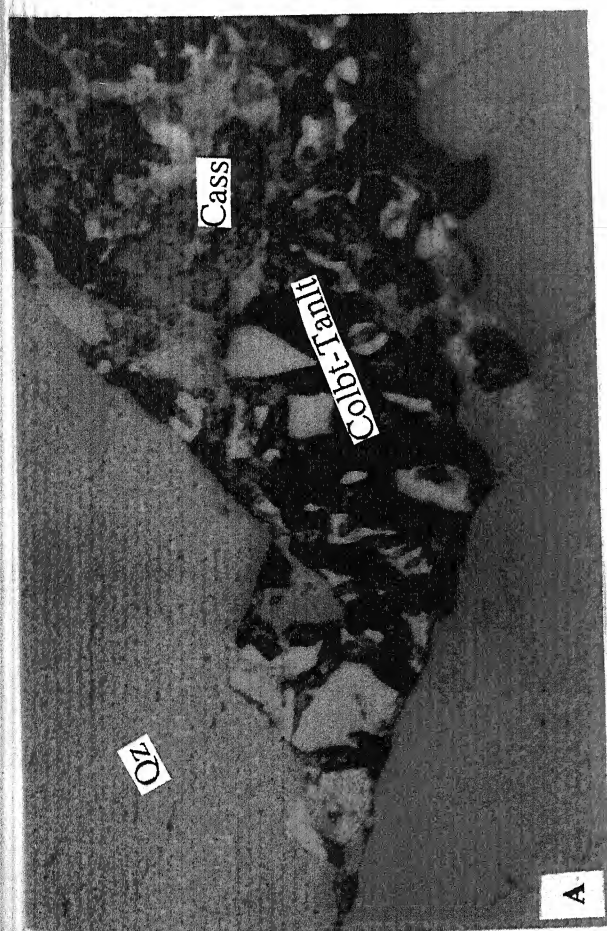
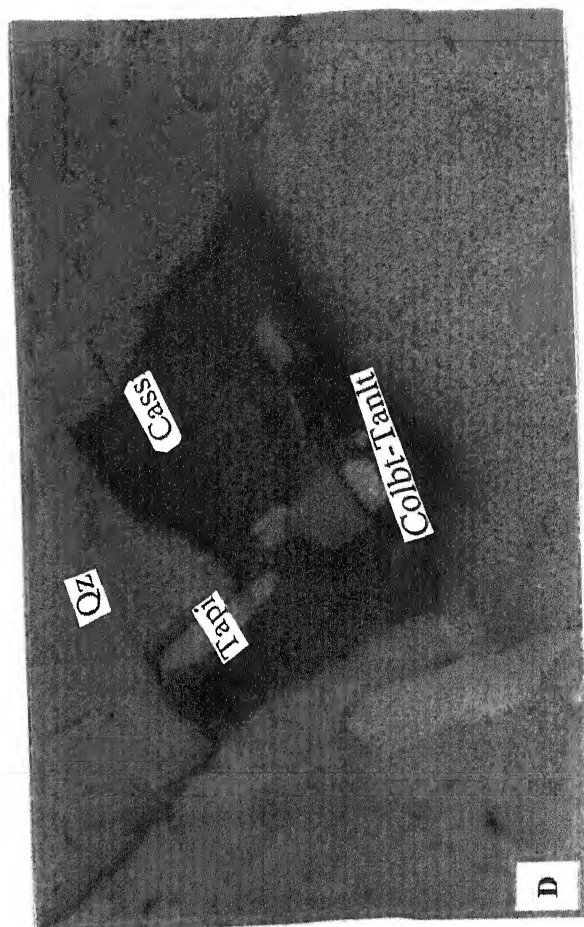
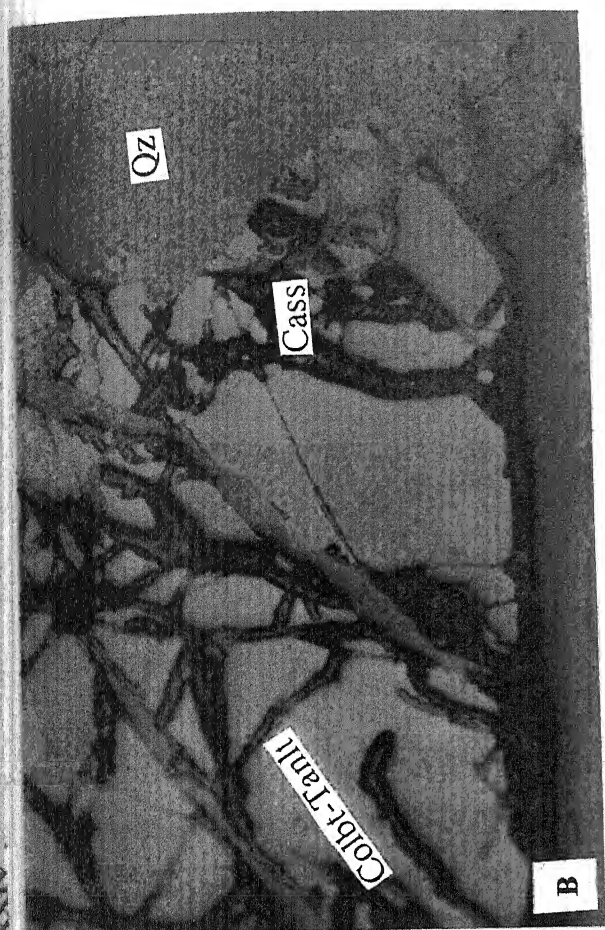


PLATE – XXV

Fig (A): Photomicrograph of coarse-grained cassiterite (light gray) having triangular Pitts with zoned surfaces of colourless to brown shades are present.

(Reflected Light, 10×7)
[Uncrossed]

Fig (B): Photomicrograph of coarse cassiterite (brownish) with exsolved grains of columbite-tantalite (whitish gray) having alternate irregular in shape and varying in size from globules to large lamellar grains. Microlite is also present having the white internal reflection.

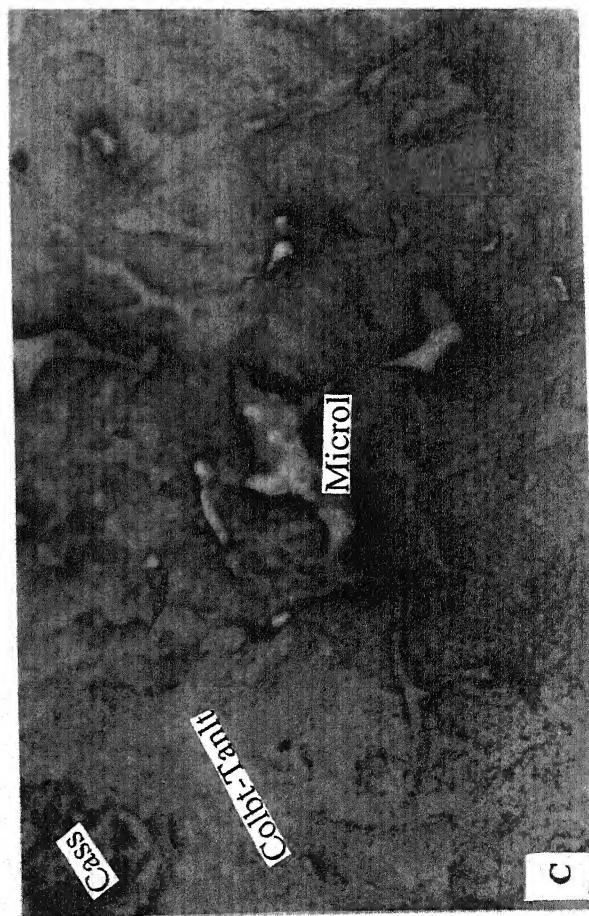
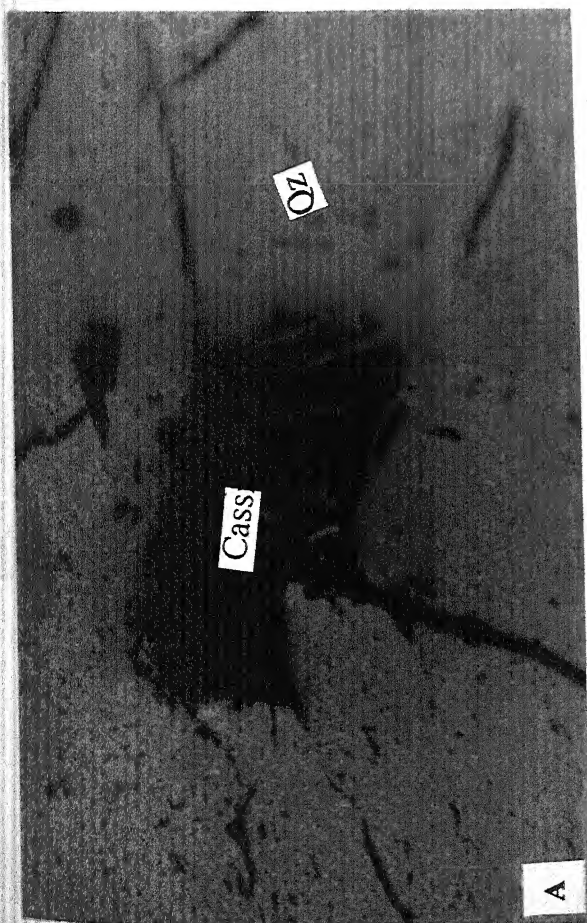
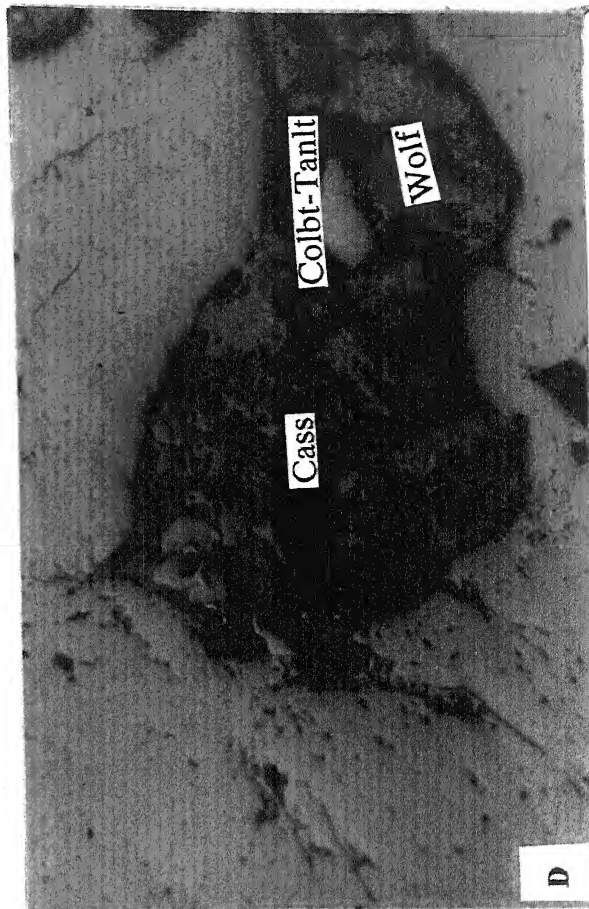
(Reflected Light, 10×7)
[Uncrossed]

Fig (C): Photomicrograph of cassiterite (brownish gray) shows the inclusions of columbite-tantalite (whitish gray) and also microlite (white internal reflection) in the form of irregular, disconnected and randomly oriented patches.

(Reflected Light, 10×7)
[Uncrossed]

Fig (D): Photomicrograph of coarse-grained cassiterite (brown) shows the inclusions of columbite-tantalite (whitish gray) and wolframite (grayish white).

(Reflected Light, 10×7)
[Uncrossed]



FLUID INCLUSION STUDIES

6.1. Introduction

Fluid inclusions are present as small amounts of fluid body that was trapped at the time of mineral formation or afterwards during the changed geological conditions. Depending upon their physical state at room temperature they may be further differentiated as gas inclusions or liquid inclusions and/or both. To understand the genetic conditions of the tin mineralisation of the Katekalyan area, fluid inclusion studies of cassiterite were carried out.

Fluid inclusions are abundant in many common tin ore and associated gangue minerals and can be observed with a standard petrographic microscope. Tin ore deposits are particularly suitable for an investigation of the inclusions in these minerals, because it contains many excellent fluid cavities.

The most useful and widely applicable classification of fluid inclusions is proposed by Roedder (1979) which categorized these inclusions into primary, secondary and pseudosecondary on the basis of their origin. Primary inclusions are trapped within crystals at the time of crystallization of host mineral and represent the parent fluid. They do not cross grain boundaries. But the secondary inclusions are epigenetic and are entrapped either after mineral formation or during isolated recrystallisation along fractures. Generally, they are found in trails or clusters, which cross grain boundaries. The pseudosecondary inclusions are primary in genetic sense but resemble with secondary inclusions as they are trapped by healing of the growth planes or fractures generated at the time of crystal formation. They represent the parent fluid of the crystal formation. The trails of these inclusions abruptly end within the single crystal while those of secondary inclusions transgress the crystal boundary.

The choice of significant inclusions is exceedingly valuable in extracting the appropriate thermobarometry and compositional informations. This is because of the possible presence of several generations of inclusions in one sample. The inclusions with sign of leakage, necking down or those adjacent to the cracks are not suitable for getting reliable data. The temperature of trapping can be estimated by heating the sample to the point at which the bubbles disappear i.e., the temperature of homogenization. This marks a minimum temperature of formation of the mineral, provided no leakage exists.

6.2. Method of sample preparation

Cassiterite samples of fluid inclusion interest were collected from the different pegmatitic veins of the Katekalyan area. The samples were collected from various lateral locations from different tin-bearing pegmatite veins, the representative of geological events. Thin sections of uniform thickness (0.3 mm to 1.0 mm) polished on both surfaces were prepared for the visual observation of fluid inclusions. Profuse water supply to prevent the damage of inclusions due to local heating and fine polishing on both the surface was helpful for better results. The polished chips were mounted on glass slides for fluid inclusion petrography while for the thermometric runs dismounted chips of less than 1 cm size, convenient as per the size of heating-cooling chamber were selected. At last, final polishing was carried out using a cotton cloth smeared with a thin pulp of fine alumina suspension.

Initial observation and identification of inclusions were carried out by a microscope with high power objective combined with a long focusing light and condenser. Field illumination was increased accordingly by using a separate light source.

6.3. Fluid inclusion petrography

The size, shape, contents and their phase proportion, degree of fill and the type of inclusion and bubble movement can be studied through

optical observations. These observations help in determining the density and viscosity of the fluid. The disposition and distribution of inclusions, their relation with other inclusions and with the host grain suggests the type and origin of the inclusion and also the relative chronology.

The types of inclusions in the cassiterite of the study area have been classified into four categories by using the compositional criteria given by Roedder (1984). The distinction among the different types of fluid inclusions was made by the presence of different phases, i.e., aqueous liquid, liquid CO₂, CO₂ gas, vapour and solids at room temperature (23°C). Due to uncertainty of clear-cut distinction between the pseudosecondary and secondary inclusions only primary inclusions were selected for the study.

The different types of inclusions identified are described below:

Type – I (CO₂ Inclusions): It is a monophasic carbonic fluid (at room temperature) and is dominated by CO₂ of the primary in nature. It resulted in partitioning of most of the CO₂ into a vapour phase, which might have carried a small amount of salts in solution. Most important, however, the evolution of this vapour phase apparently changed the ore-fluid chemistry enough to cause the precipitation of cassiterite and quartz. The fluid inclusion of type – I is lying more or less along a diagonal cleavage planes (Plate XXVI Fig. A) of cassiterite. These inclusions are primary in nature as suggested by their distribution pattern and morphologies such as six sided, euhedral to subhedral negative crystal shapes. Maximum number of CO₂ inclusions was homogenized between –7.4 to –6.8°C, whereas few inclusions of CO₂ were homogenized between –12.8°C to –6.8°C. So the isochore (Fig. 6.1) was highest as well as of low-density CO₂ inclusions. Kelly and Turneaure (1970) suggested a magmatic source for the brines and metals but progressive cooling and dilution of these brines might reflect gradual influx of meteoric water into the magmatic-hydrothermal system.

Type II (CO₂-H₂O Inclusions): These inclusions are somewhat subrounded double bubbles due to constriction of the chamber. They generally have tabular or negative crystal forms, and are similar in size and shape. However,

there is a marked difference in the relative size of the bubbles of the two types of inclusion, when then are observed in the two-phase conditions at room temperature. These inclusions are characterized by the presence of CO_2 with rich aqueous liquid (Plate XXVI Fig. B). All inclusions with bubbles occupying over 60% of the cavity were shown to be of the CO_2 - H_2O type (i.e., a third phase appeared). But other inclusions with bubbles occupying less than 40% of the cavity were shown to be of the H_2O type (i.e., no additional phase appeared), that were considered too small for the cooling tests. Bubbles occupying over 60% of their cavities are considered likely to be CO_2 - H_2O type of inclusion. The mode of occurrence of CO_2 - H_2O inclusion (H_2O rich) suggested that they were primary in nature and has lower density in comparison to CO_2 inclusions.

Type III (H_2O - NaCl -Halite Inclusions): This type of inclusions are present in the most part of crystalline material, but are characterised by relatively small bubbles of one-quarter of the volume of the cavity or less. The outlines of these inclusions are regular to irregular and marked by different from the rounded crystal forms of H_2O and H_2O - CO_2 inclusions. (Plate XXVI Fig.C). Because of the dark colour of the cassiterite and the small size of the inclusions, it was not possible to determine whether they contained crystal or not. The solid inclusions are commonly observed in the cassiterite. It may contain small solid crystals of a reddish brown mineral, which is tentatively identified as rutile. All the inclusion refers to cassiterite are not distributed in planes and are almost certainly primary in characters. Daughter minerals having usually cubes of halite (NaCl) were formed when nearly a saturated fluid cooled from the initial temperature of entrapment. The presence of such crystals obviously indicates that the fluid was salt-saturated.

Type -IV (H_2O - NaCl Inclusions): The H_2O - NaCl inclusions (Plate XXVI, Fig C) in the cassiterite, total equivalent salinity of fluid inclusion can be determined by the freezing-point depression method. In practice, freezing the sample, then observing it through the microscope as it is warmed and measuring the temperature at which the last ice melts achieve this. This temperature is then used to read off the solution composition and represents

the freezing-point depression of water as a function of salt content. The salinity of these inclusions ranges from 2.63 to 12.4 wt% NaCl and the density varies between 0.94 to 0.96 gm/cm³. The homogenization temperature of these inclusions is observed at the ranges of 115°C to 220°C. In the H₂O-NaCl system, the principal stable phases at low temperature are liquid vapour, ice and salt hydrate, which can be recognized through their optical properties. Below -20.9°C temperature only solid exists while over this temperature at a wide range both liquid and solid can co-exist. The final melting temperature of the solid phase corresponds to its concentration in the liquid. Normally the Liquid-solid change is identified by granular appearance. If the temperature of ice is increased, it will melt gradually until last ice crystal melts at last ice-melting temperature T_m .

6.4. Microthermometric Analysis

The thermometric analysis was carried out on a Leitz 1350 heating stage and U.S.G.S. gas flow freezing stage using doubly polished crystal wafers of 0.3 mm in thickness. Selected fluid inclusions were heated in a Leitz 1350 heating stage attached to a Leitz Ortholux transmitted light microscope (Shepherd, 1981). Before heating the thin sections of cassiterite, the heating stage was calibrated carefully. For this purpose, analytical grade pure calibration standards such as naphthalene, silver nitrate, sodium nitrate and potassium dichromate were used. Using the heating stage, filling temperature measurements were made on all fluid inclusions of sufficient size for accurate observation. For freezing studies a U.S.G.S. gas flow freezing stage was used to determine the composition and salinity of the entrapped fluid. Before freezing the inclusions, the stage was calibrated using distilled water (m.p. 0°C) and octane (m.p. -57.79°C) as standards.

For the microthermometric study only selected primary and some pseudosecondary inclusions were chosen and treated using above techniques. The observation is summarized in tables (6.1,2,3,4). These data

and their interpretation are more applicable to the formulation and refining the models on which genetic strategies are based.

6.5. Results of the Microthermometric Study

The observations related to types of inclusion in the cassiterite and the filling temperature is shown in tables (6.1,2,3,4). For both the measured and calculated filling temperature, the limits of variations refer to the differences between the different inclusions in the cassiterite rather than the probable errors involved.

The characteristics of each type of inclusion can be summarized as follows :

On heating the type I CO₂ inclusions, homogenized in two stages. The small bubbles of CO₂ gas disappeared first on heating and CO₂ homogenised between the temperature ranges of -57.8 to 56.2°C. On further heating, the CO₂ liquid inclusions were completely homogenized in the temperature range of -12.8 to 6.8 in a few type I inclusions. But the maximum number of CO₂ inclusions was homogenized between -7.4 to 6.8°C. The observation of the vol.% of the CO₂ liquid phase in type I inclusions is less than 5 by visual estimation at 20°C. The temperature of homogenization (T_H) of type I inclusions increases from -12.8 to 6.8°C, but the density decreases from 0.998 to 0.963 gm/cm³. It is apparent from table (1) that the carbonic fluid of cassiterite-hosted inclusions varies in both salinity and carbonic compositions. However, it is important to note that for a given host mineral, there is no correlation between the carbonic ice or clathrate melting temperature.

The results from heating studies for type I inclusions are shown in table 6.1. The plotting of the isochore of the type I CO₂ inclusions shows the highest temperature with the representation of low density (Fig. 6.1).

The type II CO₂-H₂O inclusions are characterised by visible amount of both CO₂ and H₂O in early formed granite phase. The H₂O : CO₂ ratio in

the inclusion varies between 60 : 40 to 80 : 20 volume percent which is indicated by the relative small size of CO₂ bubble at room temperature. They are subrounded in shape and their size varies from less than 8 to 25 micron in length and occurs usually as isolated primary and pseudosecondary trails. These CO₂-H₂O inclusions have tabular or negative crystal forms. The inclusions with bubbles occupying less than 40 percent of the cavity on which cooling tests were made, were shown to be of the CO₂-H₂O type (Plate XXVI Fig B). In cassiterite, the only CO₂-H₂O inclusions having the bubbles, which consist of CO₂ gas at room temperature, expand to fill the cavities at the filling temperature. The filling temperature measurements should represent more or less equal to the temperatures of formation of the cassiterite. These CO₂-H₂O inclusions contain a mixture of the two phases at the time of formation, which represent the H₂O rich member of the system.

The inclusions of type II were firstly cooled up to -100°C to solidified the CO₂ during freezing method. On slow heating the CO₂ as first liquid appeared in between temperature range of -57.6 to -56.5°C . This result represents that there was no other species present except CO₂ in the inclusion of type I. The clathrate melting temperature (T_{mC}) was recorded in between the range of $+5.1$ to $+7.1^{\circ}\text{C}$. The temperature of last melting of ice has not been measured because it will give over estimation of true salinity whereas clathrate melting temperature will give actual salinity as per the opinion of Collins (1979). The freezing experiment results indicate that salinity of the aqueous component of CO₂-H₂O inclusions varies between 5.4 to 8.2 wt percent NaCl equivalent. The data of the experiments (Table 6.2) suggested that the total homogenization of CO₂ into liquid phase mostly took place between $+5$ to $+16^{\circ}\text{C}$, whereas few inclusions of type II homogenized at the temperature of -1.2 as well as at $+17^{\circ}\text{C}$. The correct homogenization temperature on this estimate may be recorded in the order of 220 to 285°C for the fluid entrapment of inclusion type-II. The isochors plotting (show in Fig.) for the CO₂ density of type II CO₂-H₂O inclusions yield the value between 0.93 to 0.80 gm/cm³. In the CO₂-H₂O inclusion the "filling" is a matter

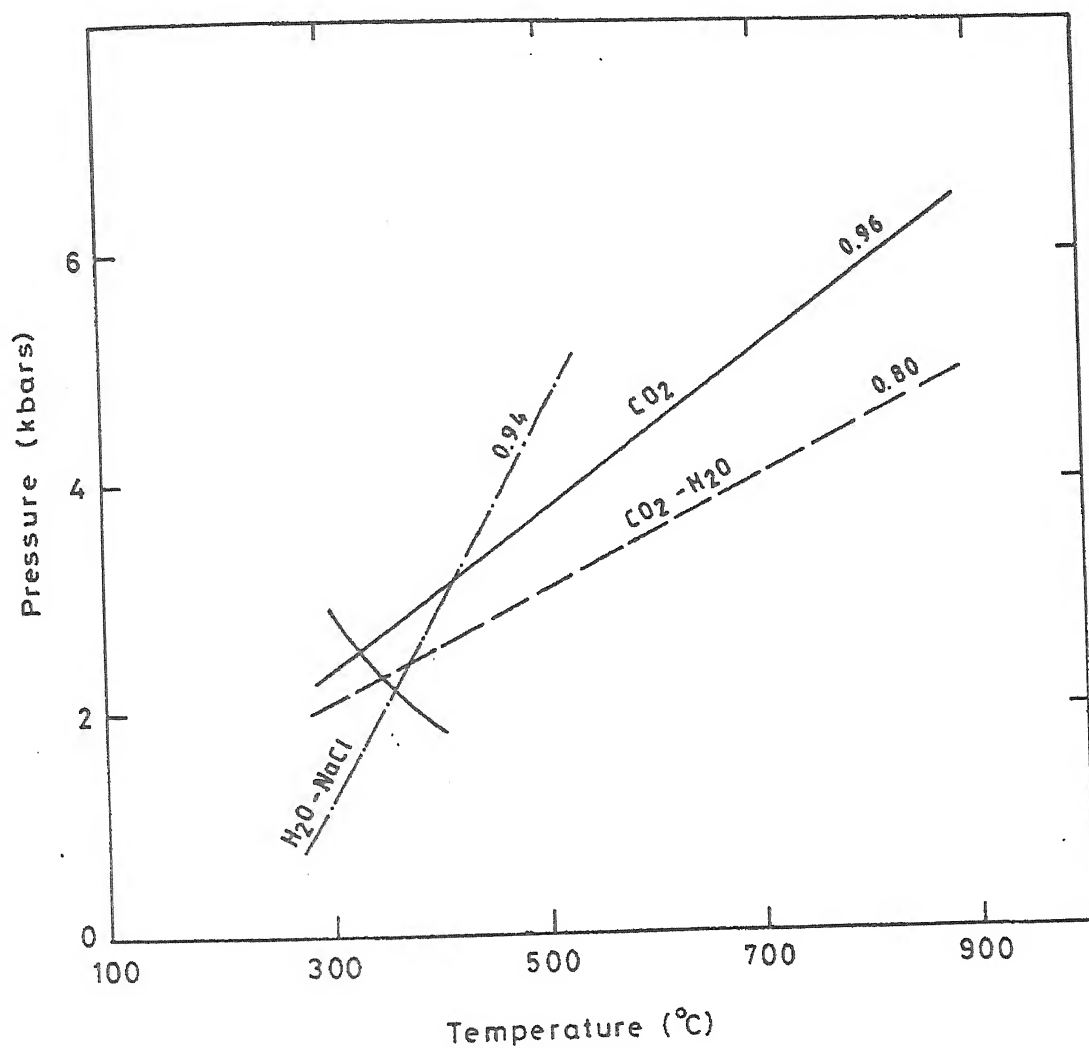


Fig. 6.1. Intersecting isochors for CO₂ and H₂O rich inclusion showing estimated P-T conditions for cassiterite associated with Katekalyan granitoids.

of mutual solubility in this two-component system. The detailed heating and freezing data noticed during the experiment are shown in table (6.2, 6.4).

Type III (H_2O -NaCl-Halite) inclusions are present as three phases shown in (Plate XXVI Fig. B). Their contents consist for the most part of crystalline material but relatively small bubbles. The volume of the liquid phases varies between 25 to 55 percent at 20°C by visual estimation. The outline of these inclusions is invariably regular to irregular in shape and size and is referred to as complex inclusions. Type III inclusions are characterized by ragged outlines in the cassiterite owing to dark colour of the cassiterite and the small size (< 5 to 10). The solid (halite) is dissolved into the aqueous liquid on heating of the type III inclusions. On further heating, the vapour disappeared and inclusions become homogenized into liquid phase in the temperature range of 160 to 360°C . It gives the salinity values in the range of 25 to 40 wt% equivalent NaCl. The freezing studies in type III inclusions were not possible, because liquid was present in very small amount.

The type IV (H_2O -NaCl) inclusions in cassiterite were freezed up to -100°C . After complete freezing of the inclusions, only solid ice crystal was observed. On heating, the ice crystals melted until last ice crystal melts at final ice melting temperature (T_{mI}) in between the temperature range of -8.6 to -1.6°C . The salinities of type IV inclusions was found between 2.63 to 12.4 equivalent weight percent NaCl with an average of 8.21 equivalent weight percent NaCl. The densities of the type IV inclusions vary between 0.94 to 0.98 gm/cm^3 with an average of 0.96 gm/cm^3 . The homogenization temperature for the fluid inclusion studies in cassiterite sample was observed from 115 to 220°C . The results from the heating-freezing studies for type IV in cassiterite are shown in table 6.3.

6.6. Conclusions

Based on the microthermometric observations summarized in table 6.4, it can be suggested that the entrapped fluids in cassiterite crystals were

magmatic to hydrothermal phases of low to high salinities (2.63 to 40 equivalent wt% NaCl) and were active over a temperature range of 115°C to 410°C. The different homogenization temperatures of fluid inclusions obtained in cassiterites indicate that the crystallization of cassiterite mainly initiated from the magmatic fluids within the temperature range of 360°C to 410°C at the pressure range of 2.4 to 3.1 Kbars i.e. 8 to 15Km depth (Fig6.1).

The heating and freezing study for many fluids reveal the mixing of low salinity magmatic with high salinity external fluids and was responsible for increasing salinities and contents of bivalent cations in the system with time (primary to pseudosecondary to halite bearing secondary). The fluid inclusion study suggests that magmatic nature of fluid was prevailed for a longer time followed by the hydrothermal process. The meteoric water (2.63 wt% NaCl equivalent) came into the picture. This is also evidenced by the decrease in salinity with lowering of temperature i.e. 40 wt% NaCl equivalent at 360°C to 2.63 wt% NaCl equivalent at 115°C at the last stage of fluid. The fluid inclusion study suggests that the progressive evolution of the hydrothermal system in the formation of tin deposit. The variable salinities (2.63 to 40 wt% NaCl equivalent) of the fluid inclusions in cassiterite from the Katekalyan tin deposit point that either two fluids of different salinities but approximately of similar composition co-existed during the main stage of ore deposition or may be related to metastability of halite in a single fluid. Roedder (1984) suggested that the gap of the salinity might be due to the halite metastability. This supports the existence of a single fluid with salinities varying from 2.63wt% to 40 wt% NaCl equivalent during the main stage of the ore deposition. On the other hand, the wide gap in salinity may be explained by of halite as metastable phase in single fluid composition process.

The fluids responsible for the tin mineralisation was probably the product of a devolatilisation of granite at depth. The most probable scene for the generation of the tin bearing fluids may be related to the fluids exsolved from the main mass of the granitic magmatic body when its upper parts was solidified and existing adjacent to the ore mineralisation. The similar opinion

also accorded by Kelly and Rye (1979) and Plimer (1987) for the granite related Sn-W deposits.

Granitic magma in system which later evolved into the pegmatite phase and finely crystallized as quartz veins with cassiterite. This magmatic fluid composition should possibly evolved from CO_2 -rich phase to the saline H_2O -rich during crystallization. The deduced concentration of CO_2 demonstrates that significant amounts of CO_2 was carried over by granitic magmas through the crust. Cassiterite associated with columbite and tantalite minerals are found as disseminated ore in the pegmatite of the Katekalyan area. The study reveals the orthomagmatic fluid is preserved as primary fluid inclusions in the core of cassiterite crystals at Katekalyan. These fluid inclusions have a composition of 2.63 wt% NaCl equivalent. The low salinity suggests that at vapour saturation, tin was partitioned in favour of the melt, which allowed cassiterite to initially crystallize directly from the melt. The regional geology of Dantewada reveals that tin-bearing pegmatite are intrusive into all other rocks except the newer dolerite. The Paliam granite, the last intrusive phase of acid magmatism may be consideration for tin mineralisation. The field and laboratory method suggest that granite magma would be the source for the hydrothermal fluid in system. Cassiterite deposition was also controlled by increasing oxygen fugacity ($f\text{O}_2$) and decompression, cooling in addition of volatiles & fluids phase contributed to mineralisation. It was commonly noted that the concentration of tin in the granitic melt increases with fractionation, and in subsequent stages melt locally saturated in cassiterite. LINNEN and WILLIAMS-JONES (1993) showed that saturation of the melt with vapour coincides with a high content of tin.

Prior to vapour saturation, pressure of the pegmatites probably decreased with cooling. Immediately after saturation of the pegmatite melt with vapour, pressure would have raised, making it more likely that the primary fluid inclusions in cassiterite were trapped at a pressure slightly higher than the emplacement pressure of the pegmatite. The occurrence of primary fluid inclusions in cassiterite suggests that orthomagmatic fluid co-

existed with melt and crystals (including cassiterite). The temperature and pressure determined by the density isochore intersection (Fig. 6.1) are, therefore, interpreted to represent the P-T conditions of disseminated cassiterite mineralisation.

The present fluid inclusion data provides an understanding of the circulation of mineralizing fluids from magmatic to hydrothermal within the fracture zones of the rocks. Based on the above study it can be said that, complete fluid evolution took place in the four stages. The first stage represented by magmatic is known as type I CO_2 inclusion characterized by monophasic carbonic fluid at room temperature and is primary in nature with low salinity. In the second stage of type II $\text{CO}_2\text{-H}_2\text{O}$, inclusions were identified by a double meniscus of an outer aqueous liquid, inner carbonic liquid and inner most carbonic vapour bubble of primary in nature with lower density in comparison to type I inclusions. The type III $\text{H}_2\text{O-NaCl-Halite}$ inclusions are characterized by saline aqueous fluids of three phase inclusions and occur with a salinity of 25 to 40 wt% NaCl equivalent without carbonic components. The fourth and final stage was characterized by the $\text{H}_2\text{O-NaCl}$ inclusions and homogenised at the temperature range of 115° to 220°C .

Tin formation is a result of the mixing of (dominant) magmatic fluid and meteoric fluid. Meteoric fluid equilibrated with igneous rocks under low water/rock ratio. Thus, it can be concluded that tin mineralisation in Katekalyan would be related to the low to high salinity (2.63 to 40 wt% NaCl equivalent) environment where CO_2 -rich complex fluids derived from the post-magmatic granitic melt at the temperature between 360° to 410°C and pressure ranges from 2.4 to 3.1 Kbars.

Table 6.1. Type-I CO₂ inclusions in cassiterite

T _h (°C) = -12.8°C Molar value = 44.106 Density = 0.998		T _h (°C) = -10.5 Molar value = 44.62 Density = 0.986		T _h (°C) = -8.4 Molar value = 45.12 Density = 0.97		T _h (°C) = -7.3 Molar value = 45.39 Density = 0.969		T _h (°C) = -6.8 Molar value = 45.52 Density = 0.96	
T (°C)	P (K.bars)	T (°C)	P (K.bars)	T (°C)	P (K.bars)	T (°C)	P (K.bars)	T (°C)	P (K.bars)
300	2.73	300	2.63	300	2.54	300	2.49	300	2.47
400	3.43	400	3.31	400	3.21	400	3.15	400	3.12
500	4.13	500	3.99	500	3.87	500	3.80	500	3.77
600	4.83	600	4.67	600	4.53	600	4.45	600	4.42
700	5.52	700	5.34	700	5.18	700	5.10	700	5.06
800	6.21	800	6.01	800	5.83	800	5.74	800	5.70
900	6.90	900	6.68	900	6.48	900	6.38	900	6.33
1000	7.50	1000	7.35	1000	7.13	1000	7.02	1000	6.97

Table 6.2. Type-II CO₂-H₂O inclusions in cassiterite.

Serial No.	1	2	3	4	5	6	7	8
T _h (°C)	-2°C	-1.2°C	+2°C	+5°C	+8°C	+11°C	+14°C	+17°C
Density of CO ₂	0.93	0.93	0.91	0.89	0.87	0.85	0.83	0.80
Bulk Density	0.96	0.95	0.94	0.92	0.91	0.89	0.86	0.84
T (°C)	P R E S S U R E (K.bars)							
300	3.5	3.4	3.17	2.89	2.71	2.4	2.1	2.1
400	4.2	4.12	3.84	3.50	3.30	3.004	2.6	2.5
500	6.3	5.18	4.82	4.40	4.16	3.77	3.3	3.1
600	6.5	6.32	5.90	5.30	5.06	4.60	4.08	3.8
700	7.7	7.48	6.48	6.32	6.004	5.42	4.8	4.5
800	8.9	8.65	8.06	7.30	6.92	6.26	5.5	5.2
900	10.1	9.81	9.14	8.27	7.86	7.09	6.2	6.6
1000	11.38	10.98	10.2	9.25	8.77	7.93	6.9	-

Table 6.3. Type-IV H₂O-NaCl inclusions in cassiterite.

T _m Ice (°C)	-8.6	-7.9	-7.4	-6.4	-5.4	-4.4	-2.4	-1.6
Salinity (wt% NaCl)	1.2.4	11.53	10.17	9.71	8.37	6.96	3.91	2.63
Density (gm/cm ³)	0.94	0.94	0.96	0.98	0.98	0.97	0.973	0.96
T _h (°C)	220	190	155	145	138	123	120	115
T (°C)	P R E S S U R E (K.bars)							
300	1.31	1.51	1.87	2.56	2.76	2.89	3.12	3.3
400	2.9	3.17	3.56	4.33	4.54	4.68	4.91	5.09
500	4.5	4.83	5.25	6.10	6.32	6.46	6.69	6.8
600	6.1	6.49	6.95	7.86	8.18	8.25	8.48	8.6
700	7.7	8.15	8.64	9.63	9.80	10.03	10.02	10.4

Table 6.4. Summary of microthermometric data of cassiterite.

Inclusion Type	Type-I CO ₂	Type-II CO ₂ -H ₂ O (H ₂ O-rich)	Type-III H ₂ O- NaCl-Halite	Type-IV H ₂ O-NaCl
Size (Micron)	< 10 to 15 (μ)	< 8 to 10 (μ)	< 5 to 10 (μ)	< 5 to 22 (μ)
Volume % of Aqueous like liquid phase at 20°C (Visual estimates)	< 5	60 to 80	25 to 55	80
T _h CO ₂ (°C)	-57.8 to - 56.2	-57.6 to - 56.5	-	-
T _h CO ₂ -liquid (°C)	-12.8 to 6.8	-2 to 17	-	-
T _m C (°C)	-	5.1 to 7.1	-	-
T _m I (°C)	-	-	-	-8.6 to -1.6
T _h (°C)	-	220 - 285	160-360	15-220

Abbreviations :

T_h = Temperature of homogenization.

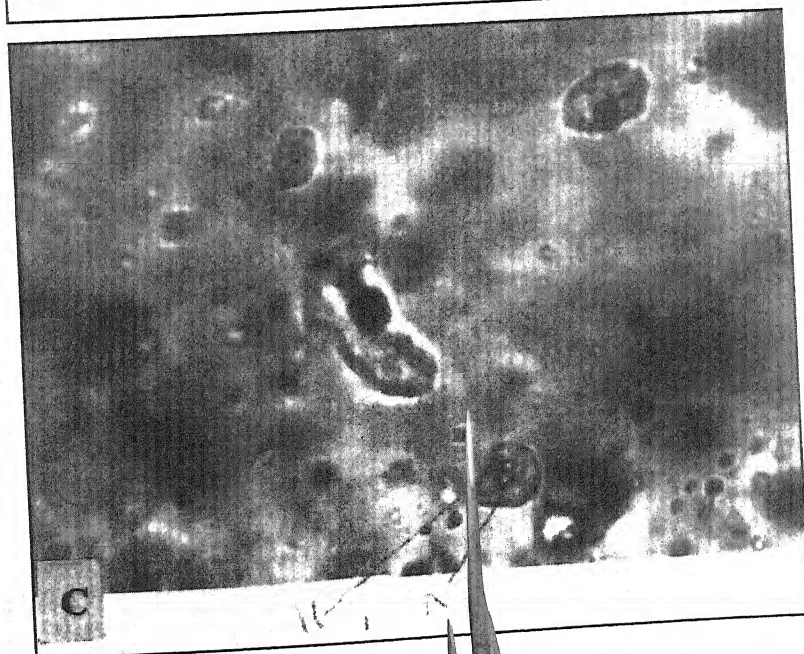
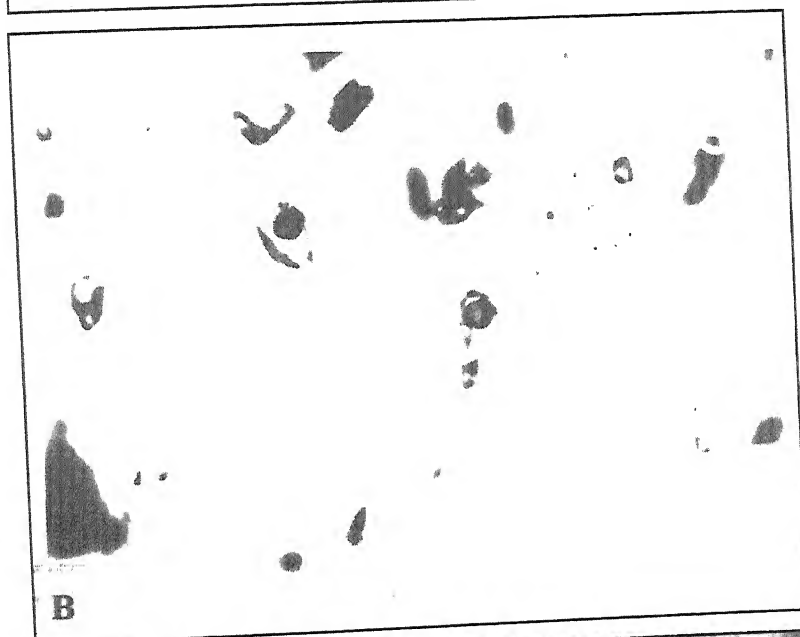
T_m C = Temperature of last melting (dissociation) of clathrate.

T_m I = Temperature of last melting of ice.

PLATE – XXVI

- Fig (A): Photomicrograph of Type-I (CO_2) primary fluid inclusion in cassiterite showing the presence of monophasic carbonic fluid.
- Fig (B): Photomicrograph of Type-II (CO_2 - H_2O) primary fluid inclusion in cassiterite showing the presence of double meniscus of CO_2 with rich aqueous H_2O .
- Fig (C): Photomicrograph of Type-III (H_2O - NaCl -Halite) and Type-IV (H_2O - NaCl) primary inclusions in cassiterite showing the presence of aqueous liquid and solid phase.

PLATE - XXVI



DISCUSSION

7.1. Introduction

In the foregoing chapters the author has recorded all his field observations and laboratory investigation results. The genesis of tin bearing granitoids (KG) except KHG as found in the area under investigation has received much attention in the background of all relevant data recorded in this work.

In the present investigations the author has made an attempt to provide a detailed geological and petrological accounts of the Katekalayan tin deposit, which may be of practical utility for searching new tin deposits associated with granitoids. At the end of this chapter the author has tried to find out some physical and geochemical parameters based an integral observation of Katekalyan granite (KG) and granite gneiss (KGG) and its relation with tin deposits to assess the nature of tin bearing granite plutons considering economic as well as academic importance.

7.2. Field evidences of tin mineralisation

The present area under investigation covers the southeastern part of the Southern Baster Craton of Dantewada district in Peninsular India (Fig.2.4). The lithology of the area is dominated mainly by andalusite sericite schist (ASS), quartz-sericite schist (QSS), banded magnetite quartzite (BMQ), grunerite-magnetite quartzite (GMQ), metabasic extrusive (MBE), metabasic intrusive (MBI), granite (KG) and basement granite gneiss (KGG).

On the basis of mode of occurrence, mineral assemblage and their mineralising characteristics, three types of pegmatites viz; simple unzonal pegmatites, recrystallised granite pegmatites and metasomatic pegmatites have been recognised and summarised in table 7.1. These pegmatites are characterised by graphic, non-greisenised, greisenised, and albitic in nature,

which are mainly emplaced into the metabasic intrusive, granites (KG), granites gneiss (KGG) and rarely metasediments with different trends and dimensions.

Pegmatites are generally 10m to 100m long but rarely exceed 100m, with width varying from less than 1 meter to 10 meters, trending mainly along NNW-SSE, N-S and NE-SW directions with steep northeasterly and easterly dips. Since, pegmatites are found extending in all directions, hence there is a general preference to NW-SE trend. Pinching, swelling, extending laterally and vertically and even sub-horizontal pegmatites are common.

From the field studies and petrographic observations to conclude that the granite-pegmatitic activity have lead to the formation of tin and associated rare metal mineralisation. The pegmatites are mainly composed of quartz, feldspars (albite, microcline, orthoclase), lithium mica, garnet, beryl, fluorite, cassiterite and columbite-tantalite. Cassiterite crystals are irregularly disseminated through the pegmatites bodies and also contain considerable columbite-tantalite minerals. The pegmatite bodies (metasomatic) emplaced into the metabasic intrusives (amphibolites/metagabbro compositions) of highly mineralising nature and also in the granite (KBG) and granite gneiss (KGG) and rarely mineralised (unzoned simple pegmatite) in metasediments. It suggested that the emplacement of these highly mineralised pegmatitic bodies are mainly found due to the availability of the joints and fracture planes in metabasic intrusives (MBI), granite (KBG) and granite gneiss (KGG) than the impermeable schistose rocks. For the first time, cassiterite-bearing pegmatites emplaced in the granite at Kondaras Dongri and Benglur areas (Babu, 1983) of the Katekalyan have been reported.

7.3. Petrographical mineral assemblages of granite gneiss (KGG), granite (KG) and its relationships with pegmatites (KP)

7.3.1. Granite gneiss (KGG)

This rock represent the gneissic foliation planes along which quartzo-feldspathic mass showing more or less preferred orientation with alternate micaceous bands. In biotite rich variety of KGG, where the mica

which are mainly emplaced into the metabasic intrusive, granites (KG), granites gneiss (KGG) and rarely metasediments with different trends and dimensions.

Pegmatites are generally 10m to 100m long but rarely exceed 100m, with width varying from less than 1 meter to 10 meters, trending mainly along NNW-SSE, N-S and NE-SW directions with steep northeasterly and easterly dips. Since, pegmatites are found extending in all directions, hence there is a general preference to NW-SE trend. Pinching, swelling, extending laterally and vertically and even sub-horizontal pegmatites are common.

From the field studies and petrographic observations to conclude that the granite-pegmatitic activity have lead to the formation of tin and associated rare metal mineralisation. The pegmatites are mainly composed of quartz, feldspars (albite, microcline, orthoclase), lithium mica, garnet, beryl, fluorite, cassiterite and columbite-tantalite. Cassiterite crystals are irregularly disseminated through the pegmatites bodies and also contain considerable columbite-tantalite minerals. The pegmatite bodies (metasomatic) emplaced into the metabasic intrusives (amphibolites/metagabbro compositions) of highly mineralising nature and also in the granite (KBG) and granite gneiss (KGG) and rarely mineralised (unzone simple pegmatite) in metasediments. It suggested that the emplacement of these highly mineralised pegmatitic bodies are mainly found due to the availability of the joints and fracture planes in metabasic intrusives (MBI), granite (KBG) and granite gneiss (KGG) than the impermeable schistose rocks. For the first time, cassiterite-bearing pegmatites emplaced in the granite at Kondaras Dongri and Benglur areas (Babu, 1983) of the Katekalyan have been reported.

7.3. Petrogrphical mineral assemblages of granite gneiss (KGG), granite (KG) and its relationships with pegmatites (KP)

7.3.1. Granite gneiss (KGG)

This rock represent the gneissic foliation planes along which quartzo-feldspathic mass showing more or less preferred orientation with alternate micaceous bands. In biotite rich variety of KGG, where the mica

bands are observed in continuous as waning and waxing patterns along the direction of foliation planes and the quartzo-feldspathic portions form small lenticular patches along this planes. At some places, granite gneiss (KGG) shows the development of linear and straight alternate banding of leucocratic and melanocratic minerals as lit- par- lit relation pattern in nature (plate VI, Fig. A). The recrystallised unzoned pegmatite (granite pegmatite) veins consisting of quartz and feldspar (non-graphic) are cut across the gneissic foliation at an angle confirming later origin and shows poorly mineralising characters.

So far as the mineral constituents of these granite-gneisses (KGG) are concerned, the following essential minerals viz., microcline, micro perthite, orthoclase (also sericitised), plagioclase and quartz have been recorded. The accessory minerals (biotite, muscovite, sphene and apatite) and also secondary minerals (sericite, epidote, chlorite and opaques) are found in this rock (Plate XII, Fig. A, B & C). Among the feldspars, the most dominant mineral is microcline perthite. This perthite shows intergrowth of thin lamellae of albite in the groundmass of microcline. The initial stage of replacement of microcline-perthite by sodic feldspars is marked by the fine cracks developed in the former (plate XVII, Fig. A).

The alteration products such as sericite and chlorite are derived from the breakdown of feldspars and biotite. Often such alteration brought about through the agency of volatiles and hydrothermal solutions.

7.3.2. Granite (KG) and its varieties

The Katekalyan granite (KG) is represented by biotite granite (KBG), tourmaline granite (KTG) and hornblende granite (KHG) of the non-foliated in nature. These varieties of granite show medium to coarse-grained and leucocratic characters. However, at places, fine-grained variety of KBG, appears aplitic in character. But the porphyritic texture is however shown by quartz and feldspars (Plate XIII, Fig. D). These phenocrysts appear to be formed prior to the quartzo-feldspathic constituents of the granite. Subsequently these phenocrysts might have introduced along the contact of

the biotite granite (KBG) and have attained the large size with subsequent pegmatitic emplacement. At the contact of granite and pegmatite, highly crushed, fine-grained quartzo-feldspathic mass is accompanied with tiny greenish biotite crystals often associated with cassiterite. Such greenish variety of biotite in KBG is indicative of pneumatolytic action. Feldspar in KBG is represented by orthoclase, microcline and plagioclase. These feldspars show intense alteration to sericite. The orthoclase feldspars are altered into sericite to some extent. The sodic intergrowth within microcline (Plate XV, Fig. B) might have also subsequently undergone alteration through the process of metasomatism. In plagioclase feldspars, the saussuritisation phenomenon is quite predominant, responsible for the formation of epidote.

The albitic twin lamellae show distinct zoning, tapering and bundle shaped (plate XV, Fig. C) and others are present as bent (plate XV, Fig. D) with the development of minute microcline grain also. The fine albite lamellae are observed as microfaulted and also hair perthite texture (Plate XVIII, Fig. D).

Quartz grains show crushing appearing at places and give rise to the formation of different grain sizes varying from very fine-grains to megacrysts. These megacrysts show undulose extinction (Plate XIV, Fig. B) due to strain effect. At the contact of granite (KBG) and pegmatite (KP), phenocrysts of quartz contains many tiny inclusions of other minerals namely biotite, apatite, zircon and dot-like inclusions of opaque. In the vicinity of the mineralisation, biotite is found to be distinctly of brownish green colour, which undergoing alteration give rise to dark green chlorite and muscovite particularly at margin of the biotite grains (Plate XVII, Fig. B, C). It is observed that the cassiterite grains are intimately associated with these altering and fractured rounded grains of brownish green biotite (plate XVII, Fig. B). Often, sphene has been also developed as subhedral to anhedral grains with very dark margins and it's associated with altered brownish green biotite (Plate XVII, Fig. A) in the hornblende granite (KHG). In this granite, hornblende is changed into biotite along the periphery (plate XVIII, Fig. B). Apatite is occurring as inclusions within quartz, feldspars, mica and hornblende (plate

XVIII, Fig. B, C). Abundant apatite proves the presence of phosphorous saturated volatile phase at the time of felsic magmatism emplacement. Zircon is mostly observed as inclusions within the nucleus of the pleochroic halos in hornblende granite (KHG) and also bleached portion of the prismatic flakes of biotite.

In the study area, tourmaline (greenish variety) is rarely found in KTG but clustered into radiating needles like appearance ("tourmaline Sun"). These needles of tourmaline on an intensive scale are suggestive of sustained pneumatolytic action through the introduction of boron.

Sericite is abundantly found as secondary minerals noted in granites (KBG, KTG and KHG). The intense alterations of the potash feldspars occur along the albite lamellae through the process of the sericitisation tiny, flaky grains. It may be recorded that extensive activity of the volatiles during the late magmatic stage was mainly responsible for the widespread alteration of the feldspar. Epidote is found to be usually an aggregate of anhedral grains occurring randomly in quartz, hornblende and altered plagioclase feldspars (plate XVIII, Fig. A, C). Hence, it appears that the formation of epidote has been pronounced by the breakdown of the plagioclase feldspars, which has supplied the required calcium (Ca) and Aluminum (Al) during the course of fluid activity. By the activity of the hydrothermal fluids in the biotite to developed the chlorite patches as dirty greenish to brownish in colour with weakly pleochroic in nature. Opaque minerals (magnetite and ilmenite) are observed as patchy, irregular masses or rarely as subhedral crystals in these granitic rocks. It is also found as inclusions in quartz, feldspars, biotite and hornblende minerals.

7.3.3. Pegmatite phase and its parents

In the study area, three types of pegmatite (KP) viz; simple unzoned, recrystallised and metasomatic pegmatites are found emplaced within the granite gneiss (KGG), granite (KG), metabasic intrusive (MBI) and also rarely metasediments as mineralised and non-mineralised characters. The examination of mineralised pegmatite veins reveals that it is varying widely in

grain size (coarse-to very-coarse grained) from one specimen to another. Large crystal of different minerals like quartz, feldspar, mica, beryl, garnet, fluorite and cassiterite are observed. At some places, crude graphic texture (Plate VII, Fig. D) is noticeable in pegmatites, where quartz and feldspars are intergrowth, having step-like relation shown by both the minerals.

From the microscopic observations, feldspar is dominant mineral in pegmatites and is found as microcline, microcline perthite, and orthoclase and then followed by albite- oligoclase and cleavelandite. The microcline grains are showing typical two sets of lamellar twinning on albite and pericline laws giving as cross hatched (plate XIX, Fig. C) characteristic. It is very interesting to note that the sericitisation has taken place along the cross hatched lamellae of the microcline. Orthoclase is present in large rectangular crystals showing common simple twinning on carlsbad law. This orthoclase has altered to sericite and is also being replaced by lithium mica in and around the margins. It is also noted that the original orthoclase has been changed into albite and cleavelandite variety (plate XX, Fig. A and B). These cleavelandite varieties are believed to have been formed due to metasomatic activity of sodium (Na) bearing vapours during or after the emplacement of the pegmatites. Due to fracturing in cleavelandite, its lamellae are not only micro-faulted but they become non- continuous and slightly bends.

Quartz of varying sizes encloses the minerals muscovite, feldspar, garnet and dust of the opaque as inclusions, which confirm that the quartz is the last mineral in the crystallising sequence of pegmatites. At places, myrmekitic texture (plate XX, Fig. B) is developed by the intergrowth with plagioclase and vermicular quartz.

Mica is another important and dominant constituent and is represented mainly by muscovite, lepidolite and biotite in the forms of books and also as small flakes associated with other minerals in the pegmatites. Primary muscovite occurs in the thick tabular crystals but the secondary muscovite is appears due to the alteration product of feldspars. Lepidolite (plate XX, Fig. C) appears to be micro-folded and usually show inclusions of cassiterite and other tiny opaque minerals. The presence of lithium mica

within the fracture of cassiterite indicates that while its crystallisation, the deformational forces were also acting upon them. During the regime of vapour stage, lepidolite got deposited within such irregular cracks and fissures.

The other mica like biotite shows variable colours and it subjected to alteration gave rise to muscovite and also limonitic secondary materials (plate XX, Fig. D). Sphene is found in a number of small aggregate grains in and around the mica flakes. In the greisenised pegmatites, fluorite shows patchy occurrence of bluish colour and sometimes, it is present as veins within fractured cleavelandite variety of albite (plate XXI, Fig. D).

From the above observations, it concluded that the pegmatites are related to diverse factos of metasomatic alterations like microclinisation (potash metasomatism), albitisation (soda-metasomatism), greisenisation (pneumatolysis) and also hydrothermal activity leading to the enrichment of tin content. It is of also recorded that the mineralisation event in an individual pegmatite is non-uniform and erratic in distribution, possibly due to combination of above two or more processes involve.

7.4. Fluid-rock interactions

To study the nature and intensities of mineralogical changes in the granitic rocks by the metasomatic processes (volatile rich fluids), it reflects the successive phases of volatile rich hydrothermal fluids, derived from the parent magma, had interacted with the host rocks. The presence of pegmatites of the different phase in the study area reflects the volatile and aqueous rich phase co-existing with residual granitic magma. The continued fractional crystallisation causes enrichment in volatiles and incompatible elements in the last rest melt. The efficiency of enrichment of incompatible elements is critically dependent on the degree of separation of melt from solids throughout crystallisation.

When the vapour pressure rises during the late stage of cooling of the parent magma and it results into fracturing in the plutons and emplacement of the residual melt produced in the different successive phases of the magmatic evolution. These volatile rich aqueous fluids resulted into the

emplacement of pegmatites and quartz veins, which existed during the last stage of cooling of the parent magma migrated towards the margins of plutons and caused greisenisation. At the contact zone contains abnormally high silica and feldspar as a result of silicification and feldspathisation.

7.5. Mineralogical evidences of boron and fluorine activity

Tourmaline occurs as patches of needle forms within the granite, which reflects that boron was enriched in the late stage of parent magmatic evolutionary phases. Boron and water bearing granitic magma raised solubility of water with the increasing content of boron. The presence of fluorite in mineralised pegmatites, also supported the fluorine rich magma source of granitic composition which reflects that differentiation processes was involved for the segregation of above minerals.

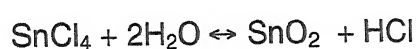
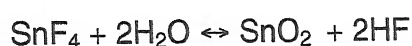
7.6. Vapor phase separation from granitic magma and its role in Sn-mineralisation

Tin-poor vapor may separate after initial water saturation of the magma is achieved, and this collects under the roof, commonly forming an impermeable barrier to later tin-bearing fluids. Continue fractional crystallisation on the floor further enriches incompatible elements, and at a very late stage, an Sn-rich vapor separates within the intercumulus phase and becomes concentrated by progressive crystallisation of the intercumulus melts. At a late stage of solidification, this vapour losses equilibrium with the earlier formed feldspars and greisenisation ensues, accompanied by the crystallisation of cassiterite and other associated ore minerals. This predicts the changes in trace element geochemistry with crystallization, which provide useful tools for assessing the tin-potential of a granitoid.

Variation in pegmatite geochemistry and mineralogy due to heterogeneity in fluid, space and time, it is not possible to individually discuss the detail tin transport mechanism in all the fluids of diverse origin. Probably, therefore, it is more meaningful to discuss the current status of knowledge regarding possible modes of tin transport and evaluate these against the

geological evidence including the fluid inclusion data. Thus, transport of tin can be described with reference to two major fluids like the gas phase and the aqueous phase.

On the basis of the association of cassiterite, lepidolite (mica) and fluorite in the pegmatites it may be possible that the tin was transported in the gaseous stage as SnF_4 or SnCl_4 and precipitated with the addition of water mainly in the condition of aqueous volatile solutions:



By this above method, the fluid SnF_4 and SnCl_4 can move in vapour phase to apical regions of intrusive where they reacted with wall rocks and are hydrolysed to give cassiterite. These mechanism is also favoured by Daubree (1841) with experimental studies and has got the association of cassiterite with other minerals contain fluorine and chloride in fluid inclusions. It is interesting to noting that the SnF_4 and SnCl_4 probably not stable in presence of water under geologically reasonable conditions.

In the aqueous phases, Baruskov (1964) has suggested that tin as a salt of complex hexa-basic acid type of $[\text{NaSn}(\text{F}, \text{OH})_6]$ breaks down in a neutral or slightly alkaline medium at pH value 7.0 to 7.5 at which $\text{Sn}(\text{OH})_4$ is precipitated and further disintegration of $\text{Sn}(\text{OH})_4$ to yields cassiterite (SnO_2). Thus the formation of cassiterite mineral in the granite (KBG) and pegmatite (KP) of the area is mainly connected with the metasomatic replacement processes which are recrystallised by hot gaseous, aqueous mineralised solutions that are chemically not in equilibrium with primary pegmatitic materials.

In spite of the suggestion by many authors that tin occurs in alumino-silicate melts of granitic composition as Sn (IV) either as free Sn^{4+} or as stannic-alumino-silicate complexes (Rankama & Sahama, 1950; Stemprok, 1969; Hesp and Rigby, 1972) depending upon either the behavior of tin in such melts or its partitioning into an associated aqueous-rich phase. If tin is indeed present in melt system as Sn (IV) then, if transport in the aqueous phase is to be as Sn (II), the partitioning must be dependent upon the oxygen

fugacity. The highest tin concentrations in the aqueous phase would thus occur at the lowest oxygen fugacities. At higher oxygen fugacities, tin as Sn (IV) would partition into the melt phase and may become relatively enriched in mineral phases such as biotite, where high tin contents may correlate with high $\text{Fe}^{3+}/\text{Fe}^{2+} + \text{Mg}^{2+}$ ratios (Durasova, 1967). Once tin is involved directly in the processes of magmatic crystallisation then any variable such as partial pressure of CO_2 , Cl, F and H_2O fugacities affecting the crystallisation of the solid phases and it will profoundly influence the partitioning of tin into different phases.

Based on the above conceptual views, it can be said that the nature of the ore fluids in the Katekalyan area were initially alkaline and became weakly acidic at the last, forming tin ore under the favourable physico-chemical condition.

Tin in granites is normally concentrated in the biotite. Therefore, biotite granite (KBG) should be given more attention for tin exploration. The content of tin in micas of the pegmatites is also important for the search of tin mineralisation. Since tin mineralisation is essentially in the last phase of granitic process and magmatic evolution, the mineral get concentrated in domel parts (apical) particularly in the margins of the granite masses where fissuring is more pronounced.

7.7. Evidences from fluid inclusion study

Fluid inclusion evidences in the cassiterite reveals the presence of monophasic carbonic (CO_2 inclusion), aqueous-carbonic biphasic ($\text{CO}_2\text{-H}_2\text{O}$), triphasic ($\text{H}_2\text{O-NaCl-halite}$) and $\text{H}_2\text{O-NaCl}$ biphasic inclusions. Three types of significant inclusion in cassiterite are exceedingly valuable and supply genetic physico-chemical conditions about the mineralising parent fluids.

The fluid inclusion studies suggest that the mineralising hydrothermal fluids in cassiterite of the study area were complex with low to high salinities 2.63 to 40 equivalent wt % NaCl) and were active over a temperature range of 115° to 360°C . The continue increases in salinitic and decreases temperatures of the fluid with time supports the magmatic nature of

the ore fluids. The different homogenisation temperature of fluid inclusions in cassiterite indicate the crystallisation of cassiterite from the fluids within the temperature range of 360° to 410°C at the pressure range of 2.4 to 3.1 Kbars. This estimated pressure range corresponds to 8 to 15 Kms, assuming a purely lithospheric regime based on intersection of density inclusions isochores.

There are several lines of evidence point to mixing between low salinity magmatic and high salinity external fluids. This magmatic nature of fluid was prevailed for a longer time and at the end of the hydrothermal process come into the picture. The fluid inclusion study suggest that the progressive evolution of the hydrothermal fluids which helped in the formation of tin deposit. The variable salinities of the fluid in cassiterite ranges from 2.63 to 40 wt % (NaCl equivalent) of the study area is suggested that the two fluids of different salinities but approximately having same composition co-existed during the main stage of the ore deposition. But Roedder (1984) suggested that the gap of the salinity may be due to the halite metastability.

The most probably scene for the generation of tin bearing fluids that it may be exsolved from the main mass of the granitic magmatic body, when its upper parts were already solidified. Silmilar opinions are also accorded by Kelly and Rye (1979) and Plimer (1987) for the granite related Sn-W deposits.

The orthomagmatic fluid is preserved as primary fluid inclusions in cores cassiterite crystals that have high tin concentrations. These fluid inclusions have a composition of 2.63 wt% NaCl equivalent. The low salinity suggests that at vapour saturation, tin was partitioned in favour of the melt, which allowed cassiterite to initially crystallise directly from the melt. Cassiterite deposition was controlled probably by increasing oxygen fugacity (f_{O_2}) and also decompression, cooling and addition of volatiles may have contributed to mineralisation. It is noted that the high concentration of tin in the granitic melt increased with fractionation and that the later stage, the melt was locally saturated with vapour (Linnen and Williams-Jones, 1993). Prior to vapour saturation, pressure of the pegmatites probably decreased with cooling. Immediately after saturation of the pegmatite melts with vapour,

pressure would increase making likely that the primary fluid inclusions in cassiterite trapped at a slightly lower pressure than the emplacement pressure of the pegmatites. The occurrence of these primary fluid inclusions in cassiterite suggests the orthomagmatic fluid co-existed with melt and cassiterite crystals.

During magmatic crystallisation, tin probably exists as Sn^{4+} or in the form of complexes and as such may isomorphously substitute for Fe^{3+} , Mg^{2+} and Li^+ in minerals including biotite (Hesp, 1975) or may have accumulated in the residual silicate melt. Nedaskovskii and Narnov (1968) demonstrated that crystallisation proceeded from lower to upper crustal levels. At upper crustal level, the more silicic rocks containing less biotite and hornblende, which are located in the apical parts of the younger intrusives. At lower levels, tin was isomorphously present in biotite and hornblende whereas in the upper (higher) levels, it was present as accessory cassiterite.

From the above laboratory work with different author's views, content of tin in granites is normally concentrated in the biotite. Therefore, biotite granite (KBG) of the study area should be given more attention for tin exploration. The content of tin in micas to pegmatites in Katekalyan is also important. Because, pegmatites showing pneumatolytic and hydrothermal effects with the presence of fluorite and albite which are indicate the more promising to search for tin-mineralisation. Since tin mineralisation is essentially in the last phase of granitic process and magmatic evolution, the mineral get concentrated in the apical parts of the granite plutons particularly in the margins where fissuring is more pronounced.

7.8. Evidences from wall-rock alteration

The kind and degree of wall-rock alteration is an important guide to tin mineralisation. Different alteration zones associated with tin mineralisation have been delineated based on field evidences, petrographic and geochemical studies of the granites and pegmatites. The influence of different zones with the changes of mineralogical and petrochemical variants shows different alteration activities. The hydrothermal fluids associated with tin

deposition which frequently react with the enclosing rocks to produces different wall-rock alteration zones are observed namely microclinisation, albitisation, biotitisation, muscovitisation, greisenisation, sericitisation, fluoritisation and silicification.

Feldspathisation takes from of microclinisation or albitisation. Normally it is seen that the feldspathisation predates greisenisation and is less influenced by fracture or fissure controls. Microclinisation usually predates albitisation and in some places, there is evidence to support additional feldspathisation following greisenisation. Albitisation seems more frequent than microclinisation and may be accompanied by lithium enrichment. The phenomenon of albite enrichment is occasionally accompanied by the presence of disseminated cassiterite \pm columbite/tantalite. Greisenisation is manifested by the decomposition of feldspars and biotite and produces the different minerals, such as quartz, mica and cassiterite (\pm columbite/tantalite) in the mantle of the granitic and pegmatitic rocks. Geochemically, the import of OH, F, Li, Sn, W, B and the removal of alkalines (especially Na, less pronounced K) are the most significant, while Si, Al remain essentially constant (Janecka and Stenprok; 1967).

Barsukov (1957) has suggested that a process of albitisation by alkali-Na rich hydrothermal solutions would also result in muscovitisation of biotite. The high tin contents within crystal lattice of biotite could theoretically be displaced enters into the hydrothermal solution and migrateto other parts before precipitating. It suggest the decomposition of quartz-cassiterite type in the pegmatites resulted from the processes of albitisation and muscovitisation of stanniferous granite. Both the albitisation and muscovitisation processes were sucessfully utilising the solutions containing chloride sodium and potassium with the addition of sodium silicates and fluorine.

In this way, the apical zones of many tin-bearing granitoids are areas of intense and complex metasomatic activity. In the area under study mainly northern part, the alteration zones occur on a local scale.

Table 7.1: *Different types of pegmatite and their mineralizing characteristics*

S. No.	Types of Pegmatite	Locality and Trend	Host Rocks	Mineralogy	Remarks
1	Simple Un-zoned pegmatite	Gatam NW-SE	A.S.S	Qz, microcline, plagioclase, muscovite, garnet	Non-greisenised, graphic intergrowth, no mineralisation (rarely).
2	Recrystallised Unzoned Pegmatite (Granitic Pegmatite)	Benglur, Kondars-Dongri, Lakharas, Tumakpal, Naynar NW-SE N-S, NE-SW	KBG and KGG	Qz, feldspar, rich mica at fringe, cassiterite, columbite-tantalite	No graphic intergrowth poorly mineralized.
3	Metasomatic Pegmatite (a) Greisenised Pegmatite	Kondaras-Dongri, Lakharas, Tumakpal, Naynar NW-SE, N-S, NNE-SSW	M.B.I. and KBG	Qz, and mica intercalations with, lepidolite, cassiterite, columbite-tantalite fluorite, beryl	Dimension of the pegmatites varies from 1 to 3m wide and 25 to 100m lengths, highly mineralized.
	(b) Albitised Pegmatite	Lakharas area to the north of the Katekalyan block NNW-SSE, NE-SW	M.B.I. and KBG	Monomineralic nature, predominantly feldspathic mainly albite or cleavelandite variety with qz and lithium mica, rich cassiterite, minor columbite-tantalite, beryl, fluorite and apatite	Highly mineralized.

7.9. Geochemical affinity for the tin-bearing granitoids

In order to understand the association of tin \pm tungsten deposits related with the granitic rocks in the upper parts of the crust, it is necessary to examine the distribution characteristics and geochemical behavior of tin and related to other rare elements, which often accompany such deposits. An examination of the table 7.2 will help in understanding this.

Table 7.2. Ionic radii and valencies of certain elements relevant to the geochemistry of tin (After Hosking, 1965a)

Sn ⁴⁺ 0.73	W ⁶⁺ 0.67	Nb ⁵⁺ 0.70	Ta ⁵⁺ 0.68	Bi ⁶⁺ 0.74	Mo ⁴⁺ 0.67
	Na ¹⁺ 0.98	K ¹⁺ 1.33	Ca ²⁺ 1.01	Al ³⁺ 0.57	
		Fe ²⁺ 0.79	Mg ²⁺ 0.75		
			Si ⁴⁺ 0.41		

From the above table (7.2), it may be seen that the ionic radius of Sn and those of W, Nb, Ta, Bi, Mo are varying within the difference of 15% and as such they have an affinity to occur together whenever the melt contains them and crystallizes under favorable conditions. One can also observe the significant difference in the ionic radius of tin and those of Na, K, Ca, Al and Si. As much tin should not have an affinity to go along with minerals of these elements. But in nature we find that tin is usually concentrated in acid igneous rocks in which quartz, feldspars, etc., dominate, which are constituted by Na, K, Al, Ca, Si etc. Further, it is clear that Fe²⁺ and Mg²⁺ have ionic radii, which are very near to that of tin, and as such it is quite likely that the metal will be concentrated in ferromagnesian minerals. But the common observation is that in rocks rich in ferromagnesian minerals, that is, in basic and ultrabasic rocks where tin deposits are not found. In general, the minerals of early crystallisation of magma, tin is absorbed as dispersed phase by the replacement of Fe and Mg ions and when magmatic differentiation proceeds with gradual conversion of olivine to pyroxene, pyroxene to amphibole, amphibole to biotite and so on, tin gets released from the ferromagnesian minerals. Thus it becomes more and more concentrated in

end members (rocks) of magmatic differentiation. Thus in rocks having granodioritic to granitic composition, the metal along with its usual associates comes out as separate phase.

The geochemical character of biotite granites (KBG) of the Katekalyan indicates the increase in silica and potash and appreciable decrease in ferromagnesian constituents especially MgO , CaO , Fe_2O_3 and TiO_2 . The concentration of tin appears to have taken place at an optimum proportion of 72.5% SiO_2 , 5% K_2O and 3% Na_2O . From the tin field granitoids of the world, when plotted in ternary diagram (Fig.4.7) it shows the more than 80% SiO_2 , the combined ferromagnesium constituent are less than 4% and alkalis around 8% (Babu, 1993). Besides these, when compared to normal granites, the appreciable enrichment of trace elements especially B, F, Li, Rb and Be and depletion of Cr, Ni, Co and V are significant characteristics of tin fertile granites.

7.9.1. Major element geochemistry

Twenty-five representative samples of KGG ($N = 7$), KG ($N = 11$) and pegmatite ($N = 7$) from the Katekalyan area were analysed [Table 4.1a,b, d] by X-ray Fluorescence Spectrometer Philips Exam Six and PV 9100 at *Wadia Institute of Himalayan Geology, Dehradun*.

Na_2O vs K_2O weight percentage diagram (Fig. 4.1) for the Katekalyan granites (KG) and gneisses (KGG) were plotted, where majority of the samples fall in the field of granite, but few of them (KGG) are in the adamellite to granodioritic fields. On the basis of Q-A-P ternary Streckeisen's diagram (Fig. 4.3) and R_1 - R_2 multicaticonic classificatory diagram (Fig. 4.4) after De La Roche *et al.* (1980), the hornblende granite (KHG) plots in the tonalite field due to poor content of potassium in it.

According to the data on tin-bearing granites and pegmatites of Kazakhstan and Erzjebirdge studied by Greig-Stemprok (1969) through ternary diagram (Fig.4.6) of silica (SiO_2), ferro-calc-magnesium ($\text{FeO}_T + \text{MgO} + \text{CaO}$) and alkalis ($\text{Al}_2\text{O}_3 + \text{Na}_2\text{O} + \text{K}_2\text{O}$), the "tin compositional zone" is

indicative of moderately higher silica, alumina and alkalis content with marked depletion of ferro-calc-magnesium constituents. Almost all tin-bearing granitoids (KG and KGG) and pegmatites (KP) of the Katekalyan area fall within this ternary tin zone. However, a few of the tin-bearing granitoids are represent the excess of FeO and CaO, perhaps due to digested mafic xenoliths, fall outside the tin zone (Fig. 4.6).

The chemical-mineralogical based on multicationic parameters (major elements) delineated by Debon and Le-Fort (1982) define the peraluminous and metaluminous characters depending on its positive and negative values respectively. This A-B plot (Fig. 4.8a) reflects the nature and proportions of their characteristics minerals other than quartz and feldspars. The A-B diagram [where $A = Al - (K + Na + 2Ca)$ and $B = (Fe + Mg + Ti)$] shows clearly that all the Katekalyan granite (KG) and gneiss (KGG) have occupy the delineated I and II fields of the peraluminous domain. This indicate that they belong to the association of muscovite > biotite and biotite > muscovite respectively.

Solubility of tin in melts

Naski and Hess (1985) demonstrating that the influence of the alkali concentration (and temperature) of the solubility of SnO_2 in melts are less apparent in peraluminous magmas. However, changes in the dominant alkali component of peraluminous melts (from Na in albite-quartz melts to K in K-feldspar quartz melts) can be responsible for significant variations in the solubility of SnO_2 in the melts. Since the solubility of SnO_2 in albite-quartz melts increases far more rapidly with decreasing fO_2 than in K-feldspar-quartz (or haplogranite) melts. It is clear that the incorporation of Sn^{2+} into melts is more strongly influenced by the presence of Na than K.

The high molar A/CNK i.e., $Al_2O_3 / (CaO + Na_2O + K_2O)$ ratio of the analysed granite (KG) and gneiss (KGG) samples are plotted against SiO_2 (Fig. 4.8b).

The most of the samples fall in the field of peraluminous composition having molar A/CNK ratio more than 1.1, which suggest that the granitoids though igneous in origin but have crustal components (Chappel and White, 1974). Presence of normative corundum and high molar concentration ($Al/(Ca+Na+K) > 1.1$) also suggests the S-type nature of Katekalyan granite (KG) and gneiss (KGG). The criteria used for distinguishing I- and S-type granites (Chappel and White, 1974 and Takahasi *et al.*, 1980) are given in Table 4.2 and have been compared to Katekalyan granite (KG) and gneiss (KGG).

Blevin and Chappel (1995) pointed out that the granites are commonly misclassified; the most common being an assumption of peraluminous (corundum normative) chemistry and presence of muscovite and/or ilmenite is diagnostic of S-type origin. However, these features may also be found in granites derived from an igneous protolith. Therefore, I- and S-type granite scheme (Table 4.2) of White and Chappel (1974) is considered a genetic classification of source not a descriptive chemical-petrographic scheme. Further, Blevin and Chappel (1995) argued that the granite compositions are reflected in their metallogenic relationship when plotted Rb/Sr ratio against SiO_2 (Fig. 7.1a). The KG evolved and coincides with the compositional trend similarly shown by tin-specialized granite of Australia, which are normally peraluminous and highly differentiated.

Ishihara (1977) have classified the granites into magnetite series and ilmenite series on the basis of magnetic susceptible, which are broadly equivalent to I- and S-type granites of White and Chappel (1974). Takagi and Tsukinura (1977) have proposed of oxidised type and reduced type equivalent to magnetite and ilmenite series respectively on the basis of thermodynamic consideration such as fO_2 and fHO_2 etc. These classifications are characterized by distinct mineralisation type e.g., magnetite series granite accompanies sulphide deposits of Cu, Pb and Mo whereas ilmenite-series granite usually forms oxide deposits of Sn and W.

The magnetic susceptible (MS) of selected granite gneiss (KGG) and granite (KG) of the study area was measured using SM 20-MS meter.

The MS values ($\times 10^3$ SI unit) measured mostly on smooth rock surface is given in Table 7.3. Most of the measured values of KG and KGG are below 0.3×10^{-3} SI unit which belongs to the ilmenite series granite (Ishihara *et al.*, 1977) with which most of the Sn-W deposits are commonly worldwide. The supporting characteristic features viz., presence of ilmenite in place of magnetite and deep brown titanium-rich biotite in place of green biotite indicate that magma was containing relatively low oxygen fugacity and low ferric-ferrous ratios.

Table 7.3. Measured magnetic susceptibility (MS) related to samples of Katekalyan granite (KG) and granite gneiss (KGG)

S. No.	Sample No. (Rocks)	Magnetic Susceptibility ($\times 10^{-3}$ SI unit)	Inferred granite series (Ishihara, 1977)
1.	F/47,B (KGG)	(a) 0.060 (b) 0.066 (c) 0.062 Av. 0.0622 (n=5) (d) 0.063 (e) 0.060	Ilmenite Series
2.	F/2,A (KBG)	(a) 0.047 (b) 0.048 (c) 0.053 Av. 0.0502 (n=4) (d) 0.053	Ilmenite-Series
3.	F/10, A (KBG)	(a) 0.061 (b) 0.060 (c) 0.046 Av. 0.0542 (n=5) (d) 0.047 (e) 0.057	Ilmenite-Series
4.	F/42, A (KGG)	(a) 0.041 (b) 0.046 (c) 0.046 Av. 0.0432 (n=5) (d) 0.039 (e) 0.044	Ilmenite-Series

(S. Kumar, Pers. Comn.)

The Katekalyan granite (except KHG) and gneiss (KGG) represent the calc-alkaline differentiated trend, evident from A-F-M diagram (Fig. 4.9) as given by Irvine and Baragar (1971). Another supporting this view, when plotted in SiO_2 vs $\text{Na}_2\text{O} + \text{K}_2\text{O}$ variation diagram (not shown) according to Fung *et al.* (1990) and compared with granite compositional variations of Tischendorf (1985). Most of KG has shown affinity with alkali feldspathic granite and syenogranite being subalkaline in nature and highly differentiated granite in the silica range of 64.11 to 72.19 wt.% except one hornblende granite (KHG) with 57.75 wt.% SiO_2 , and tourmaline granite (KTG) with 62.08 wt.% SiO_2 which are relatively depleted in SiO_2 content. On the other hand, most granite gneiss (KGG) plot in the trondhjemite field of calc-alkaline nature except one sample, which plot into subalkaline and another much depleted in alkalis. These compositional features of KG and KGG suggest that KG is much more evolved in their silica and alkali contents and therefore most likely responsible for tin mineralisation, in comparison to KGG.

To identify the nature of the Katekalyan granite (KG) and granite gneiss (KGG), author has attempted $\text{K}_2\text{O}/\text{Al}_2\text{O}_3$ vs $\text{Na}_2\text{O}/\text{Al}_2\text{O}_3$ (wt.%) plot (Fig. 4.17) which discriminates igneous and sedimentary/metasedimentary protolith as has been outlined by Garrels and Mackenzie (1971). The diagram suggests that almost all samples plot in the sedimentary/metasedimentary field.

Major elements: Source characterization

In the presence of the high pressure and temperature conditions that prevailed resulted in anatexis and acid magmatic activities in the study area. The support of the view of the partial melting vectors and metasedimentary sources, author has attempted R_1 - R_2 multicationic scheme (Fig. 4.16b) based on Batchelor and Bowden (1985). They proposed that the first liquid to separate from the fusion of felsic crustal source such as gneiss, metapelite, intermediate metaigneous rocks, having the composition equivalent to alkali feldspar and quartz \pm sodic plagioclase. It indicates the felsic melt is completely mobilized in the crust and emplaced at a higher level,

and its composition will be equivalent to a syenogranite or monzogranite. Sequential intrusions within an igneous complex, trend towards more silicic and alkaline compositions with time. If it were assumed that lower crustal sources had compositions represented by A, B and C (Fig. 4.16b), then increasing degree of equilibrium, partial melting would generate compositions whose vectors could have represented by PM-A, PM-B and PM-C respectively (PM = zone of anatectic melts).

The major oxides variation study between felsic ($\text{SiO}_2 + \text{Al}_2\text{O}_3 + \text{Na}_2\text{O} + \text{K}_2\text{O}$) and mafic ($\text{FeO}_t + \text{MgO} + \text{MnO} + \text{CaO}$) constituents (Fig. 4.18) appear to mark inverse relationship.

It is noted that the comparatively felsic constituents (wt.%) in the granite (KG) except KTG is higher than the granite gneiss (KGG). The antipathic relationship between the felsic and mafic constituents marked the similar crystallisation differentiation pattern to that of the other tin bearing granites of the magmatic origin (Babu, 1993).

More recently Frost *et al.* (2001) has proposed three tier geochemical classification scheme for granitoids in a view to decipher; (i) differentiated history of granite magma determined by $\text{FeO}^*/\text{FeO}^* + \text{MgO}$ ratio of these rocks; (ii) source of magma based on alkali-lime index of the rock ($\text{Na}_2\text{O} + \text{K}_2\text{O} + \text{CaO}$) and (iii) sources and conditions of the melting based on aluminous saturation index (ASI). The granites (KG) and granite gneiss (KGG) have been plotted based on $\text{FeO}_{(t)}/\text{FeO}_{(t)} + \text{MgO}$ vs SiO_2 (Fig. 7.1b) which suggest that the KG is typically magnesian except a few one whereas KGG has affinity with ferroan type except one sample which is much depleted in $\text{FeO}_{(t)}/\text{FeO}_{(t)} + \text{MgO}$ ratio. The magnesian and ferroan-differentiated series of granitoids are indeed equivalent to tholeiitic and calc-alkalic magma types respectively as originally discriminated by Miyashiro (1974). However, a little overlapping in the fields of magnesian and ferroan have been noted towards high silica content of rocks which is more likely related to the late-stage compositional evolution of granitoids during their differentiation. What so ever the reason may be but KG is apparently distinct from KGG but both have experienced different degree of chemical differentiation in different episodes.

It is more likely that the magnesian enrichment trend of KG may be responsible for tin mineralisation in the study area.

Modified alkali-lime index (MALI) plotted against K_2O weight percentage (Fig. 7.1c) show compositionally affinity of KGG with Mesozoic Cordilleran granitoids, though scattered calcic to calc-alkaline. In order to discriminate the various igneous series $Na_2O + K_2O - CaO$ vs SiO_2 wt.% diagram (Fig. 7.2a) was plotted which failed to show any specific trend for both KG and KGG, rather spread over calcic to alkalic fields through calc-alkaline and alkalic-calcic, which suggest that the processes other than crystal-liquid separation might have played an important role in the evolution of KG and KGG. Alternatively, the data scattered in this diagram can be explained by metasomatism, which resulted in modifying the alkali content. The molar $A/(CNK)$ ratio of KG and KGG points in nature similar to as peraluminous granites (S-type). Whereas, aluminium saturation index ($ASI = A/(Na + K + Ca - 1.67 \times P)$) by Frost *et al.* (2001), takes into account of apatite also and ASI greater than 1.0 is considered peraluminous noted for most KG ($ASI = 0.99-2.17$) and KGG ($ASI = 1.19-1.82$). The MALI being unable to classified the KG and KGG rocks.

Further geochemical classification of KG and KGG as per scheme of Frost *et al.* (2001) is not possible. Nevertheless, magnesian and peraluminous for KG and ferroan and peraluminous for KGG can be very well suggested.

7.9.2. Trace element geochemistry

For trace element analysis, twentyfive samples of KGG ($n = 7$), KG ($n = 11$) and pegmatite ($n = 7$) were analysed by XRF-ED (X-ray Fluorescence-Energy Dispersive) for Cu, Zn, Zr, Ga, Y, Rb, Ba, Sr and Nb using Philips Exam Six and PV 9100 spectrometer. Sn and Ba were determined by AAS (Perkin-Elmer 4000) after total decomposition with an $HF-HClO_4-HNO_3$ acid mixture (Word *et al.*, 1969). Analytical results are given in Table (4.4a,b and d).

When plotted on Rb-Sr log-log variation diagram (Fig. 4.14) of Condie (1973), the most of the Katekalyan granite (KG) and gneiss (KGG) samples are clusters between the lines defined by $Rb/Sr = 0.1$ and $Rb/Sr = 1$, at the depths relevant to 20 to 30 kms. But few samples are emplaced at depths greater than 30 kms.

Rb-Ba-Sr ternary diagram of El Bouseilly and El Sokkary (1975) has pointed out the usefulness for the tracing differentiation trends and also detect specialization of tin-bearing nature of the granitic rocks. When plotted in this ternary diagram (Fig. 4.15), most of the Katekalyan granite (KG) and granite gneiss (KGG) are plotted in considerable range from granodiorites to normal granites through anomalous granitic fields. Among the granite (KG), the KTG and KHG fall in the granodiorites field, whereas, KBG fall in the anomalous granites field upto some extent normal granites field. The Rb levels in the anomalous granite (KBG) field having relatively somewhat higher as compared to that of the normal granites field. It concluded that the Ba is not depleted in the magma until very late stages of the differentiation sequence; but Sr is depleted relative to Ca. Thus the geochemical behaviour of Rb and Sr indicates that they have a greater sensitivity to magmatic processes than K and Ca. In the KG and KGG group of rocks, Sr shows more or less uniform distribution (low concentration) while the increase in Ba is accompanied by decrease in Rb. The normal granites are indicated similar in their chemistry to the well-known low-Ca granite, whereas anomalous granites represent metasomatised, granitised, magmatic granites that suffered from chemical changes and they were not formed by a simple mechanism.

Based on Whalen *et al.* (1987), the diagrams (Fig. 4.16 a,b) $Zr + Nb + Ce + Y$ (ppm) vs FeO^*/MgO (wt.%) and $Zr + Nb + Ce + Y$ (ppm) vs $K_2O + Na_2O/CaO$ (wt.%) show the nature of biotite granite (KBG) as fractionated felsic granites (FG) whereas granite gneiss (KGG) represent the orogenic granite type (OGT) of the unfractionated S-type granite.

Winchester and Max (1983) have used the trace element parameters viz., Rb/Sr vs Sn (Fig. 7.2b) and TiO_2 vs Sn (Fig. 7.2c) as originally proposed by Lehman (1982), which discriminate Sn-rich and Sn-

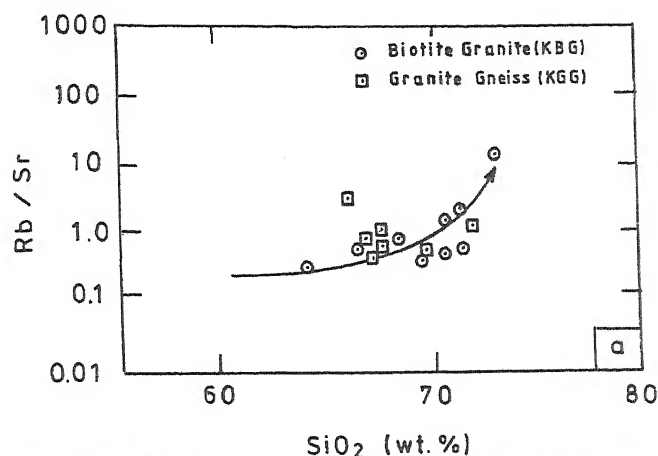


Fig. 7.1a. Rb/Sr vs SiO_2 plots for KG (KBG, KHG and KTG) and KGG. Note that the KG is evolved to a most SiO_2 differentiated and has affinity with Sn-granitic of Australia (Blevin and Chappel, 1995). See text for detail discussion.

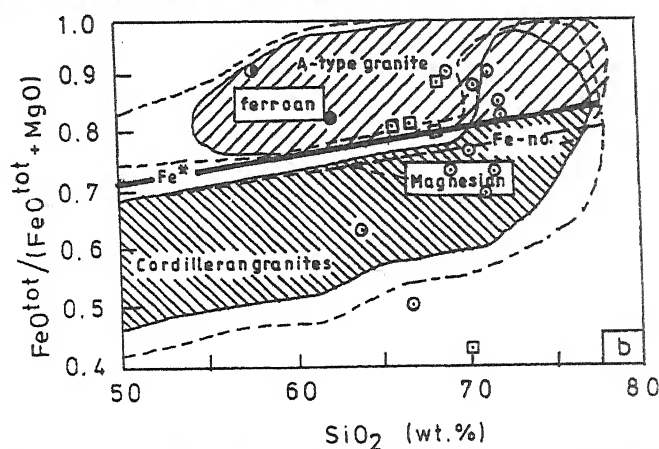


Fig. 7.1b. $\text{FeO}^{\text{tot}}/(\text{FeO}^{\text{tot}} + \text{MgO})$ vs weight percent SiO_2 diagram plotted for KG and KGG and compared with ferroan plutons and magnesian plutons shown by continuous line (Frost *et al*; 2001). Bold dashed line is the boundary between calc-alkalic and tholeiitic magmas defined by Miyashiro (1970).

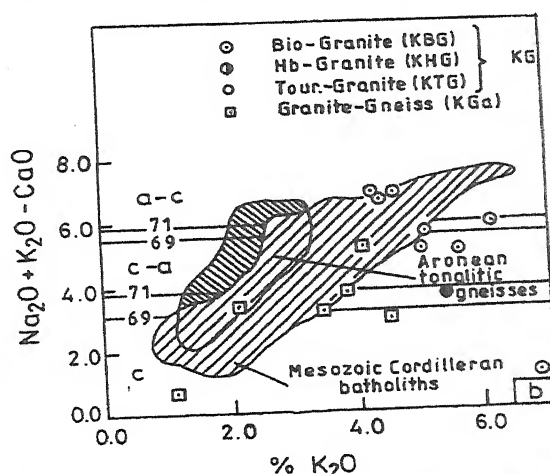


Fig. 7.1c. $\text{Na}_2\text{O} + \text{K}_2\text{O} - \text{CaO}$ vs K_2O diagram plotted for KG and KGG compared with the compositional trends of Archean tonalitic gneisses and Mesozoic granites of the Cordilleran batholiths a-c, alkali - calcic; c-a, calc-alkalic; c, calcic. The number refers to the position of the respective boundaries at that percentage of SiO_2 , $n=83$ for the cordilleran batholiths; $n=17$ for the Archean Gneisses - as used by Frost *et al* (2001).

poor compositional trends while studying the Greenville granite gneiss. When granite (KG) and granite gneiss (KGG) are plotted in the same diagrams (Fig. 7.2b,c), the trend of both KG and KGG follow Sn-enriched trend. This feature of tin enrichment trend of KG and KGG may probably indicate that generation of KG melt by melting of KGG protolith and further enriched in the late stage fractionation of KG, because the later is relatively richer in tin content compared to the former one.

The concept of geochemical specialization is commonly used for rare metal bearing potential of acidic rocks with certain elements concentration taken as indicators of mineralisation. Tischendorf (1977) proposed averages of some content specific rare elements in the specialised granite viz., Sn (40 ± 20 ppm), W (7 ± 3 ppm), Rb (580 ± 200 ppm), Li (400 ± 200 ppm), F (3700 ± 1500 ppm) and Be (13 ± 5 ppm) in comparison to normal granites. Compared to these averages in the specialised granites further granitophile elements (Sn, W, Nb, Ta, Cs, U, Th, Rb and REEs) are enriched whereas granitophobe elements (Ni, Cr, Co, V, Ba and Sr) are impoverished. Such type of rare metal concentrations are usually products of the late stage differentiates of the granitoids. Based on the data for granitoid rocks, Imeokparia (1985) also suggested that the enrichment of Rb, Li, F, Nb and depletion of Ba, Sr and Zr or element pairs (Low K/Rb and Ba/Rb ratios) might use of the lithogeochemical exploration for Sn and W deposits. Sn-W mineralisation is commonly associated with peraluminous granites (Stemprok and Sulcek, 1969; Jarchovsky, 1974; Groves, 1972 and 1978). Smirnov (1968) also studied the several metallogenic provinces to show that Sn, W, Nb, Ta and Li are deposits were associated with the S-type granites formed due to palingenesis of crustal rock materials.

The distribution of trace elements in the granite gneiss (KGG), granite (KG) and pegmatite (KP) of the study area are given in the Table 4.4a,b,d. In the granite gneiss (KGG), the concentration (ppm) of various trace elements are varied such as Sn 4.0-50 ppm (16.14); W, 16.36-39.65 (25.26); Rb, 75-666.86 (217.43); Ba, 112-1150 (727.67); Th, 18.64-59.53 (39.06); Nb, 16.67-30.03 (23.63); Sr, 117.43 – 190.53 (153.83); Zr, 132.72 – 193.56

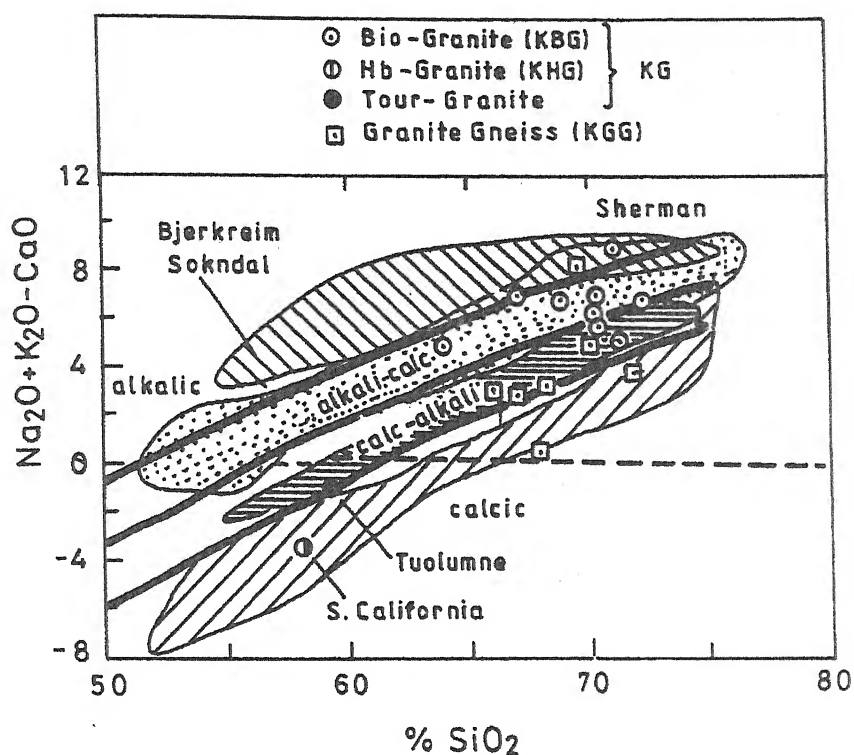


Fig 7.2a. $\text{Na}_2\text{O} + \text{K}_2\text{O} - \text{CaO}$ vs SiO_2 diagram plotted for KG and KGG compared with the compositional trends of various plutons (Frost *et al*, 2001). The thick boundary lines separating the various series are taken after Frost *et al* (2001). See text for detail explanation.

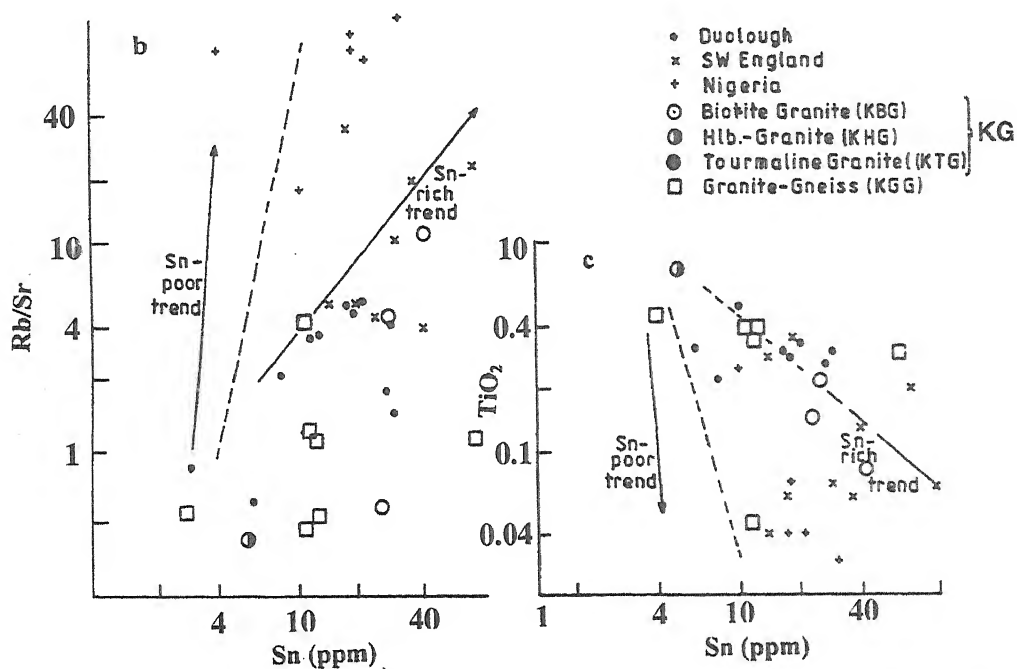


Fig 7.2b,c. Rb/Sr vs Sn (b) and TiO_2 vs Sn (c) variation diagrams (after Lehmann, 1982; Winchester and Max, 1983) contrasting Sn-rich and Sn-poor trends. Note that KG (KBG and KHG) and KGG mostly coincides with Sn-rich trends. The broken line separates the Sn-poor and Sn-rich fields.

(175.09); etc. whereas in the granite (KG) the content of trace element ranges (ppm) in the Sn, 6.0 – 151(69.45); W, 5.782-32.69(21.24); Rb, 78 – 316.33 (142.53); Ba, 228 – 1019 (525.83); Th, 25.20 – 45.14 (33.48); Nb, 14.29 – 35.64 (21.67); Sr, 15.06 – 202.97 (146.32); Zr, 138.69 – 155.05 (144.91); etc.

Besides the above, different type of pegmatites having the concentration (ppm) of trace element viz; Rb, 962 – 2436.70(461.74); Ba (285); Th, 17.44 – 193.33(105.38); Nb, 9.67 – 102.18(55.92); Sr, 70.15 – 378.01 (150.36) and Zr, 16.97 – 124.73(70.85).

All these above data of the granite gneiss (KGG) granite (KG) and pegmatite (KP) of the study area are presented in the form of spider diagram (Fig. 7.3a, b, c).

However, when the trace elements for Katekalyan granite gneiss (KGG) and granite (KG) are plotted against SiO_2 in Harker's variation diagram (Fig. 4.18), they show some genetic features. Rb, Ba, Sn, W and Nb increasing with SiO_2 showing the similar differentiation trend. This supports the view that these KGG and KG were of the same in nature and possibly have got same petrogenetic history. There is a tendency for rise in tin content with increasing silica at the initial stage up to 50 ppm. The enrichment of tin content in granites is more than the saturation level up to 50 ppm, might be due to the effect of post – magmatic and metasomatic processes. There is no definite relationship observed between the variations of tin with other major oxides.

7.9.3. Rare earth elements (REE) geochemistry

Rare earth elements of seven selected samples of KGG (n=2) and KG (n=5) of the study area were analyzed table 4.5 by the ICP – AES (Jobin Yvon, Model J Y 70 plus) and further chondrite normalized patterns by Taylor and McLennan, 1985 (1.5 X values of Evenson *et al*; 1978) are shown in figure 4.20. All the suites exhibit enriched LREE pattern relative to HREE along with variable negative Eu anomalies. The most of the granitoid samples show steep by inclined pattern and are highly fractionated.

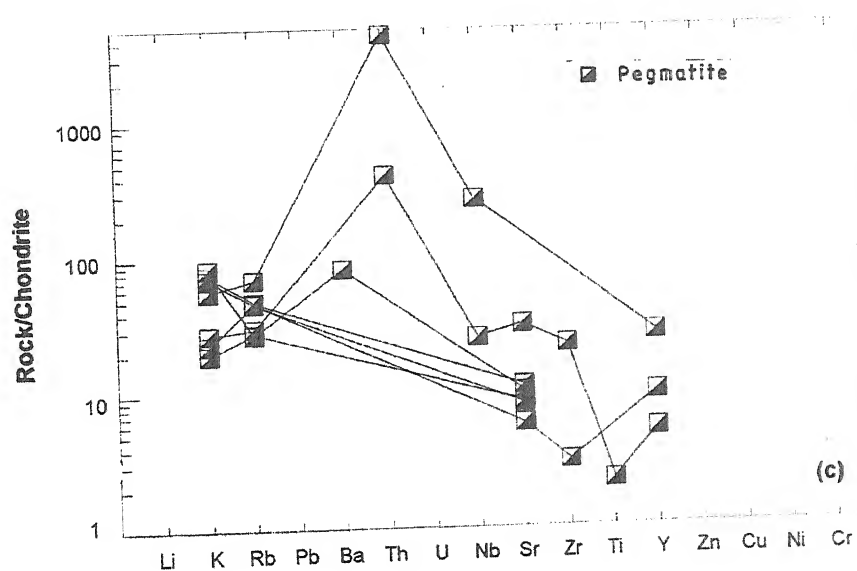
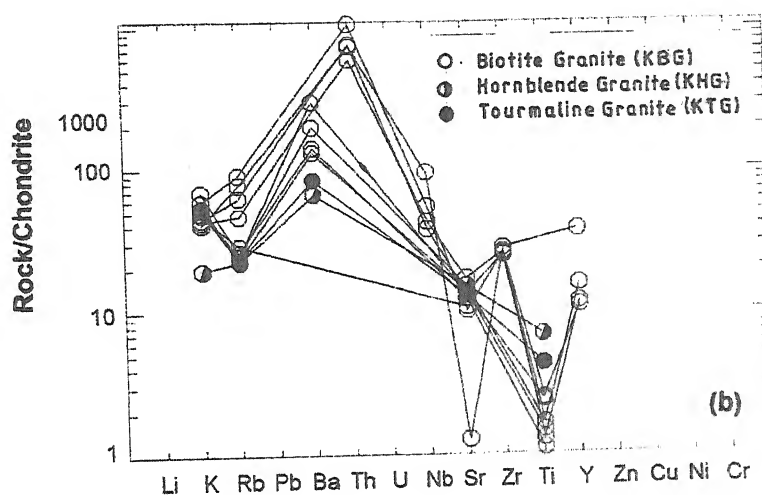
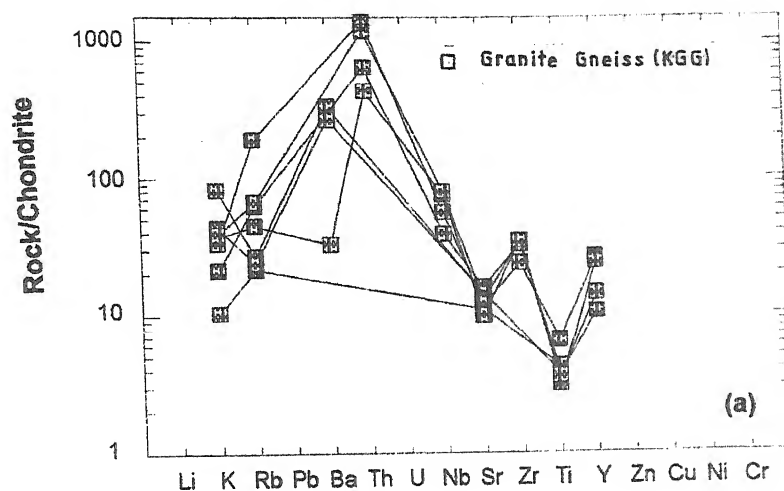


Fig. 7.3a,b,c. Spider diagrams of the trace elements for the Katekalyan KGG (a), KG (b) and pegmatite (c). (After Taylor and Mc Lennan, 1985).

The ΣREE of KG ranges between 114.25 – 277.99 ppm (\bar{X} = 174.79 ppm) and KGG 297.96 – 343.71 ppm (\bar{X} = 320.83 ppm) are significantly different but continuous to decreases from KGG to KG. This feature can be very well illustrated when LREE (La + Ce + Nd) and ΣLREE are separately plotted against B (Fe + Mg + Ti) content (Fig. 7.4 a and b) for KG and KGG. B components calculated other Debon *et al*, 1987) whole rock data actually represent ferromagnesian minerals of granitoids. In present study, the ferro-magnesian minerals in KG and KGG are mostly represented by biotite, which is relatively more in KGG compared to KG. In +ve correlation noted between LREE vs B ΣREE vs B for the samples of KG and KGG reflect that KG variation can be explained in terms of varying degree of melting of KGG source but an internal differentiation within KG by fractionation cannot be fully ruled out. The striking chondrite normalized REE pattern is similar where REE pattern is inclined composed to the relatively flatter HREE pattern with some degree of negative Eu anomalies except few samples. This feature strongly suggests that KG stanniferous melt could be derived by partial melting of protolith of KGG having feldspar depleted signature source. A limited range of Eu – anomalies noted for KG ($\text{Eu}/\text{Eu}^* = 0.45$) reflects the source character whether than fractionation (feldspar) during its evolution. The HREE pattern of KG are distinctly depleted compared to that of KGG points the mechanism of melt separation from the probable sources KGG particularly noted for one KGG sample which show flatter REE pattern (sample no. F/15A). Tourmaline granite (KTG) has more REE resemblance with one sample of KGG with signites its generation by low degree of melting of KGG source composed two other biotite granite (KBG). The overall REE feature of KG and KGG has resemblance with that of tin –bearing granitoids reported elsewhere (Jingwen, 1989).

7.10. Geochemical modeling of KG and KGG melt generation

Several lines of field photographic and bulk geochemistry of KG, KGG and pegmatites (KP) reveal with origin from crustal anatexis i.e.; partial melting of crustal source generating the peraluminous KG and KGG melts.

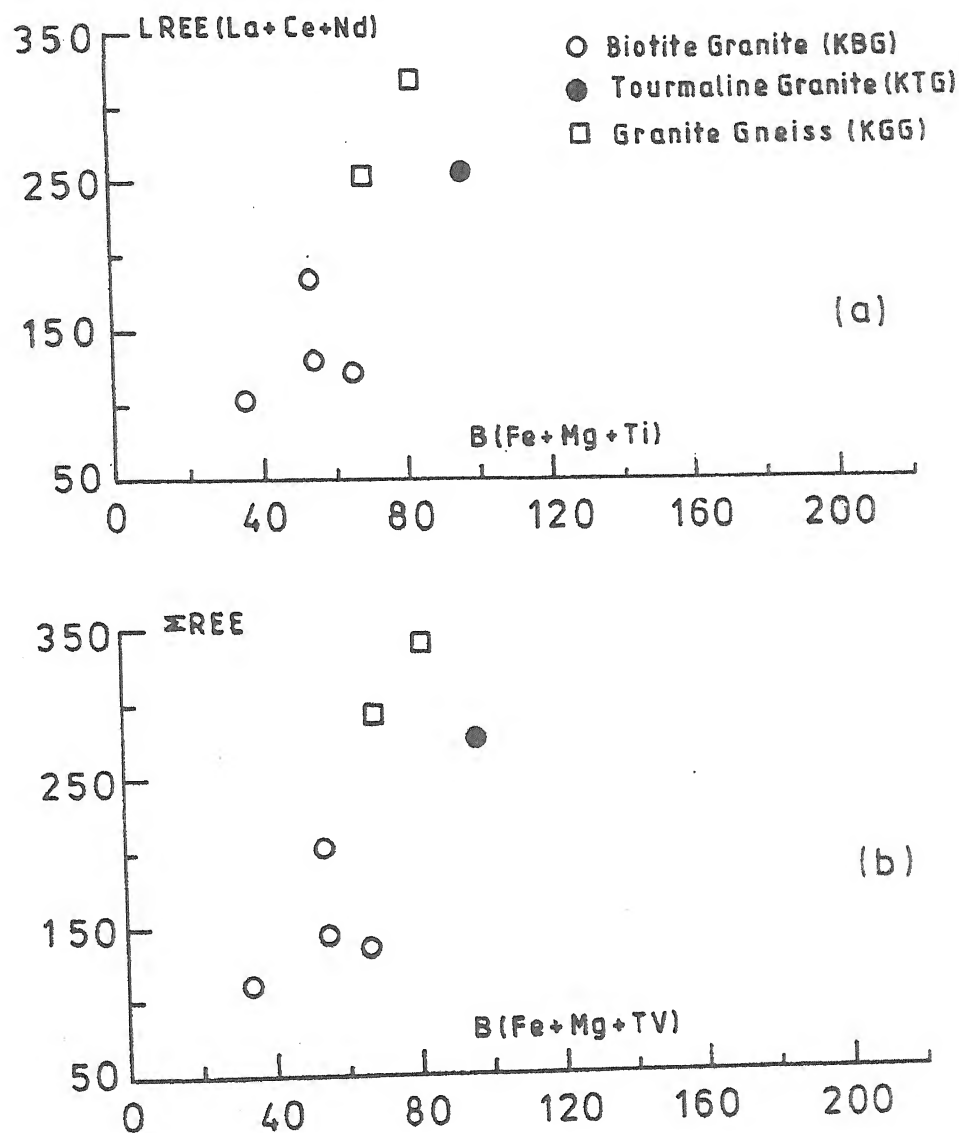


Fig. 7.4a. Distribution of the KBG, KTG and KGG granitoid samples in the $LREE = (La + Ce + Nd)$ in ppm vs $B = (Fe + Mg + Ti)$ diagram. $(La + Ce + Nd)$ is proportional to the amount of monazite. $(Fe + Mg + Ti)$ reflects the amount of biotite content in granitoids. B values are calculated after Debon and Le Fort (1983) and Debon *et al* (1986).

b. Distribution of KBG, KTG and KGG samples in the total REE (in ppm) vs $B = (Fe + Mg + Ti)$ diagram.

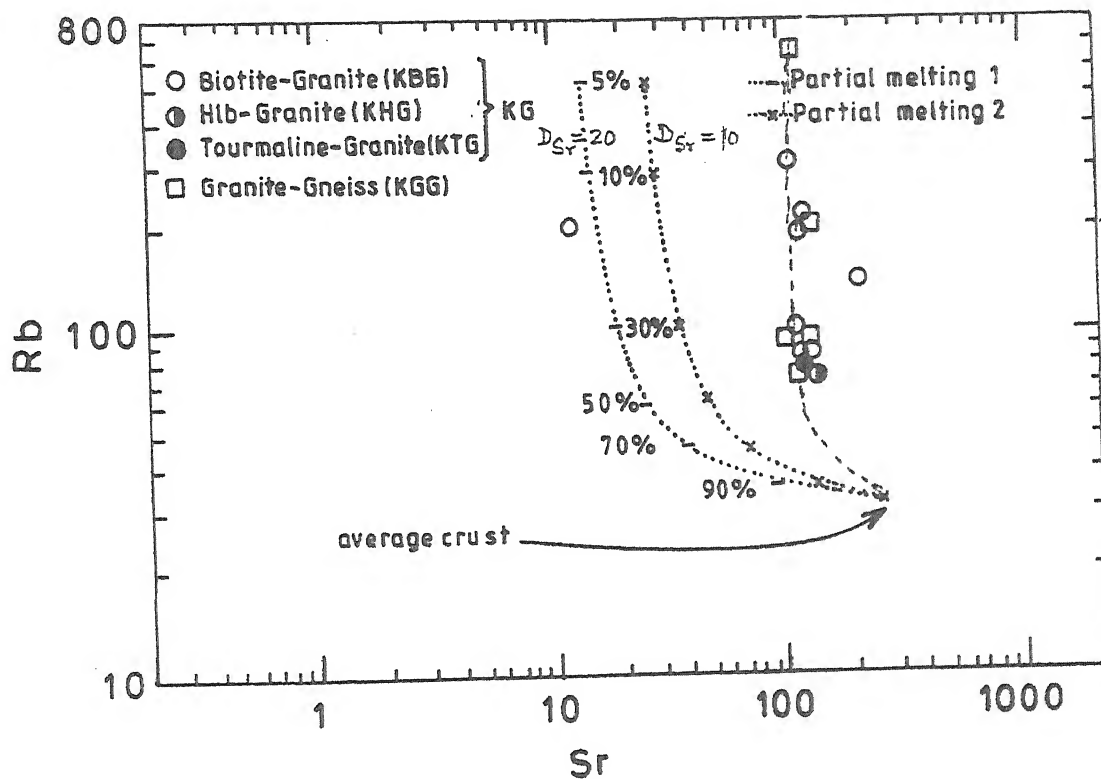


Fig. 7.5. Partial melting models (1 and 2) of bulk crust composition ($Sr = 260$ ppm, $Rb = 32$ ppm) of Taylor and Mc Lennan (1985) calculated at $D_{Sr} = 20$ and $D_{Sr} = 10$ respectively as shown by Gasparon *et al.* (1983) and compared with the variation of KG and KGG, approximately by 5-50% melting of average crust silicate. $D_{Sr} < 10$. See text for discussion.

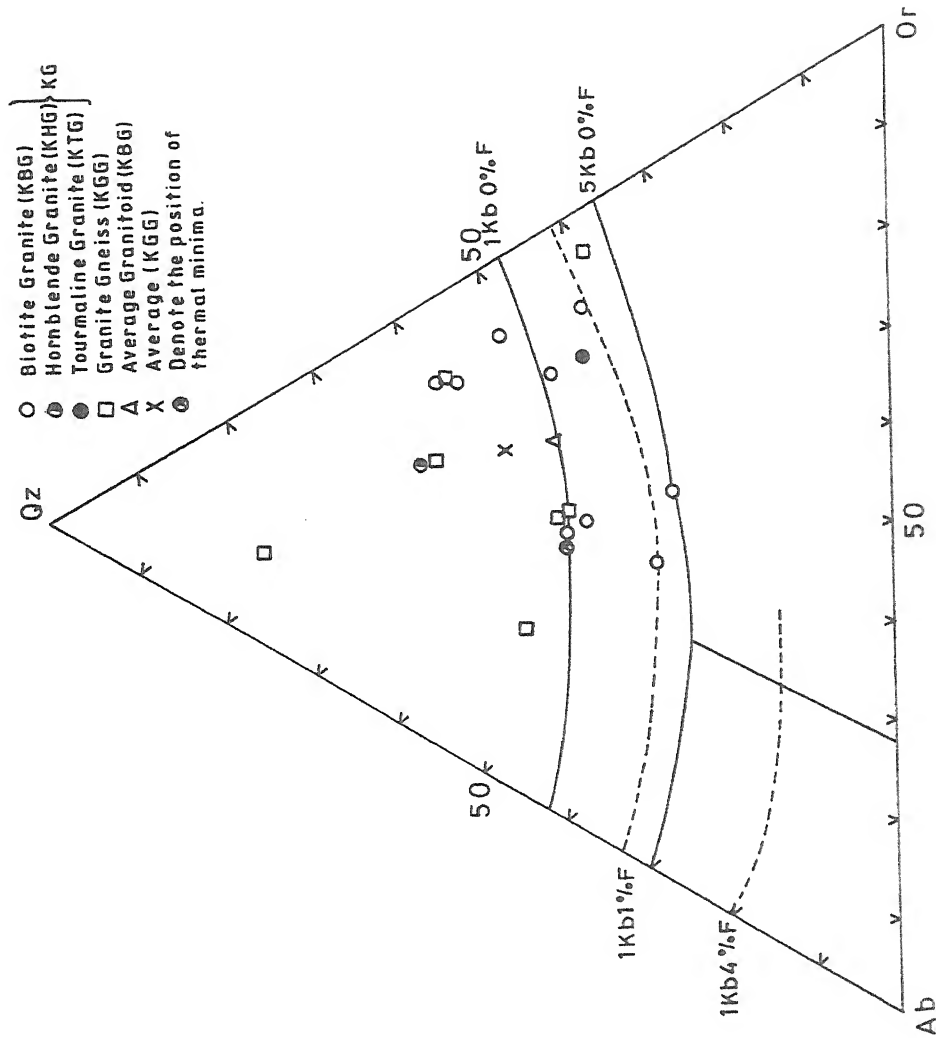


Fig. 7.6. Plots averages for Katekalyan granite (KG) and granite gneiss (KGG) in the Qz-Ab-Or-H₂O-F system (Tuttle and Bowen, 1958; Manning *et al*, 1980).

Therefore, it is now pertinent to model the partial melting in terms of Rb, Sr content where Rb is incompatible in an acid igneous system. The partial melting model of bulk continental crust (Taylor and McLennan, 1985) as calculated and presented by Gasparon *et al.* (1993) have been used to explain variation of KG and KGG. The partial melting model given in figure 7.5 and this shows that the variation of KG as well as KGG can be explained by varying degree of partial melting (5 to 50%) of bulk continental crust but distribution coefficient for Sr (D_{Sr}) must be very low i.e. $\ll 10$. The anorthite content of feldspar is very sensitive to determine the distribution coefficient of Sr, therefore, a small changing D_{Sr} will shift the vertical trend of partial melting of source towards higher or lower sides of Sr content. The result of partial melting modeling at least suggests that the differentiation of KG and KGG melt are more governed by partial melting of bulk crust rather than fractional crystallization. The estimates upper limit of partial melting i.e., 50 % of bulk crust noted for KG and KGG are consistent with required rheological, critical melt percentage to leave the source region has decreased granite melt which were capable to mineralised tin ore elements.

7.11. Geotectonic environments and its relevance tin-bearing granitoids

In order to characterize the tectonic environment for the genesis of Katekalyan granites (KG) and gneisses (KGG) are classified on the basis of major oxides criteria based on the fields (Fig 4.10 a-d) of the Maniar and Piccoli (1989) and compared inferred tectonic environment for Katekalyan granite (KG) and granite gneiss (KGG) based on discriminants functions given in table 4.3b.

When the plotted of the KG and KGG in the fields of Maniar and Piccoli (1989) diagram (Fig 4.10 a-d), all the KG and KGG fall in the field of orogenic granites which is distinctly away from the field of anorogenic granites in the discrimination diagram by the weight percentage of SiO_2 vs K_2O (Fig 4.10a). Further classified on the basis of the projection diagrams (Fig 4.10b and c) among the MgO (wt%) vs FeO^* and CaO (wt%) vs $FeO^* + MgO$ (wt%), it does not fall in the field defined for post- orogenic granitoids (POG). The KG

and KGG are originated by the continental collision with highly peraluminous nature, which is clearly evident on the basis of the discriminate variation diagram (Fig 4.10d) of molar $A/(CNK)$ vs $A/(NK)$. It results from the anatexis of metasedimentary rocks mainly during continental collision. The S- type of KG and KGG are the assumed product of the continent collision.

Petrogenetic modeling demonstrates that the observed discrimination diagram based on Pearce *et al* (1984) can be explained by the volatiles induced enrichment in Rb and Ta during the genesis of Syn- collision granites (syn-COLG). It is apparent that the Rb enrichment is a likely consequence of K-silicate and sericitic alteration due to growth of secondary biotite and muscovite respectively and Rb- depletion a likely consequence of chloritisation and argillic alteration due to the breakdown of feldspar and mica. Using classical system in terms of Qz – Ab- Or (Tuttle and Bowen, 1958, Manning *et al*, 1980) diagram in the (Fig 7.6) presence of water and fluorine. The emplacement of KG can be estimated at shallow level (1 Kb) plotting on the quartz – orthoclase cotectic close to the granite thermal minima. However, the average KGG plots into the quartz saturated granite melt field, therefore its unsuitability estimates its physical conditions of emplacement.

CONCLUSION

Favorable geological setting, nature of plutons, and composition of host rocks, are the most significant tools to assess the degree of ore potential and also, to know the genetic history of the granitic rocks of the study area.

Based on texture, structural and compositional peculiarities, the granitoids can be classified into two broad groups viz., non-foliated (KG) and foliated (KGG) granitic rocks. The non-foliated granites (KTG, KHG and KBG) are found to be medium-to coarse-grained leucocratic in nature. Some are, however, fine-grained where the texture appears aplitic in character. The biotite rich micaceous bands in granite gneiss (KGG) are often very continuous as wanning and waxing pattern along the direction of foliation planes and also the quartzo-feldspathic portion form small lenticular patches along these planes.

So far as the mineral constituents of these granite-gneisses (KGG) are concerned, the following essential minerals viz., microcline, micro perthite, orthoclase (also sericitised), plagioclase and quartz have been recorded. The accessory minerals (biotite, muscovite, sphene and apatite) and also secondary minerals (sericite, epidote, chlorite and opaques) are found in this rock. The alteration products such as sericite and chlorite are derived from the breakdown of feldspars and biotite. Often such alteration brought about through the agency of volatiles and hydrothermal solutions. The mineral assemblage granites (KG) are more or less the same except the tourmaline, hornblende, biotite (less) and cassiterite. At places, the porphyritic texture is represented by quartz and feldspars. These phenocrysts appear to be formed prior to the quartzo-feldspathic constituents of the granite. Subsequently these phenocrysts might have introduced along the contact of the biotite granite (KBG) and have attained the large size with subsequent pegmatitic emplacement. At the contact of granite and pegmatite,

highly crushed, fine-grained quartzo-feldspathic mass is accompanied with tiny greenish biotite crystals often associated with cassiterite.

Apatite particularly the prismatic one is crystallised late in the sequence whereas the needle-shaped apatite might have formed early in the sequence but relatively under cooled at the initial stage of felsic magmatism. Zircon is mostly observed as inclusions within the nucleus of the pleochroic halos of hornblende. Tourmaline is found as comparatively rare accessory mineral of granitoid rocks. At places, clusters of radiated needles of greenish tourmaline are observed giving an appearance like "tourmaline Sun". These needles of tourmaline on an intensive scale are suggestive of sustained pneumatolytic action through the introduction of boron. Sericite is the most predominant of all the secondary minerals noted in the granitoids. The intensity of sericitisation is increasing along the zones of fracture present in the granite body. It may be recorded that extensive activity of the volatiles during the late magmatic stage was mainly responsible for the widespread alteration of the feldspar.

From the field relations and petrographic observations of different litho-units of the area, it appears that the tin mineralisation is primarily associated and genetically related to the Katekalyan granitoids (KG and KGG). It is characterised by high silica (KG = 57.75 to 72.19 wt%, KGG = 65.87 to 75.49 wt%), moderate to high alumina (KG = 14.06 to 22.53 wt%, KGG = 14.28 to 18.48 wt%), higher K_2O (KG = 2.02 to 7.15 wt%, KGG = 1.07 to 8.48 wt%) than Na_2O (KG = 0.72 to 3.95 wt%, KGG = 0.49 to 3.37 wt%) and low TiO_2 (KG = 0.02 to 0.75 wt%, KGG = 0.05 to 0.71 wt%).

The Katekalyan granitoids have been chemically classified on the basis of different oxide, norm and cationic parameters. On these parameters, majority of the samples plot in the fields of granite, adamellite and granodiorite. However, the hornblende granite (KHG) due to poor potassium content falls in field of tonalite.

The data (Greig and stemprok, 1969) of the tin bearing granites and pegmatites of Kazaksthan and Erzjebirdge area have been also used and compared with present data of Katekalyan granite (KG), granite gneiss (KGG)

and pegmatites (KP) in ternary diagram [SiO_2 - ($\text{FeO}_T + \text{CaO} + \text{MgO}$) - ($\text{Al}_2\text{O}_3 + \text{Na}_2\text{O} + \text{K}_2\text{O}$)]. It is interesting to note that the most of the tin-bearing pegmatites fall within the tin-bearing granite field to favour the same genetic history. Most of data fall within the tin compositional zone, however, few of the tin-bearing granitoids (KGG, KTG and KHG) represent the excess of FeO and CaO, perhaps due to partial digested of mafic xenoliths which takes the sample away from the tin zone.

The chemical-mineralogical typology based on multicationic parameters delineated by Debon and Le-Fort (1982) defined the peraluminous and metaluminous characters depending on its positive and negative values respectively reflect the nature and proportions of their characteristics minerals other than quartz and feldspars. The $A[\text{Al}-(\text{Na} + \text{K} + 2\text{Ca})] - B(\text{Fe} + \text{Mg} + \text{Ti})$ diagram shows clearly that Katekalyan granitoids (KG and KGG) occupy the delineated I and II fields of the peraluminous domains which indicate that they belong to the association of muscovite>biotite and biotite>muscovite respectively. The high molar A/CNK i.e., $\text{Al}_2\text{O}_3/(\text{CaO} + \text{Na}_2\text{O} + \text{K}_2\text{O})$ ratio against SiO_2 indicate peraluminous compositional field. The molar A/CNK ratio more than 1.1 suggests that the granitoids is mainly igneous origin with some crustal component (Chappel and White, 1974). Presence of normative corundum and high molar concentration of A/CNK (>1.1) is also suggestive of S-type nature of Katekalyan granites.

The other characteristic features, viz., low ferric/ferrous ratios appearance of ilmenite mostly in place of magnetite and deep brown titanium-rich biotite in place of green biotite, indicate that the magmas was evolved in the condition of relatively low oxygen fugacity. The alkalinity ($\text{Na}_2\text{O} + \text{K}_2\text{O}$) not more than 10% exceed, which is evident from the TAS ($\text{Na}_2\text{O} + \text{K}_2\text{O}$ Vs SiO_2 wt%) diagram (Middlemost 1985). Most of the granitoids (KG and KGG) are hypoalkalic but few of them as silicic nature also yield that the possibility of local metasomatism may be possible in the present area. The AFM ($\text{Na}_2\text{O} + \text{K}_2\text{O} - \text{FeO}_T - \text{MgO}$) diagram (Irvine and Baragar, 1971) indicates that most of the KG and KGG granitoids represent the calc-alkaline differentiation trend, which were evolved towards alkalis corner.

Blevin and Chappel (1995) argued that the granitic compositions are reflected in their metallogenic relationship. The KG evolution coincides with the compositional evolution trend and is normally peraluminous and highly differentiated when plotted Rb/Sr ratio against SiO_2 similarly shown by tin specialized granite of Australia.

The magnetic susceptible (MS) of selected granite (KG) and granite gneiss (KGG) of the study area was measured using SM-20-MS meter. The MS values ($\times 10^{-3}$ SI unit) measured mostly on smooth rock surface. Most of the measured values of KG and KGG are below 0.3×10^{-3} SI unit, which belongs to the ilmenite series granite (Ishihara *et al.*; 1977).

The SiO_2 versus $\text{Na}_2\text{O} + \text{K}_2\text{O}$ variation diagram for the Katekalyan granite (KG) and granite gneiss (KGG) and compared with granite compositional variations of Tischendorf (1985) suggest that KG is much more evolved in their silica and alkali contents and therefore most likely responsible for tin mineralisation, in comparison to KGG (Fung *et al.*, 1990).

In order to compare the characteristics of the inferred tectonic environment for the Katekalyan granitoids (KG and KGG), the classification scheme proposed by Maniar and Piccoli (1979) have been followed. The Katekalyan granitoids fall in the field of orogenic granites distinctly away from the field of anorogenic granites in the discrimination diagram due to the presence of K_2O content of KG (av. 5.08 wt%) and KGG (av. 3.94 wt%) being greater than one does not support anorogenic oceanic plagiogranite (OP) and post orogenic granitoids (POG). It concludes that the Katekalyan granitoids represent continental collision and peraluminous in nature. It is also suggested that Katekalyan granitoids were formed by the anatexis of metasedimentary (crustal) source rocks during continent collision.

Considering the geochemical pattern, based on selective trace elements (Y, Nb and Rb) criteria, most of the Katekalyan granitoids can not be assigned collectively of any one tectonic regime but cluster near the triple junction demarcating lines of VAG, syn-COLG and WPG fields, when plotted on Y + Nb vs Rb log-log (ppm) and Y vs Nb log-log (ppm) based on Pearce *et al.* (1984). Nevertheless, syn-COLG appears an appropriate tectonic

environment due to the presence of highly content of Rb and Ta during the genesis of syn-COLG for the Katekalyam granitoids. It is apparent that Rb enrichment is a likely consequence of K-silicate and sericitic alteration due to the growth of secondary biotite and muscovite respectively. Discriminated tectonic environment for the granitoids of the study area based on $R_1 [4\text{Si} - 11(\text{Na} + \text{K}) - 2(\text{Fe} + \text{Ti})]$ and $R_2 [6\text{Ca} + 2\text{Mg} + \text{Al}]$ is other supporting evidence the pre-to syn-COLG (Pitcher, 1982 and Harries *et al*, 1986).

For the partial melting vectors and metasedimentary sources, the Katekalyan granitoids (KG and KGG) plotted in R_1 - R_2 multicationic scheme (Batchelor and Bowden, 1985). Most of the granitoids (KG and KGG) occupied the anatectic granite field which indicates the first liquids to get separated from the fusion of felsic crustal source (gneiss and metapelite) would have compositions equivalent to alkali feldspar and quartz \pm sodic plagioclase. This felsic melt was completely mobilized in the crust and was emplaced at a higher level and its composition will be equivalent to a syenogranite or monzogranite.

Based on $\text{Zr} + \text{Nb} + \text{Ce} + \text{Y}$ (ppm) vs FeO^*/MgO (wt%) and $\text{Zr} + \text{Nb} + \text{Ce} + \text{Y}$ (ppm) Vs $\text{K}_2\text{O} + \text{Na}_2\text{O}/\text{CaO}$ (wt%) diagrams of Whalen *et al*; (1987). The Katekalyan granitoids represent the fractionated felsic granite (FG) of the biotite granite (KBG) whereas granite gneiss (KGG) as unfractionated orogenic granite type (OGT) in nature. Besides these, author has attempted to find out the KG and KGG as the sedimentary/metasedimentary protolith based on $\text{K}_2\text{O}/\text{Al}_2\text{O}_3$ vs $\text{Na}_2\text{O}/\text{Al}_2\text{O}_3$ (wt%) diagram (Garrels and Mackenzie, 1979). The Rb-Sr log-log variation diagram (Condie, 1973), the granitoid samples were found to cluster between the lines defined by $\text{Rb}/\text{Sr} = 0.1$, which is equivalent to the depth relevant to 20-30 Kms. But few samples are emplaced at depth greater than 30 Kms. According to El Bouseilly and El Sokkary (1973), the tourmaline granite (KTG) and granite gneiss (KGG) fall in the fields of granodiorite and normal granite respectively in Rb-Ba-Sr ternary diagrams. But the biotite granite (KBG) falls in the anomalous granite field chiefly due to its relatively lower Rb levels as compared to that of the normal granites. This is possibly brought by late

residual aplitic liquid whereby Rb may be fractionated during differentiation in the formation of these granitic rocks. Thus studies of these individual granitoids (KTG, KBG and KGG) represent their own characteristics. The changes in major and trace element chemistry towards more felsic granitoids indicate fractional crystallization processes. The variation between felsic ($\text{SiO}_2 + \text{Al}_2\text{O}_3 + \text{Na}_2\text{O} + \text{K}_2\text{O}$ wt%) and mafic ($\text{FeO} + \text{CaO} + \text{MgO} + \text{MnO}$ wt%) constituents, it appears to marked inverse relation in the Katekalyan granitoids (KG and KGG)

Most of the Katekalyan granitoids fall within true granitic field when examined in the ternary system of normative quartz, albite and orthoclase proposed by Tuttle and Bowen's (1958).

The calculated normative quartz, albite and orthoclase value of Katekalyan granitoid plotted in the Qz-Ab-Or-F system (Manning *et al*, 1980) point out that their average fall in a restricted and evolved compositional field approaching the thermal granitic minima but slightly deviated towards quartz-orthoclase joint. Assuming the average content of fluorine in Katekalyan granitoid about 0.5%, which is several times higher than the average fluorine content the normal granite. The pressure of crystallising fluid observed from this diagram can be constrained more or less 2 kb and the final temperature of crystallization about 650 °C. This depict about the occurrence of shallow level of pluton emplacement.

In the Katekalyan granitoid, the enrichment of tin (Sn) content in KBG (av. 76.55 ppm) is found more than the saturation level of 50 ppm, comparison to KGG (av. 16.14 ppm) might be due to the effect of post-magmatic and late metasomatic processes. There is no definite relationship observed among the variation of tin with other major oxides.

Rare earth elements (REEs) of the Katekalyan granitoid (KBG, KTG and KGG) were analyzed and it chondrite normalized were made by Taylor and McLennan, 1985 (1.5X values of Evensen *et al*, 1978) scheme. All the granitoids are enriched towards LREE pattern relative to HREE along with variable negative Eu anomalies. The variation in LREE/HREE ratio can be interpreted by the presence or absence of accessory phases like monazite

residual aplitic liquid whereby Rb may be fractionated during differentiation in the formation of these granitic rocks. Thus studies of these individual granitoids (KTG, KBG and KGG) represent their own characteristics. The changes in major and trace element chemistry towards more felsic granitoids indicate fractional crystallization processes. The variation between felsic ($\text{SiO}_2 + \text{Al}_2\text{O}_3 + \text{Na}_2\text{O} + \text{K}_2\text{O}$ wt%) and mafic ($\text{FeO} + \text{CaO} + \text{MgO} + \text{MnO}$ wt%) constituents, it appears to marked inverse relation in the Katekalyan granitoids (KG and KGG)

Most of the Katekalyan granitoids fall within true granitic field when examined in the ternary system of normative quartz, albite and orthoclase proposed by Tuttle and Bowen's (1958).

The calculated normative quartz, albite and orthoclase value of Katekalyan granitoid plotted in the Qz-Ab-Or-F system (Manning *et al*, 1980) point out that their average fall in a restricted and evolved compositional field approaching the thermal granitic minima but slightly deviated towards quartz-orthoclase joint. Assuming the average content of fluorine in Katekalyan granitoid about 0.5%, which is several times higher than the average fluorine content the normal granite. The pressure of crystallising fluid observed from this diagram can be constrained more or less 2 kb and the final temperature of crystallization about 650 °C. This depict about the occurrence of shallow level of pluton emplacement.

In the Katekalyan granitoid, the enrichment of tin (Sn) content in KBG (av. 76.55 ppm) is found more than the saturation level of 50 ppm, comparison to KGG (av. 16.14 ppm) might be due to the effect of post-magmatic and late metasomatic processes. There is no definite relationship observed among the variation of tin with other major oxides.

Rare earth elements (REEs) of the Katekalyan granitoid (KBG, KTG and KGG) were analyzed and it chondrite normalized were made by Taylor and McLennan, 1985 (1.5X values of Evensen *et al*, 1978) scheme. All the granitoids are enriched towards LREE pattern relative to HREE along with variable negative Eu anomalies. The variation in LREE/HREE ratio can be interpreted by the presence or absence of accessory phases like monazite

and zircon. The Katekalyan granitoids (KBG, KTG and KGG) contain variable amounts of apatite, zircon and monazite as accessory minerals. Most of the LREE are controlled by monazite (Mittlefehldt and Miller, 1983). Hanson (1978) suggested that middle rare earth element (MREE) is controlled by apatite while zircon controls the HREE (Charoy, 1986). These minerals are soluble in a peraluminous melt, and they are mostly inherited from the original source rocks and included in early-formed minerals like biotite.

There is some significant variations in REE distribution patterns among these granitoids, because of the scattered distribution of KGG rocks probably implies that the initial amount of LREE was different from granite gneisses (KGG) to KBG granites, perhaps represent the different segments source of the same crustal materials. This genetic history relationships is evident from the LREE (La + Ce + Nd) corresponds to the amount of monazite plotted against B parameter (Fe + Mg + Ti) equivalent to the amount of biotite (B values are calculated after Debon and LeFort, 1983 and Debon *et al.*, 1986).

The Σ REE of KG ranges from 114.2.5 to 277.99 ppm (av. 174.79 ppm) and KGG range 297.96 to 343.71 ppm (av. 320.83 ppm) are significantly different but continuous to decrease from KGG to KG. The striking chondrite normalized REE pattern of KG and KGG are similar where REE patterns are inclined composed to the relatively flatter HREE patterns with same degree of negative Eu anomalies except few samples. This feature strongly suggests that KG stanniferous melt could be derived by partial melting of protolith of KGG having feldspar-depleted signature in the source. The overall REE feature of KG and KGG has close resemblance with that of tin bearing granitoids reported elsewhere.

The Eu/Eu* ratio in the Katekalyan granitoid rocks (KBG, KTG and KGG) range from 0.32 to 0.57 (av. 0.45) indicates negative Eu anomalies. Taylor and McLennan (1985) recommend using the geometric mean i.e., $Eu/Eu^* = Eu_N / \sqrt{[Sm_N \cdot Gd_N]}$.

The REE patterns of the granitoid rocks also show steeper pattern and highly fractionated trend. It is enriched in LREE and depleted in HREE

and show moderate and large anomalies. In the same figure, one sample of KGG (granite gneiss) show almost flat pattern with large negative Eu anomaly and enriched HREE due to the presence of accessories phase as zircon and apatite concentration. This flat pattern of HREE in the KGG might have resulted due to the presence of ample apatite that are entrapped within large feldspar grains. The increase of size of negative Eu anomalies indicates the rock is highly evolved during differentiation processes.

From the above discussion, the Katekalyan granitoid (KBG, KTG and KGG) representing the product of peraluminous melt generated by the partial melting of somewhat heterogeneous older crustal rocks perhaps the quartz- feldspathic psammopelitic composition with the over saturation of Al_2O_3 as indicated by high normative corundum value, is being well comparable with those for S-type granitoid of White and Chappel (1988). The influence of the alkali concentration (and temperature) of the solubility of SnO_2 in melts are less apparent in peraluminous magmas. However, changes in the dominant alkali component of peraluminous melts (from Na in albite-quartz melts to K in K-feldspar quartz melts) can be responsible for significant variations in the solubility of SnO_2 in the melts. Since the solubility of SnO_2 in albite-quartz melts increases far more rapidly with decreasing $f\text{O}_2$ than in K-feldspar-quartz (or haplogranite) melts. It is clear that the incorporation of Sn^{2+} into melts is more strongly influenced by the presence of Na than K. The significant changes in measure in trace element towards more leucocratic granitoids (KBG and KTG) with inverse relationship between felsic and mafic constituents and also evident by the relative enhancement in SiO_2 , K_2O and Rb as well as Rb/Sr ratio and decrease in FeO^* , MgO , CaO , TiO_2 , Sr and Zr from granite gneisses (KGG) to granite (KBG and KTG) indicate the fractional crystallization processes with the initial crystallization of biotite and plagioclase followed by muscovite, quartz and K-feldspar. The geochemical data, shows very clearly that the decrease in REE content with enhanced SiO_2 , moderate $\Sigma\text{LREE}/\Sigma\text{HREE}$ ratio (av. 17.45) and more pronounced negative Eu anomalies (av. 0.85) are also support the fractional crystallization processes.

It is impossible to establish the chronology of inclusion entrapment due to repeated fracturing and healing accompany quartz deposition which have resulted into complex distribution of inclusions.

Fluid inclusion microthermometric studies of cassiterite reveal the presence of monophasic carbonic (CO_2 inclusion), aqueous-carbonic biphasic (CO_2 - H_2O), triphasic (H_2O - NaCl -Halite) and H_2O - NaCl biphasic inclusions. The fluid inclusions data provides an understanding of the circulation of mineralizing fluids from magmatic to hydrothermal within the fracture zones of the rocks is common in the study area.

Tin formation was the result of the mixing of (dominant magmatic fluid with meteoric fluid. Meteoric fluid equilibrated with igneous rocks under low water/ rock ratio. Thus it can be concluded that tin mineralisation in Katekalyan was deposited from the low to high salinity (2.63 to 40 wt% NaCl equivalent) and CO_2 rich complex fluid derived from the post magmatic granitic melt at the temperature between 360 to 410 $^{\circ}\text{C}$ and pressure ranges from 2.1 to 3.1 Kbars. This estimated pressure range corresponds to 8 to 15 km, assuming a purely lithospheric regime.

The granite (KG) and granite gneiss (KGG) have been plotted in $\text{FeO}^{\text{tot}}/\text{FeO}^{\text{tot}} + \text{MgO}$ vs SiO_2 diagram Frost *et al.* (2001), which suggest that the KG is typically magnesian except a few one whereas KGG has affinity with ferroan type except one sample, which is much depleted in $\text{FeO}^{\text{tot}}/\text{FeO}^{\text{tot}} + \text{MgO}$ ratio. The magnesian and ferroan-differentiated series of granitoids are indeed equivalent to tholeiitic and calc-alkalic magma types respectively as originally discriminated by Miyashiro (1974). However, a little overlapping in the fields of magnesian and ferroan have been noted towards high silica content of rocks which is more likely related to the late stage compositional evolution of granitoids during their differentiation. Whatsoever the reason may be but KG is apparently distinct from KGG but both have experienced different degree of chemical differentiation in different episodes. It is more likely that the magnesian enrichment trend of KG may be responsible for tin mineralisation in the study area. Modified alkali-lime index (MALI) plotted against K_2O percentage show compositionally affinity of KGG with Mesozoic

Cordilleran granitoids, though scattered calcic to calc-alkaline. The alumina saturation index, ASI ($= A/Na + K + Ca - 1.67 \times P$) proposed by Frost *et al*, (2001) takes into account of apatite also and ASI greater than 1.0 is considered peraluminous has been noted for most KG (ASI= 0.99 – 2.17) and KGG (ASI= 1.19 – 1.82). Magnesian and peraluminous for KG and ferroan and peraluminous for KGG can be very well suggested.

Several lines of field petrographic and bulk geochemistry of KG, KGG and pegmatites (KP) reveal that stanniferous peraluminous KG and KGG granitic melt originated from the crustal anatexis i.e. partial melting of crustal source. The partial melting model shows that the variation of KG as well as KGG can be explained by varying degree of partial melting (5 to 50%) of bulk continental crust but bulk distribution coefficient for Sr (D_{Sr}) must be low i.e. $\ll 10$. In this context the anorthite content of feldspar is very sensitive to determine the distribution coefficient of Sr, therefore, a small changing D_{Sr} will shift the vertical trend of partial melting of source towards higher and lower sides of Sr content. The result of partial melting modeling at least suggests that the differentiation of KG and KGG melt is more governed by partial melting of bulk crust rather than fractional crystallization. The estimates upper limit of partial melting i.e. 50% of bulk crust noted for KG and KGG are consistent with required rheological, critical melt percentage to leave the source region has decreased granite melt which were capable to mineralised tin ore elements.

In the study area, three types of pegmatite with the different phases viz., simple unzoned, recrystallized (granitic pegmatite) and metasomatic pegmatites (greisenised and albitised pegmatites) are found emplaced within the pre-existing rocks of metabasic intrusive (MBI), granite (KG), granite gneiss (KGG) and also rarely metasediments as mineralised and non-mineralised characters along the fractures and foliation planes trending N-S, E-W and more frequently are observed NNW-SSE trends.

Those pegmatites emplaced in Bengapal metasediments (ASS), are generally unzoned, non-greisenised, simple albitic to graphic and practically devoid of noticeable cassiterite mineralisation. It is interesting to noted that

the emplacement of mineralised pegmatites is more frequent in metabasic intrusive (MBI), granite (KG) and granite gneiss (KGG) than the Bengpal metasediments (ASS). The recrystallised unzoned pegmatites (granite pegmatites) appear to have formed along the shear and fracture planes in granites due to recrystallization of granite by autometasomatic process within the granite. The metasomatic pegmatites (greisenised and albitised pegmatites) are found mainly in metabasics (MBI) and biotite granites (KBG) with the highly concentration of tin mineralising nature in the study area. The mineral assemblages in these pegmatites are represented by quartz, K-feldspar, plagioclase (albite and cleavelandite), mica (also lithium mica), fluorite, apatite, beryl, cassiterite, garnet and columbite-tantalite etc. The cleavelandite variety of albite is believed to have been formed due to metasomatic activity of sodium bearing vapours during the emplacement of the pegmatites. So the presence of cleavelandite is strong support in favour of soda-metasomatism in the pegmatites. There is presence of fluorite in the mineralised pegmatites, also supported the fluorine rich magma source of granitic composition which reflects that differentiation processes was involved for the segregation of above minerals. The association of smoky quartz within pegmatite veins suggests that the mineralisation was accompanied by most probably radioactive emanations from the granitic melt.

On the basis of the association of cassiterite, lithium mica (lepidolite) and fluorite in the pegmatites, it may be possible that the tin was transported in the gaseous stage as SnF_4 or SnCl_4 and precipitate with the addition of water mainly in the condition of aqueous volatile solutions. The above fluid SnF_4 or SnCl_4 can move in vapour phase to apical regions of intrusive where they reacted with wall rocks and are hydrolysed to give cassiterite. It is interesting to noting that the SnF_4 and SnCl_4 probably not stable in presence of water under geologically reasonable conditions.

From the above observations, the nature and intensities of mineralogical changes in the granitic rocks by the metasomatic processes (volatile rich fluids), it reflects the successive phases of volatile rich hydrothermal fluids, derived from the parent magma, had interacted with the

host rocks. The presence of pegmatites of the different phase in the study area reflects the volatile and aqueous rich phase co-existing with residual granitic magma. The continued fractional crystallisation causes enrichment in volatiles and incompatible elements in the last rest melt. The efficiency of enrichment of incompatible elements is critically dependent on the degree of separation of melts from solids throughout crystallisation. When the vapour pressure rises during the late stage of cooling of the parent magma and it results into fracturing in the plutons and emplacement of the residual melt produced in the different successive phases of the magmatic evolution.

The alteration zones of the study area are very narrow. The apical zones of tin-bearing granitoids are sites of intense and complex metasomatic activity with the transportation of tin ions leading to the formation of discrete crystals of cassiterite. Source of the alteration solutions is highly debated.

REFERENCES

- Acharya, S.K. and Roy, A. (2000): Tectonothermal history of the Central Indian tectonic zone and reactivation of major fault/shear zones. *Jour. Geo. Soc. Ind;* 55, pp239-256
- Acharya, S; Sarangi, S.K.; and Das, N.K. (1982): The tin ore deposit of Orissa, India Ore-Genesis – The state of the arts Eds: Amstutz, G.C., et al. *Springer-Verlag Berlin Heidelberg*.
- Aktanov, M.T. (1971): Behaviour of tin in postmagmatic alteration of granitoids of Southern Tien Shan (Southern Kirghigiya). *Geochemistry International*, 8: 367-370.
- Anon (1978a): New age data by $K^{40} - Ar^{40}$ method. *Geol. Sur. India, News*, 9:3.
- Aranyakanon, P. (1970): Tin deposits in Thailand. *Second Tech. Conf. On Tin, 1960. ITC*, 83-102.
- Babu, T.M. (1979): Regional assessment of cassiterite and associated rare minerals in colluvial horizons of Kudripal and Jangarpal blocks, Bastar district, Madhya Pradesh (F.S. 1978-79), *Geol. Surv. India, Unpub. Report*.
- Babu, T.M. (1983): Different phases of tin, niobium and tantalum mineralization in Bastar district, M.P. Workshop of mineralisation associated with acid magmatism, IGCP-26 [MAWAM] under IUGS, UNESCO, *Geol. Surv. India, Spl. Publ. No. 13*, pp. 77-80.
- Babu, T.M. (1990): Metallogeny of tin in Bastar craton, Central India, Seminar on Evolution of Precambrian Crust in India. Abs. Volume, *Geol. Surv. India, Publn. Sec. 5*. pp. 64.
- Babu, T.M. (1993): Comparative Studies of Tin Granitic Rocks in Space and Time, *Resource Geology*, V. 43(5), pp. 355-363.

- Ball, V. (1877): On the geology of the Mahanadi basin and its vicinity. *Rec. Geol. Surv. India*, V. 10, pp. 167-186.
- Balasundaram, M.S. and Balasubramanyan, M.N. (1973): Geochronology of the Indian Precambrian. *Geol. Soc. Malaysia Bull.* 6, pp. 213-226.
- Balasubramanyam, M.N. (1983): Chronology of mineralisation episodes associated with acid magmatism in India - A review. Mineralisation Associated with Acid Magmatism. *Geol. Surv. India, Spl. Pub. No. 13*, pp. 31-36.
- Bandyopadhyay, B.K., Bhoskar, K.G., Ramachandra, H.M., Roy, A., Khadse, V.K., Mohan, M., Sreeramachandra Rao, K., Ray Barman, T., Bishui, P.K., Gupta, S.N. (1990): Recent geochronological studies in parts of Precambrian of Central India, *Geol. Surv. India. Spl. Publ. 28*, pp. 199-210.
- Barsukov, V.L. (1957): The Geochemistry of tin. *Geochemistry International*, V. 1, pp. 41-51.
- Barsukov, V.L. (1967): Source of ore substance of tin deposits. Symp. of the international association on genesis of ore deposits. *Abstracted Transactions of the Inst. of Mining and Metallurgy, Sec. B. Applied Earth, Science*, V. 76, pp. 220.
- Barsukov, V.L. (1964): On the Metallogenic Specialisation of Granitic Intrusions - Volume II, Moscow Izd-VOAN U.S.S.R.
- Barsukov, L.V. and Volosov, A.G. (1968): New approach to geochemical prospecting for mineralisation located deep below the surface. *Geologiya Rudnykh Mestorozheniy. (Academy of sciences of the U.S.S.R., November-December 1968) 10(6): 3-9. English Abstract: Chemical Abstracts 70(1969) 117.027a.*
- Batchelor, R.A. and Bowden, P. (1985): Petrogenetic interpretation of granitoid rock series using multicationic parameters. *Chem. Geol.*, V. 48, pp. 43-55.

- Beckinsole, R.D.; Drury, S.A. and Holt, R.W. (1980): 3360 Myr. Old Gneisses from South Indian Craton, *Nature (London)*, V. 283, pp. 469-470.
- Beus, A. (1976): Mission report of Alexie A. Beus Technical Adviser, Minerals Sec. Energy and Mineral Development Branch, New York, *CNRET/ESA 6-11-Dec. 1975, UNDP Unpub. Report.*
- Beus, A.A. and Zalashkova, N.Ye. (1964): Post magmatic high temperature metasomatic process in granitic rocks. *International Geological Review*, 6:668-681.
- Bhowmik, S.K., Pal, T. Roy, A. and Pant N.C. (1999): Evidence for Pre-Grenvillian High-Pressure Granulite Metamorphism from the Northern Margin of the Sausar Mobile Belt in Central India, *Jour. Geol. Soc. Ind.* 53, pp. 385-399.
- Blevin, P.L. and Chappel.B.W. (1995): Chemistry, origin and evolution of mineralized granites in the Lachlan Fold Belt, Australia: The metallogeny of I- and S-Type granites. *Econ.Geol.* v.90, pp. 1604-1619.
- Bose, S.K. *et al.* (1979): Tin mineralisation in Bastar district. Madhya Pradesh. *Proc. Int. Sym. on Resour. Engg. and Tech., Vol. II, Sect. 4 II*, pp. 1-14.
- Chappel S.W. and White, A.J.R. (1974): Two contrasting granite types. *Pacific Geology*, v. 8, pp. 173-174.
- Charoy, B. (1986): The genesis of the Cornubian batholith (South West England): The example of the Carnmenellis pluton. *J. Petrol.*, 27, pp. 571-604.
- Chatterjee, A. (1970): Structures, tectonics and metamorphism in a part of South Bastar, M.P.Q.J. *Geol. Min. Met. Soc. Ind.*, v. 42, pp. 75-95.
- Chaudhary, A; Mukhopadhyay, P.K. and Yedekar, D.B.(1994): Petrology and Petrochemistry of the volcanic suites in the Precambrian Dongargarh Supergroup, Central India, *Geol. Surv. Ind. Unpub. Rep.* 52p.

- Church, S.E. (1981): Multielement analysis of 54 geochemical reference samples using inductively coupled plasma atomic emission spectrometry. *Geostandard Newsletter*, v. 5, pp. 133.
- Cleg, E.L.G. (1944): Notes on Tin and Wolfrum with description of tin and wolfram deposits in Burma and India, *Rec. Geol. Surv. Ind. Bull.* 76(15), 1-168.
- Clemen, J.D. (1989): The importance of residual source material (restite) in granite petrogenesis; A Comment. *Jour. Petrology* v. 30, pp.-1313-1316.
- Condie, K.C. (1973): Archaean magmatism and crustal thickening, *Geol. Soc. Am. Bull.* v. 84, pp. 2981-2992.
- Condie, K.C. (1981): Archaean Greenstone Belts, *Elsevier, Amsterdam*, 434 p.
- Crawford, A.R. (1970): The Precambrian geochronology of Rajasthan and Bundelkhand, Northern India. *Can. J. Earth Sci.*, v. 7, pp. 91-110.
- Crock, J.J., Lichte, F.E., Riddle, G.O. and Beech, C.L. (1986): Separation and preconcentration of the rare earth elements and yttrium from geological materials by ion exchange and sequential acid elution. *Talanta*, v. 33, No. 7, pp. 601-606.
- Crookshank, H. (1938b): Iron ores of Bailadilla range, *Trans. Min. Geol. Met. Inst. India*, v. 34(3), pp. 254-281.
- Crookshank, H. (1963): Geology of Southern Bastar and Jeypore from Bailadilla range to the Eastern Ghats, *Geol. Surv. India, Memoir* 87, 149 p.
- Daubree (1841): Memoir sur is gisement, la constitution at 1' origine des amas de minerai detain. *Analos des Mines, 3.e Serie, t. XX*, 65-112.
- Debon, F. and Le Fort, P. (1982): A chemical - mineralogical classification of common plutonic rocks and associations. *Trans. Royal Soc. Edinburg, (Earth Sci.)*, v. 73, pp. 135-149.

- Debon, F., Sheppard, S.M.F. and Sonet, J. (1986): The four plutonic belts of the Transhimalaya-Himalaya: A chemical, mineralogical, isotopic and chronological synthesis along a Tibet-Nepal section. *Jour. Petrol.* v. 27, pp. 219-250.
- De La Roche, H., Leterrier, P., Grandclaude, P. and Marchal, M. (1980): A classification of volcanic and plutonic rocks using R_1 - R_2 diagrams and major element analyses - its relationship with current nomenclature. *Chem. Geol.*, v. 29, pp. 183-210.
- Despande, M.L. (1975a): Note on the prospects and exploration of the cassiterite-lepidolite bearing pegmatites in Sukma Sub-Tahsil, Bastar district, M.P. *Unpub. Rep. Geol. Surv. India*.
- Despande, M.L. and Bose, S.K. (1979): Mineralisation associated with granite and pegmatites in India - *Guidelines for future work. Ind. Minerals*, V. 33, pp. 1-18.
- Dhoundial, D.P., Paul, D.K., Amitabha Sarkar, Trivedi, J.R., Copalan, K. and Potts, P.J. (1987): Geochronology and Geochemistry of Precambrian granitic rocks of Goa, SW India. *Precamb. Res.*, v. 36, pp. 287-302.
- Didier, I., Duthou, J.L. and Laymere, J. (1982): Mantle and crustal granites: genetic classification of orogenic granites and the nature of their enclaves. *Jour. Volcanol. Geotherm. Res.*, v. 14, pp. 169-186.
- Dmitriyev, L.V., Barsukov, V.L. and Dura Sova, N.A. (1968) : Change in paragenesis as a factor in the distribution and mobilisation of one elements in granites, *Geochemistry International*, v. 5, pp. 268-270.
- Drabek, M. and Stemprok, M. (1974) : The system Sn-S-O and its geological application. *Neues Jahrbuch für Mineralogie Abhandlungen*, v. 122, No. 1, pp. 90-118.
- Durasova, N.A. (1967) : Some problems of the geochemistry of tin. *Geochemistry International*, v. 4, pp. 671-681.

- Dutta, S.M., Mishra, V.P., Dutta, N.K. and Pandhare, S.A. (1981): Precambrian Geology of a part of Narainpur and Kondagaon tahsils, Bastar district, with special reference to Rowghat iron ore deposit. *Spec. Publ. Geol. Surv. Ind.*, No. 3, pp. 55-67.
- El Bouseilly, A.M. and El Sokkary, A.A. (1975): The relation between Rb, Ba and Sr in granitic rocks. *Chem. Geol.*, v. 16, pp. 207-219.
- Evans, A.M. (1980): Introduction to ore geology. *Geoscience texts. Black Well Scientific Publn.* v. 2.
- Evensen, N.M., Hamilton, P.J. and O'Nions, R.K. (1978): Rare earth abundances in chondritic meteorites. *Geochim. Acta* 42, pp. 1199-1212.
- Fermor, L.L. (1935): General Report for the year 1933. *Rec. Geol. Surv. Ind.*, v. 68. Pt. 1, pp. 85-88.
- Fermor, L.L. and Kellerschön (1909): Notes on the mining section of the Central Province and Berar exhibition, 1908, *Trans. Mining Geol. Inst. India*, v. 4(2), pp. 115.
- Frost R. B., Bornes C. G., Colling W. J., Arculus R. J., Ellis D. J. and Frost C. D. (2001): A Geochemical classification for granitic rocks. *Jour. Petrology*, v-42, pp. 2033-2048
- Garrels, R.M. and Mackenzie, F.T. (1971): Evolution of sedimentary rocks, W.W. Norton, New York, 394 p.
- Gasparon, M., Inuocentri, F., Hanneti, P., Peccerillo, A. and Tsegaye, A. (1993): Genesis of the Pliocene to Recent bimodal mafic-felsic volcanism in the Debrezeit area, Central Ethiopia: Volcanological and Geochemical constraints. *JOUR> African. Earth Sci.*, vol. 17, pp. 145-165.
- Ghosh, P.K. (1941): The charnockite series of Bastar State and Western Jeypore. *Geol. Surv. Ind. Rec.*, v. 75, Paper No. 15, pp. 55.
- Ginzburg, L.N., et al. (1972) : Genetic types of tantalum ore deposits and their economic importance. Review-14, No. 7, International Geological Review.

- Goldschmidt, V.M. (1954): *Geochemistry*, Carendon, Press, Oxford, pp. 730.
- Govindaraju, K. (1989): Compilation of working values and sample description for 272 geostandards. *Geostand. Newsletter*, v. 13, Special issue, pp. 1-113.
- Govindaraju, K. and Mevelle, G. (1987): Fully automated dissolution and separation methods for inductively coupled plasma atomic emission spectrometry rock analysis. Application to the determination of rare earth elements. *Jour. of Analytical Atomic Emission Spectrometry*, v. 2, No. 1, pp. 615-621.
- Groves, D.I. and McCarthy (1978): Fractional crystallization and the origin of tin deposits in granitoids, *Mineralium Deposita*, v. 13, pp. 11-26.
- Guha, R. and Raychowdhury, (1983): X-ray investigation of Bastar casiterite. *Geol. Surv. India. Spl. Pub. No. 13*, pp. 115-116.
- Haack, U.K. (1969): Trace elements in biotites from granites and gneisses. *Contributions to Mineralogy & Petrology*, v. 22, pp. 83-126.
- Haapla, (1988): Metallogeny of the Proterozoic rapakivi granites of Finland. In: Taylor, R.P. and Strong, D.F. (eds.). Recent advances in the Geology of granite – Related mineral Deposits, *Can. Inst. Mining Metall. Spec. v. 39*, pp. 124-132.
- Hanson, G.N. (1980): Rare earth elements in petrogenetic studies of igneous rocks. *Ann. Rev. Earth Planet. Sci.*, 8, pp. 371-406.
- Harker, A. (1909): The natural history of igneous rocks. Methuen, London, pp. 384.
- Harpum, J.R. (1963): Petrographic classification of granitic rocks by partial chemical analysis. *Tanganyika Geol. Surv. Rep.*, v. 10, pp. 80-86.
- Harries, N.B.W., Pearce, J.A. and Tindle, A.G. (1986): Geochemical characteristics of collision-zone magmatism. In: Coward, M.P. and Ries, A.C. (Eds.) *Collision Tectonics, Blackwell Scientific Publication 19, London*, pp. 67-82.
- Heron, A.M. (1937): General Report for 1935. *Rec. Geol. Surv. Ind.*, v. 71, Pt. 1, pp. 86-89.

- Heron, A.M. (1938): General Report for 1937. *Rec. Geol. Surv. Ind.*, v. 73, Pt. 1, pp. 101-102.
- Hesp, W.R. (1975): Aspects of tin metallogenesis in the Tasman geosyncline, Eastern Australia, as reflected by cluster and factor analyses. *Jour. Geoche. Expln.* v. 4, pp. 331-347.
- Hesp, W.R. and Rigby, D. (1972): The transpect of tin in acid igneous rocks, *Pacific Geology*, v. 4, pp. 135-152.
- Hosking, K.F.G. (1965a-c): The search for tin: *Mining Mag.*, v. 113, pp. 261-273, 368-383, 448-461.
- Hosking, K.F.G. (1977) : Known relationships between the hard rock tin deposits and the granites of South East Asia. *Bull. Geol. Soc. Mal.* 9, pp. 141-157.
- Hunter, D.R. (1974): Crustal development in Kaapvaal Craton, I – the Archean, *Precambrian Res.*, v. 1, pp. 259-294.
- Hutchison, C.S. (1977): Granite emplacement and tectonic subdivision of Peninsular Malaysia. *Bull. Geol. Soc. Mal.* 9, pp. 187-297.
- Hutchison, C.S. and Chakraborty, K.R. (1979): Tin: a mantle or crustal source? *Geol. Soc. Malaysia Bull.* v. 11, pp. 71-79.
- Imeokparia, E.G. (1985): Rare metal mineralisation in granitic rocks of the Tongolo Anorogenic complex – Northern Nigeria. *Mineralum Deposita*, v. 20, pp. 81-88.
- Irvine, T.N. and Baragar, W.R.A. (1971): A guide to the chemical classification of the common volcanic rocks. *Canad. Jour. Earth, Sci.*, v. 8, pp. 523-548.
- Ishihara, S., (1977): The magnetite-series and ilmenite series granitic rocks. *Mining Geology* 27, 293-305.
- Iyengar, S.V.P., Chandy, K.C. and Narayanaswamy, R. (1981): Geo-chronology and Rb-Sr systematics of the igneous rocks of Simlipal complex, Orissa, *Ind. Jour. Earth Sci.*, v. 8(1), pp. 61-65.

- Jarvis, K.E. and Jarvis, I. (1988): Determination of the rare earth elements and yttrium in 37 International silicate reference materials by inductively coupled plasma atomic emission spectrometry. *Geostandard Newsletter*, v. 12, pp. 1-12.
- Jahns, R.H. and Burnham, C.W. (1969): Experimental studies of pegmatite genesis: I. a model for the derivation and crystallization of granitic pegmatites. *Econ. Geol.*, 64, 843-864.
- Jingwen, M. (1989) The igneous rock series and tin polymetallic minerogenetic series in the Tengchong area, Yunnan. *Acta, Geol. Sinica*, v- 2 pp. 175-187
- Kanasiewicz, J.S., Purkar, P.M. and Srivastava, C.H. (1980b): Report on exploration and preliminary evaluation of the Govindpal and Chitalnar tin primary and colluvial-deluvial placer deposits, Bastar area, *Madhya Pradesh State Geology and Mining with U.N.D.P. collaboration. Unpub. Report.*
- Kelly, W.C. and Turneure, F.S. (1970): Mineralogy, paragenesis and geothermometry of the tin and tungsten deposits of the Eastern Andes, *Bolivia Econ. Geol.*, 65, 609-680.
- King, W. (1881): The geology of Pranhita Godavari Valley, *Memoir Geol. Surv. India*, v. 18, pt. 3.
- Krishnamurthy, P., Chaki, A., Pandey, B.K., Chimote, J.S. and Singh, S.N. (1988): Geochronology of the granitic-rhyolite suites of the Dongargarh supergroup, Central India, *IV National Symp. Mass Spec. (Extended Abs.), Preprint Vol.*, pp. Eps. 2/1- Eps. 2/5.
- Lamba, V.J.S. and Agarkar, P.S. (1988): The tin potential of Precambrian rare metal bearing pegmatites of Bastar district, M.P., India. *Mineralium Deposita*, v. 23, pp. 218-221.
- Lehmann, B. (1982): Metallogeny of tin: Magmatic differentiation versus geochemical heritage. *Econ. Geol.* 77. 50-59
- LeMaitre, R.W. (1989): A classification of igneous rocks and glossary of terms. *Blackwell, Oxford*, 193 p.

- Linnen, R.L. and Williams-Jones, A.E. (1993): Mineralogical constraints on magmatic and hydrothermal Sn-W-Ta-Nb mineralisation at the Nong-Sua aplite-pegmatite deposit. *Eur. J. Mineral.* 5, 721-736.
- Luth, W.C. (1976) : Granitic rocks. In: Bailey, D.K. and McDonald, R. (eds.). The evolution of the crystalline rocks. *Academic Press, London*, pp. 335-417.
- Manning, D.A.C., Hamilton, D.L., Henderson, C.M.B. and Dempsey, M.J. (1980) : The probable occurrence of interstitial Al in hydrous, F-bearing and F-free aluminosilicate melts. *Contrib. Mineral. Petrol. Springer-Verlag*, v. 75, pp. 257-262.
- Maniar, P.D. and Piccoli, P.M. (1989): Tectonic discrimination of granitoids. *Geol. Soc. Am. Bull.* v. 101, pp. 635-643.
- McCarthy, T.S. and Kable, E.J.D. (1978): On the behaviour of rare-earth elements during partial melting of granitic rock. *Chem. Geol.*, 22, 21-29.
- McClelland, J. (1849): Progress report for the field season, 1848-49. *Geol. Surv. India, Unpub. Report*.
- Middlemost, E.A.K. (1985): The potassic rocks, their nomenclature, origin and evolution with examples from Australia. *IAVCET Scientific Assembly Abst.*
- Mishra V.P., Dutta N.K., Kanchan V.K., Vatsa U.S. and Guha K. (1984): Archaean granulite and granite gneiss complexes of Kondagaon area, Bastar district, M.P. *Rec. Geol. Surv. Ind.*, vol. 113, pt. 6, pp. 150-158.
- Mishra, V.P., Pushakar Singh and Dutta, N.K. 1988): Stratigraphy, structure and metamorphic history of Bastar craton, *Rec. Geol. Surv. Ind.*, vol. 117, Pts. 3 to 9, pp. 1-26.
- Moorbath, S., Taylor, P.N. and Jones, N.W. (1986): Dating the oldest terrestrial rocks – Facts and Fiction. *Chem. Geol.*, v. 57, pp. 63-86.

- Mukerjee, N.K. (1975): A preliminary study of tin mineralisation in Bihar pegmatites, Chakrabandah region, District Gaya, India. *Fortschritte der Mineralogie*, v. 52, pp. 317-328.
- Mukerjee, N.K. and Rai, D. (1978): The position of tin prospects of India. *Third Regional conference in Geology and Mining. Res. of SE Asia, Thailand, 14-18 Nov.*
- Murthy, K.S., Jaiswar, H.P. and Jesani, R.S. (1979): Geology in relation to tin mineralisation in Bastar District, M.P. Presented at the Workshop on mineralisation associated with acid magmatism, Nagpur, *Geol. Surv. India. Spl. Publ., No. 13*, pp. 61-70.
- Nag, D.C. (1929): On the occurrence of a tin-tungsten deposit in Gaya, Bihar and Orissa. *Quart. Jour. Geol. Min. Met. Soc. India*, vol. 2, No. 1.
- Naski, G.C. and Hess, P.C. (1985): SnO solubility: Experimental results in peraluminous and peralkaline high silica glasses (abs.) *EOS*, v. 66, pp. 412.
- Nedaskovskii, P.G. and Narnov, G.A. (1968): Tin distribution in tin bearing granites apo-granites and replaced pegmatites on the Soviet Far East. *Geochemistry International*, v. 5, pp. 687-695.
- Norman, M.D., Leeman, W.P. and Mertzman, S.A. (1992) : Granites and rhyolites from the northern U.S.A. : temporal variation in magmatic processes and relations to tectonic setting. In: Brown, P.E. and Chappel, B.W. (Eds.) *Proc. 11th Hutton Symposium on the origin of granites and related rocks; Geol. Soc. Am. Spl. Pap.*, v. 272, pp. 71-81.
- O'Connor, J.J. (1965): A classification for the quartz-rich igneous rocks based on feldspar ratios. *U.S. Geol. Surv. Prof. Pap.*, pp. 525.
- Pandey, B.K., Prasad, R.N., Veena Krishna, Sagar, S., Gupta, J.N. and Saraswat, A.C. (1989): Early proterozoic Rb-Sr isochron ages for the granitic rocks from parts of Koraput District, Orissa, India, *Ind. Minerals*, v. 43 (3 and 4), pp. 273-278.

- Pearce, J., Harris, N.B.W. and Tindle, A.G. (1984) : Trace element discrimination diagrams for the tectonic interpretation of granitic rocks. *Jour. Petrol*, v. 25, pp. 956-983.
- Pitcher, W.S. (1982): Granite type and tectonic environment. In: K.J. Hsc (ed.) Mountain building processes, *Academic Press, London*, pp. 19-40.
- Pitakpaivan, K. (1969): Tin-bearing granites in Thailand. Second Tech. Conf. on Tin I.T.C., London, pp. 283-298.
- Pitchavant, M. and Manning, D. (1984): Petrogenesis of tourmaline granites and topaz granites. The contribution of experimental data. *Phys. Earth. Planet. Inter.*, v. 35, pp. 31-50.
- Plimer, I.R. (1987): Fundamental parameters for the formation of granite-related tin deposits. *Geol. Rundschau*, 76, 23-40.
- Radhakrishna, B.P. (1989): Suspect tectonostratigraphic Terrain Elements in the Indian subcontinent. *J. Geol. Soc. Ind.*, v. 34(1), pp. 1-24.
- Radhakrishnan, B.P. and Naqvi, S.M. (1986): Precambrian continental crust of India and its evolution. *J. Geol.*, vol. 94, pp. 145-166.
- Rajesham, T.; Rao, B. Y. J. and Murti, K. S. (1993): The Karimnagar Granulite Terrane- A new Sapphirine bearing Granulite Province, South India. *Jour. Geol. Surv. Ind.*; 41, pp 51-59.
- Rajurkar, S.T., Bhate, V.D. and Sharma, S.B. (1990): Lineament fabric of Madhya Pradesh and Maharashtra and its techonic significance. Spl. Publ. No. 28, Nagpur, Aug., 1990, pp. 241-259.
- Ramachandra, H. M. (1999): Petrology of the Bhandara – Balaghat granulite belt in parts of Maharashtra and Madhya Predesh. *Geol Sur. Ind. Unpub. Rep.*
- Ramachandra, H. M.; Mishra V. P., Roy, A. and Dutta, N. K. (1998): Evolution of the Bastar Craton- A critical review of gneiss- granitoids and supracrustal belts (Abs.) *M. S. Krishnan Centenary Commemorative National Seminar*; Calcutta, pp. 144-150

- Ramakrishnan, M. (1969a): Preliminary investigation of the known andalusite occurrences in the Netapur-Kuhasras area, Bastar district, Madhya Pradesh, *Unpub. Prog. Rept. Geol. Surv. Ind.* (F.S. 1968-69).
- Ramachandra, H. M. and Roy, A. (1998): Geology of intrusive granitoids with particular reference to Dongargarh granite and their impact on tectonic evolution of the Precambrian in Central India. *Ind. Min.*; 52 (1 and 2) pp. 15-33.
- Ramachandra, H. M., Roy, A., Mishra, V. P. and Dutta, N. K. (2001): A Critical review of the tectonothermal evolution of the Bastar Craton. *Geol. Surv. Ind. Spl. Publ. no. 55* pp.161-180
- Ramakrishnan, M. (1973): Facies series in the polymetamorphic complex of Southern Bastar, Madhya Pradesh. *Symposium on Peninsular Shield, Hyderabad*, pp. 13-14 (Abs.).
- Ramakrishnan, M. (1990): Crustal development in Southern Bastar, Central Indian Craton, *Geol. Surv. Ind. Spl. Publ., No. 28*, pp. 44-46.
- Ramaswamy, C., Deshpande, M.L., Murti, K.S., Jaiswar, H.P. and Jesani, R.S. (1981): Tin-bearing pegmatites from Bastar, M.P. *Geol. Surv. Ind. Spl. Pub. No. 3*, pp. 185-189.
- Ramdohr, P. (1969): The ore minerals and their intergrowths", *Pergamon Press, New York, Braunschweig*, pp. 1174.
- Ramesh Babu, P.V., Dwivedi, K.K. and Jayaram, K.M.V. (1984): Geochemistry of tin-rich granites of Paliam & Darba, Bastar, M.P. *Proc. Fifth Ind. Geol. Congress, Bombay, 1984*, pp. 313-319.
- Ramesh Babu, P.V., Pandey, B.K. and Dhana Raju, R. (1993): Rb-Sr ages on the granite and Pegmatitic minerals from Bastar-Koraput Pegmatite Belt, M.P. and Orissa, India. *Jour. Geol. Soc. India*, v. 42, pp. 33-38.
- Rankama, K. and Sahama, Th.G. (1950): Geochemistry: *The Univ. of Chicago Press, Chicago, Illinois, U.S.A.*

- Rao, G. V. (1981): Sausar Group: Distribution and correlation. *Geol. Surv. Ind. Spl. Pub* 3, pp. 1-7.
- Rathi, M.S., Khanna, P.P., Mukherjee, P.K., Purohit, K.K. and Saini, N.K. (1994): Working values for major, minor and trace elements for meta-basic reference sample (MB-H). *Jour. Geol. Soc. India*, v. 43, No. 3, pp. 295-303.
- Ray, Burman, T., Bhanumati, L., Biswi, P.K. and Gupta, S.N. (1982): Thermo-chronometric implications of isotopic data from Bastar district, M.P. *Geol. Surv. India. Unpub. Report*.
- Roedder, E. (1979): Silicate liquid immiscibility in magmas. In: Yoder, H.S. (ed.). *The Evolution of the Igneous Rocks, Fiftieth Anniversary Perspectives, Princeton University Press*, 15-57.
- Roedder, E. (1984): Fluid Inclusions; *Review in Mineralogy*, 12, 644 pp. *Mineralogical Society of America*.
- Rogers, John, J. W. (1993): India and Ur, *Journ. Of Geol. Soc. of Ind.*, v. 42, pp. 217-222.
- Roy, A.; Bandyopadhyay, B. K.; Huin, A. K.; Mony Charles, D. and Saha, A. K. (1995): Geology of the Sakoli Fold Belt Nagpur, Bhandara and Gadchiroli district, Maharashtra, Central India. *Geol. Surv. Ind.unplb. Rep.*
- Sarang, S.K. and Das, N.K. (1977): Tin prospecting in South Orissa. A case study. *Prelim. report, D.G.M., Orissa, Bhubaneswar*.
- Sarkar, A., Sarkar, G., Paul, D.K. and Mitra, N.D. (1990): Precambrian geochronology of the Central Indian Shield – review. *Geol. Surv. India, Spl. Pub. 28*, pp. 453-482.
- Sarkar, S.N., Gerling, E.K., Polkanov, A.A. and Chukrov, F.V. (1967): Precambrian Geochronology of Nagpur-Bhandara-Durg, India. *Geological Magazine*, v. 104(6), pp. 525-549.
- Sarkar, S.N., Gopalan, K. and Trivedi, J.R. (1981): New data on the geochronology of the Precambrians of Bhandara-Durg, Central India, *Ind. Jour. Earth Sci.*, V. 8, pp. 131-151.

- Sarkar, G. and Gupta, S.N. (1989): Dating of early Precambrian granite complex of Bastar district, Madhya Pradesh, *Rec. Geol. Surv. Ind.*, v. 122, pt. 2, pp. 22-30.
- Sarkar, G., Paul, D.K., McNaughton, N.J., De Laeter, J.R. and Misra, V.P. (1990): A geochemical and Pb, Sr isotopic study of the evolution of granite gneisses from Bastar Craton, Central India. *Jour. Geol. Soc. India*, v. 35(5), pp. 480-496.
- Schuiling, R.D. (1967): Tin Belts on the continents around the Atlantic Ocean. *Econ. Geol.*, v. 62, pp. 540-550.
- Shukla, B.D. and Singh, A.K. (1988): Tin mineralization in Almora district, Uttar Pradesh, *J. Geol. Soc. Ind.*, v. 31, pp. 347-349.
- Singh, S. (1981): *Geology of the granitic and associated rocks with special reference to their mineralisation in Govindpal-Tongpal region*, District, Bastar, M.P. Unpubl. Ph.D. Thesis, Banaras Hindu University.
- Singh, S., Shankar, B., Kumar Santosh (1996): Trace and rare earth element geochemistry of rocks associated with tin-tungsten mineralization in the Jalali area, Kumaun Lesser Himalaya, *Geol. Surv. Spl. Publ.*, 21(1), pp. 463-467.
- Smirnov, V.I. (1968): The sources of ore forming material, *Eco. Geol.*, v. 63(4), pp. 380-389.
- Smith, F.G. (1947): Transport and deposition of the non-sulphide vein materials. II Cassiterite. *Economic Geology*, v. 42, pp. 251-264.
- Smith, J.V. (1974): *Feldspar Minerals*, vols. 1, 2, 3, Springer-Verlag, New York.
- Stemprok, M. and Sulcek, Z. (1969): Geochemical profile through an ore bearing lithium granite. *Economic Geology*, v. 64, pp. 392-404.
- Stemprok, M. (1970): Geochemical association of tin. In. W. Fox (Editor), A second technical conference on tin, Bangkok, *International Tin Council, Dept. of Mineral Resources of Govt. of Thailand*, pp. 159-176.

- Stemprok, M. and Skvor, P. (1974): Composition of Tin Bearing Granites from the Krusne Hory Metallic Province of Czechoslovakia *Shornik Geologických Ved, Losiskova Geologie, vol. 16*, pp. 7-87.
- Stemprok, M. and Voldan, J. (1975): *Rozpustnost SnO_2 vs Sodnokremicitychsklech. Silikaty*, 19.3: 211-222.
- Stemprok, M. and Voldan, J. (1978): Solubility of tin dioxide in dry sodium rich granite melts. Proceedings of the XI. *General Meeting of IMA: 125-133, Novosibirsk 4-10. Sept. 1970. Izd. Nauka-Leningrad.*
- Streickeisen, A.L. (1967): Classification and nomenclature of igneous rocks, *Neues. Jahr. Mineral. Abhandl, v. 107*, pp. 144-240.
- Suryanarayana, M. et al. (1979): On the occurrence of cassiterite, tantillam-columbite-tantilite and other uranium minerals in Bastar district. *M.P. Geol. Sur. India. Ind. Min.33: 2*, 36-38.
- Takagi, T. and Tsukinura, K. (1997): Genesis of oxidised and reduced- type granites. *Econ. Geol. V. 92*, pp.81-86
- Tauson, L.V. (1968): Distribution regularities of trace elements in granitoid intrusions of the batholith and hypabyssal types. In Ahrens. L.H. ed. *Origin and distribution of the elements*: Oxford, Pergamon. pp. 629-639.
- Tauson, L.V. and Kozlov, Y.D. (1973): Distribution functions and ratios of trace element concentrations as estimators of the ore-bearing potential of granites. *Proc. Int. Geochem. Explor. Symp. 1972, Inst. Min. Metall. London, 4*: 37-44.
- Taylor, R.G. (1979): Geology of tin deposits, *Developments in Economic Geology-11. Elsevier Scientific Publishing Company, Amsterdam*. 543 p.
- Taylor, S.R., Heier, K.S. and Sverdrup, P.L. (1960): Contribution to the mineralogy of Norway. No. 5. Trace element variations in three generations of feldspars from Landsverk I Pegmatite, Evje, Southern Norway, *Norsk. Geol. Tidsskr. v. 40*, pp. 135-156.

- Taylor, S.R. and McLennan, S.M. (1985): The continental crust : its composition and evolution. *Blackwell, Oxford*, 295 p.
- Tischendorf, G. (1977): Geochemical and Petrographic Characteristics of Silicic Magmatic Rocks associated with Rare Elements Mineralisation. In *Metallisation Associated with Acid Magmatism*, v. 2, pp. 41-96.
- Tripathi, C.; Ghosh, P. K.; Thambi, P. I.; Rao, T. V. and Chandra, S. (1981): *Elucidation of the stratigraphy and structure of the Chilpi Group*. *G. S. I. Spl. Pub.* 3; 17-30
- Tuttle, O.F. and Bowen, N.L. (1958): Origin of granite in the light of experimental studies in the system $\text{NaAlSi}_3\text{O}_8\text{-SiO}_2\text{-H}_2\text{O}$. *Geol. Soc. Am. Mem.*, v. 74, pp. 153.
- Walker, T.L. (1900): Geological sketch of the central portion of Jeypore Zamindari Vizagpatnam district. *Gen. Rep. Geol. Surv. Ind.*, 1899-1900.
- Walsh, J.N., Buckley, F. and Barker, J. (1981): The simultaneous determination of the rare earth elements in rocks using inductively coupled plasma source spectrometry. *Chem. Geol.*, v. 33, pp. 141-153.
- Whalen, J.B., Currie, K.L. and Chappel, B.W. (1987): A-type granites: Chemical characteristics, discrimination and petrogenesis. *Contrib. Mineral. Petrol.* 95, pp. 407-419.
- White, A.J.R. and Chappel, B.W. (1988): Some supracrustal (S-type) granites of the Lachlan Fold Belt. *Trans. Roy. Soc. Edinburgh*, 79, pp. 169-181.
- Winchester, J. A. and Max, M. D. (1983): A note on the occurrence of stanniferous granite gneiss in County mayo. *Geol. Surv. Ire. Bull.* 3; 113-119
- Yedekar, D. B; Jai, S. C.; Nair, K, K, and Dutta, K. K. (1990): The Central Indian Collision Suture. *G. S. I., spl pub*; 28 1-43.